# All-India Survey of Photovoltaic Module Reliability: 2018


## National Centre for Photovoltaic Research and Education (NCPRE), IIT Bombay

## &

## National Institute of Solar Energy (NISE), Gurugram

NCPRE

NISE

March-May 2018

# All-India Survey of Photovoltaic Module Reliability: 2018

Yogeswara Rao Golive, Sachin Zachariah, Sonali Bhaduri, Rajiv Dubey, Shashwata Chattopadhyay, Pratik Joshi, Nilesh Kusher, Arpit Nandi, Amey Chindarkar, Devan P Vasudevan, Pratik Mundle, Sugguna Rambabu, Ajeesh M.V, Ritesh Ingle, Ali Asger Khattab, Hemant Kumar Singh, Brij Mohan Arora, K. L. Narasimhan, Anil Kottantharayil, Juzer Vasi and Narendra Shiradkar

*National Centre for Photovoltaic Research and Education (NCPRE)*
*Indian Institute of Technology Bombay*
*Powai, Mumbai 400076, India*

and

Yogesh Kumar Singh, Ramayan Singh, Sahan Raghava, Manander Bangar, Gowri Ganesh, Avinash Kumar Haldkar, Birinchi Bora, Sanjay Kumar, Rajesh Kumar and A.K. Tripathi

*National Institute of Solar Energy (NISE)*
*Gwalpahari, Gurugram, Haryana 122003, India*

Survey conducted in March-May 2018

# Contents

# Acknowledgements

The 2018 All-India Survey of Photovoltaic Module Reliability is the fourth in the series of such surveys conducted to assess the reliability and durability of photovoltaic (PV) modules in different parts of India. It was conducted during March to May of 2018. As in the case of the previous surveys, the 2018 Survey was also conducted jointly by the National Centre for Photovoltaic Research and Education (NCPRE) at the Indian Institute of Technology Bombay (IITB) and the National Institute of Solar Energy (NISE).

NCPRE and NISE would like to thank the various participants in the 2018 survey at different levels (PV system owners, State Renewable Energy nodal agencies, private EPC contractors and local installers) who have helped us in multiple ways to bring the survey to fruition. Their names and organizations are not individually mentioned in order to preserve anonymity of the sites. We would also like to thank SenseHawk and Air Probe-14W Technologies for helping us with aerial thermography of solar power plants at a few sites.

Thanks are due to many people at NCPRE and NISE who have helped in making the Survey possible. We thank Prof. B. G. Fernandes and Prof. Chetan Singh Solanki, Principal Investigators of NCPRE, and Dr. Chandan Banerjee, Deputy Director-General of NISE, for their support of the survey. We thank Ms. Ruchita Korgaonkar for help in preparation of report. We also thank Ms. Smita Wangikar, Mr. Gaurav Hande, Dr. Diksha Makwani, Ms. Mallika Moolya, and Ms. Pushpa Jadhav of IIT Bombay, and all the staff members of NISE for logistic and other support. The team also wishes to thank Mr. Ajit Singh who made the arrangements for the vehicles for the cross-country travel, and the drivers Mr. Rakesh, Mr. Yadav, and Mr. Shafiq who drove the 18,000 plus kilometers safely in sometimes difficult terrain.

We are also thankful to several persons who have given advice and feedback on the Survey. Mr. Hemant Lamba gave the initial suggestion which launched the surveys in 2013, and has continued to be actively involved over the years. Thanks are also due to Dr. S. P. Gonchaudhuri and Dr. B. Bhargava for their support and encouragement. We are also thankful to Dr. Lawrence Kazmerski and Dr. Rajiv (Rajeewa) Arya, both of whom are Visiting Professors at IIT Bombay, and Dr. G. Tamizhmani of Arizona State University, USA, for their valuable inputs.

Both NCPRE and NISE would like to thank the Ministry of New and Renewable Energy (MNRE), Government of India, for funding which enabled this survey to be undertaken.

# Executive Summary

The 2018 All-India Survey of Photovoltaic Module Reliability is the fourth in a series of such Surveys conducted to monitor the reliability and durability of photovoltaic (PV) modules in different parts of India. It was carried out during March to May of 2018. The modules in Cold & Sunny climate of Ladakh were surveyed in the month of September 2018. As in the 2013, 2014 and 2016 Surveys, the 2018 Survey was also conducted jointly by the National Centre for Photovoltaic Research and Education (NCPRE) at the Indian Institute of Technology Bombay (IITB) and the National Institute of Solar Energy (NISE).

The 2018 Survey built upon the experience gained from the previous Surveys. The number of large utility-scale power plants surveyed in 2018 was significantly larger than earlier, reflecting the pattern of PV installations in the country in the last few years. The team visited a total of 36 sites distributed in 5 (of the 6) climatic zones of India, and of these 27 were 'large' (> 100 KW) sites. Another important difference in 2018 from the earlier Surveys was that instead of choosing modules at random, we followed a more systematic procedure wherever possible, by selecting modules from good, medium and poor performing strings. This procedure meant that we obtained gross string level data on a total of 11270 modules. Out of these, a total of 1199 modules were inspected and analyzed in detail, of which 975 were in the large sites. The age of the modules was varied from 1 year to more than 25 years, and 7 different technology types were represented, though the main type was c-Si. Of the 36 sites, 17 were 'repeat' sites which had been inspected in one or more earlier Surveys. The sites visited in 2018 are shown in Fig. 1. The outdoor characterization tests undertaken in 2018 included: visual inspection, measurement of *I-V* characteristics under light, infra-red (IR) thermography under light, electroluminescence (EL) imaging, interconnect integrity test, measurement of irradiance, ambient and module temperatures.

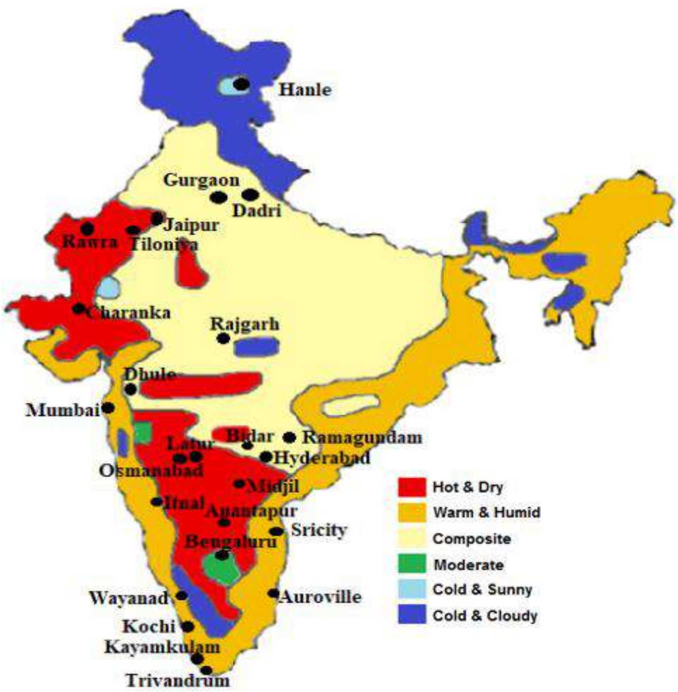


Fig. 1. Climatic zones of India and sites visited during the 2018 All-India Survey. Note that the Survey did not include any sites in the Cold & Cloudy zone.

At each of the 36 sites, between 25 and 50 modules were typically taken up for detailed analysis. Some modules (46 in number) showed Overall Degradation Rates of more than 5.2 %/year, and these modules, termed 'outliers', were not included in the main analysis as they appeared to suffer from serious quality problems and other extraneous issues, such as over-rating. Finally a total of 1199 modules were taken up for detailed analysis, and their distribution is shown in Fig. 2.

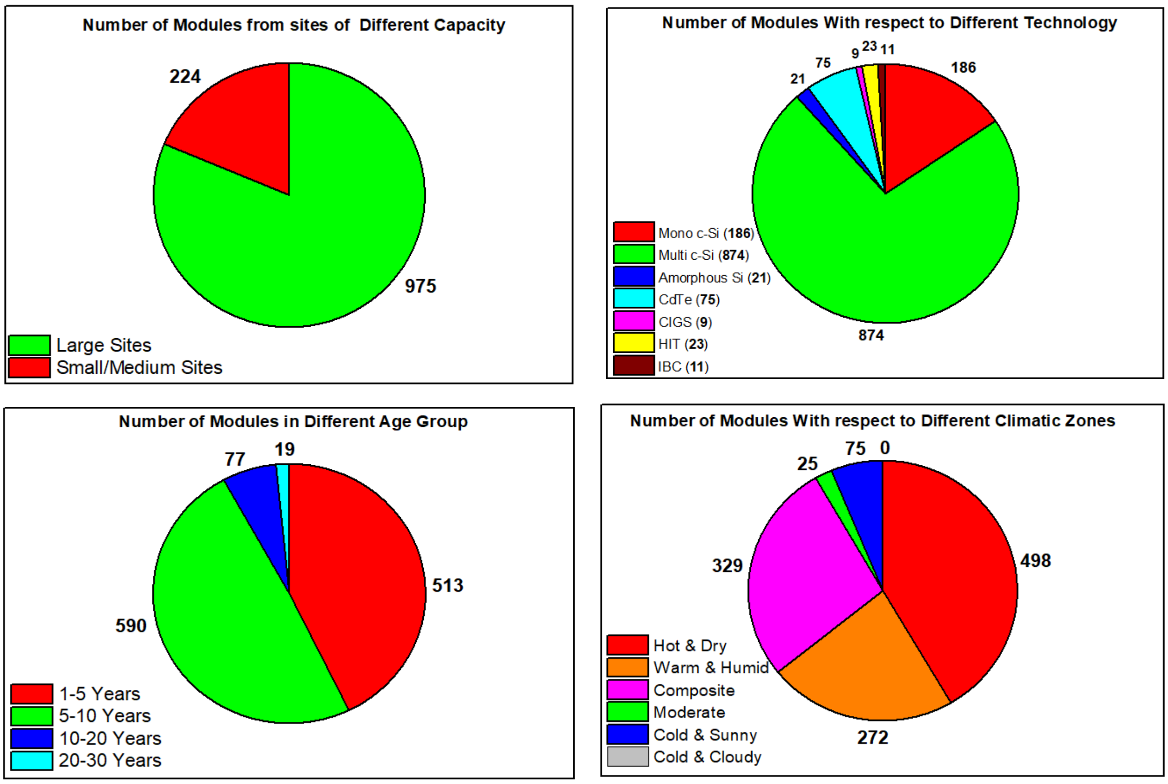


Fig. 2. Distribution of sites and modules in terms of installation size, technology used, age and climatic zone. Large size refers to installations > 100 kW, and small/medium to installations < 100 kW.

An important observation of the 2018 Survey is that there was a wide distribution in the performance of the modules. This phenomenon was also observed in previous Surveys. The histogram of the 'Overall Degradation Rate' of the modules, that is, the rate at which the output power $P_{max}$ decreases per year *without* accounting for initial rapid Light Induced Degradation (LID), as well as the LID-discounted 'Linear Degradation Rate', for which a 2% initial degradation in $P_{max}$ is used for Si modules, are shown in Fig. 3.

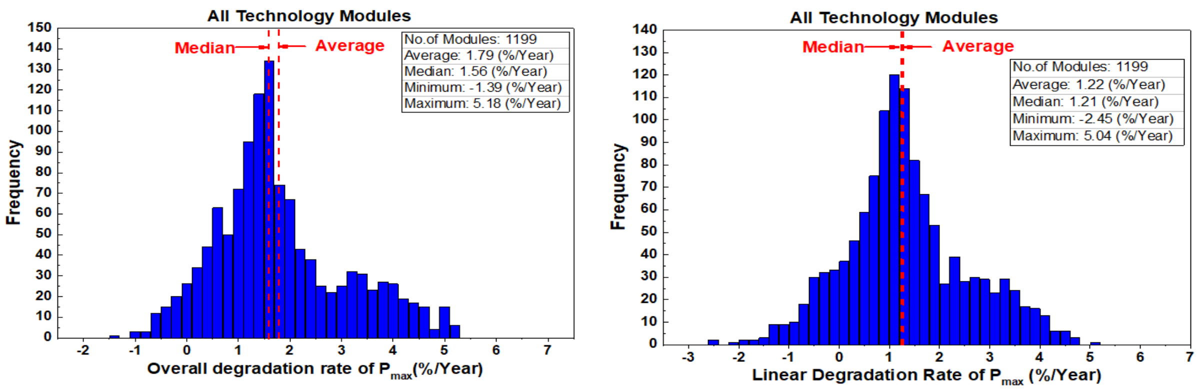


Fig. 3. Histograms of 'Overall' and 'Linear' $P_{max}$ Degradation Rates for modules of all technologies.

It can be seen that the rates vary over a large range, from less than 0 %/year to more than 5.2 %/year, with the average at 1.79 %/year and 1.22 %/year for the Overall and Linear Rates. (The LID-discounted Linear Rate is more appropriate when comparing the long-term trends in Young and Old modules.) It should be noted that the international benchmark is about 0.6-0.8 %/year. Since most of the installations in India now use c-Si modules, we look at the histograms for only c-Si technologies (both mono and multi), shown in Fig. 4. It can be seen that the average Linear Rate for c-Si technologies (1.47 %/year) is higher than the Linear Rate for all technologies. This is because the thin film technologies are observed to have low degradation rates. Whether this difference is due to an intrinsic technology effect, or is a reflection of the quality of manufacturing (all thin film modules come from a handful of reputed manufacturers whereas the c-Si modules come a wide variety of manufacturers), is unclear.

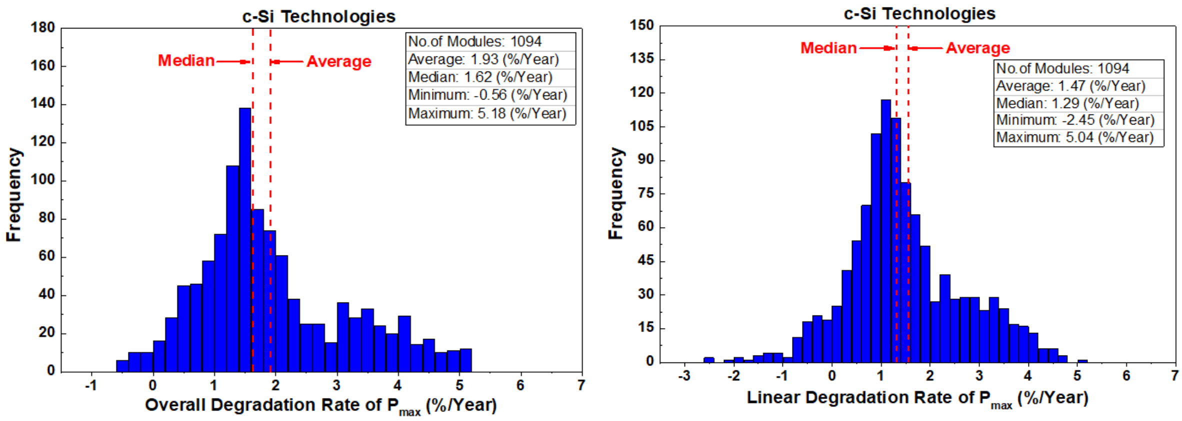


Fig. 4. Histogram of Overall and Linear $P_{max}$ Degradation Rates (%/year) for c-Si technologies only.

It is well known that PV modules in different climates degrade differently, and this has been seen in all the All-India Surveys, including 2018. While we have looked at the degradation rates in all climatic zones, we find it is most instructive to separate these zones into two broad categories: *'Hot' zones* (comprising the Hot & Dry, Warm & Humid, and Composite zones), and *'Non-Hot' zones* (comprising Moderate, Cold & Sunny and Cold & Cloudy zones). The Linear Degradation Rates for c-Si modules in the Hot and Non-Hot zones are shown in Fig. 5. Modules in the Hot zones degrade distinctly faster. This is a cause for concern since many of the solar installations in India will come up in Hot zones (which also have plentiful sunshine). Our detailed visual analysis indicates that the main reasons for modules to degrade faster in Hot zones is that the encapsulant (EVA) discolors faster, and there is more metal and interconnect corrosion in the Hot zones. Moreover, several degradation mechanisms get accelerated due to high temperature, thus resulting in faster wear out of modules in Hot zones.

Another disturbing factor observed is that the Linear Degradation Rate for Young modules is higher than that for Old modules. This result has been seen in both the 2016 and 2018 Surveys. This is shown in Fig. 6 for c-Si modules. The Young modules have an average Linear Degradation Rate of 1.85 %/year, while the Old modules have 1.14 %/year. For Young modules, the main contributor for $P_{max}$ degradation is the fill factor (*FF*) which is often related to poor quality and cracks, whereas for the Old modules, besides *FF*, short circuit current ($I_{sc}$) degradation, symptomatic of encapsulant discoloration, also plays a role.

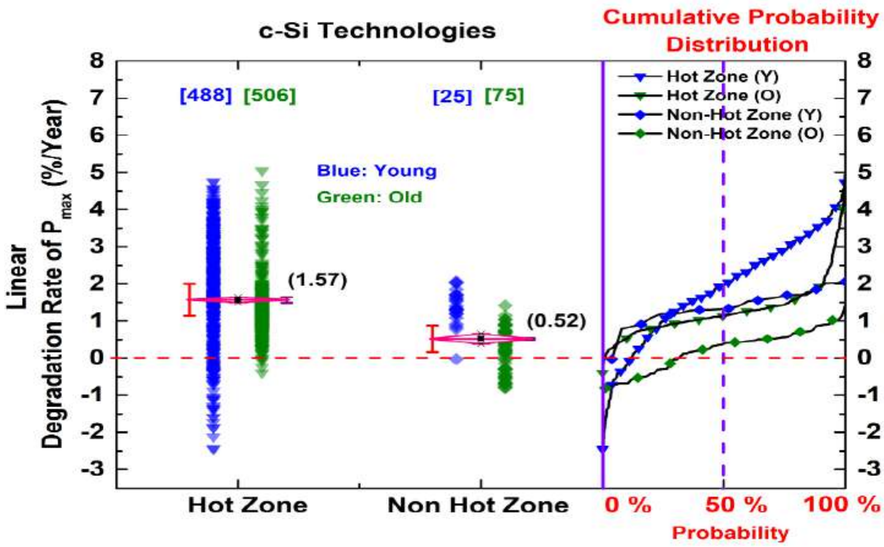


Fig. 5. Comparison of the Linear Degradation Rate of $P_{max}$ in Hot and Non-Hot climatic zones. The blue and green symbols represent Young (<5 year) and Old (>5 year) modules. The numbers on top are the total number of modules in that zone and age group, and the horizontal red bar is the average degradation rate in that zone. Error bars due to nameplate and measurement error are also shown. The right segment shows the cumulative probability distribution.

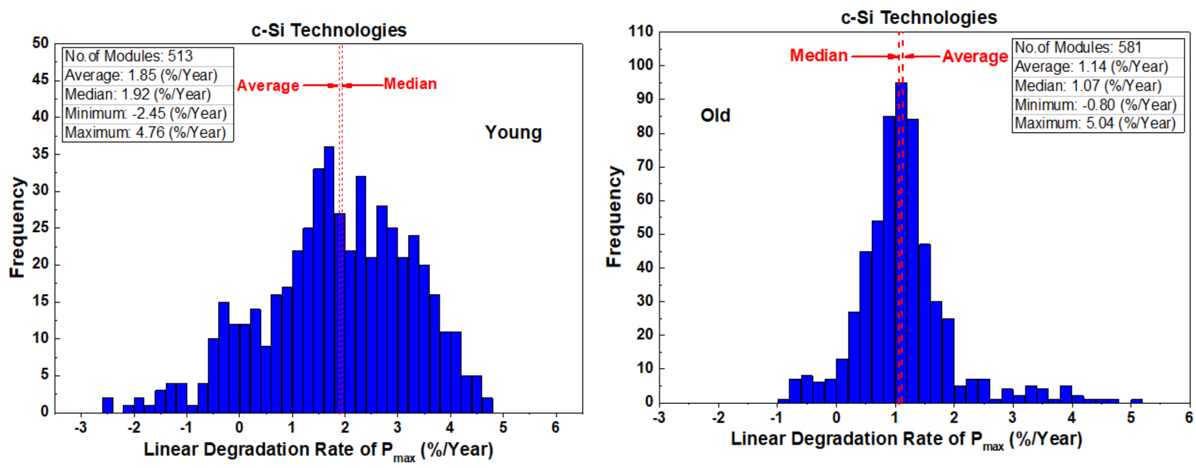


Fig. 6. Histograms of Linear $P_{max}$ Degradation Rates for Young and Old c-Si modules.

The Young versus Old differentiation is also well brought out in Fig. 7, which shows the average Linear Degradation Rates for the various *sites* as a function of the age of the site. It is again seen that the Young sites have a higher degradation rate. Further, based on the detailed analysis of the performance of the modules, we have been able to assign causes for the higher degradation rates for Young sites, as shown in the figure. It is seen that Potential Induced Degradation (PID) and interconnect degradation are key causes of poor performance. It can be seen in Fig. 7 that there were four Young sites where significantly high linear degradation was observed, however, no specific signature of any failure mechanism was seen in any of the characterization tests. This observation, and existence of several modules with >3 %/year linear degradation rates indicates that Young category is beset by poor quality and possibly also unethical over-rating of panels.

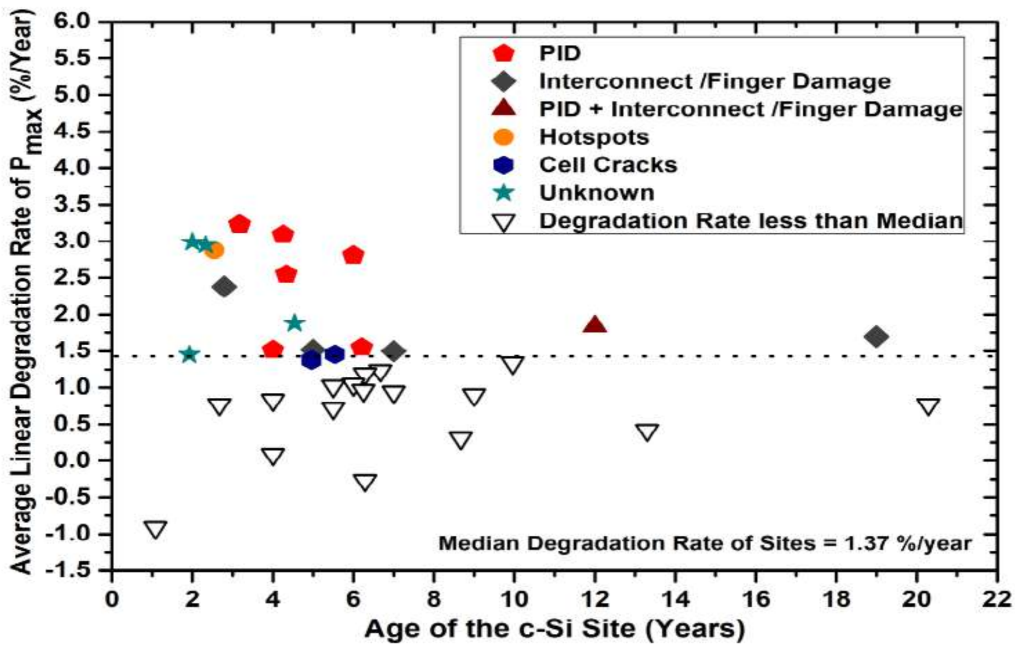


Fig. 7. Average Linear Degradation Rates of $P_{max}$ for all c-Si sites with respect to their Age and dominant degradation modes observed in sites with degradation rates higher than the median (1.37 %/year)

A final observation which calls for serious attention relates to the relative performance of roof-mounted versus ground-mounted modules. As seen in Fig. 8, the roof-(rack)-mounted modules show a degradation rate of 1.99 %/year compared to 1.33 %/year for ground-mounted c-Si modules. This result (consistent with results from previous Surveys) means that special attention is needed for the design and deployment of PV systems for India's rooftop target.

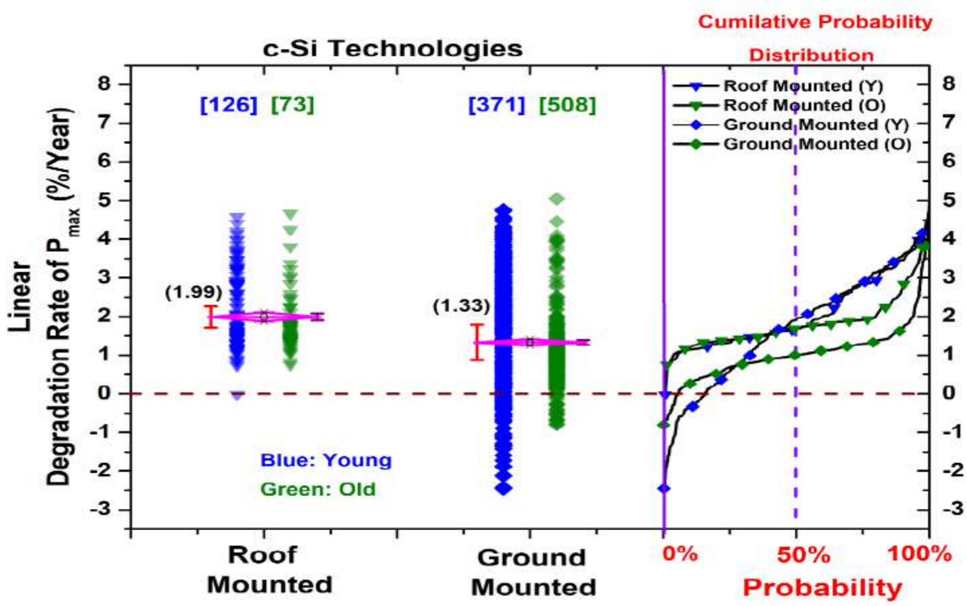


Fig. 8. Linear Degradation Rate of $P_{max}$ for Roof Rack and Ground Rack mounted c-Si PV modules

We have performed a detailed study of the visual degradation seen in modules, using an enhanced NREL visual checklist. Some key results are as follows. Encapsulant discoloration (yellowing or browning), shown in Fig. 9(a), occurs in all climatic zones, but is faster in Hot zones. Delamination (Fig. 9(b)) is seen to occur most frequently in Warm & Humid climates, but its prevalence is not very high. Snail trails, shown in Fig. 9(c), are usually associated with cracks in the cells, and are again seen mainly in Hot climates. Metallization discoloration or staining (Fig. 9(d)) is seen in all climatic zones, but the severity is higher in Hot zones. Metal discoloration/staining can be due to corrosion or improper soldering.

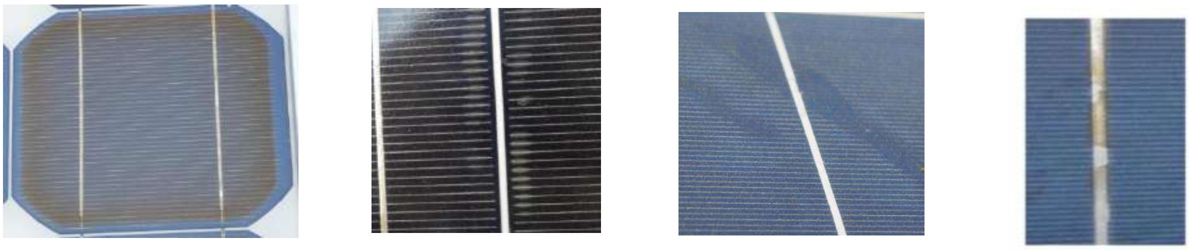

(a) (b) (c) (d)

Fig. 9. (a) Encapsulant browning (b) Delamination (c) Snail trails (d) Metallization discoloration.

The visual defects seen can cause power degradation, and we have explored the correlation between these. Fig. 10 shows the correlation between power degradation and (a) encapsulant discoloration, and (b) metal discoloration. Note that in all cases, the y-axis shows the *total* percentage power loss suffered by the module since installation, and not the annual power degradation rate. It can be clearly seen that these visible defects do indeed result in power loss. Further, the higher incidence of these defects in Hot climates is clearly at least part of the reason for higher degradation rates seen in Hot zones.

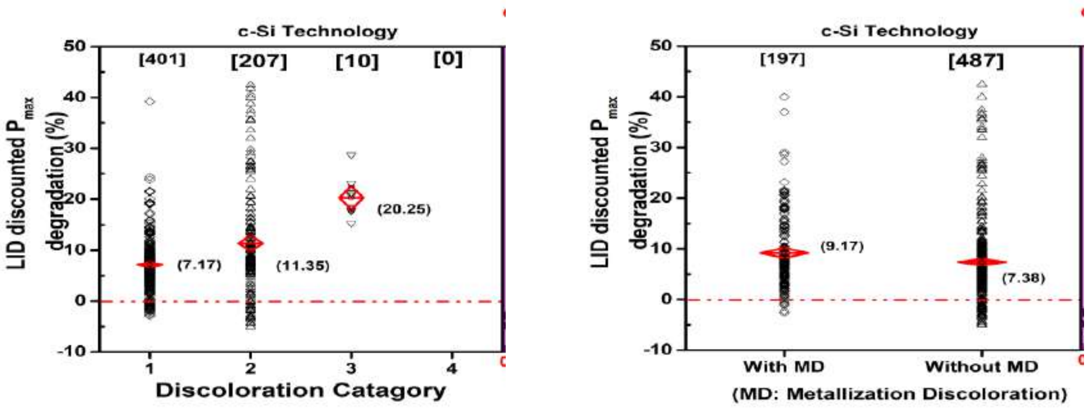


(a) (b)

Fig. 10. Correlation of total $P_{max}$ degradation with (a) Encapsulant discoloration (binned into 4 categories, with 4 indicating highest discoloration) and (b) Metallization discoloration.

Using a special low-light electroluminescence (EL) technique developed by NCPRE for the 2014 Survey, and rugged lightweight DSLR based EL cameras developed by NCPRE for the 2016 Survey, we have taken EL images of over 700 modules during the 2018 Survey. This perhaps represents the most exhaustive field EL data taken anywhere in the world. The EL images allow us to detect microcracks in the c-Si solar cells which cannot normally be seen with the naked eye, and also to detect the presence of PID. Fig. 11 shows examples of EL images of modules without and with cracks. In the 2018 Survey, we did not observe a statistically significant correlation between number of cracks and power degradation (unlike in the 2016 Survey).

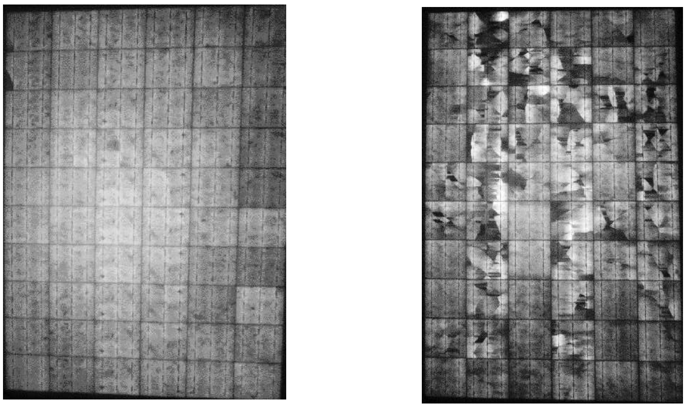

Fig. 11. Field EL image of a module with few micro-cracks (left) and with many micro-cracks (right).

During the 2018 Survey, we also used infra-red (IR) thermography, which shows the temperature distribution over the module. This is particularly useful for identifying hot spots, which can cause significant long-term degradation. The highest modal temperature seen during the Survey for a module operating under MPPT conditions was 72 °C, and highest hot cell temperature seen was 122 °C. We have defined a Thermal Mismatch Index (TMI), where a higher TMI indicates the possibility of hot spots. Fig. 12(a) shows a typical IR image and Fig 12(b) shows how the Total $P_{max}$ Degradation is correlated with the presence of hot spots as measured by the TMI category. Our analysis also shows that PV modules with hot cells have higher degradation in all climatic conditions (both Hot and Non-Hot zones), and further that hot cells ($\Delta T > 4$ °C) in Hot zones have a significantly more deleterious effect on power degradation than in Non-hot zones.

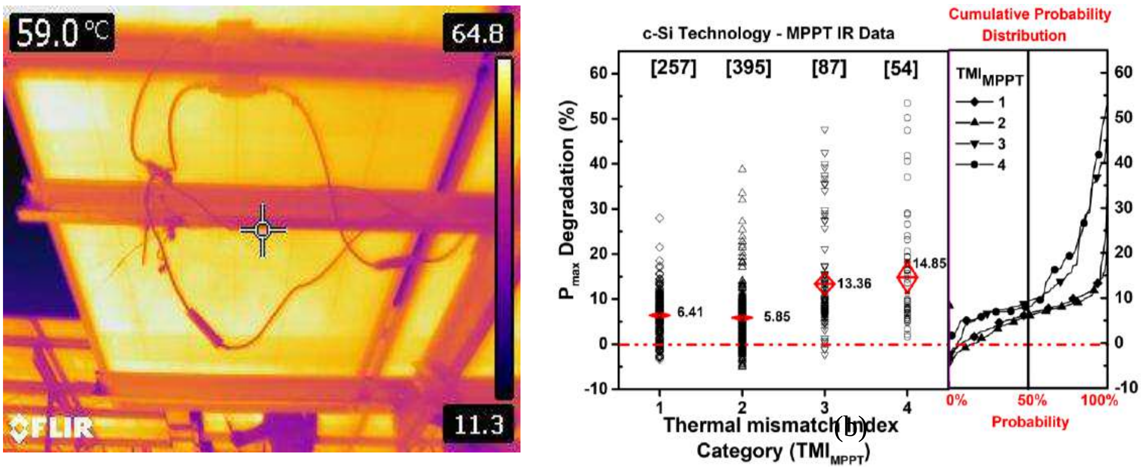


Fig. 12. (a) IR image of a module under MPPT condition (b) correlation of Total $P_{max}$ Degradation with Temperature Mismatch Index (TMI) category.

For the first time, the 2018 Survey also undertook a drone-based IR study at one of the sites, and compared it with the ground-based IR measurement. The modules with hot spots or hot cells identified by the drone were also seen to have high module $\Delta T$ (a measure of the temperature of the hot spot above the rest of the module) in the ground IR measurement. The conditions during drone based IR imaging resulted in higher sensitivity for detection of modules with $\Delta T > 4$ °C, thus some modules with lower $\Delta T$ were not flagged. However, it was observed that drone based IR imaging, coupled with intelligent image processing software is a promising technique for quick, 100% inspection of PV plants to identify modules with catastrophic failures or extreme hot spots.

A special effort was made during the 2018 Survey to identify the presence of Potential Induced Degradation (PID) in the modules, which can cause a substantial decrease in $P_{max}$. We made measurements on modules at the positive end of the string, the middle of the string and the negative end of the string, since PID is known to affect mainly modules near the negative end. We also analysed the *I-V* and EL data, since it is known that PID causes a decrease in shunt resistance and in *FF*, and is accompanied by dark EL near the edges of the module. Fig. 13 shows (a) the EL image of a module near the positive end of String 4, (b) the EL image near the negative end of the same string and (c) the power degradation of modules of 3 strings, including String 4. PID is very likely to have occurred in String 4. Using this methodology, we have seen PID in 7 of the 36 sites surveyed in 2018.

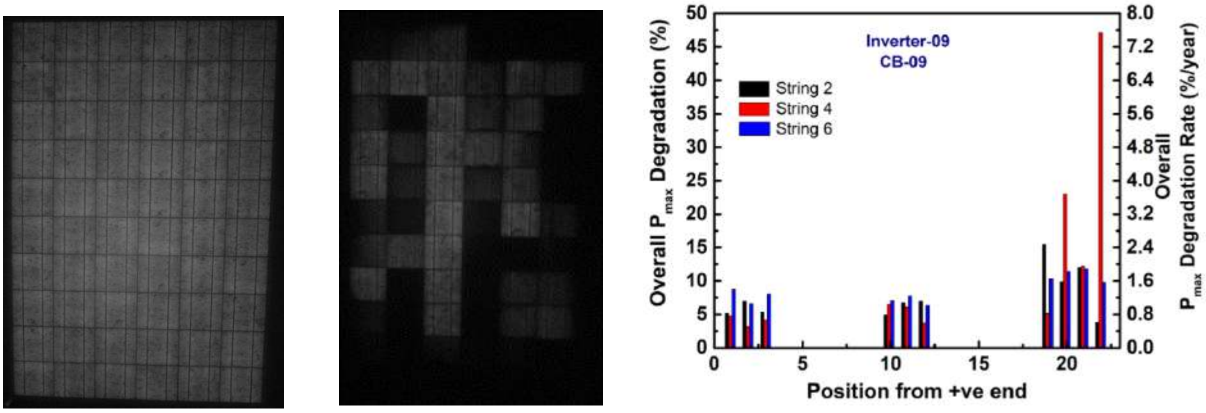


(a) (b) (c)

Fig. 13. (a) EL image of the 2nd module in String 4 (b) EL image of the 22nd module in String 4 and (c) Positional dependence of $P_{max}$ degradation in 3 strings.

We have also performed a Risk Priority Number (RPN) analysis of the failure modes. Such an analysis would help to identify which failure mode(s) pose the most risk in different climatic zones, and would thus enable power plant operators to specifically look out for such failure modes. Our analysis has found that solder bond failure has high RPN in all climatic zones, and in the Hot climatic zones, PID, delamination and junction box issues also pose high risk. Modules in the Cold & Sunny climatic zone show very few failure modes. An important 'safety' RPN in all climatic zones corresponds to hot spots with high temperatures. An example of the RPN analysis for 'performance' reliability based on various defects in Young modules in different climatic zones is shown in Fig. 14.

In summary, an excellent picture of the durability and reliability of PV modules in the country has emerged from the 2018 All-India Survey. Broadly, the results agree with those of the previous 2014 and 2016 Survey. Again, one of the important observations is that there is wide variability in the quality and degradation rates of the modules. Many modules show excellent performance, but there are many others showing alarmingly high degradation rates. Crystalline-silicon modules show an average Linear Degradation Rate of 1.47 %/year, much higher than the international benchmark of 0.6-0.8 %/year. Young modules (< 5 years) show higher degradation rates than Old modules, pointing to poor quality and also perhaps over-rating of Young modules in recent years. As seen during the past Surveys, the 2018 Survey also shows that modules in Hot zones and on rooftops are seen to degrade faster.

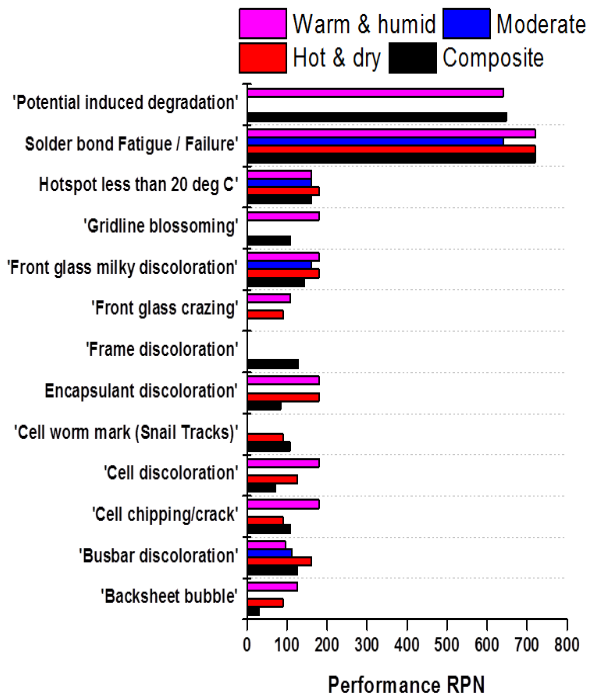


Fig. 14. 'Performance' Risk Priority Number (RPN) of various failure modes in Young PV modules in different climatic zones (high RPN value indicates high risk of performance failure).

Based on the field observations, analysis and results of the 2018 All-India Survey, some high-level recommendations which can be made are the following:

– Due diligence should be exercised while selecting and procuring modules. This may include verifying the antecedents of the manufacturer, and independent checks on the quality of the module(s). Although most modules available in the market carry the IEC certification, it should be noted that this does not guarantee that the module will perform adequately through its intended life.

– The tender specifications need to be much more elaborate than currently being used. EVA and backsheet particularly can be of different qualities, and should be specified carefully in the tender document for procurement.

– Cases of 'over-rating' of modules have been observed. Owners and installers of power plants should be vigilant about this malpractice. Random measurements should be made on modules, and such checks should be specified in the tender documents as well. An independent audit of modules and installations by third party is recommended.

– It is recommended that a field-based electroluminescence (EL) study be performed after receiving the modules at site and after installation to reveal micro-cracks which may have been caused during the transport and installation phases.

– The presence of PID seen in the 2018 Survey indicates the need to be cognizant of this failure mode, and to take appropriate steps, including attention to grounding, and installation of 'PID-free' modules.

– It has been noted that the 'Hot' climates present a harsh operating environment for PV modules. An intensive study of degradation phenomena in hot climates, which has not been emphasized sufficiently by the PV community so far, is needed. This is particularly important for India, since much of the 100 GW is expected to come up in the 'Hot' zones of the country.

- The IEC certification protocols (e.g. 61215), and other standards are currently being updated to take into account the hot climate phenomena. This has arisen partly out of our All-India Survey reports which have consistently shown in 2013, 2014, 2016, and now in 2018 that modules in Hot climates degrade faster. The upcoming IEC technical specification (IEC 63126) would provide harsher accelerated tests for modules deployed in high temperature end use environments.
- Modules and sites perform very well in the ‘Cold & Sunny’ climate of Ladakh. We had recommended earlier that power plants should be set up in this region, as these would enjoy not only low degradation rates & high performance ratios, but also excellent irradiance and easy availability of land. With the proposed grid links to Ladakh under construction, it is now appropriate that MNRE is pursuing 23 GW of solar PV in the region.
- It is felt that some of the quality issues seen especially in the young modules are the result of aggressive pricing and timelines and improper handling/installation. Reverse bidding has been extremely valuable to discover lower tariffs and bring down the cost of PV in India. However, now that the cost of PV electricity is comparable (or lower) with that of fossil fuel based generation in most parts of the country, it is recommended that elaborate clauses to ensure quality and reliability be included in the tenders. These clauses should attempt to go beyond the minimum IEC certification criteria to proactively ensure good quality of PV modules in the entire chain - from manufacturing to installation. This may result in stabilization of the tariffs to current values for some time (instead of further lowering), however, the benefit in terms of increased energy production during the service life of PV plants would outweigh the slightly higher initial costs. While reverse bidding is a good strategy in many situations to discover lowest tariffs, this has a major negative implication in solar PV, where the price of modules varies significantly based on quality.

# 1. Introduction

## 1.1 Introduction to Survey

India has set an ambitious target of deploying 100 GW of solar Photovoltaic (PV) capacity by 2022 under the National Solar Mission (NSM) in an effort to combat climate change and avoid over-dependence on fossil fuels for electricity generation. By December 2018, 26 GW had been installed [1], and rapid additional deployment is expected to occur over the next 4 years. The 100 GW target is part of the overall goal to achieve 175 GW of non-fossil fuel energy by 2022, and resonates well with India's COP-21 obligation in Paris to have 40% of its electricity generated by renewables by 2030. A recent announcement that the 175 GW goal may be increased to 227 GW further emphasizes India's commitment to renewables [2]. The success of the National Solar Mission in de-carbonizing the power generation sector will depend not just on meeting the 100 GW installation target but also on the satisfactory long-term performance of the photovoltaic systems. This is because eventually, only the GW-hours of electricity generated per GW of PV installation would contribute towards addressing the issues for which the NSM was created. The expected lifetime of solar PV modules in the field is 25 years. Considering the lack of information with regard to the long-term performance of PV systems of various technologies in different climatic conditions of India, the High Powered Task Force of MNRE had in March 2013 requested the National Centre for Photovoltaic Research and Education (NCPRE), at the Indian Institute of Technology Bombay (IITB) to survey the performance of PV systems installed in the country. NCPRE requested the National Institute of Solar Energy (NISE) to partner in conducting the survey. Accordingly, a joint team was formed which surveyed PV modules in the summer of 2013, and followed this up with Surveys with enhanced scope in 2014 and 2016. The full reports of these Surveys are available online [3-5], and briefer descriptions elsewhere [6-15]. With the wealth of useful data emerging from these Surveys, it was important to continue the Surveys biennially, in 2018 and 2020. This would then make available the most comprehensive, consistent and repeated (year-on-year) set of data on reliability and durability of PV modules to policy makers, PV developers, manufacturers and others in the PV community in India and abroad. This report describes the results of the 2018 All-India Survey of PV Module Reliability.

The 2018 All-India Survey was performed jointly by NCPRE and NISE during the early summer months (early March to late May) of 2018. Since, by 2018, utility-scale PV power plant installations dominated the solar landscape in India, the 2018 Survey contained many more 'large' (> 1 MW) sites than earlier, and correspondingly fewer 'small/medium' rooftop sites. A total of 36 different sites covering five of the six climatic zones of India were chosen. Of these 36 sites, 17 were 'repeat' sites, and 19 were 'new' sites which had not been surveyed earlier. In most sites, we first inspected several strings which contained a total of 11270 modules. Of these, 1199 modules were chosen for detailed measurement and analysis. About 75% of the sites covered in 2018 were 'large' sites, containing 81% of the modules (both these numbers are significantly higher than in previous Surveys). For the 2018 Survey, the field assessment of the 1199 modules included (as in the 2014 and 2016 Surveys) a visual checklist, a detailed electrical characterization of the modules (illuminated *I-V*, insulation resistance test and electroluminescence imaging), thermal characterization (illuminated IR), and measurement of the relevant weather and irradiance data.

The survey methodology and a review of some related literature are presented in the forthcoming sections of this chapter, including a brief discussion on the climatic zones of India. Chapter 2 deals with the survey statistics and some general information about the survey sites. Since the field data have been collected under various ambient conditions (different irradiance and module temperatures), it was necessary to convert all the data to Standard Test Condition (STC) of 1000 W/m$^2$, 25 °C and AM1.5G solar spectrum for comparison and calculation of degradation rates. Chapter 3 deals with this conversion and assesses the errors associated with such conversions as well as due to other reasons. Chapters 4 to 7 deal respectively with illuminated *I-V* analysis, visual analysis, electroluminescence (EL) imaging and infrared (IR) thermography and Potential Induced Degradation (PID) analysis. Results from Risk Priority Number (RPN) analysis are presented in Chapter 8. Finally, we present our concluding remarks in Chapter 9 with recommendations for the PV community.

A new protocol to choose the strings and modules for detailed characterization and analysis was developed for the 2018 Survey, and that is described later in this chapter. During the 2018 Survey, we also undertook a detailed inspection and characterization of BOS components, and overall power plant performance, but those results are not included in this report, which focuses on the module reliability.

## 1.2 Literature Review

A comprehensive review of the relevant literature has already been presented in the previous reports [2-4], and the reader is referred to these documents for relevant scientific literature. Here, we briefly mention some recent important publications which have appeared, including the literature on Light Induced Degradation (LID) with the aim to obtain the most appropriate values for the rapid initial degradation.

Field studies provide information about the performance degradation of photovoltaic modules in actual operating conditions. A publication by Jordan *et al.* [16] shows that the average degradation rate in hot climates is higher than those in cold climates. This has also been the experience in the All-India Surveys. They have reported that the average degradation rate of crystalline silicon modules is in the range of 0.8-0.9 %/year, while it is higher than 1% for HIT and thin film technologies. Other recent publications by Jordan *et al.* [17, 18] have reviewed the relevant literature on various degradation modes and indicated that encapsulant discoloration is the most common degradation mode, particularly in the older systems. Hot spots have also been identified as a matter of concern for the modules aged less than 10 years. Glass breakage and absorber layer delamination are the common problems in thin film modules. Jordan *et al.* [19] have recently suggested a robust year-over-year calculation of degradation rates.

One important effect to consider while estimating the degradation rate (percentage loss of power per year), especially for relatively young modules, is the non-linearity involved in the degradation of PV modules, as discussed by Jordan *et al.* [18]. This includes the rapid initial degradation observed in crystalline silicon modules upon exposure to sunlight, referred to as Light Induced Degradation (LID), and similar meta-stabilities in various thin film technologies, owing to which the power output decreases rapidly upon outdoor exposure (as in the case of the Staebler-Wronski effect in amorphous silicon modules [20, 21]) or even increase initially followed by long term degradation (for example, in CdTe modules [22, 23]). In case of CdTe, the performance enhancement due to light soaking effects can be up to 10%, and it shows a strong temperature dependence as well [24]. LID is commonly seen in crystalline silicon modules from almost all manufacturers, and the manufacturers usually incorporate this in their warranty documents, as a 2% to 3% initial rapid degradation in power output within the first year of operation [25-27]. It is primarily caused due to dissolved impurities like boron, iron, and oxygen in the silicon ingot, and hence the extent of LID depends on the quality of wafer and cell manufacturing processes [28]. Though LID varies from manufacturer to manufacturer, PVSyst software recommends a value of 2% LID for energy generation simulations [29]. PERC modules are known to suffer from enhanced amount of LID [30], however, note that none of the sites inspected in this Survey had PERC modules. A detailed survey of the literature [28, 31-34] gave varying values of $P_{max}$ degradation, and we found that 2% is a reasonable number to choose. The literature also mentioned how the 2% is divided into degradation in short circuit current, open circuit voltage, and fill factor. As described in the report of the 2016 All-India Survey [5], 40% of the degradation in power output is assigned to short circuit current ($I_{sc}$) degradation, another 40% to open circuit voltage ($V_{oc}$) degradation, and the rest 20% to fill factor (*FF)* degradation. Accordingly, for the purpose of our analysis, we have divided the 2% LID in power output into 0.8% for $V_{oc}$, 0.8% for $I_{sc}$ and 0.4% for *FF*.

## 1.3 Survey Methodology

An important difference between the 2018 Survey and the earlier Surveys was in the methodology used to select the modules in the new sites which had not been visited earlier. In earlier Surveys, the modules were chosen at random, in the hope that this sample would capture the behavior of the group. In the 2018 Survey, a more systematic procedure was followed for the 19 new sites, which is described below.

At the new sites, we selected two inverters based on either the SCADA information available to us (for 4 sites), or from the inputs of site engineers (for 15 sites). From the SCADA data, we chose the best performing and worst performing inverters based on their energy generation. (We have seen that the difference in power between the best and worst performing inverters was not significant.) We then chose a Combiner Box (CB) randomly based on its accessibility and the availability of an AC power supply close to it. Once the CB was chosen, we performed *I-V* measurement on all the strings connected to it, without cleaning the modules. Based on *I-V* and power measurements, we identified the best, medium and worst performing strings. Once these three strings were selected, we cleaned all the PV modules in these three selected strings. We performed *I-V* measurements of the selected strings after cleaning as well. We then chose three or four PV modules from the beginning (or positive end), three or four PV modules from the middle, and last three or four PV modules from the end (or negative end) of each of the selected three strings. Finally we performed all the detailed characterization on these selected PV modules. If the SCADA data was not available, we found out from the site engineers which they considered the best and worst performing inverters, and then proceeded further as described above.

For the 17 repeat sites, we used the same modules as in earlier Surveys, as this would enable us to estimate year-on-year degradation rates. In addition, at some of the repeat sites, we surveyed some more (new) modules, for which we selected a random inverter, and then used the subsequent procedure as described above.

Another innovation employed in the 2018 Survey at one of the sites was to use drone-based IR imaging, followed by a correlation of the drone image with the actual ground performance of the modules. This methodology has the potential advantage of first identifying mal-performing modules (in terms of their IR image) out of a very large number, and then checking the reasons for this by detailed on-ground measurements.

The methods and protocols used on individual modules in the 2018 Survey were broadly similar to those used in 2016, with some differences. The protocol is repeated here for completeness. An extensive array of characterization tools was taken to the field for detailed inspection of the modules, as shown in Table 1.1.

The first activity on reaching the site was to collect dust samples from the top of a few modules for further analysis later in the laboratory for a parallel soiling study. After choosing the strings and modules as described above, and after cleaning the modules, we first did infrared (IR) thermography without disconnecting the system. The system was then disconnected, and visual inspection, illuminated *I-V*, short-circuited IR thermography, and Insulation resistance test were performed. All of the above tests were conducted in daylight with high solar irradiance. Electroluminescence (EL) imaging was performed on selected set of modules (more than 50% of the total number) in the late afternoon and early evening, using a special low-cost EL camera augmented with a quad-pod. It was followed by dark IR measurements. The methodology of the various tests is briefly explained below.

Table 1.1. Equipment Specifications

| Instrument | Make & Model No. | Specifications |
|---|---|---|
| *I-V* Tracer | Solmetric PVA-1000S | Voltage Range (& Accuracy) : 0-1000 V DC, (+/-0.5% +/-0.25V)<br>Current Range (& Accuracy) : 0-20 A DC, (+/-0.5% +/-40mA)<br>Irradiance Sensor Range & accuracy: 0-1500 W/sq.m., (+/-2%) |
| Infrared Camera | FLIR E60 | Temperature Range : -20 $^oC$ to 650 $^oC$<br>Thermal Sensitivity : <0.05 $^oC$ at 30 $^oC$<br>Detector Type (& size) : Uncooled Microbolometer, 320 x 240 Pixels |
| Electroluminescence Camera | Modified SONY camera | No. of Pixels (& pixel size) : 20.1MPixel<br>Sensor Technology: CMOS |
| Insulation Resistance Tester | FLUKE 1550C | Insulation test voltage : 250 V / 500 V / 1000 V / 2500 V / 5000 V<br>Leakage current measurement range : 1 nA – 2 mA |
| DC Power Supply | GWInstek PSW 160-14.4 | Rated Output Voltage: 160 V dc<br>Rated Output Current: 14.4 A dc |
| Digital camera | Nikon D3200 | Effective Pixels : 24.2 Million<br>Image sensor : 23.2 x 15.4 mm CMOS sensor |
| Shading Analyzer | Solar Pathfinder | NA |

### *a) Visual Inspection*

Visual inspection of the modules was done to record the physical degradation visible in various parts of the module. A visual inspection checklist, which is a slightly modified and enhanced version of the NREL Visual Inspection Checklist [35], was filled up. Images of the modules were taken using a high resolution camera. The high resolution images enable us to magnify the region of interest in the captured image to get a better view of the defect zone. A sample checklist sheet is given in Appendix A.

### *b) Current-voltage (I-V) Measurement under illumination*

The current-voltage (*I-V*) characteristic is the most important diagnostic tool for determining the electrical performance of a PV module [36]. Two sets of portable *I-V* tracers, which were cross-calibrated before starting the survey, were used in the survey, enabling us to collect data of multiple PV modules in parallel. Both the tracers had additional accessories for measurement of the Plane of Array (POA) global solar irradiance and module temperature. The POA was also measured by using a reference PV module (mini-module) of the same technology (for mono c-Si, multi c-Si) of the tested PV modules at the particular site. Along with these two, we also measured POA with a pyranometer. At least 5 sets of *I-V* readings were taken for each module, at intervals of about 1 minute. The ambient temperature and relative humidity were also recorded at the time of *I-V* measurement, which would aid in the spectral correction during STC translation of the field data [37], if required.

### *c) Infrared Thermography under Illumination*

Infrared (IR) images enable us to detect hot spots in the module which can degrade the module performance significantly [38]. IR images were taken from the backside of the module. One set of IR images were taken at MPPT, before disconnecting the system and a second set of IR images were taken after disconnecting the system and short circuiting individual PV modules. These images were taken only when the irradiance is above 700 W/m$^2$, so as to enable proper detection of hot spots.

Through drone-based IR imaging one can identify PV modules with hot spots over large areas of the site. This was done at three sites. However, the detailed ground-based measurements on the corresponding modules which showed the presence of hot spots were performed only on one site. Therefore, data (drone based and ground based IR images) corresponding to that site are discussed in this report.

### *d) Insulation Resistance Measurement*

Insulation resistance is an important measure of the quality of insulating materials used in the module, like the encapsulant and backsheet [39]. Low values of insulation resistance can be a cause several issues such as ground faults, electrical hazard and fire hazard etc. The test we performed for measurement of Insulation resistance (Wet and Dry) of the PV module is not compliance with actual IEC 61215 standard, so we did not include the results of this test in this report

### *e) Electroluminescence Imaging*

Electroluminescence (EL) imaging of modules is an important diagnostic tool that provides information about the extent and nature of cracks and various other defects like interconnect failures, PID, and current crowding effects in the solar cells [40]. Based on our positive experience in the 2016 Survey, we used our low-cost standard DSLR camera having a silicon CMOS sensor, suitably modified to take good EL images, to capture the luminescence emitted by the selected PV module, when forward biased to carry the rated short circuit current using a DC power supply. By using two such cameras, we were able to take considerably more EL images in the 2018 Survey. An image difference technique, developed in-house at IIT Bombay specifically for such field Surveys, was utilized to capture the EL images in the late afternoon hours under low irradiance conditions in the field. This technique takes the difference of two images of the module captured by the camera – one taken with, and another without, forward biasing the module [41]. The EL images are later analyzed to calculate statistics of various types of defects observed in modules.

### *f) Dark IR Measurement*

Dark IR imaging was done in the evening hours by covering the selected module. The module was forward biased at its rated short circuit current, and it was allowed to heat up for about 1 minute before taking the image using the infrared camera. The image was usually taken from the back side of the module, unless the installation structure prevented access to its back side.

## 1.4 Climatic Zones of India

The National Building Code of India [42] divides India into 5 climatic zones based on average annual temperature and humidity – Hot & Dry, Warm & Humid, Composite, Temperate and Cold. However, as argued in our 2014 report [4], it is better to use the six-zone classification system of Bansal and Minke [43], the criteria for which are described in Table 1.2.

Table 1.2. Climatic Zone Classification criteria as per Bansal and Minke [43]

| Climate | Mean Monthly Temperature (deg. C) | Mean Relative Humidity (%) |
|---|---|---|
| Hot & Dry | >30 | <55 |
| Warm & Humid | >30 | >55 |
| Moderate | 25 – 30 | <75 |
| Cold & Cloudy | <25 | >55 |
| Cold & Sunny | <25 | <55 |
| Composite | This applies when six months or more do not fall within any of above categories | |

As per the six-zone classification, the coastal areas of India (like Mumbai, Chennai and Kolkata) fall in the Warm & Humid zone, whereas some central parts of India (Hyderabad and Delhi) fall in Composite zone. Places in the central western part of India like Jaipur, Jodhpur, Jaisalmer and Charanka lie in the Hot & Dry zone. Bangalore falls in the Moderate climatic zone. Sites in Ladakh fall in the Cold & Sunny climatic zone, whereas sites in Jammu, Kashmir Valley and Himachal Pradesh experience Cold & Cloudy climate. The various climatic zones in India have been shown in Fig. 1.1, along with the sites where the 2018 Survey has been conducted (in black dots). As evident from the figure, five of the six zones have been covered in this Survey (we did not have any sites in the Cold & Cloudy zone). The number of sites (refer to Table 1.3) is not quite evenly distributed, with many sites falling in the Hot & Dry, Warm & Humid and Composite zones, but nevertheless there are enough modules in the five zones to gauge climatic variations. Further, it has been found (in 2014 and 2016, and again in 2018) that many aspects of module degradation are similar between the 'Hot' zones, that is, Hot & Dry, Warm & Humid and Composite zones. Similarly, the cooler ('Non-Hot') climates, namely Moderate, Cold & Cloudy and Cold & Sunny zones also have similar kind of module degradation. Hence the six climatic zones will sometimes be classified into Hot and Non-Hot zones for the sake of analysis wherever found necessary.

Table 1.3. Survey site and PV module statistics based on six zone climatic classification

| Climatic Zone | No. of Sites | No. of PV Modules |
|---|---|---|
| Hot & Dry | 12 | 498 |
| Warm & Humid | 9 | 272 |
| Composite | 11 | 329 |
| Moderate | 1 | 25 |
| Cold & Sunny | 3 | 75 |
| Cold & Cloudy | 0 | 0 |

While the six-climate classification of Bansal and Minke is being used for the analysis of the 2018 Survey data, we have provided some of the important climate-dependent analysis also in terms of the internationally accepted Koppen-Geiger climate classification system, in Appendix B.

In any case, neither the Bansal-Minke nor the Koppen-Geiger climate classifications are well-suited for photovoltaic performance and degradation. Attempts are under way to come up with more relevant classification schemed, which may be used in future Surveys [44].

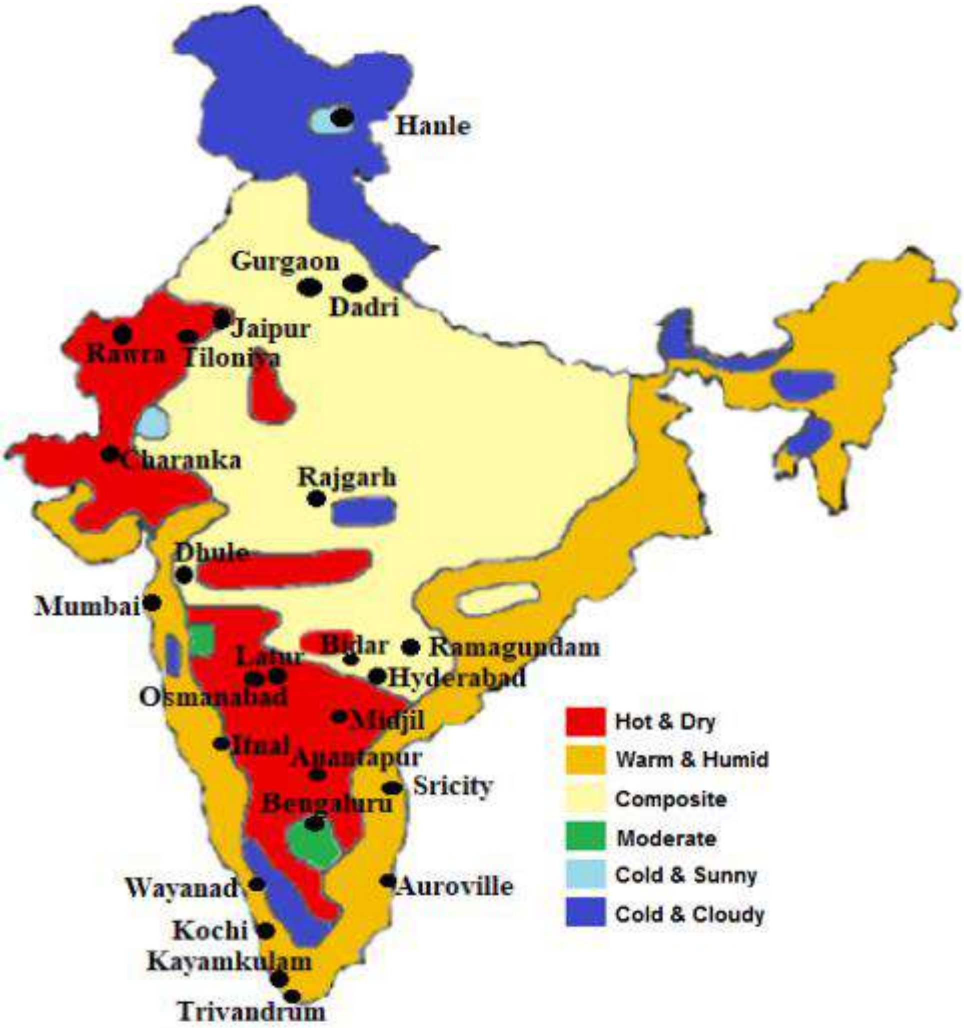


Fig. 1.1. Climatic Zones of India as per Bansal and Minke [43]. The black dots represent the sites visited in the 2018 Survey.

## 1.5 Summary

This chapter has given an overview of All-India Survey of PV Module Reliability undertaken in 2018, together with a brief review of some relevant literature. The survey methodology, types of inspections and measurements undertaken, and the details of the equipment used in the field have been described. Since India has a variety of climatic zones, from extremely hot climates in Rajasthan to cold climates in Ladakh, the six-zone climatic classification of India has been described. Before going into the analysis of the survey data, it is important to understand the distribution of the data, in terms of the age, technology, type of mounting, and various other aspects. The following chapter discusses some of these vital statistics related to the 2018 Survey.

# 2. Information on PV Modules Surveyed

## 2.1 Introduction

This chapter focuses on the statistics of different sites and PV modules inspected. The inspected sites include both large and small/medium scale systems which are installed on different mounting structures like Ground Rack, Roof Rack, and Floating. The inspected sites also contain modules of various technologies, and furthermore, they are located in five different climatic zones of India. The sites also belong to different Age categories.

## 2.2 Statistics of Sites Surveyed

In the 2018 edition of the All-India Survey of PV Module Reliability, we have surveyed 40 different sites, but of these 4 sites were not considered for analysis as they are very new (less than one-year-old), in order to avoid excessive uncertainties due to LID etc. while calculating the degradation rates. Thus, a total of 36 sites were considered for the analysis, out of which 27 sites (75%) belong to large scale installations (> 100 KW), and 9 sites (25%) belong to small/medium scale installations. The selection of sites reflects the current scenario of installations across India, where significant amount of large (utility) scale PV plants are being installed in recent years. Note that this is a change from the 2016 and earlier Surveys, where many more small/medium sites were surveyed. Fig. 2.1 shows the total analysed sites of different capacity in the 2018 Survey.

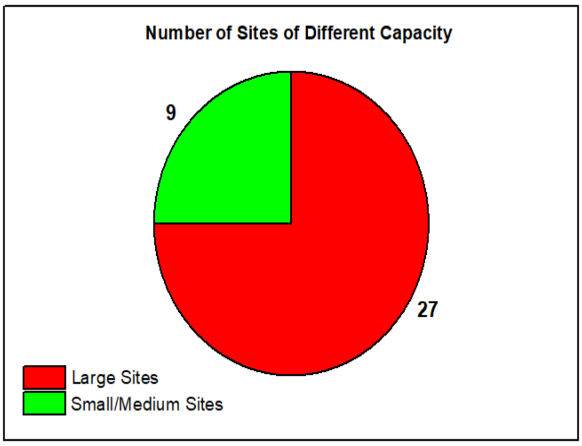


Fig. 2.1. Sites of Different Capacity (Size)

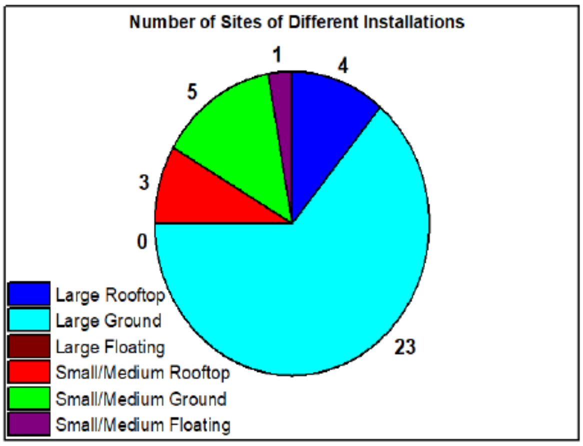


Fig. 2.2. Sites based on Type of Installation

Fig. 2.2 shows the distribution of sites based on the type of installation. Out of the 36 sites we analysed, 23 sites belong to large ground rack-mounted installations, 4 belong to large roof rack-mounted, 5 belong to small/medium ground rack-mounted, 3 belong to small/medium roof rack-mounted, and 1 site is a small/medium floating installation (this is the first time we have inspected a floating PV plant in our All-India Surveys.)

## 2.3 Statistics of PV Modules Inspected

The statistics of PV modules surveyed in All-India Survey of PV Module Reliability 2018 are shown in Fig 2.3 to Fig 2.10. Fig. 2.3 shows the number of PV modules inspected in large sites and small/medium sites. Out of a total of 1199 PV modules inspected in this Survey, 975 (81.3%) are from large PV installations, and 224 (18.7%) are from small/medium PV installations. Fig. 2.4 shows the number of PV modules of different technologies inspected, and out of 1199 PV modules, a majority (1094) belong to c-Si technologies, and 105 belong to thin film technologies. Out of 1094 c-Si technology PV modules, 186 belong to mono c-Si, 874 belong to multi c-Si, 23 belong to HIT, and 11 belong to IBC technologies. It can be seen that the major share is of multi c-Si technology, which reflects well the current scenario of installations in the country. Out of 105 thin film PV modules inspected, 75 are CdTe, 21 are a-Si, and 9 are CIGS.

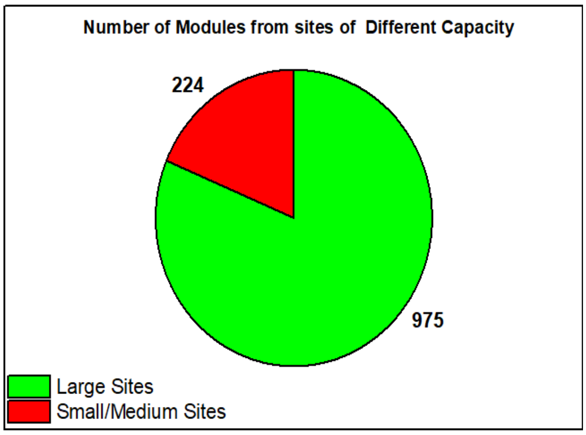


Fig. 2.3. PV modules from large and small/medium sites

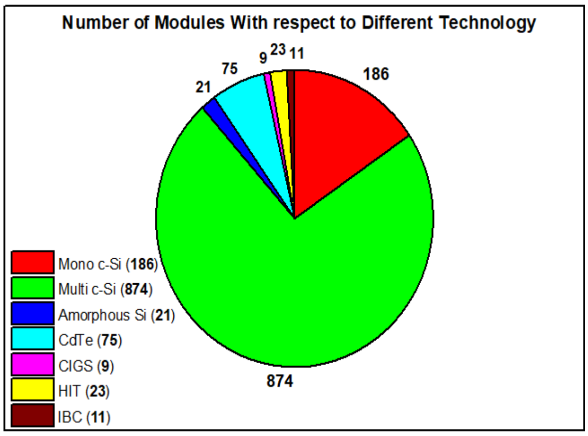


Fig. 2.4. PV modules of different technologies

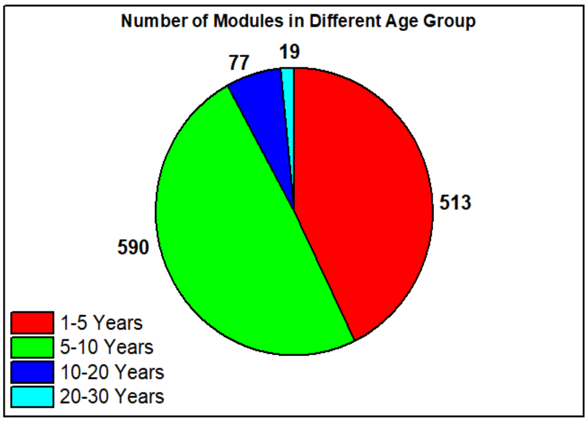


Fig. 2.5. Age distribution of PV modules

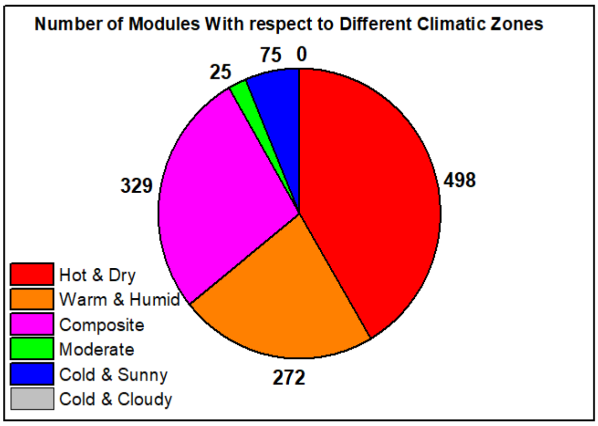


Fig. 2.6. PV modules from different climatic zones

Fig. 2.5 shows the distribution of PV modules from the 2018 All-India Survey with respect to their age. It is seen that most of the modules lie in the 1-5 year and 5-10 year categories, though there are some which are more than 20 years old. Fig 2.6 shows the distribution of the PV modules in different climatic zones across the country. We have the PV modules from 5 climatic zones (Hot & Dry, Warm

& Humid, Composite, Moderate, and Cold & Sunny) out of the 6 climatic zone classification of India [43] (we did not have any modules from the Cold & Cloudy climatic zone). Out of all the analysed PV modules, 498 (41.5%) are from Hot & Dry, 272 (22.7%) are from Warm & Humid, 329 (27.4%) are from Composite, 25 (2.1%) are from Moderate, and 75 (6.3%) are from Cold & Sunny climatic zones. The PV modules for each climatic zone are sufficient in number to draw reasonable statistical conclusions, except the Moderate climatic zone, in which only 25 modules were analysed.

Fig. 2.7 shows the power rating distribution of the PV modules. It is seen that a majority (843 out of 1199) lie in the 201-300 Wp range. Fig. 2.8 shows the PV modules with different packaging types. Out of the 1199 modules, 1094 (91.2%) have Glass-Polymer packaging, 96 (8%) have Glass-Glass packaging, and 9 (0.75%) have Glass-Metal type of packaging.

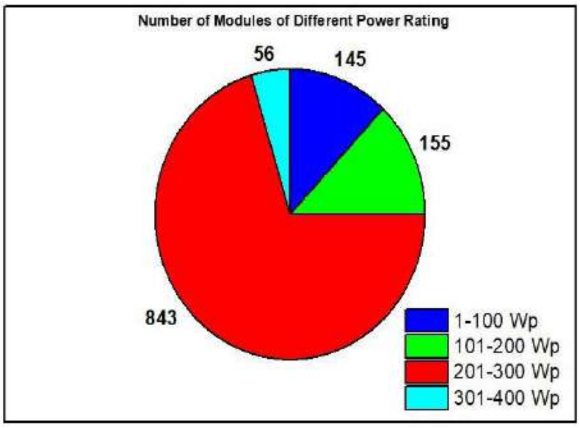


Fig. 2.7. PV modules with different power ratings

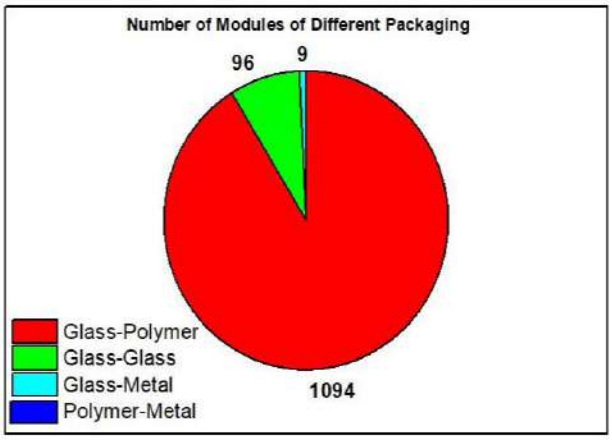


Fig. 2.8. PV modules with different packaging

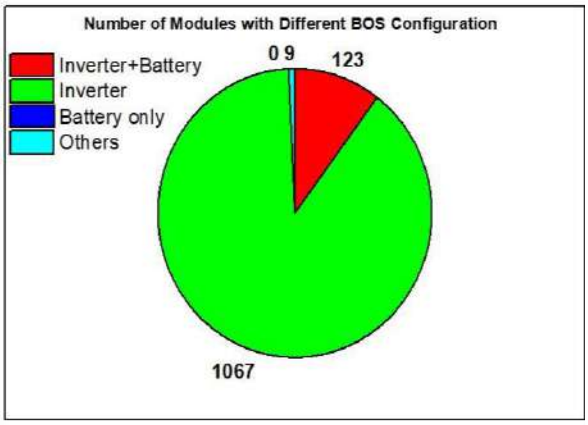


Fig. 2.9. PV modules with different Balance of System configuration

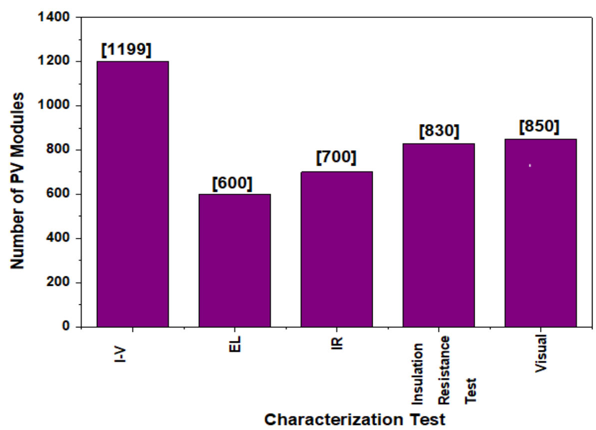


Fig. 2.10. Number of PV modules subjected to different Characterization Tests

Fig. 2.9 shows the Balance of System (BOS) configurations, and it is seen that a majority of them (1064 modules, or 88.7% of the total) are connected to Inverter, 123 (10.3%) are connected to both Inverter and Battery and 9 (0.75%) of them are left open due to some reasons. Finally, Fig. 2.10

shows the number of different performance characterization tests performed on the PV modules during the 2018 All-India Survey. Current-Voltage (*I-V*) measurements were performed on all 1199 PV modules, whereas Infrared Imaging (IR) was performed on 700 PV modules, Electroluminescence (EL) Imaging was performed on 700 PV modules, Visual Inspection was performed on 850 PV modules, and Insulation Resistance test were performed on 830 PV modules. One notable difference compared to earlier Surveys was that EL imaging was performed on half of total number of modules.

## 2.4 Summary

In this chapter we have provided the statistical distribution of all the PV sites and modules analysed in the All-India Survey of PV Module Reliability 2018, with respect to different Size, Climatic Zones, Age, Type of Mounting, Technology, etc. In most of the cases we have a statistically significant number of PV modules to deduce reasonable conclusions. Two significant differences of the 2018 Survey compared to earlier ones were (1) the increased number of large size (typically > 1 MW) installations, many of which were of a young age, and (2) a smaller number of roof-mounted systems. These differences reflected the changing patterns of PV installations in India. Another difference was that EL images were taken on many more modules, and this constitutes perhaps the most comprehensive EL study of fielded PV modules. In the next chapters, we will discuss the detailed Electrical, Thermal, Electroluminescence, and Visual analysis of the data, and correlating these with the degradation rates and reliability.

# 3. Correction Procedures and Statistical Methods Applied to Survey Data

## 3.1 Introduction

The Current-Voltage (*I-V*) measurements of PV modules were performed at different irradiance and temperature conditions in the field during the All-India Survey of PV Module Reliability 2018. To compare the present performance of a PV module with the initial performance, the measured *I-V* curves should be translated to the Standard Test Conditions (STC), namely, 1000 W/m$^2$ irradiance with AM 1.5G spectrum and 25 $^0$C module temperature. International Electrotechnical Committee (IEC) has proposed three correction procedures to translate the measured data to any other condition, including STC [45]. Along with the IEC translation procedures, there exist some other translation procedures in the literature, like the Anderson procedure [46], and the Standard Irradiance and Desired Temperature (SIDT) procedure [47]. In this chapter, we discuss the procedure that we have chosen and the simulation study we have done to justify the selection of this procedure. We also discuss the errors associated with the translation, measurement, and nameplate. The templates of the graphs that we have used throughout the report and the notations used in those graphs are also discussed in this chapter. Finally, this chapter ends with the statistical method we applied to determine the outliers and selection of mean versus median to represent statistical significance for the data that we have plotted.

## 3.2 IEC 60891 Correction Procedure

The IEC 60891 standard has three procedures to convert the measured *I-V* data of solar PV devices from different irradiance and temperature conditions to the STC (1000 W/m$^2$, 25 $^0$C) condition. All the three procedures are based on entire curve translation. The first procedure IEC 60891 Procedure 1 consists of two equations, one for translating the currents and the other for translating the voltages. It is suggested that the measured irradiance conditions should be within ± 20% to the STC irradiance, in order to reduce the translation error. The second procedure IEC 60891 Procedure 2 consists of an alternative algebraic method, but it can be used for more accurate conversion of the *I-V* curves measured at irradiances with a margin greater than ± 20% to STC. In both these procedures, the correction parameters must be determined prior to the correction. The third procedure IEC 60891 Procedure 3 is an interpolation based procedure and it does not require any correction parameters. All the three IEC 60891 correction procedures were comprehensively reviewed in the report of All-India Survey of Photovoltaic Module Degradation 2013 [3], and the interested readers can refer to that report.

The IEC 60891 correction Procedure 1 requires four correction parameters for translating the entire *I-V* curve. These are: $\alpha$ (temperature coefficient for short circuit current), $\beta$ (temperature coefficient for open circuit voltage), $R_s$ (internal series resistance of the test specimen) and $K$ (curve correction factor). It is recommended to use all four parameters for better accuracy. Obtaining the values of $R_s$ and $K$ requires *I-V* measurements at three different irradiance and temperature values, which is difficult in field where conditions are largely uncontrolled and high throughput is desired. In previous Surveys, we have used a modified procedure, which we call IEC 60891-1a or Modified IEC 60891 Procedure 1. In this modification, we use only two parameters i.e. $\alpha$ (temperature coefficient for short circuit current) and $\beta$ (temperature coefficient for open circuit voltage) while keeping $R_s$ and $K$ equal to zero. This was shown to give fairly good accuracy in translation [4]

## 3.3 Standard Irradiance and Desired Temperature (SIDT) Correction Procedure

Recently Singh *et al.* have proposed an STC correction procedure especially suitable for the field measured *I-V* data called the Standard Irradiance and Desired Temperature method (SIDT) [47]. This is basically a point translation procedure in which only the Short Circuit Current ($I_{sc}$), Open Circuit Voltage ($V_{oc}$), and Maximum Power ($P_{max}$) will be translated to STC conditions. SIDT is a two-step procedure: in the first step, the measured currents, and voltages will be corrected to the Standard Irradiance (1000 W/m$^2$), and in the second step, only the above mentioned three points will be corrected to the Desired Temperature of 25 $^0$C. The equations of this procedure are following:

Step 1: Correction for Irradiance

$$V_{SIDT} = V_{Measured} \qquad \ldots\ldots\ldots (3.1)$$

$$I_{SIDT} = \frac{I_{Measured}}{G_{Measured}} \times 1000 \qquad \ldots\ldots\ldots (3.2)$$

Step 2: Correction for Temperature

$$X_{STC} = X_{SIDT} + \Phi(25 - T_{Module}) \qquad \ldots\ldots\ldots (3.3)$$

Where $X$ is the required (current/voltage/power) parameter, and $\Phi$ is the temperature coefficient of that parameter.

In the next section, we explain the correction procedure that we have used and the simulation study we have performed which provides the basis for the choice.

## 3.4 Selection of Appropriate STC correction Procedure for Survey Data

It is crucial to choose a STC correction procedure which provides the least translation error, reasonable throughput and is practically feasible during All-India Surveys. For this purpose, we have performed a simulation study by comparing three STC correction procedures: IEC 60891 Procedure 1, Modified IEC 60891 Procedure 1 [48] which was used on the data of previous All-India Surveys, and SIDT procedure. The translational equations of IEC 60891 Procedure 1 and Modified IEC 60891 Procedure 1 are as follows.

**IEC 60891 Procedure 1:**

$$I_2 = I_1 + I_{SC} * \left(\frac{G_2}{G_1} - 1\right) + \alpha * (T_2 - T_1) \qquad \ldots\ldots\ldots (3.4)$$

$$V_2 = V_1 - R_S * (I_2 - I_1) - K * I_2 * (T_2 - T_1) + \beta * (T_2 - T_1) \qquad \ldots\ldots\ldots (3.5)$$

**Modified IEC 60891 Procedure 1:** This procedure is very similar to the IEC 60891 Procedure 1, except considers $\mathrm{R_S}$ and K as zero. The conversion equations of this procedure are as follows.

$$I_2 = I_1 + I_{SC} * \left(\frac{G_2}{G_1} - 1\right) + \alpha * (T_2 - T_1) \qquad \ldots\ldots\ldots (3.6)$$

$$V_2 = V_1 + \beta * (T_2 - T_1) \qquad \text{.........} (3.7)$$

The translational equations for the SIDT procedure were already mentioned in Section 3.3. We have considered datasheets of five different PV modules for the simulation study that we have performed to compare translation error produced by the above mentioned three STC correction procedures. Out of these, four PV modules were among those surveyed in the All-India Survey 2018, and one is a commercial PV module from a leading manufacturer. In this simulation study, we generated *I-V* curves at different irradiances (ranging from 600 W/m$^2$ to 1300 W/m$^2$, with a step of 100 W/m$^2$) and temperatures (20 $^0$C to 80 $^0$C, with a step of 5 $^0$C) using some of the standard equations available in literature [49], [50], [51] based on single diode model of a PV module. The set of equations we have used for generating *I-V* curves were named as Method 1 (as we tested different sets of equations, but reporting the results with the best set (Method 1)). The generated *I-V* curves were given as inputs for all the three STC correction procedures, and the normalized error in maximum power ($P_{max}$) was compared. Fig. 3.1 shows the contour plots of the normalized error in $P_{max}$ for IEC 60891 Procedure 1, Fig.3.2 shows the contour plot of normalized error in $P_{max}$ for Modified IEC 60891 Procedure 1 and Fig.3.3 shows the contour plot of normalized error in $P_{max}$ for SIDT Procedure and for all the three procedures the input data sets generated from Method 1 were given.

Out of the above three STC correction procedures, IEC 60891 Procedure 1 gives the least normalized error in the maximum power for the entire range of temperature and irradiances considered for the five PV modules used in this simulation study. However, as mentioned earlier, this procedure requires us to estimate series resistance ($R_S$) and curve correction factor ($K$), which is difficult to do in our Survey, where lots of modules need to be surveyed in a span of 80 days across the county. The Modified IEC 60891 Procedure 1 was found to be more sensitive to irradiance than temperature and it produces a high value of error compared to IEC 60891 Procedure 1 due to the assumption of $R_S$, $K$ being zero. However, it produces a lower normalized error in maximum power compared to the SIDT correction procedure in the range of temperature (50 $^0$C to 70 $^0$C) and irradiance (700W/m$^2$ to 1000 W/m$^2$) conditions that correspond to those typically observed in the All-India Survey. The SIDT correction procedure performs relatively better at lower (< 700 W/m$^2$) and higher (> 1000 W/m$^2$) irradiance conditions compared to Modified IEC 60891 Procedure 1. One more interesting finding is that SIDT procedure predicts a slightly higher power after conversion than IEC 60891 Procedure 1 and Modified IEC 60891 Procedure 1, and it is more sensitive to temperature than irradiance. Fig.3.4 shows the normalized error in $P_{max}$ with respect to the irradiance for all the three procedures at 55 $^0$C temperature, Fig.3.5 shows the normalized error in $P_{max}$ with respect to the irradiance for all the three procedures at 65 $^0$C temperature and Fig.3.6 shows the normalized error in $P_{max}$ with respect to the irradiance for all the three procedures at 75 $^0$C temperature. We can observe in all these figures the SIDT procedure estimates higher power, IEC 60891 Procedure 1 estimates the power with lowest normalized error, and Modified IEC 60891 Procedure 1 estimates power with lower normalized error compared to SIDT in the irradiance range of 700W/m$^2$ to 1000 W/m$^2$.

As most of our All-India Survey data falls in the range of irradiation (700W/m$^2$ to 1000 W/m$^2$) and temperature (50 $^0$C to 70 $^0$C), we decided to use the Modified IEC 60891 Procedure 1, rather than SIDT. This happens to be the same procedure that was used in the last three All-India Surveys that took place in 2013, 2014, and 2016. However, it should be noted that the Modified IEC 60891 Procedure 1 estimates higher Open Circuit Voltage ($V_{oc}$) and lower Fill Factor ($FF$) than SIDT procedure, which causes a higher normalized error estimation of these parameters. These observations are important while understanding some of the plots that we will show in the coming chapters of this report.

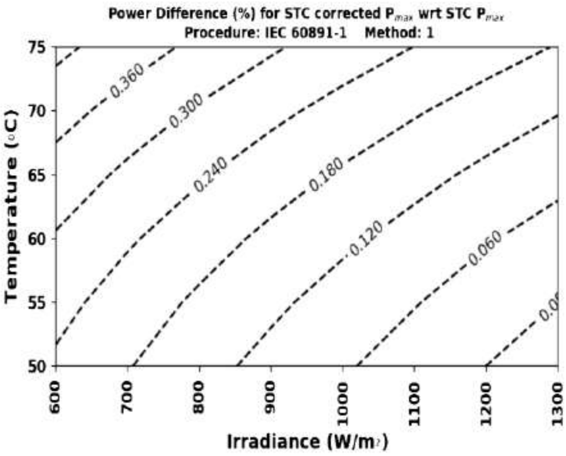


Fig. 3.1. Contour plot of normalized error in $P_{max}$ for IEC 60891 Procedure 1

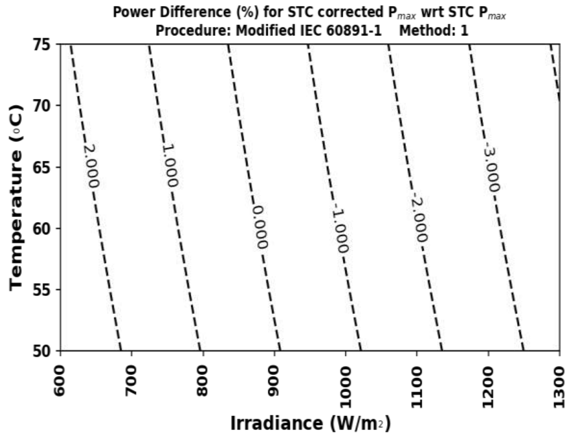


Fig. 3.2. Contour plot of normalized error in $P_{max}$ for Modified IEC 60891 Procedure 1

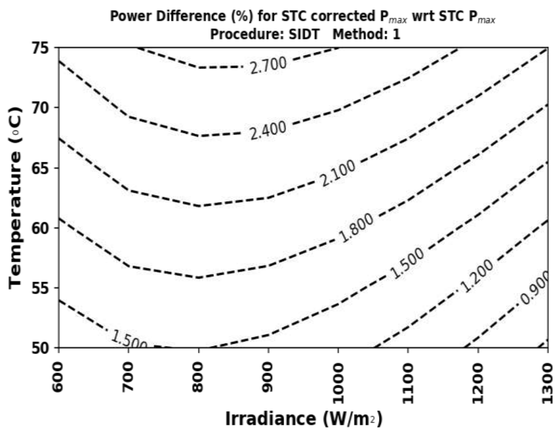


Fig. 3.3. Contour plot of normalized error in $P_{max}$ for SIDT procedure

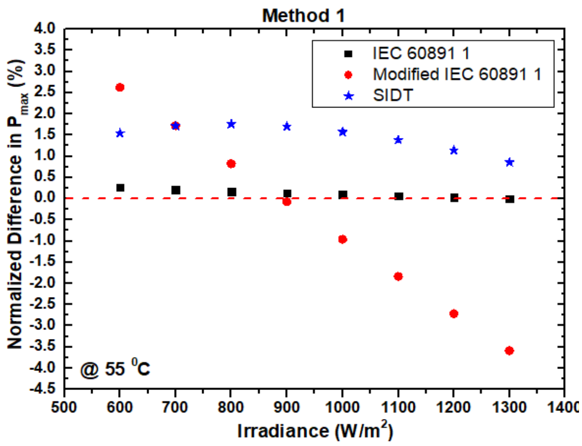


Fig. 3.4. Comparison of normalized error in $P_{max}$ for all three procedures at 55 $^0$C

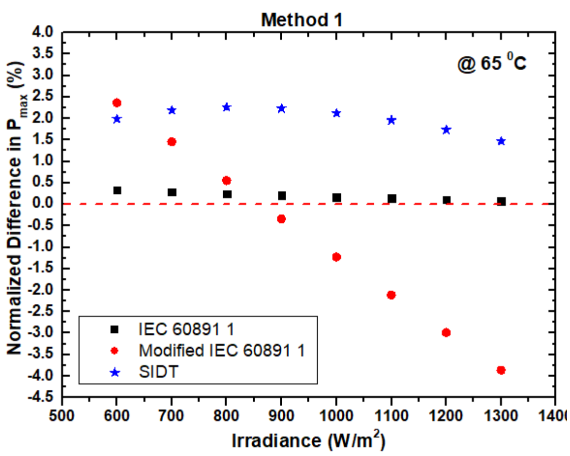


Fig. 3.5. Comparison of normalized error in $P_{max}$ for all three procedures at 65 $^0$C

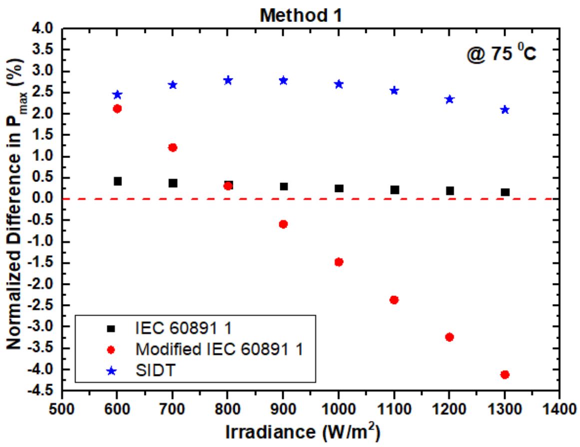


Fig. 3.6. Comparison of normalized error in $P_{max}$ for all three procedures at 75 $^0$C

## 3.4.1 Modified IEC 60891 Procedure 1 for STC correction

As discussed in the previous part of this section, Modified IEC 60891 Procedure 1 considers the Series Resistance ($R_S$) and Curve Correction factor ($K$) to be zero. In Eq. 3.6 and Eq. 3.7, $G_1$ represents the irradiance at measured condition, $G_2$ represents the irradiance at the conditions to be translated, at STC it is 1000 W/m$^2$, $V_1$ represents measured voltage of PV module, $V_2$ represents voltage at translated condition, $I_1$ represents measured current of PV module, $I_2$ represents current at translated condition, $T_1$ represents measured PV module temperature, $T_2$ represents the temperature at the conditions to be translated (at STC it is 25 $^0$C), $\alpha$ represents the current temperature coefficient in A/$^0$C, and $\beta$ represents the voltage temperature coefficient in V/$^0$C. The temperature coefficients that we considered for this 2018 Survey PV modules are from the data sheet of the manufacturer and not the field measured values.

We have used the Eq. 3.6 and Eq. 3.7 for the STC correction of field measured *I-V* curves and automated the entire process by writing a MATLAB code. As we already mentioned this procedure estimates higher $V_{oc}$, and lower *FF* values compared to IEC 60891 Procedure 1 and SIDT, but gives good values for $P_{max}$.

## 3.4.2 Low Irradiance/High Temperature Correction

The IEC the standard 60891 Procedure 1 is recommended to be used for an irradiance variation of ± 20%, so for STC translation, the *I-V* curves should be measured within the range of 800 to 1200 W/m$^2$. We planned our All-India Survey in the early summer months of March to May of 2018 to meet those irradiance conditions. Nonetheless, we do have a few PV module *I-V* curves that were measured at irradiances as low as 600 W/m$^2$. But based on our experimental study on some sample PV modules in the laboratory [4], the translational error will be within ± 4% down to the irradiance condition of 700 W/m$^2$ and a temperature as high as 70 $^0$C, as shown in Table 3.1. So we have only considered the PV modules for analysis which are measured at an irradiance condition of greater than or equal to 700 W/m$^2$ (others were simply discarded).

Table 3.1. Error in translation of $P_{max}$ to STC using Modified IEC 60891 Procedure 1

| **Δ$P_{max}$ (%)** | **Module Temperature (Deg. C)** | | | | | | | | | |
|---|---|---|---|---|---|---|---|---|---|---|
| **Irradiance (W/m$^2$)** | **25** | **30** | **35** | **40** | **45** | **50** | **55** | **60** | **65** | **70** |
| **500** | 4.59 | 4.12 | 4.05 | 4.10 | 4.37 | 4.59 | 4.90 | 5.08 | 5.41 | 5.91 |
| **550** | 4.09 | 3.58 | 3.48 | 3.51 | 3.74 | 3.93 | 4.22 | 4.37 | 4.69 | 5.17 |
| **600** | 3.69 | 3.17 | 3.03 | 3.07 | 3.25 | 3.37 | 3.65 | 3.78 | 4.07 | 4.51 |
| **650** | 3.08 | 2.61 | 1.78 | 1.57 | 1.38 | 1.29 | 1.20 | 1.07 | 0.94 | 0.84 |
| **700** | 2.62 | 2.16 | 1.30 | 1.04 | 0.82 | 0.72 | 0.60 | 0.44 | 0.27 | 0.16 |
| **750** | 2.22 | 1.72 | 0.82 | 0.52 | 0.28 | 0.13 | -0.01 | -0.19 | -0.39 | -0.51 |
| **800** | 1.70 | 1.18 | 0.96 | 0.94 | 1.03 | 1.19 | 1.25 | 1.32 | 1.00 | 1.28 |
| **850** | 1.25 | 0.72 | 0.44 | 0.39 | 0.49 | 0.60 | 0.63 | 0.66 | 0.35 | 0.40 |
| **900** | 0.86 | 0.29 | 0.00 | -0.07 | -0.03 | 0.07 | 0.07 | 0.07 | -0.29 | -0.28 |
| **950** | 0.37 | -0.37 | -0.94 | -1.24 | -1.56 | -1.67 | -2.00 | -2.47 | -2.73 | -2.90 |
| **1000** | 0.00 | -0.60 | -1.40 | -1.75 | -2.10 | -2.24 | -2.59 | -3.08 | -3.36 | -3.58 |

The shaded cells in the table indicate that the irradiance and temperature conditions that were *not* encountered in the All-India Survey 2018. Most of the modules that we surveyed fall in the range of 700 W/m$^2$ to 1000 W/m$^2$ (few were measured at an irradiance greater than 1000 W/m$^2$) and 50 $^0$C to 70 $^0$C. This means that the maximum translation errors for power that we expect are +1.32/-3.58 percent. The simulation study we performed was only used to select the STC translation procedure for our analysis, but the errors that were obtained from that study yet to be experimentally validated. The translational errors presented in Table 3.1 are from the experiment conducted on a single PV module immediately after 2014 All-India Survey.

## 3.5 Definition of Degradation Rate

In order to calculate the amount of degradation that the PV module has suffered, we should compare the present performance parameter (translated to STC) with the initial values measured at STC. However, in most cases of fielded modules, it is not possible to get the actual measured initial data of each PV module, so we considered the data sheet or nameplate values as the initial values of the PV modules that we analysed. We have used two degradation rates similar to those used in the 2016 survey report [5]: the 'overall degradation rate' (sometimes just called the 'degradation rate'), and the 'linear degradation rate'. The calculation of linear degradation rate was introduced to account for the high degradation of PV modules seen in the initial period after installation due to Light-Induced Degradation (LID) or other effects. The linear degradation rate is especially important to compare degradation of younger and older modules, as it discounts the effect of the initial rapid decrease in power. The formulas for the two degradation rates are given below.

$$(Overall)\ Degradation\ Rate\ \left(\frac{\%}{Year}\right) = \frac{\left(P_{max,nominal} - P_{max,present}\right)}{P_{max,nominal} \times Module\ Age} \times 100 \qquad \ldots\ldots.\ldots (3.8)$$

The initial $P_{max,\ nominal}$ is the 'nominal' value and it was calculated by considering the tolerance along with the actual value mentioned on the nameplate or in the datasheet of PV module. Generally, the tolerance values will be either ±X% or –0%, and +X% of the actual mentioned power. The $P_{max,\ nominal}$ for a PV module is calculated by the formula given below.

$$P_{max,nominal}(W) = \frac{P_{mp,maximum} + P_{mp,minimum}}{2} \qquad \ldots\ldots\ldots (3.9)$$

For a module with ±X% tolerance, the $P_{max,\ nominal}$ will be the same as the mentioned nameplate value, but, for example, for a 100 W nameplate power and –0%/+5% tolerance, the $P_{max,\ nominal}$ would be 102.5 W.

For the calculation of linear degradation rate, we have discounted 2% from the initial calculated nominal power or $P_{max,\ nominal}$ after referring to available literature and from PV Syst software (this 2% drop is assumed to occur within a very short time of installation). For the module mentioned above the initial LID discounted nominal power would be 100.45 W. The formula for linear degradation rate is as given below.

$$Liner\ Degradation\ Rate\ \left(\frac{\%}{Year}\right) = \frac{\left(P_{mp\ LID\_Discounted} - P_{mp,present}\right)}{P_{mp,LID\_Discounted} \times Module\ Age} \times 100 \qquad \ldots\ldots\ldots (3.10)$$

Fig. 3.7 shows graphically the calculation of linear degradation rate for a PV module of 15 years age. As can be readily appreciated, for young modules, the (overall) degradation rate would greatly over-estimate the long-term (linear) degradation rate, whereas for old modules, there would be little difference. This is particularly important for our Survey, where we have many young modules, and furthermore, we wish to compare the performance of young and old modules.

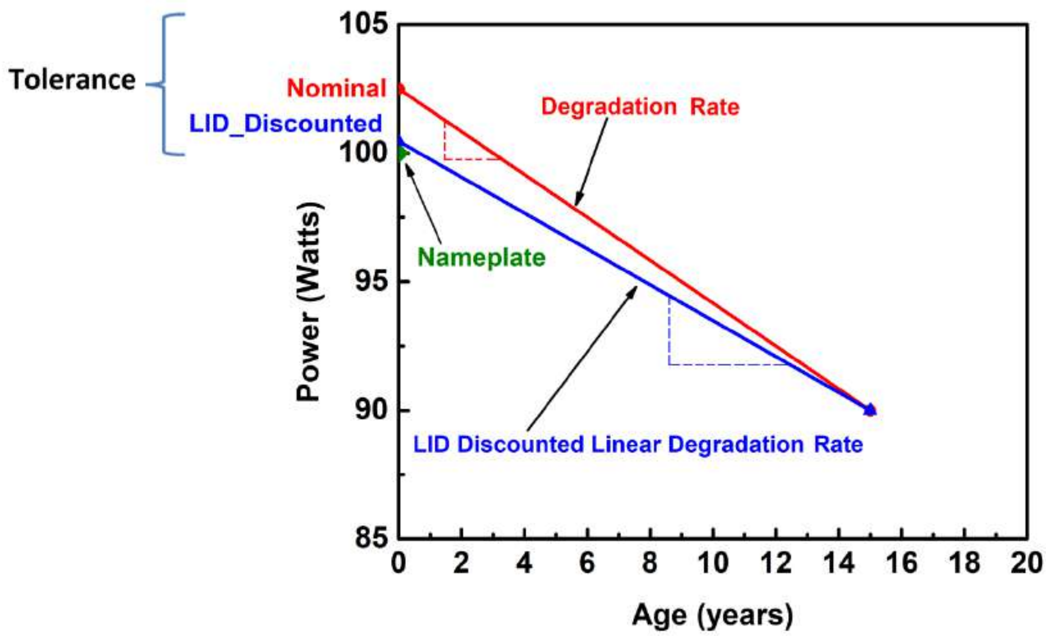


Fig. 3.7. Graphical representation of 'Linear Degradation Rate', and comparison with simple or Overall 'Degradation Rate'

## 3.6 Uncertainties in Linear Degradation Rate Calculation

*I-V* curves measured in the field at different irradiance and temperature conditions were translated to STC conditions to evaluate the present performance and to estimate the degradation rate. We have used Modified IEC 60891 Procedure 1, so along with the error in the translation as discussed above in Section 3.4, there are also other errors associated with the measurement itself, as well as the error associated with nameplate tolerance. The total uncertainty in the calculation of the degradation rate includes all these errors.

### 3.6.1 Uncertainties in Measurement

For the measurement of *I-V* curves of PV modules during the survey, we have used Solmetric PVA-1000S portable *I-V* curve tracer. The Plane of Array (POA) Irradiance was measured with Solsensor, which is a silicon photodiode, and the Solmetric has ports for K-type thermocouples to measure the PV module temperature. The typical uncertainties of measured irradiance arise from the stability, temperature coefficient, data acquisition, and spectral mismatch. The measurement uncertainty is ± 2% for the measured irradiance, and ± 2% for the measured temperature according to the manufacturer's data sheet specifications. The manufacturer's data sheet also specifies that the maximum uncertainty in voltage and current measurement is ± 0.5%. The measurement error caused by the instrument used for *I-V* measurement of a PV module was calculated in detail and included in the report of All-India Survey of PV Module Reliability 2014 [4], the interested readers can refer to it. The main findings of this calculation have been tabulated in Table 3.2. The maximum uncertainty in measurement caused by the instrument at STC is 4%.

Table.3.2. Error caused by the instrument on $P_{max}$ at STC

| $\Delta P_{max}$ (%) | Module Temperature (Deg. C) | | | | | | | | | |
|---|---|---|---|---|---|---|---|---|---|---|
| **Irradiance ($W/m^2$)** | **25** | **30** | **35** | **40** | **45** | **50** | **55** | **60** | **65** | **70** |
| **500** | 4.05 | 4.05 | 4.04 | 4.03 | 4.01 | 4.00 | 3.99 | 3.97 | 3.96 | 3.93 |
| **550** | 4.05 | 4.05 | 4.03 | 4.03 | 3.97 | 3.95 | 3.94 | 3.91 | 3.90 | 3.88 |
| **600** | 4.05 | 4.05 | 4.04 | 4.03 | 3.97 | 3.95 | 3.94 | 3.92 | 3.91 | 3.88 |
| **650** | 4.05 | 4.05 | 4.01 | 3.99 | 3.97 | 3.95 | 3.93 | 3.92 | 3.90 | 3.89 |
| **700** | 4.04 | 4.04 | 4.01 | 3.99 | 3.97 | 3.95 | 3.93 | 3.92 | 3.91 | 3.89 |
| **750** | 4.04 | 4.05 | 4.00 | 3.99 | 3.97 | 3.95 | 3.93 | 3.92 | 3.90 | 3.89 |
| **800** | 4.04 | 4.04 | 3.99 | 3.97 | 3.96 | 3.94 | 3.92 | 3.91 | 3.89 | 3.88 |
| **850** | 4.04 | 4.04 | 4.00 | 3.98 | 3.96 | 3.94 | 3.93 | 3.91 | 3.90 | 3.89 |
| **900** | 4.03 | 4.03 | 4.00 | 3.98 | 3.97 | 3.95 | 3.93 | 3.92 | 3.91 | 3.89 |
| **950** | 4.03 | 4.03 | 4.01 | 3.99 | 3.98 | 3.96 | 3.95 | 3.94 | 3.93 | 3.88 |
| **1000** | 4.03 | 4.03 | 4.00 | 3.99 | 3.98 | 3.96 | 3.95 | 3.94 | 3.93 | 3.92 |

## 3.6.2 Uncertainties in Power at STC

As discussed the total error in maximum power ($P_{max}$) at STC is mainly the sum of errors associated with translation and measurement but there will also be some uncertainty associated with the temperature coefficients used in the translation equations. Even though the temperature coefficients we used are from the datasheet, there can be some variation from the actual values. Table 3.3 shows the total error at STC for maximum power ($P_{max}$) and it will be within 6% taking into all the errors and uncertainties (measurement and translation) into consideration.

## 3.6.3 Uncertainties in Nameplate/Datasheet values

For calculating the overall and linear degradation rates we have used the nameplate or datasheet parameters as initial values at STC, as we do not have (in most cases) the actual measured initial values of all the parameters. There is always a tolerance associated with the nameplate value, generally either ±X% of the actual mentioned nameplate power, or –0%, and +Y% of the actual mentioned nameplate power. In these cases, the tolerance results in an 'error' associated with the nominal power rating of the panel of X% or (Y/2) %, and hence in the calculation of the degradation rates.

## 3.6.4 Uncertainties in Initial LID

To account for Light-Induced Degradation (LID) in the initial days of field operation of PV modules we have discounted 2% from the nominal power, as described earlier. But in reality the LID values might be higher than the discounted 2%; many of the manufacturer's data sheets specify it as 2% to 3%, and in some cases, it might be less than 2%. Variation in actual extent of LID can give rise to an additional error in LID discounted degradation rate, which we have not quantified.

Table.3.3. Total error caused by Modified IEC 60891 Procedure 1 and instrument on $P_{max}$ at STC

| $\Delta P_{max}$ (%) | Module Temperature (Deg. C) | | | | | | | | | |
|---|---|---|---|---|---|---|---|---|---|---|
| **Irradiance ($W/m^2$)** | **25** | **30** | **35** | **40** | **45** | **50** | **55** | **60** | **65** | **70** |
| **500** | 8.64 | 8.17 | 8.09 | 8.13 | 8.38 | 8.59 | 8.89 | 9.05 | 9.37 | 10.44 |
| **550** | 8.14 | 7.63 | 7.51 | 7.54 | 7.71 | 7.88 | 8.16 | 8.28 | 8.59 | 9.05 |
| **600** | 7.74 | 7.22 | 7.07 | 7.1 | 7.22 | 7.32 | 7.59 | 7.7 | 7.98 | 8.39 |
| **650** | 7.13 | 6.66 | 5.96 | 5.73 | 5.63 | 5.64 | 5.63 | 5.3 | 5.12 | 4.83 |
| **700** | 6.66 | 6.2 | 5.48 | 5.25 | 5.12 | 5.1 | 5.06 | 4.83 | 4.52 | 4.18 |
| **750** | 6.27 | 5.77 | 5.02 | 4.76 | 4.6 | 4.55 | 4.5 | 4.12 | 3.89 | 3.54 |
| **800** | 5.74 | 5.22 | 4.95 | 4.91 | 4.99 | 5.13 | 5.22 | 5.33 | 5.54 | 5.83 |
| **850** | 5.3 | 4.76 | 4.44 | 4.43 | 4.52 | 4.7 | 4.77 | 4.86 | 5.06 | 5.33 |
| **900** | 4.92 | 4.32 | 4 | 3.93 | 4.03 | 4.16 | 4.21 | 4.28 | 4.45 | 4.68 |
| **950** | 4.43 | 3.66 | 3.99 | 4.13 | 4.33 | 4.67 | 4.73 | 5.05 | 5.35 | 5.56 |
| **1000** | 4.03 | 3.43 | 3.55 | 3.66 | 3.85 | 4.15 | 4.21 | 4.51 | 4.75 | 5.01 |

## 3.7 Graph Templates

In this section, we describe the templates of the most-frequently used graphs in this report. These are shown in Fig. 3.8 to Fig. 3.10 (the values presented in these figures are indicative only). Fig. 3.8 shows the template of histograms, and the two red dotted lines represent mean and median. The box in the inset represents the values of total number of modules, average (mean), median, minimum and maximum values of the samples in that plot. Fig. 3.9 shows the template for the distribution of degradation of any electrical parameter. The blue coloured data represent the Young PV modules (age between 1 to 5 years) and green represent the Old PV modules (age greater than 5 years). Each PV module is represented by a separate data point (which often overlap). The mean of each group (value in parentheses) is shown by the pink horizontal line, while the pink diamond shows the 95% confidence interval. The number in square brackets above the data points represents the number of samples (PV modules). Also, the following errors are marked for each group:

a) Error due to measurement and STC correction (on right side of the plotted data, in purple)

b) Error due to uncertainty in name plate (nominal) value (on left side of the plotted data, in red)

For some cases, the Cumulative Distribution Function (CDF), which gives the probability of a random variable being less than or equal to a specific value, is shown on the right side of the graph. In order to improve readability, we have not marked all the data points in the CDF plot. The data point at 50% of the probability is the median of the sample data set.

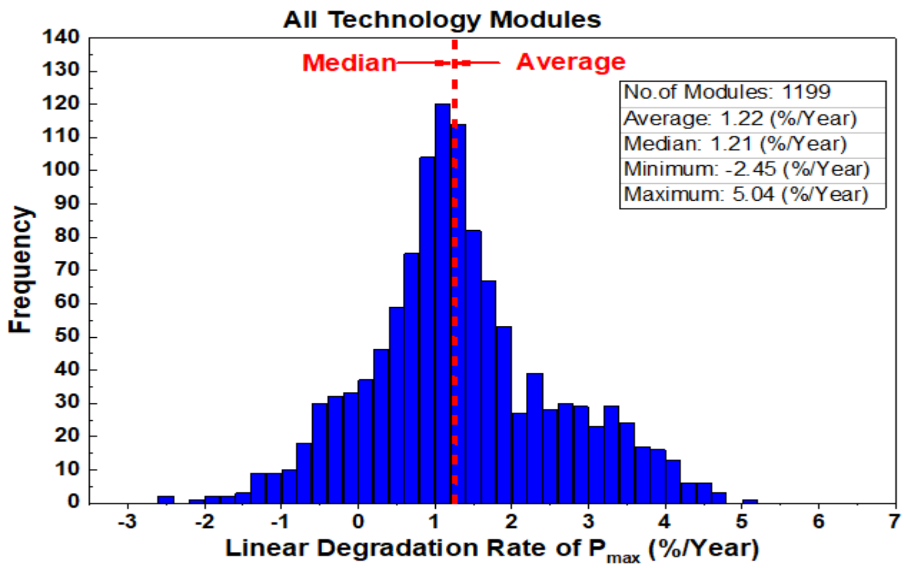


Fig. 3.8. Graph template showing the histogram of Linear Degradation Rate of $P_{max}$ of all the PV modules surveyed

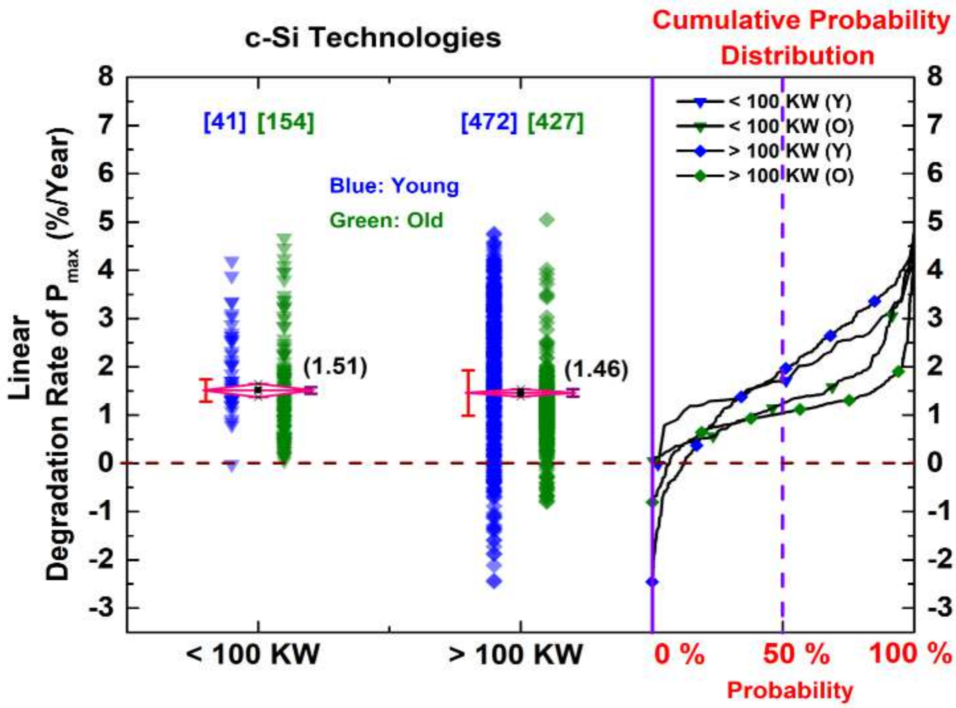


Fig. 3.9. Graph template showing Linear Degradation Rate and Cumulative Probability Distribution Function of $P_{max}$ for Young and Old PV modules and Small/medium and Large Systems

Graphs with all data points and representing density in width (see Fig. 3.10) will show the mean of samples with red horizontal bar and red colour diamond represents 95 % confidence interval but there would be no errors.

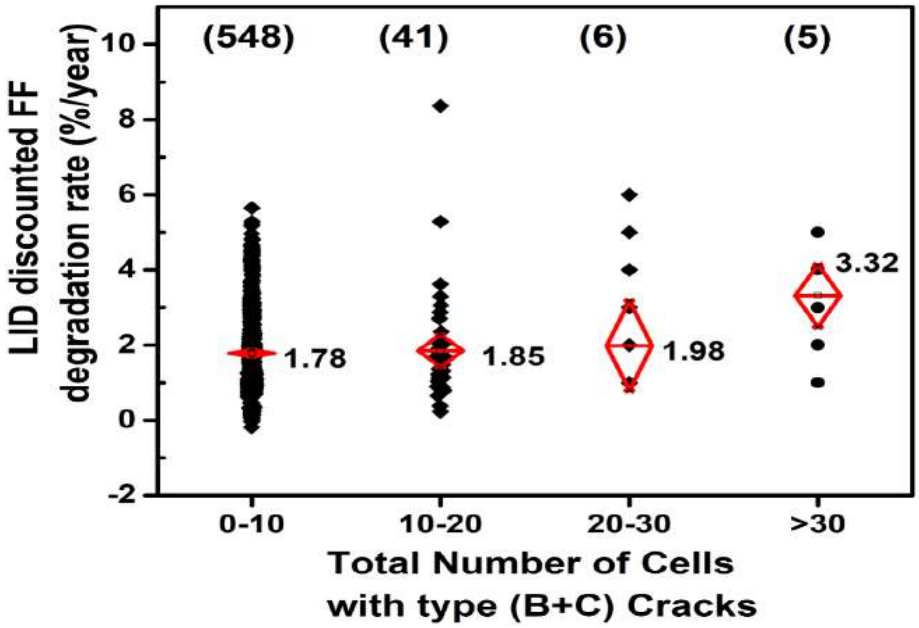


Fig. 3.10. Graph template showing Linear Degradation Rate of *FF* with respect to total number of cells with type (B+C) cracks (along with density in width)

## 3.8 Statistical Analysis

The PV modules surveyed in this and previous studies show high variability in the degradation rates. Hence it is necessary to perform a rigorous statistical analysis of the data in order to find out whether perceived differences in central tendencies of the data sets are statistically significant. The detailed methodology used for statistical analysis was reported in All-India Survey of PV Module Reliability 2016 [5] and in [52], and the interested readers can refer to it. In the 2018 All-India Survey also, we have encountered high variability in $P_{max}$ degradation rates ranging from -2.45 %/year to +7.73 %/year due to various reasons. So it is necessary to perform a statistical test to identify 'outliers' and separate them out from the analysis, otherwise we may arrive at some wrong conclusions.

### 3.8.1 Outlier Identification

The outliers of the overall degradation rate of $P_{max}$ of PV modules were identified by using a statistical approach called inter-quartile method. In this method the data points are arranged in ascending order and the total data is split into two halves. The two halves are called as lower half (lf) and upper half (uf). A measure of the spread which is resistant to outliers is given by the difference between the upper fourth and lower fourth, which is referred to as the inter-quartile range. Any observation beyond 1.5 times of inter-quartile range from its nearest fourth is considered as an outlier. For our 2018 Survey data set we found that a degradation rate of 5.21 %/year is the upper outlier limit from this method, as shown in Fig. 3.11. Subsequently, the electrical and other analyses were carried out on the samples remaining after removing the outliers (which numbered 46). An analysis on outliers was carried out to determine possible reasons for such high degradation rates, as described in Appendix–C.

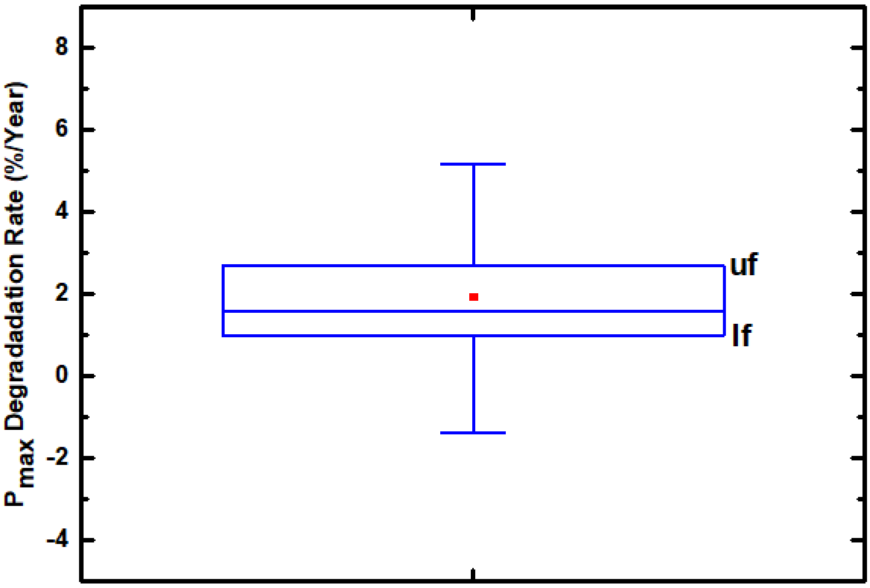


Fig. 3.11. Box plot for $P_{max}$ degradation rates for all PV modules in all sites (The red dot indicates the sample mean)

### 3.8.2 Choice of Mean vs Median

In order to arrive at meaningful conclusions, we need to present overall trends in the measurements from the large set of data collected in our survey using suitable summary statistics. We have used sample mean over the sample median for the same purpose. The reasons for choosing mean vs median were explained in detailed in All-India Survey of PV Module Reliability 2014 [5].

## 3.9 Summary

We have used the Modified IEC 60891 Procedure 1 for STC Correction for the field measured I-V data to estimate the degradation rate. We have also included a new simulation study to justify this choice. In this chapter we have also estimated various errors due to the translation procedure, and errors due to instrument or measurement uncertainties. The measurement and STC translation procedures together have been assessed to have a maximum possible error in $P_{max}$ degradation to be 6% for crystalline silicon modules measured above 700 W/m$^2$. A further error exists due to uncertainty in nameplate (or nominal) rating as we do not have actual initial measured parameters. We have defined the 'Linear Degradation Rate' which considers effect of LID on the module in degradation rate calculations by assigning a 2% discount in initial nominal power. Templates of the typical graphs used in succeeding chapters have been described here. We have also presented the significance of outlier identification by the inter-quartile method. We have laid a lot of emphasis on the errors involved, as the degradation rates calculated and presented in succeeding chapters need to be appropriately qualified. The next chapter is dedicated to the electrical analysis of the PV modules in the Survey (after separating the outliers).

# 4. Analysis of Electrical Degradation

## 4.1 Introduction

As part of India's National Solar Mission of commissioning 100 GW of solar PV across the country by 2022, 26 GW has been installed by December 2018 [1]. The growth rate of solar PV installations is predicted to increase rapidly in the coming years to achieve the target. The majority of the installations are utility-scale power plants, so the long term reliability of these power plants is very important for the eventual success of the mission. The All-India Survey of PV Module Reliability 2018 therefore gives due emphasis to the performance of these utility-scale power plants, though some small/medium installations (including rooftops) are also included.

Out of all the PV modules inspected during this Survey, only those modules for which *I-V* measurements were done at an irradiance level of at least 700 W/m$^2$ were considered for further analysis. The total number of such modules was 1245. *I-V* curves of PV modules measured at different irradiance and temperature conditions were translated to Standard Test Conditions (STC) by the Modified IEC 60891 Procedure 1, as described earlier. This is also the same procedure used in previous All-India Surveys (2016, 2014, and 2013) [5], [4], [3] which makes the translation scheme used consistent across all our Surveys.

After translating all the field-measured *I-V* curves of PV modules to STC, the interquartile method (described in Section 3.8.1) was used to find the 'outlier degradation rate limit', in order to discard modules with abnormally high degradation rates due to unknown causes. This limit was found to be 5.21 %/year. After removing the 'outlier' PV modules (46 in number) based on this limit, we have ended up with 1199 PV modules for the electrical degradation analysis. Out of these 1199 PV modules, a majority of the PV modules (1094 or 91.2%) are of c-Si technology, and the remaining 105 (8.8%) are of thin film technologies (this distribution is in consonance with the current scenario of PV installations in India). Table 4.1 summarizes the number of PV modules we inspected (at least *I-V* measurements were performed, but all other characterization tests might not be performed on all these PV modules) in various conditions at the site and it also shows the analysed PV modules.

The analysis of electrical degradation consists of finding the overall degradation rate of maximum power (using Eq. (3.8)) for all the 1199 PV modules (including the 1094 c-Si modules). We have also calculated, wherever required, the overall degradation rate of individual parameters like $I_{sc}$, $V_{oc}$ and $FF$, using equations similar to Eq. (3.8). For c-Si modules, we have also calculated the 'linear degradation rate', using Eq. (3.10), which discounts the rapid initial LID, as described earlier in Section 3.5. The linear degradation rate of other performance parameters like $V_{oc}$, $I_{sc}$ and $FF$ for c-Si PV modules was also estimated. The discounted 2% in $P_{max}$ in accounting for LID has divided in to three parts: 0.8% each for $V_{oc}$ and $I_{sc}$, and 0.4% for $FF$ [28], [33].

In this chapter, we describe the effect of the age of PV modules, type of mounting of PV modules, system size, technology and climatic zones on the performance of the PV modules. We also show the results of 4-point and 3-point analysis for cases where the modules were measured in previous Surveys also.

Table 4.1. Number of PV Modules inspected (at least *I-V*) and analysed in All-India Survey 2018

| S. No | Condition of Inspection/Analysis | No. of PV Modules |
|---|---|---|
| 1 | Inspected without cleaning | 11270 |
| 2 | Inspected after cleaning | 3165 |
| 3 | Detailed inspection performed | 1375 |
| 4 | Age with less than One Year (not considered for analysis) | 100 |
| 5 | Measured at low irradiances (<700 W/m$^2$) (not considered for analysis) | 27 |
| 6 | Outlier category (not considered for analysis – however see Appendix-C) | 46 |
| 7 | Detailed Electrical Analysis performed | 1199 |
| 8 | c-Si Technology | 1094 |
| 9 | Thin film Technology | 105 |

## 4.2 Overall and Linear Degradation Rate of $P_{max}$ for all the PV modules and for c-Si PV modules

The histogram of overall degradation rate of $P_{max}$, and of linear degradation rate of $P_{max}$ for all the 1199 PV modules are shown in Fig. 4.1 (a), and Fig.4.1 (b). We observe that the average or mean of overall degradation rate in $P_{max}$ is 1.79 %/year, and average of linear degradation rate of $P_{max}$ is 1.22 %/year. These numbers are slightly higher than the 2016 values (1.55 %/year and 1.20 %/year for overall and linear rates respectively [5]) but slightly lower than 2014 value (2.07 %/year for overall degradation rate [4]). The reason for this turn-around, we believe, is the increase in the number of large installations (from 2014 to 2016), and the increase in the number of young installations (from 2016 to 2018). As we show later, young installations tend to have higher degradation rates. The average linear degradation rate of $P_{max}$ (1.22 %/year) observed in the 2018 All-India Survey is higher than the typical expected linear degradation rate of 0.8 %/year (20% degradation in $P_{max}$ in 25 years) according to normal warranty conditions.

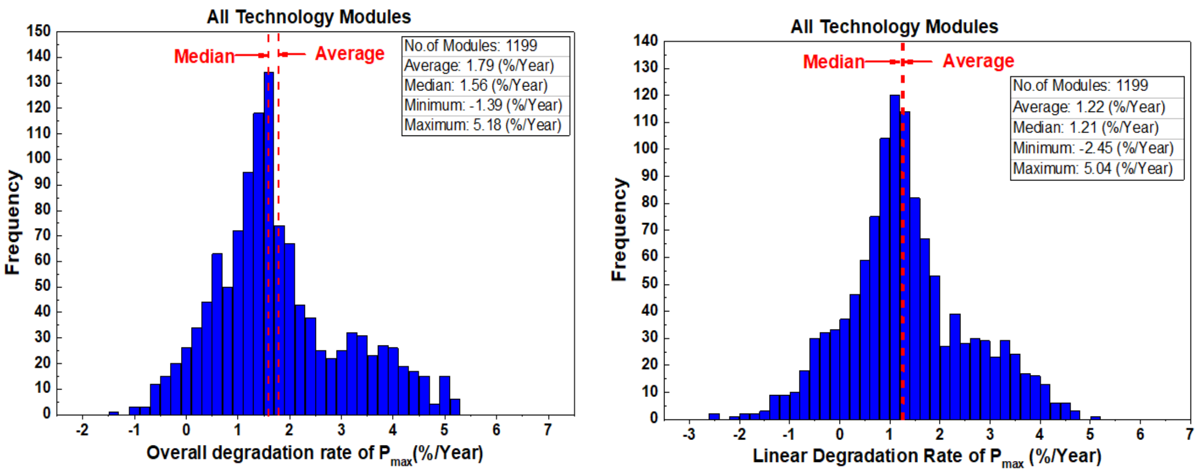


(a) (b)

Fig. 4.1. (a) Histogram of overall degradation rate of $P_{max}$ and (b) Histogram of linear degradation rate of $P_{max}$ of all the analysed 1199 PV modules which include all the technologies.

In Figs. 4.1(a) and (b), we also see that there is a wide distribution in degradation rates, from –1.39 %/year to 5.18 %/year. The wide distribution indicates that some modules (and indeed sites) are performing quite well, but that the average is being adversely affected by poorly performing modules and sites. Most of the negative degradation rates are for thin film modules, but also for some c-Si modules. They are probably due to recovery, error in STC translation and measurement, error in LID estimation, nameplate error, under-rating of modules, or a combination of all of these.

The histogram of overall degradation rate in $P_{max}$, and the histogram of linear degradation rate of $P_{max}$ for the 1094 c-Si PV modules are shown in Fig. 4.2 (a), and Fig. 4.2 (b). We can observe that the average or mean of overall degradation rate in $P_{max}$ is 1.93 %/year, and average linear degradation rate of $P_{max}$ is 1.47 %/year. These numbers are very similar to those of 2016 All-India Survey (1.90 %/year and 1.47 %/year [5]).

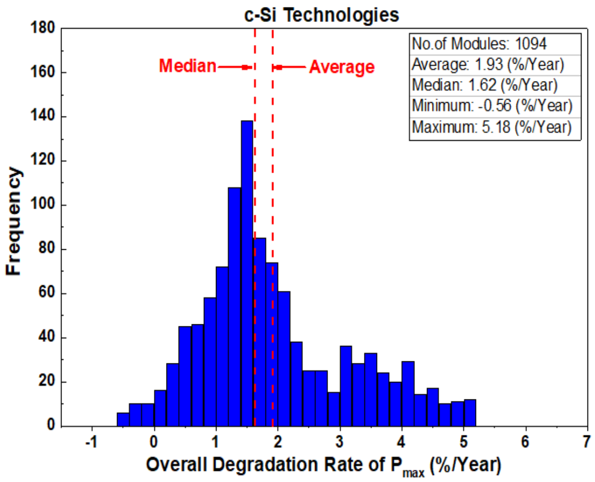


(a)

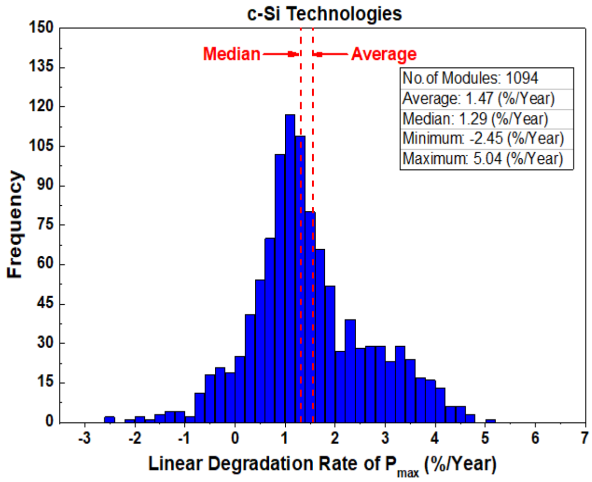


(b)

Fig. 4.2. (a) Histogram of overall degradation rate of $P_{max}$ and (b) Histogram of linear degradation rate of $P_{max}$ of all the analysed 1094 PV modules which include only c-Si technology.

In the sections which follow, we discuss the dependence of the degradation rates with age, climatic zone, technology, system size and type of installation (ground-mounted or roof-mounted).

## 4.3 Age Variation

This section focuses on the effect of PV module age on the overall and linear $P_{max}$ degradation rate of c-Si PV modules. We have classified the PV modules as Young (age between 1-5 years) and Old (age greater than 5 years), similar to 2016 All-India Survey classification. In this section we also show how the age variation effects the other parameters of PV modules like $I_{sc}$, $V_{oc}$, and *FF* along with $P_{max}$.

### 4.3.1 Effect of PV System Age on the $P_{max}$ Degradation Rate of sites

Fig. 4.3 shows the site-wise overall and linear degradation rates of $P_{max}$ for the 35 c-Si sites and one can clearly observe that the Young sites are degrading at relatively faster rate than that of Old sites. One can also observe from this figure the fact that the 2018 Survey mainly focused on recent installations (most of the sites are below seven years of age). Most of the sites commissioned during the period 2013 to 2017 (Young) show high degradation rates. We can also observe form Fig. 4.3 that not only the overall degradation rate of $P_{max}$ but also the linear degradation rate (after discounting LID) of $P_{max}$ for the Young sites is high. The key reasons for higher degradation rates in certain sites are highlighted in Fig. D.1 (Appendix-D) with different colored and symbol legends.

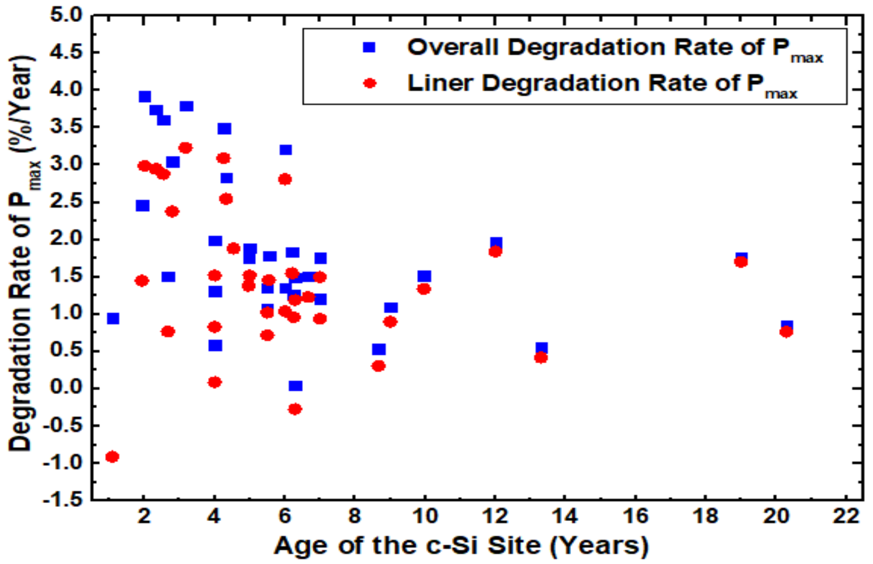


Fig.4.3. Effect of System Age on the average Overall and Linear degradation rates of $P_{max}$ for c-Si sites

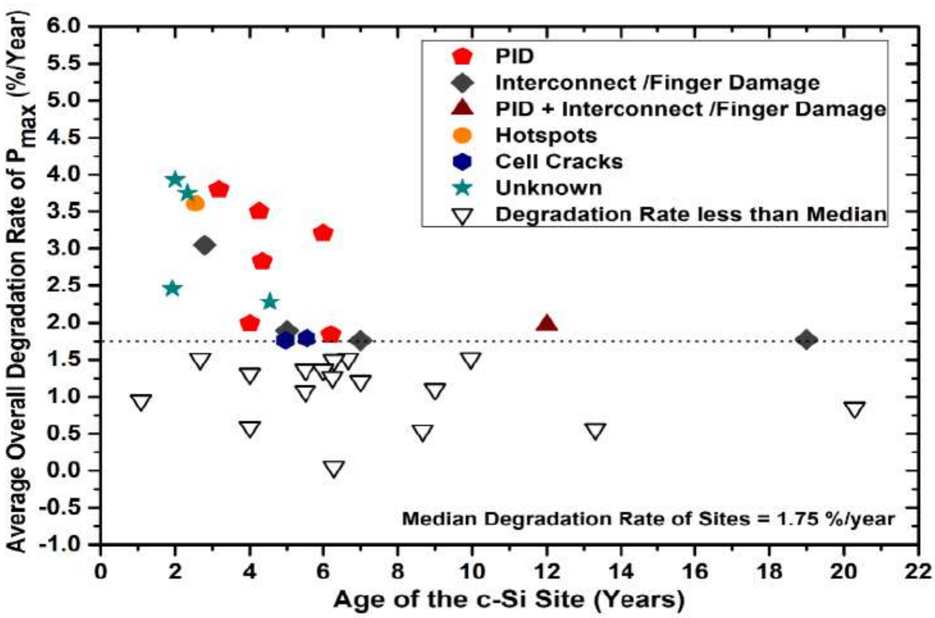


Fig. 4.4. Average overall degradation rates of $P_{max}$ for all c-Si sites with respect to their Age and dominant degradation modes observed in sites with degradation rates higher than the median (1.75 %/year)

Fig. 4.4 and 4.5 show the average overall and linear degradation rates of $P_{max}$ for all c-Si sites with respect to their Age and dominant degradation modes observed in sites with degradation rates higher than the median. We can clearly observe that Potential Induced Degradation (PID), followed by Interconnect/Finger damage are the more frequently observed degradation modes in All-India Survey 2018. In some of the "Young" sites even though the observed degradation rates are high, we could not identify any of the dominant degradation mode from our characterization and analysis techniques.

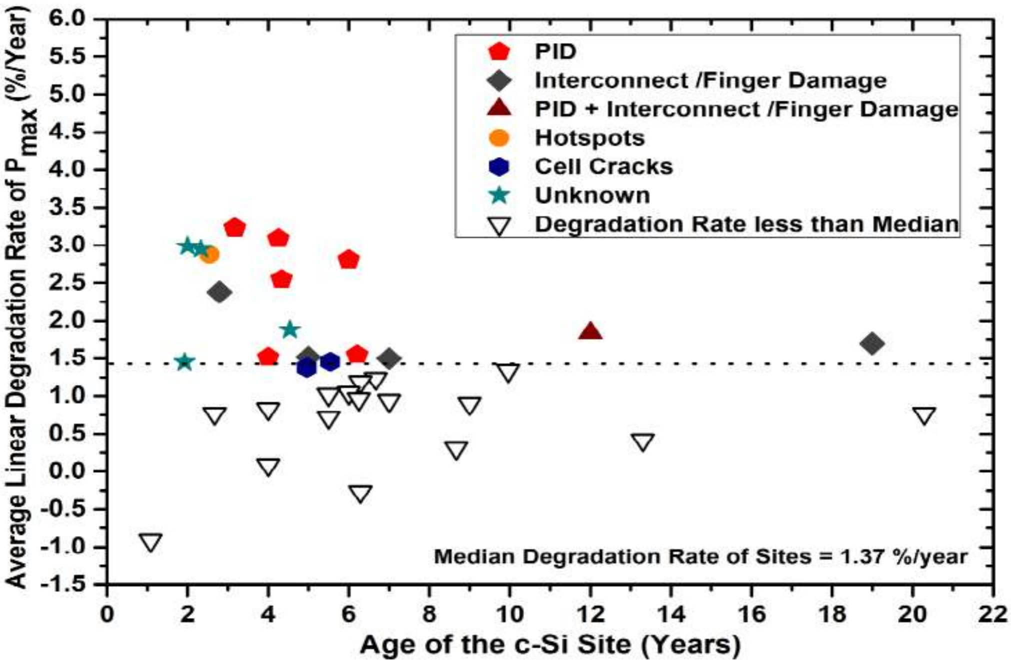


Fig. 4.5. Average linear degradation rates of $P_{max}$ for all c-Si sites with respect to their Age and dominant degradation modes observed in sites with degradation rates higher than the median (1.37 %/year)

## 4.3.2 Effect of PV Module Age on the $P_{max}$ Degradation Rate

Figs. 4.6 (a) and (b) shows the histograms of linear degradation rate of $P_{max}$ for Young and Old PV modules. The average of the linear degradation rate of $P_{max}$ for Young PV modules is 1.85 %/year, and for Old PV modules it is 1.14 %/year. In 2016, the average of linear degradation rate for Young PV modules was 1.71 %year and for Old PV modules it was 1.11 %/year, quite similar to what we see in 2018. This is surprising as one would have expected Young modules to have superior technology and durability, but the results clearly indicate that Young modules, whether because of inferior quality due to pricing pressure, poor installation due to time pressure, or some other reason, are performing significantly worse than the Old modules. Evidence for this also emerges from the broad distribution for the Young compared with the tight distribution for Old. The main reason for the linear degradation rate for all c-Si modules (Young and Old) being higher in 2018 compared to 2016 is simply that we had significantly more Young sites and modules in 2018. This important Young versus Old comparison has serious implications on future installations of > 50 GW which will come up in India during the next 3-4 years. The key reasons responsible for higher degradation rates in certain younger sites as discussed earlier also apply here.

## 4.3.3 Effect of PV Module Age on $P_{max}$, $V_{oc}$, $I_{sc}$, and *FF*

The linear degradation rate of *I-V* parameters ($P_{max}$, $V_{oc}$, $I_{sc}$, and *FF*) for c-Si Young and Old PV modules analysed in 2018 are shown in Fig. 4.7. We can observe that the major contribution for the $P_{max}$ degradation in Young PV modules is *FF* degradation. The linear degradation rate of all *I-V* parameters of Old PV modules is also shown in Fig. 4.7. Here, the $P_{max}$ degradation is due mainly to *FF*, and also $I_{sc}$ to an extent. The major probable reasons for the *FF* degradation in Old PV modules are: (i) We have observed PID in some of the old sites (ii) Corrosion of metal interconnects like fingers, and PV ribbons and which are observed in visual images of Old modules (iii) Cracks in the PV modules, which we observed through EL imaging (iv) The translation procedure as mentioned above. Except corrosion, all the mentioned reasons are valid for FF degradation in young PV modules also. We also found current crowding effects in EL images of some Young PV modules.

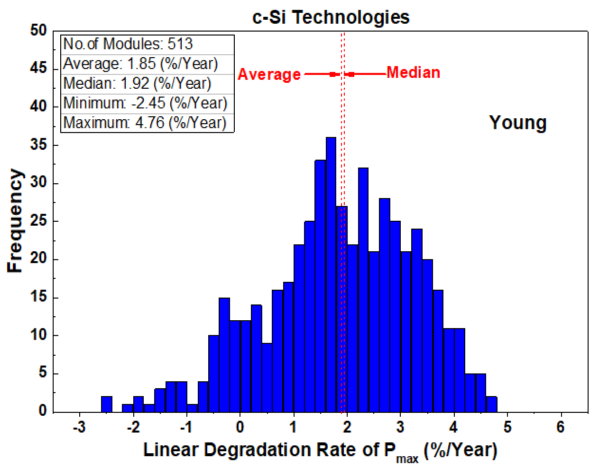


(a)

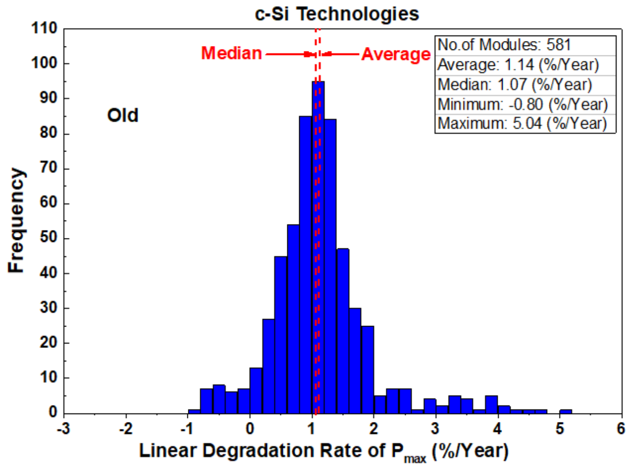


(b)

Fig.4.6. (a) Histogram of linear degradation rate of $P_{max}$ for c-Si Young PV Modules, (b) Histogram of linear degradation rate of $P_{max}$ for c-Si Old PV Modules

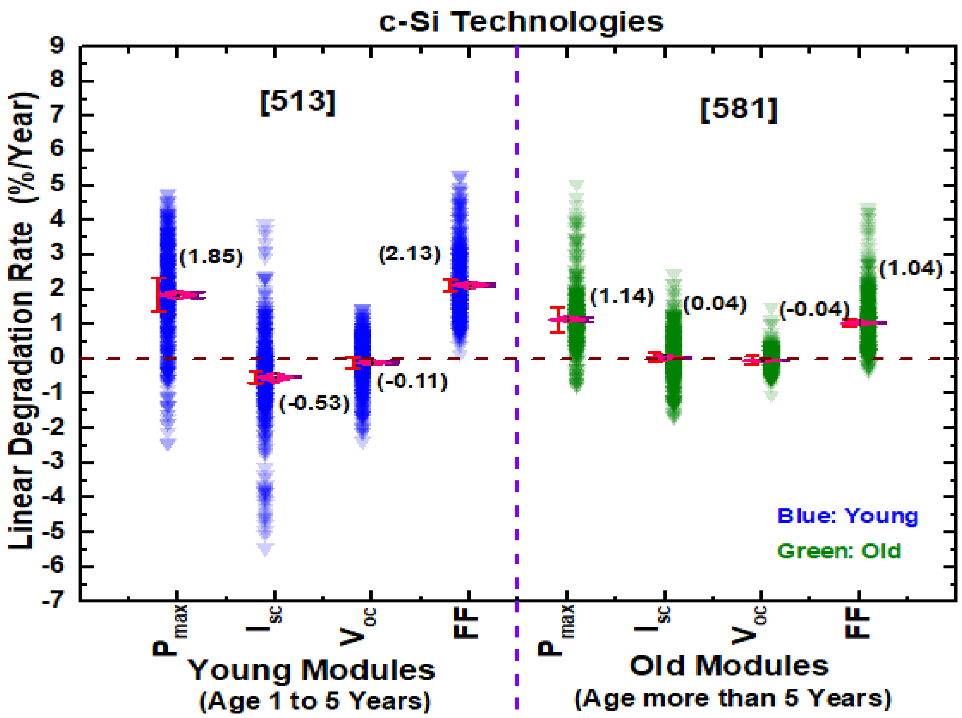


Fig. 4.7. Linear Degradation Rates of different *I-V* parameters for Young and Old c-Si PV Modules

## 4.4 Climatic Zone Variation

The performance of PV modules also depends on the climatic zone in which they have been deployed. Bansal and Minke [43] have divided India into six climatic zones, as described in Chapter 2. Initially we will present the performance of PV modules data with respect to the six-zone classification system, and then also show the data as per the internationally accepted Koppen-Geiger classification system.

### 4.4.1 Effect of Climatic Zone on $P_{max}$ Degradation

Fig. 4.8 shows the linear degradation rate of $P_{max}$ for c-Si PV modules for the different climatic zones. In all of the climatic zones, the Young and Old PV modules are distinguished by blue and green colours. Further, the six-zone climatic zones are coalesced into two major climatic zones, the 'Hot' Zone (Warm & Humid, Hot & Dry, and Composite) and 'Non-Hot' Zone (Moderate, Cold & Sunny, and Cold & Cloudy) in order to showcase the effect of hot climates on the performance of PV modules. We observe that the average linear degradation rate of $P_{max}$ is highest (2.07 %/year) in Warm & Humid zone, next highest in Hot & Dry zone (1.53 %/year), followed by Moderate zone (1.38 %/year, though it has a very small sample size of only 25 Young PV modules, and Composite zone, (1.17 %/year), and finally the least degradation occurs in Cold & Sunny zone (0.23 %year).

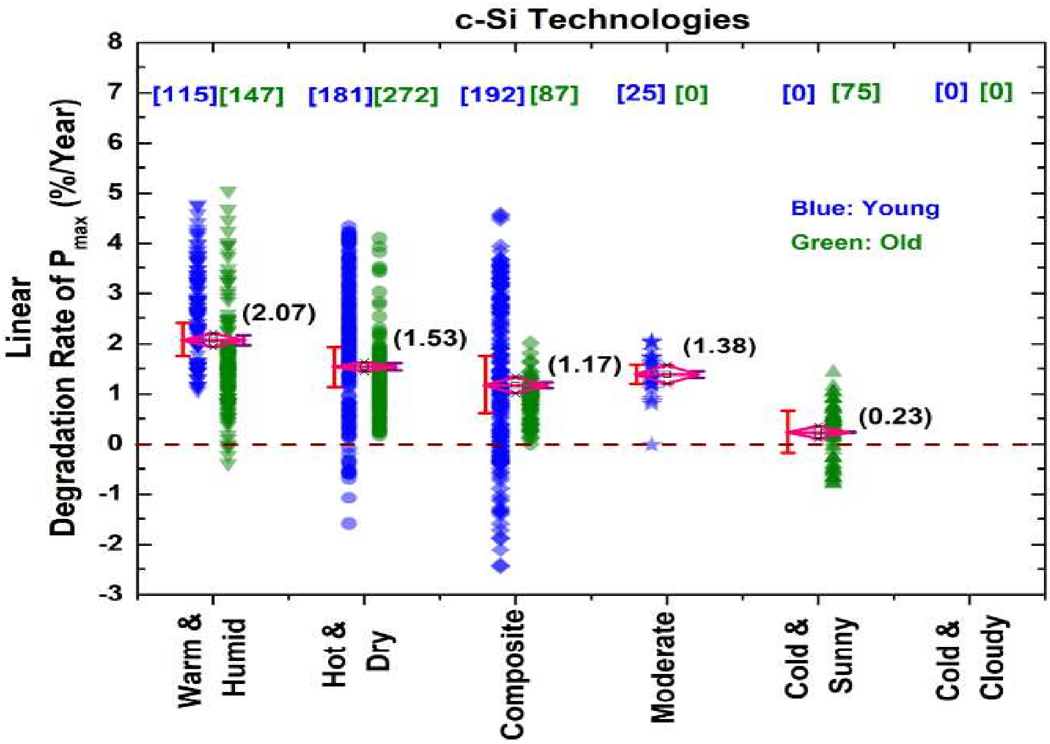


Fig. 4.8. Effect of climatic zone on the linear degradation rate of $P_{max}$ for c-Si PV modules

Fig. 4.9 shows the linear degradation rate of $P_{max}$ for Hot and Non-Hot climatic zones. From Fig. 4.9, we clearly observe that the modules in the Hot zones are degrading faster (1.57 %/year) than the modules in Non-Hot zones (0.52 %/year). Fig. 4.9 also includes the Cumulative Probability Distribution Function (CDF) of the linear degradation rate of $P_{max}$ for the Young and Old PV modules deployed in Hot and Non-Hot climatic zones. One can clearly observe that the CDF of PV modules deployed in the Hot climatic zone is always higher than in the Non-Hot zone (and also that the CDF for Young modules is above the CDF of Old modules).

Fig. 4.10 shows the effect of climatic zones (according to Koppen-Geiger classification) on the linear degradation rate of $P_{max}$, and we observe that the PV modules deployed in Tropical Monsoon climatic zone degrade at the highest rate (2.34 %/year), followed by the PV modules in Arid Semi Hot

(1.64 %/year), Arid Desert Hot (1.55 %/year), Tropical Savanna (1.32 %/year), and Arid Desert Cold (0.23 %/year). Out of all the climatic zones, the PV modules deployed in the Arid Desert Cold climate (the Ladakh region of India) are performing very well, and is part of the reason for the plan to install several GW of solar in Ladakh.

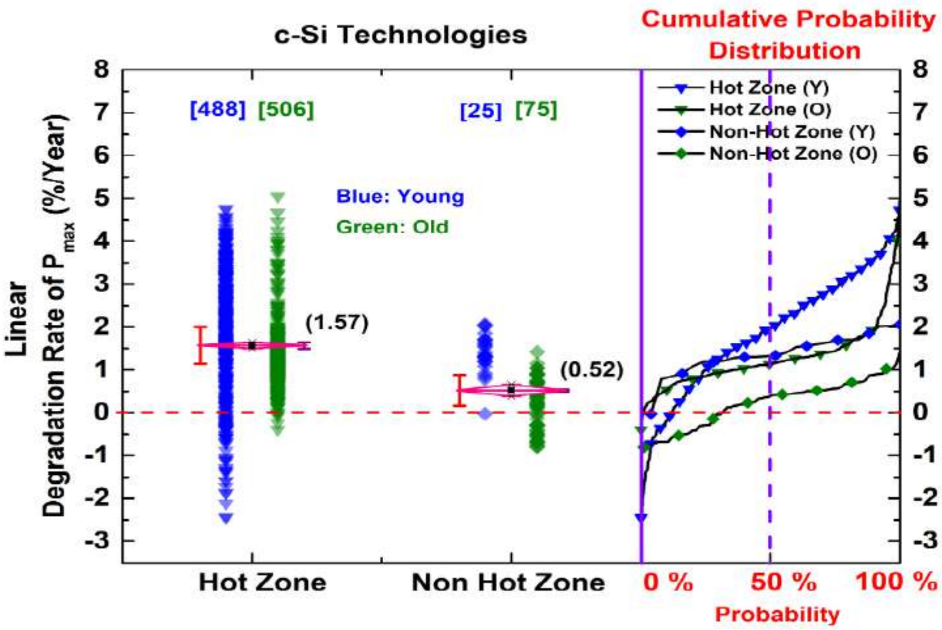


Fig. 4.9. Effect of Hot and Non-Hot climatic zones on the linear degradation rate of $P_{max}$ for c-Si PV modules, and also cumulative probability distribution

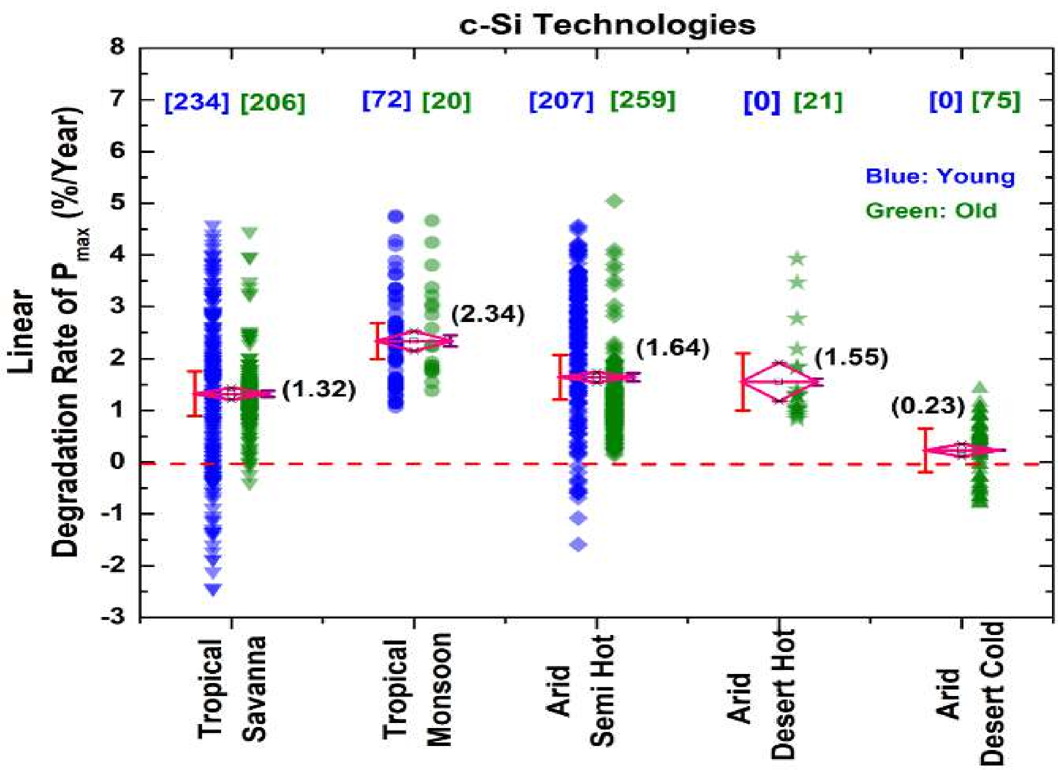


Fig. 4.10. Effect of climatic zones (Koppen-Geiger) on the linear degradation rate of $P_{max}$ for c-Si PV modules

### 4.4.3 Effect of Climatic Zone on $I_{sc}$, $V_{oc}$, and *FF* Degradation

The influence of climatic zone on the linear degradation rate of Short Circuit Current ($I_{sc}$), Open Circuit Voltage ($V_{oc}$), and Fill Factor (*FF*) is shown in Fig. 4.11, along $P_{max}$. For most of the climatic zones, *FF* degradation is the largest contributor, but in Warm & Humid climatic zone, $I_{sc}$ also contributes. The possible reasons for *FF* degradation in all of the climatic zones are mismatch between the solar cells in the PV modules due to cracks, high series resistance ($R_s$) of PV modules due to cracks and corrosion, low shunt resistance ($R_{sh}$) of PV modules due to Potential Induced Degradation (PID), other shunt paths, and the translation procedure (Modified IEC 60891 Procedure 1) which we used. The reasons for $I_{sc}$ degradation are encapsulant browning in hot climates, and enhanced UV radiation dosage for modules in cold and sunny climatic zone (Ladakh is at about 4000 m altitude), and PID at some sites.

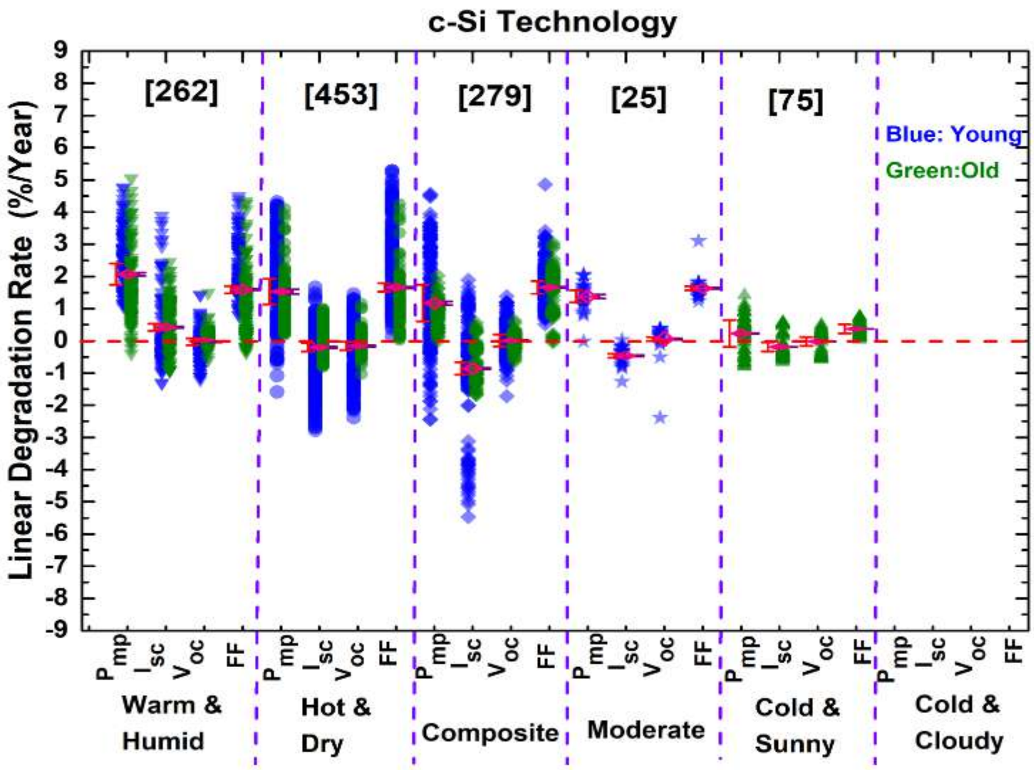


Fig. 4.11. Effect of climatic zone on the *I-V* parameters of PV modules

## 4.5 Technology Based Variation

Even though the 2018 All-India Survey mainly focused on modules of standard crystalline silicon technology (Mono as well as Multi), other technology modules like a-Si, CdTe, CIGS, HIT, and IBC were also included in the survey. In this section we discuss the linear degradation rate of $P_{max}$ and the other *I-V* parameters for these different technologies. We consider HIT, and IBC technologies as part of c-Si technologies not as a part of thin film.

### 4.5.1 $P_{max}$ Degradation for Different Technology PV Modules

Linear degradation rate of $P_{max}$ for different technologies is shown in Fig. 4.12. Out of 1199 PV modules that were analysed, 874 PV modules are multi c-Si, 186 are mono c-Si, 75 are CdTe, 23 are HIT, 11 are IBC, 21 are a-Si, and 9 are CIGS. This indicates the most of the share is of c-Si technology, and which is also reflects the current scenario of installations across the country. We observe from Fig. 4.12, that CdTe and a-Si technology (thin film) PV modules have the lowest average degradation rates compared to other technologies, and also that they are negative. The reasons for negative degradation rates might be under-rating, which is often done for thin film PV module manufacturers in order to account for stabilization effects. Also, these PV modules are manufactured by leading international manufacturers with state of the art control over their manufacturing quality and sometimes installation process. The other reason might be spectral mismatch as we have measured the irradiance with Solsensor (Photodiode), Pyranometer, and we used a reference PV module for c-Si technology but not for thin film PV modules. Within c-Si technology modules, multi c-Si modules are degrading faster than mono c-Si modules (similar results were observed in the 2016 Survey [5]). From Fig. 4.12, we also see that the 15 Young HIT PV modules are degrading much faster rate than the 8 Old HIT PV modules, primarily because of degradation of $V_{oc}$. A caveat should be noted about the conclusions of technology variation – the number of non-c-Si modules is quite small.

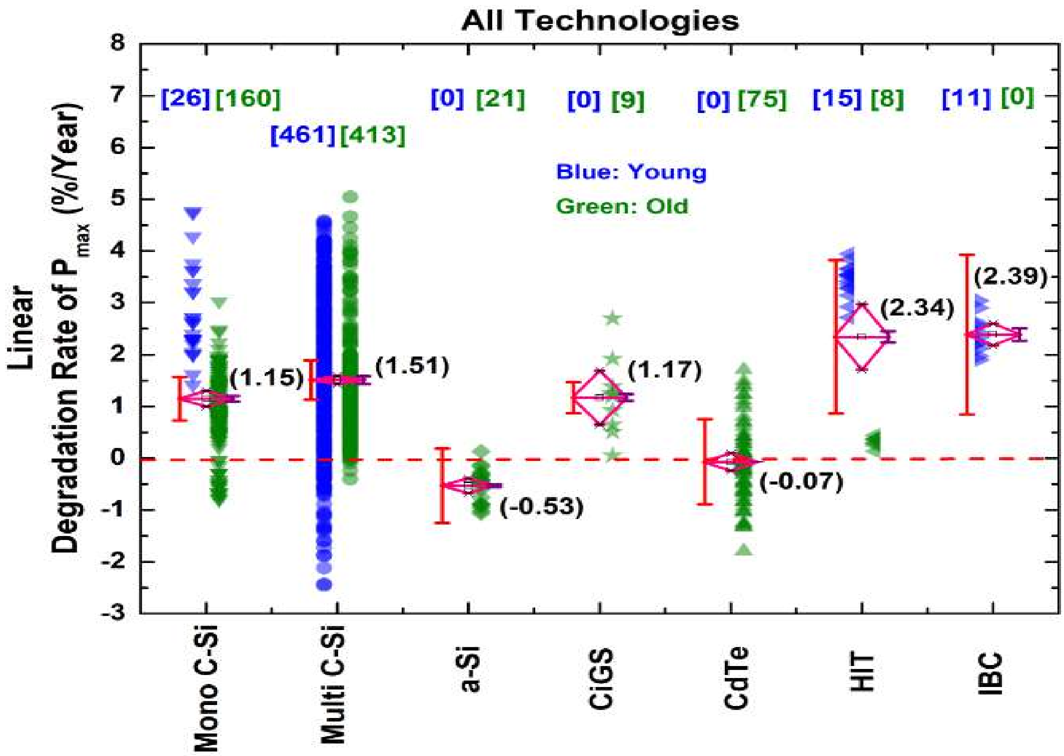


Fig.4.12. Linear Degradation Rate (%/year) of $P_{max}$ for different technology PV modules

## 4.5.2 *I-V* Parameter Degradation for Different Technology PV Modules

The linear degradation rates of $P_{max}$, together with Short Circuit Current ($I_{sc}$), Open Circuit Voltage ($V_{oc}$), and Fill Factor (*FF*) for c-Si (which includes mono c-Si, multi c-Si, HIT, and IBC) and Thin Film is shown in Fig. 4.13. The c-Si PV modules have a higher linear degradation rate of $P_{max}$ (1.47 %/year) compared to Thin Film PV modules (-0.06 %/year), and also we can observe that the degradation of *FF* is major contributor for degradation of $P_{max}$ for both c-Si and Thin Film PV modules.

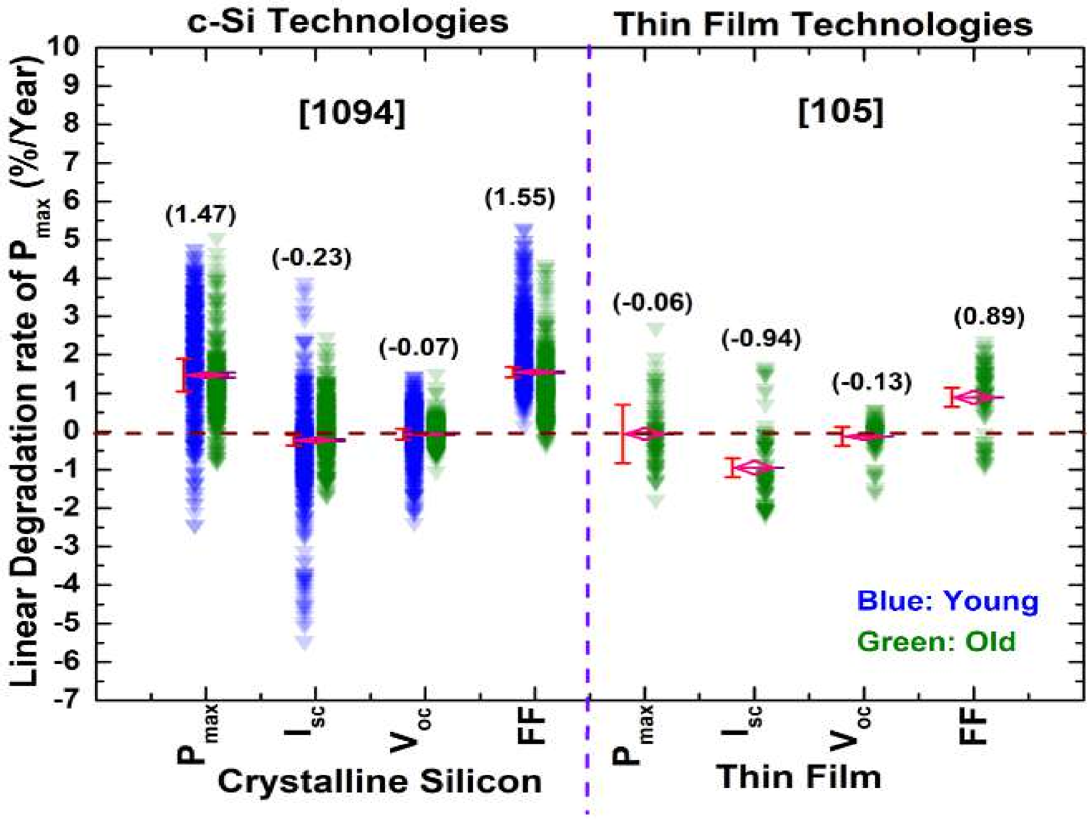


Fig. 4.13. Linear Degradation of *I-V* parameters for different technology PV modules

## 4.6 System Size Based Variation

This section focuses on PV module performance based on the size of the PV system in which they are located. We classify the PV systems that we inspected in the 2018 Survey as Small/Medium (< 100 KW) and Large (> 100 KW) systems, which is similar to our 2016 Survey. However, it should be noted that many of the Large systems are in the range of 1-100 MW.

### 4.6.1 Influence of System Size on $P_{max}$ Degradation

The linear degradation rate of $P_{max}$ of all the c-Si sites that were inspected in 2018 is shown in Fig. 4.14, which also differentiates between Young sites (blue in colour) and Old sites (green in colour). From Fig. 4.14, it is evident that system size is not an influential parameter, but the age (Young or Old) is a dominating parameter for the degradation of $P_{max}$ of PV modules.

The linear degradation rate of $P_{max}$ of all the c-Si sites split into the two system sizes (Small/medium and Large) is shown in Fig.4.15. From this figure also it is evident that there is not much difference between the degradation rates of $P_{max}$ for Small/medium (1.51 %/year), and Large (1.46 %/year) PV systems. On the other hand, we see from the CDF of degradation rates in Fig. 4.15 that the probability distribution of Young modules is above that for Old modules, re-iterating the distinction in terms of age.

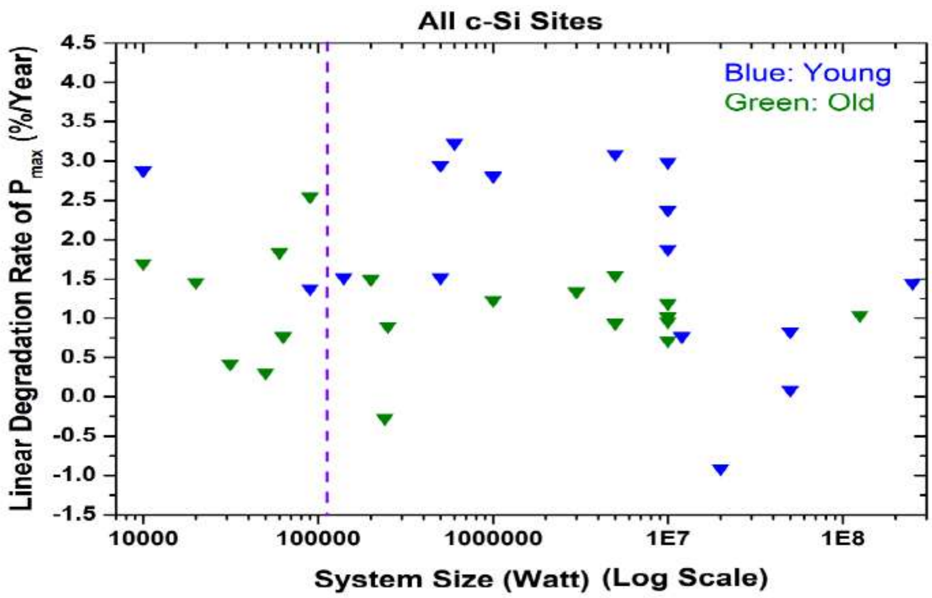


Fig. 4.14. Linear Degradation Rate of $P_{max}$ of all the c-Si systems with respect to Svstem Size.

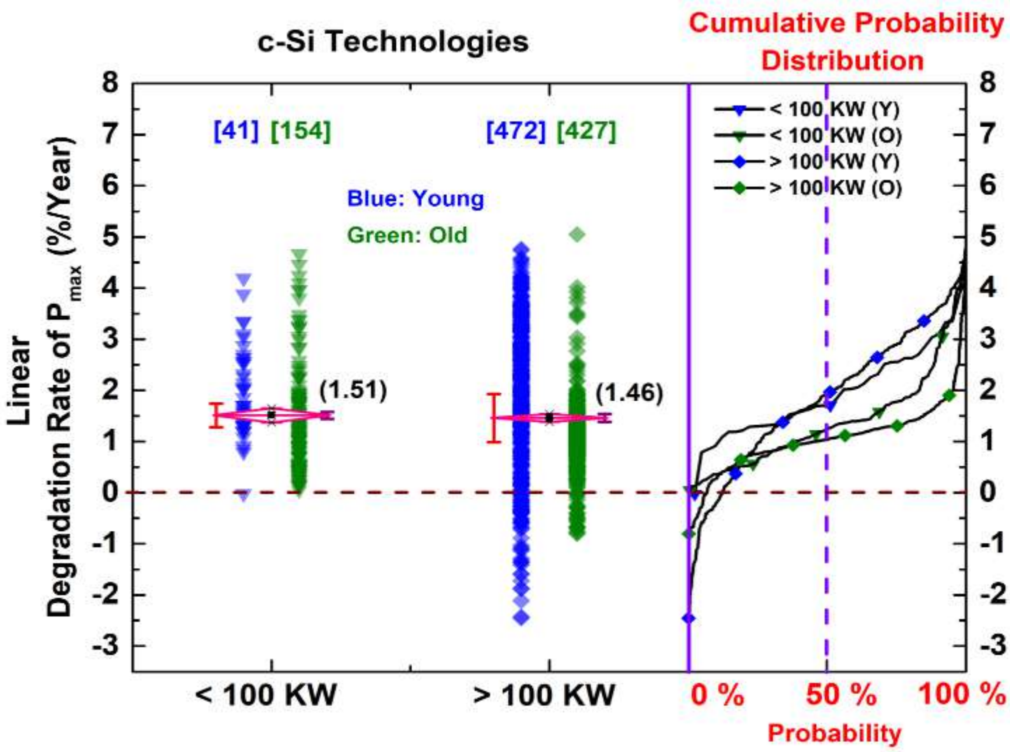


Fig. 4.15. Linear Degradation Rate and Cumulative Probability Distribution Function of $P_{max}$ for Small/medium and Large Systems

Fig. 4.16 shows that the linear degradation rate of $P_{max}$ for large (>100 KW) scale systems deployed in Hot zones, with respect to Young and Old categories. This has been done since most of upcoming installations will be Large systems located in the Hot zones. We observe that the Young PV modules deployed in Hot climatic zones are degrading at a much faster rate (1.84 %/year) than Old PV modules (1.15 %/year) deployed in Hot zones. This shows that Young modules deployed in Hot climatic zone are most susceptible to show high degradation rates.

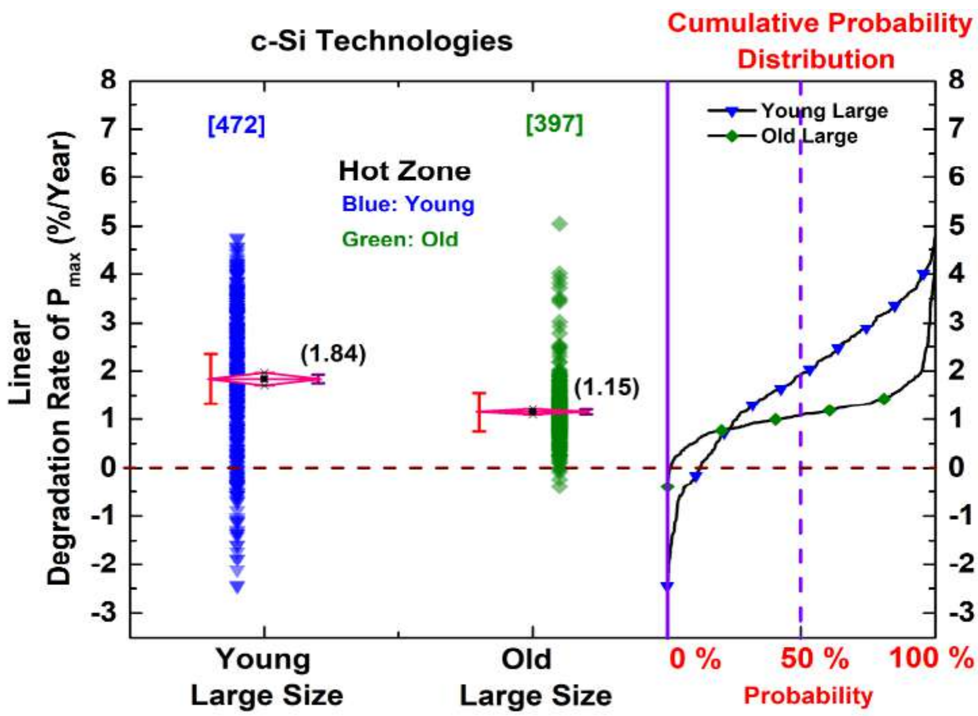


Fig. 4.16. Linear Degradation Rate and Cumulative Probability Distribution Function (CDF) of $P_{max}$ for Young and Old Large Systems in Hot Zone

## 4.7 Variation Based on Installation Type

In this section we discuss influence of type of installation of the PV system (Ground-Rack Mounted, Roof-Rack Mounted and Floating) on module performance. This discussion also includes the system size (Small/medium and Large) along with the type of installation.

### 4.7.1 $P_{max}$ Degradation Based on Type of Installation

The linear degradation rate of $P_{max}$ for c-Si PV Modules with respect to type of installation and system size is shown in Fig. 4.17. From this figure, one can firstly identify that the only floating system that we inspected in this Survey has a high degradation rate in $P_{max}$ (2.88 %/year). However, high degradation rate seen in this system is due to installation problem associated with module mounting clips, and has nothing to do with the floating nature of the system, but we would not like to draw any conclusion whether this single instance reflects problems with floating installations in general. Out of the Roof-Rack mounted and Ground-Rack mounted installations, we see that, irrespective of installation size, the Roof-Rack mounted installations show higher degradation rates in $P_{max}$ (1.84 %/year for Small/medium Systems, and 2.06 %/year for Large systems) compared to Ground-Rack mounted installations (1.14 %/year for Small/medium systems, and 1.36 %/year for Large systems). In this figure, too, from the CDF of $P_{max}$, it is evident that the Young PV modules are degrading at faster rate than the Old PV modules.

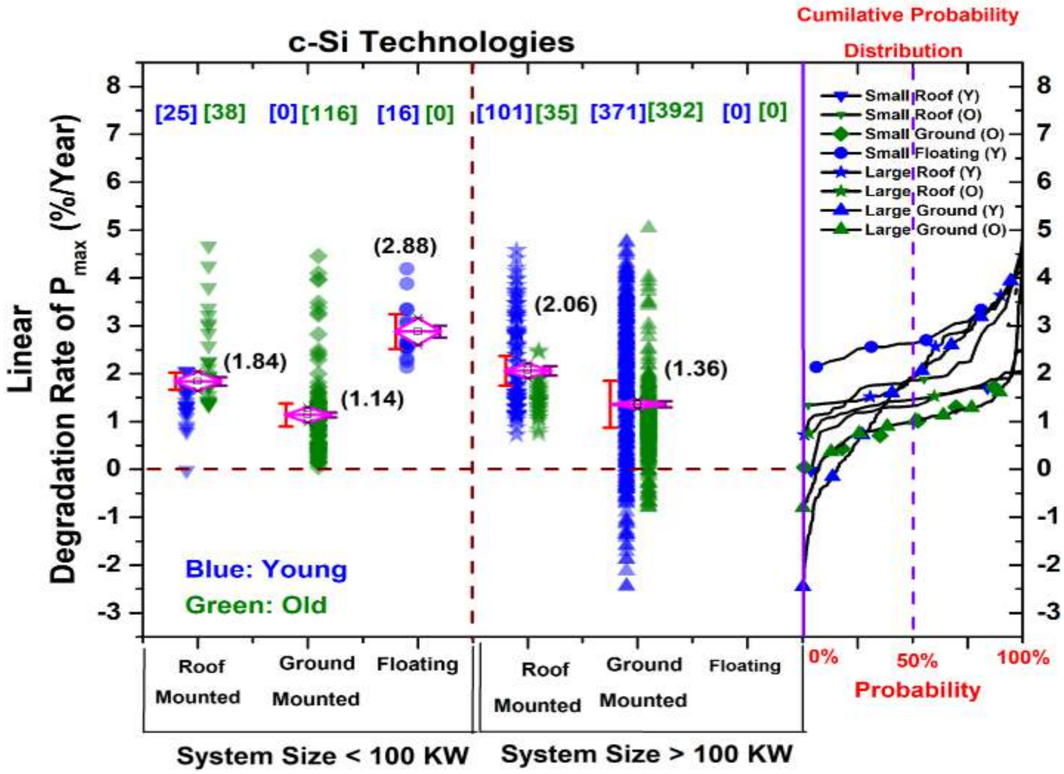


Fig. 4.17. Linear Degradation Rate of $P_{max}$ for Different Types of Installations and System Size

## 4.7.2 $P_{max}$ Degradation for Roof and Ground Mounted Installations

The comparison of linear degradation rate of $P_{max}$ for Roof-Rack mounted and Ground-Rack mounted c-Si PV installations (but not separated out by system size) is shown in Fig. 4.18. Most of the PV modules that we inspected and analysed in this Survey are of Ground-Rack mounted (80.3% of total c-Si PV modules), we also have a reasonable share of Roof-Rack mounted (18.2% of total) PV modules to draw some statistically significant conclusions. The average linear degradation rate of $P_{max}$ for Roof-Rack mounted PV installations is 1.99 %/year, and for Ground-Rack mounted PV installations it is 1.33 %/year. This indicates that the PV modules installed on roofs are degrading faster than those on ground, consistent with our results of all previous Surveys.

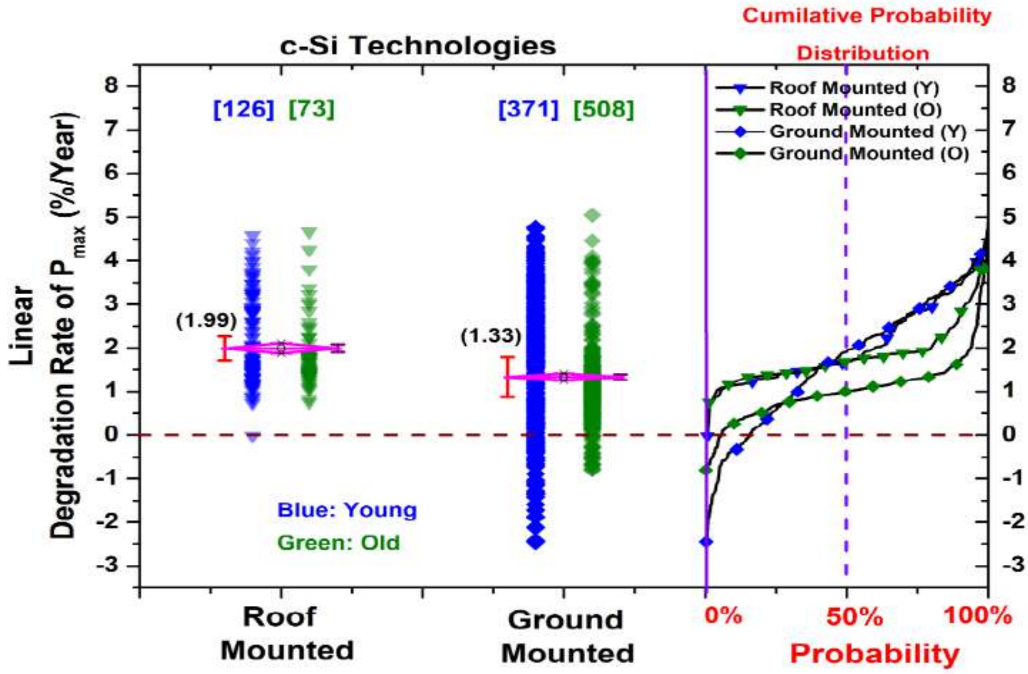


Fig. 4.18. Linear Degradation Rate of $P_{max}$ for Roof Rack and Ground Rack mounted c-Si PV modules

## 4.8 Multi-Point Data Analysis for Repeat Sites

The degradation rates calculated in the previous sections use the initial value (obtained from the nameplate), and the currently measured value. As can be imagined, this 'two-point' analysis is subject to error, due to uncertainty in the nameplate value, the LID discount, the measurement error and the translation error. All these errors have been described in Chapter 3, and also all the plots have explicitly shown these uncertainties.

It would be useful to have data on modules taken repeatedly every year or every two years to obtain a better estimate of the degradation rate. Fortunately, since we have performed the Surveys in 2014, 2016 and 2018, we do have some modules in 'repeat sites' for which data are available during all three or two of these Surveys. Including the initial nameplate data, we can therefore perform a 'four-point' or 'three-point' data analysis. In this section we present the analysis of performance of PV modules in repeat sites using four- and three-point data analysis.

### 4.8.1 Four-Point Data Analysis for Repeat Sites

Fig. 4.19 (a) to (c) show the average STC translated maximum power of all the inspected c-Si PV modules at three different repeat sites in 2014, 2016, and 2018 along with initial nameplate value. The bar in red colour indicates the tolerance in the nameplate value (after discounting LID), and the purple colour bar indicates the error in measurement and STC translation. The degradation in first two sites (Fig. 4.19 (a) and (b)) is minimal. The third site (Fig. 4.19 (c)) shows an average power degradation of nearly 35% in 19 years, which is much higher than the currently observed typical warranty conditions (20% of the power degradation in 25 years).

Fig. 4.20 (a) and (b) show the average STC translated maximum power of all the inspected Thin Film (CdTe) PV modules at two different sites in 2014, 2016, and 2018 along with initial nameplate value. The nameplate, measurement and translation errors also indicated similar to Fig. 4.19. We can see that the first CdTe site (Fig. 4.20 (a)) shows very low degradation, and the possible reasons for the observed low degradation of thin film PV modules was mentioned in Section 4.5. The second CdTe site (Fig. 4.20 (b)) shows somewhat higher degradation, but is still performing quite well.

Table 4.2 shows the average degradation rates calculated for the 5 repeat sites using a best linear fit to the four data points, compared to a two-point analysis using only the 2018 data and the initial nameplate data (The latter is the value used in all earlier plots). It can be seen that the values compare reasonably well, giving confidence in the data.

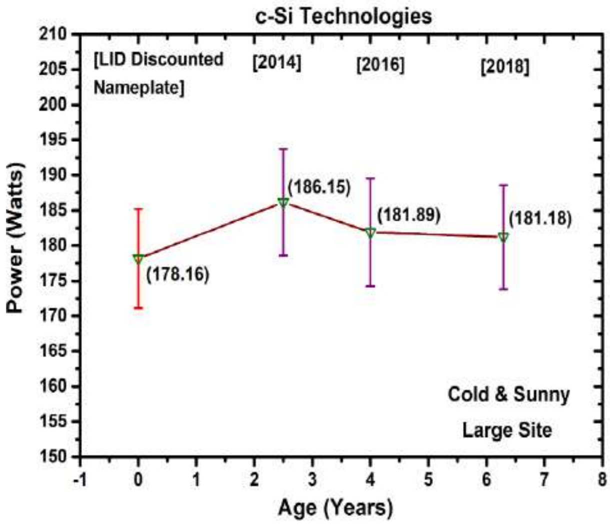


(a)

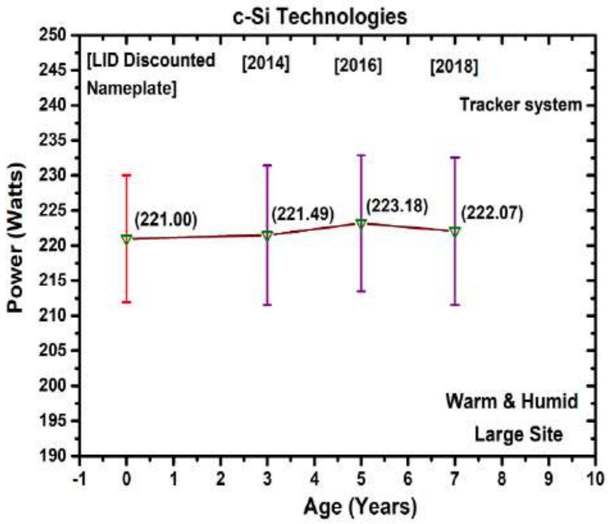


(b)

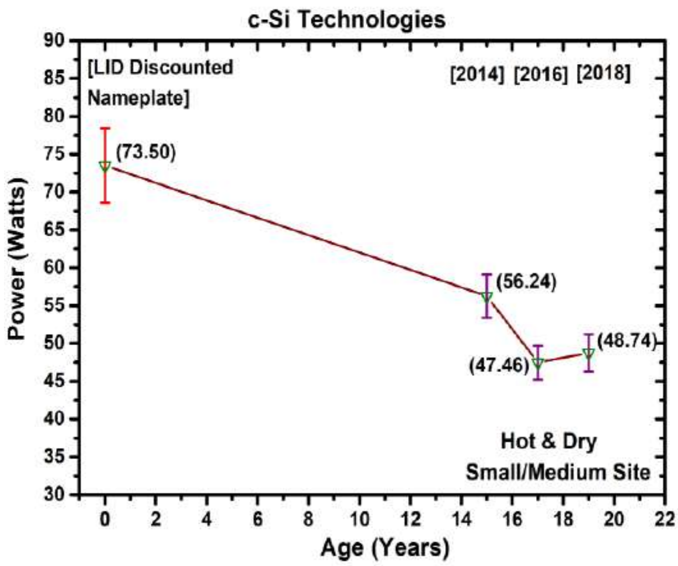


(c)

Fig. 4.19. Four-point analysis of all the c-Si PV modules installed at 3 sites, (a) through (c) which were repeated in 2014, 2016 and 2018 All-India Surveys

Table 4.2. Comparison of average degradation rates calculated for the 5 repeat sites using a best linear fit to the four data points, to a two-point analysis using only the 2018 data and the nameplate data

| Site Wise Figure Numbers | Degradation Rate With 2018 Data (%/year) | Degradation Rate With Four Point Linear Fit (%/year) |
|---|---|---|
| Fig. 4.17. (a) | -0.27 | -0.18 |
| Fig. 4.17. (b) | -0.07 | -0.1 |
| Fig. 4.17. (c) | 1.70 | 1.84 |
| Fig. 4.18. (a) | -0.28 | -0.44 |
| Fig. 4.18. (b) | 0.92 | 0.69 |

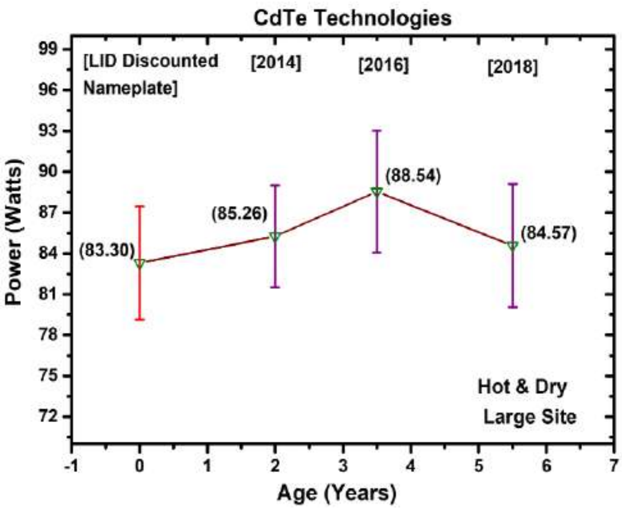


(a)

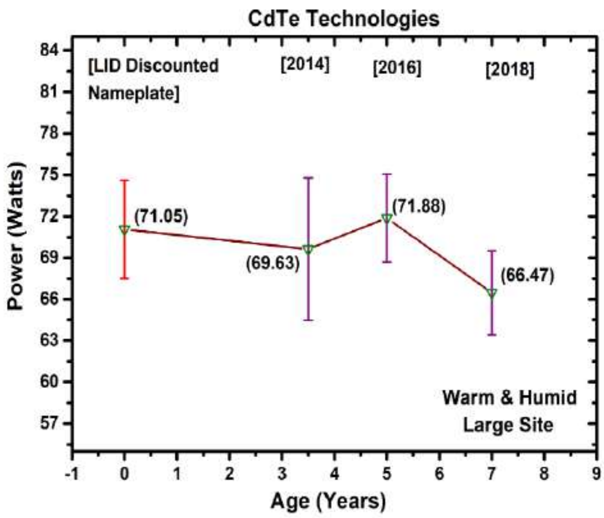


(b)

Fig. 4.20. Four-point analysis of all the Thin Film (CdTe) PV modules installed at 2 sites, (a) and (b) which were repeated in 2014, 2016 and 2018 All-India Surveys

## 4.8.2 Three-Point Data Analysis for Repeat Sites

Fig. 4.21 (a) to (m) show the average STC translated maximum power of all the c-Si PV modules inspected at thirteen different sites in 2016 and 2018 along with initial LID discounted nameplate value. We can clearly observe that some of these sites show high initial degradation (the slope of the line joining first two points is higher than the slope of line joining second and third points). This observation is surprising, as we have already discounted LID (2%) from the initial nameplate value. Two possible reasons are that LID might be higher than 2% and overrating of the PV modules. Some other sites show higher degradation rate later during service life. A few sites show nearly constant degradation rate in both regions. One site in Fig. 4.21 (m), shows an anomalous behaviour with the average maximum power being higher in 2018 than in 2016.

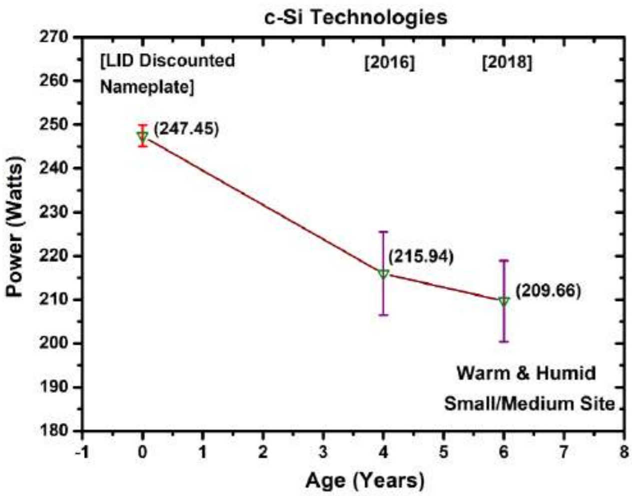
c-Si Technologies
[LID Discounted Nameplate]
[2016]
[2018]
(247.45)
(215.94)
(209.66)
Warm & Humid
Small/Medium Site
Power (Watts)
Age (Years)

(a)

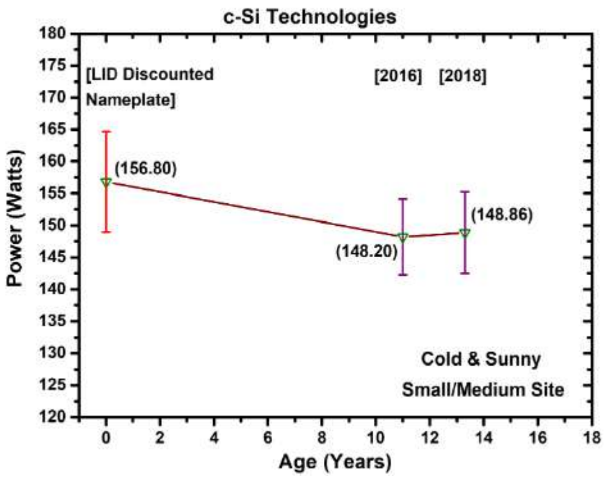
c-Si Technologies
[LID Discounted Nameplate]
[2016]
[2018]
(156.80)
(148.20)
(148.86)
Cold & Sunny
Small/Medium Site
Power (Watts)
Age (Years)

(b)

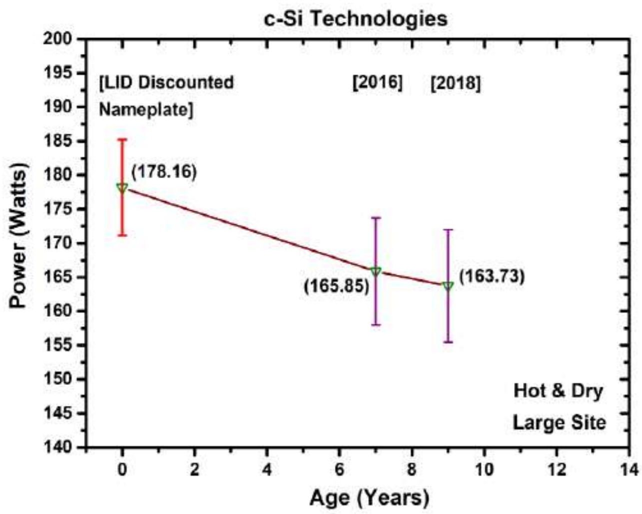
c-Si Technologies
[LID Discounted Nameplate]
[2016]
[2018]
(178.16)
(165.85)
(163.73)
Hot & Dry
Large Site
Power (Watts)
Age (Years)

(c)

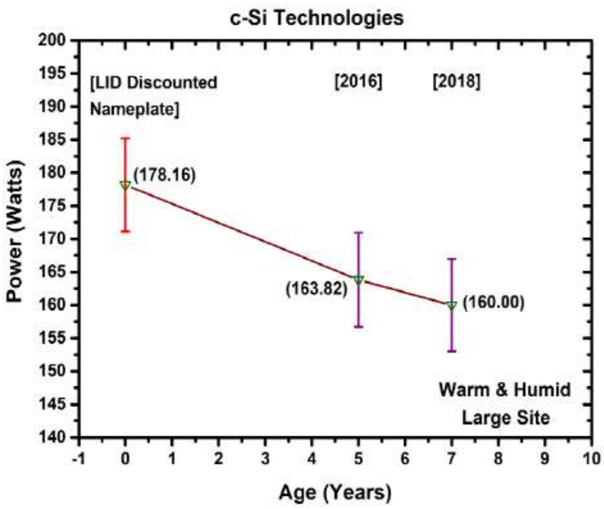
c-Si Technologies
[LID Discounted Nameplate]
[2016]
[2018]
(178.16)
(163.82)
(160.00)
Warm & Humid
Large Site
Power (Watts)
Age (Years)

(d)

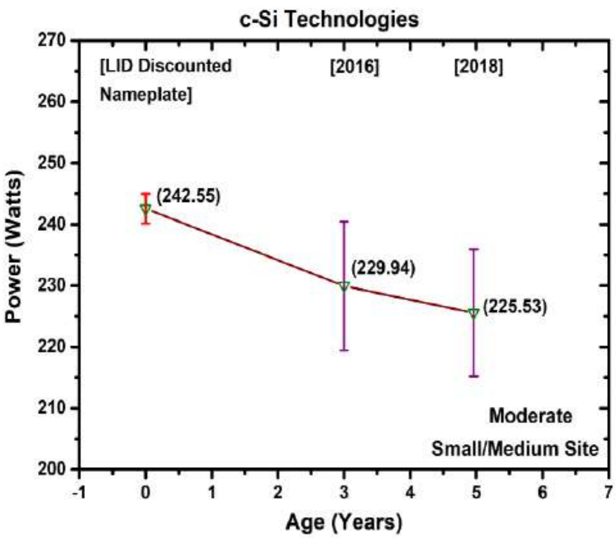
c-Si Technologies
[LID Discounted Nameplate]
[2016]
[2018]
(242.55)
(229.94)
(225.53)
Moderate
Small/Medium Site
Power (Watts)
Age (Years)

(e)

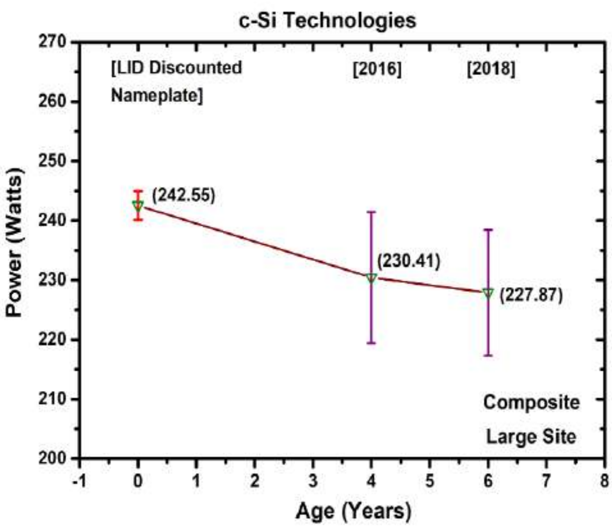
c-Si Technologies
[LID Discounted Nameplate]
[2016]
[2018]
(242.55)
(230.41)
(227.87)
Composite
Large Site
Power (Watts)
Age (Years)

(f)

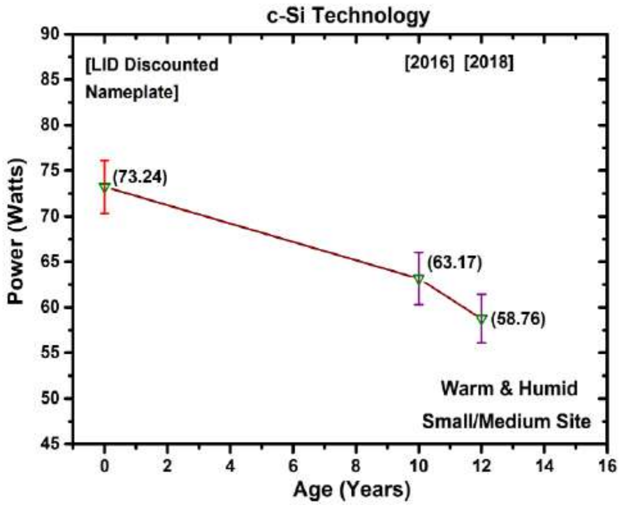
c-Si Technology
[LID Discounted Nameplate]
[2016] [2018]
(73.24)
(63.17)
(58.76)
Warm & Humid
Small/Medium Site
Power (Watts)
Age (Years)

(g)

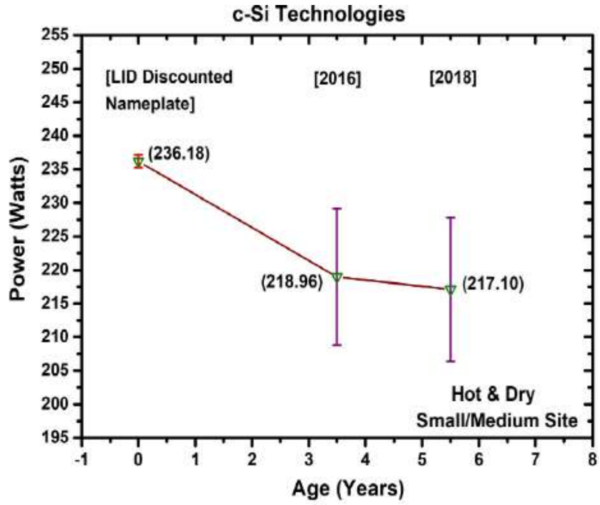
c-Si Technologies
[LID Discounted Nameplate]
[2016]
[2018]
(236.18)
(218.96)
(217.10)
Hot & Dry
Small/Medium Site
Power (Watts)
Age (Years)

(h)

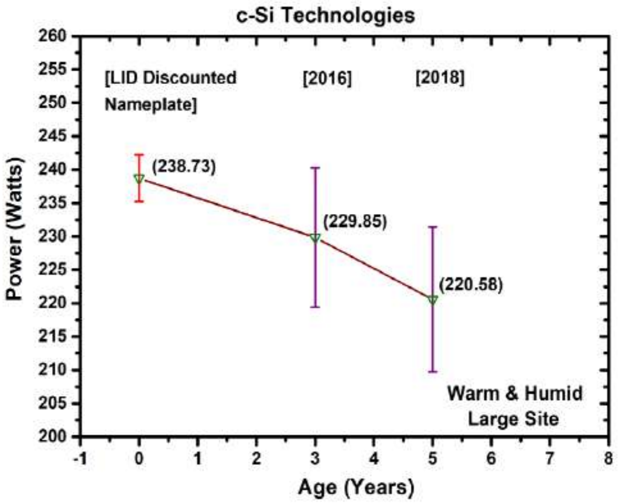
c-Si Technologies
[LID Discounted Nameplate]
[2016]
[2018]
(238.73)
(229.85)
(220.58)
Warm & Humid
Large Site
Power (Watts)
Age (Years)

(i)

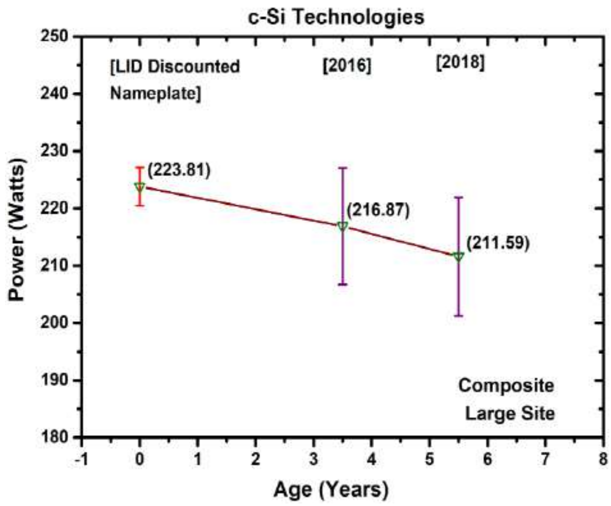
c-Si Technologies
[LID Discounted Nameplate]
[2016]
[2018]
(223.81)
(216.87)
(211.59)
Composite
Large Site
Power (Watts)
Age (Years)

(j)

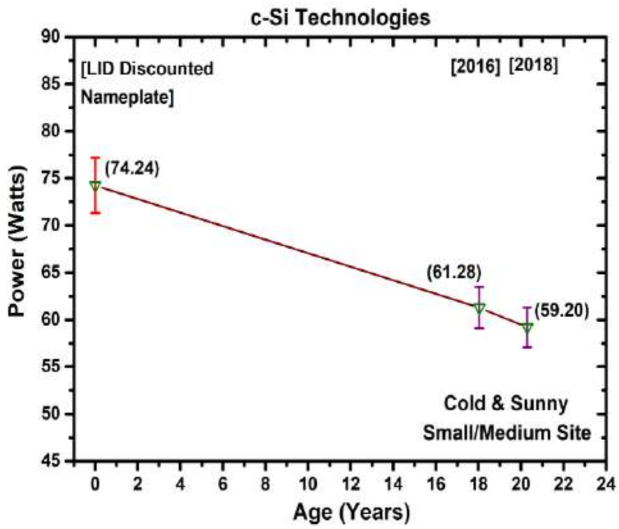
c-Si Technologies
[LID Discounted Nameplate]
[2016] [2018]
(74.24)
(61.28)
(59.20)
Cold & Sunny
Small/Medium Site
Power (Watts)
Age (Years)

(k)

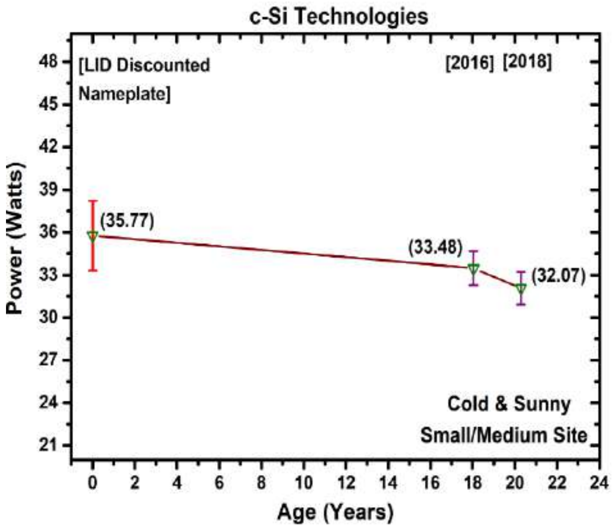
c-Si Technologies
[LID Discounted Nameplate]
[2016] [2018]
(35.77)
(33.48)
(32.07)
Cold & Sunny
Small/Medium Site
Power (Watts)
Age (Years)

(l)

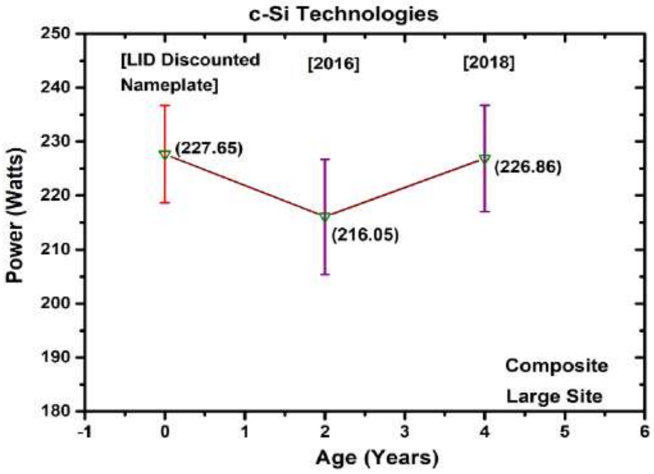


(m)

Fig. 4.21. Three point analysis of the c-Si PV modules installed at 13 sites, (a) through (m) which were repeated in 2016 and 2018 All-India Surveys

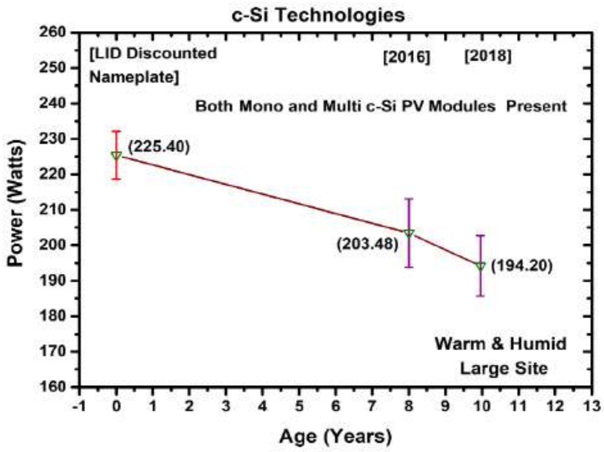


(a)

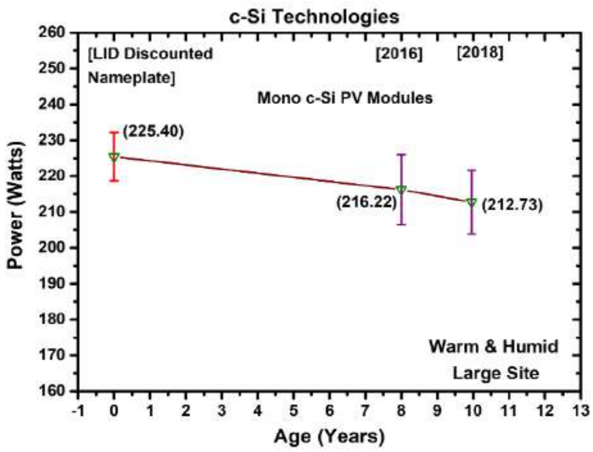


(b)

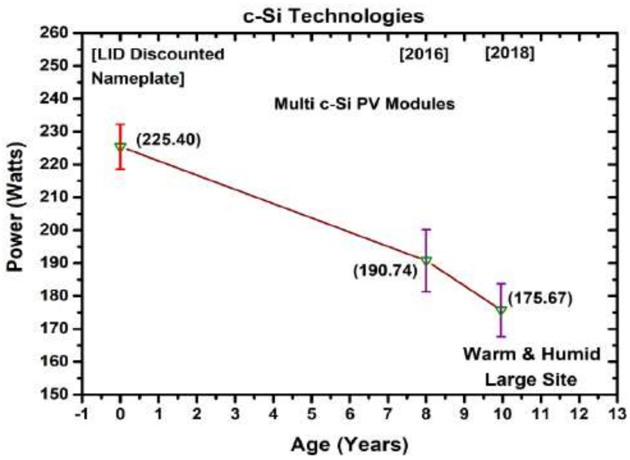


(c)

Fig. 4.22. Three point analysis of the c-Si PV modules installed at one site which was repeated in 2016 and 2018 All-India Surveys, (a) mono and multi combined, (b) only mono and (c) only multi c-Si PV modules

Fig. 4.22 shows the three point data analysis of a site consists of both multi and mono c-Si PV modules. Fig. 4.22 (a) shows the average maximum power of the site including multi and mono c-Si PV modules, Fig. 4.22 (b) and (c) show the average maximum power of only mono and only multi c-Si PV modules inspected in detail from the site.

Table 4.3 shows the average degradation rates calculated for the 14 repeat sites using a best linear fit to the three data points, compared to a two-point analysis using only the 2018 data and the initial nameplate data (The latter is the value used in the plots in earlier sections). It can be seen that the values compare quite well in most cases.

Table 4.3. Comparison of average degradation rates calculated for the 14 repeat sites using a best linear fit to the three data points, to a two-point analysis using only the 2018 data and the nameplate data

| Site Wise Figure Numbers | Degradation Rate With 2018 Data (%/year) | Degradation Rate With Three Point Linear Fit (%/year) |
|---|---|---|
| Fig. 4.21. (a) | 2.55 | 2.63 |
| Fig. 4.21. (b) | 0.42 | 0.42 |
| Fig. 4.21. (c) | 0.90 | 0.92 |
| Fig. 4.21. (d) | 1.50 | 1.38 |
| Fig. 4.21. (e) | 1.38 | 1.44 |
| Fig. 4.21. (f) | 1.04 | 1.04 |
| Fig. 4.21. (g) | 1.84 | 1.56 |
| Fig. 4.21. (h) | 1.46 | 1.54 |
| Fig. 4.21. (i) | 1.52 | 1.50 |
| Fig. 4.21. (j) | 1.02 | 0.98 |
| Fig. 4.21. (k) | 0.51 | 0.45 |
| Fig. 4.21. (l) | 0.98 | 0.98 |
| Fig. 4.21. (m) | 0.09 | 0.09 |
| Fig. 4.22. (a) | 1.34 | 1.34 |
| Fig. 4.22. (b) | 0.58 | 0.55 |
| Fig. 4.22. (c) | 1.86 | 2.13 |

## 4.9 Summary

From the analysis of electrical degradation of PV modules inspected in 2018 All-India Survey, we can draw the following major conclusions.

- The Young c-Si PV modules (age 1-5 years) show higher power ($P_{max}$) degradation rate than that of Old c-Si PV modules (age > 5 years).
- Key reasons contributing to higher degradation rate observed in certain younger sites are PID and finger / interconnect damage.
- The overall and linear degradation rates of $P_{max}$ for c-Si PV modules observed in the 2018 Survey are broadly similar to those observed in the 2016 Survey.
- The linear degradation rate of $P_{max}$ for c-Si PV modules deployed in Hot climatic zones (Warm & Humid, Hot & Dry, and Composite) is much higher (1.57 %/year) than in the Non-Hot climatic zones (Moderate, Cold & Sunny, and Cold & Cloudy) (0.52 %/year).
- The Roof-Rack mounted PV modules degrade at a much faster rate than Ground-Rack mounted PV modules.
- System size (Small/Medium, or Large) does not appear to have much influence on the degradation rate of PV modules.
- The $P_{max}$ degradation of Young PV modules is mainly due to the *FF* degradation, and the $P_{max}$ degradation of Old PV modules is due to both *FF* and $I_{sc}$ degradation.
- The main reasons for observed high FF degradation are i) Mismatch between the solar cells in the PV modules due to cracks, ii) High series resistance ($R_s$) of PV modules due to cracks and corrosion, iii) Low shunt resistance ($R_{sh}$) of PV modules due to Potential Induced Degradation (PID), and other shunt paths, iv) Light Induced Degradation (LID), v) Inaccuracy of the translation procedure (Modified IEC 60891 Procedure 1 and vi) possible over-rating of modules.
- The main reasons for $I_{sc}$ degradation are i) Encapsulant browning in hot climates, ii) Enhanced UV radiation dosage for modules in Cold & Sunny climatic zone, iii) Potential Induced Degradation (PID) at some of the sites, and iv) Light Induced Degradation (LID).
- The thin film PV modules generally show low $P_{max}$ degradation compared to c-Si PV modules, though this is more likely to be a manufacturer rather than technology related issue.
- Four-point and three-point data analysis of modules in repeat sites gives fairly consistent results compared to a simple two-point analysis, thereby validating the results even where only two-point data (single measurement plus initial nameplate value) are available.

# 5. Analysis of Visual Degradation

## 5.1 Introduction

Many degradation modes in PV modules have visible signatures, making it easy to identify them through visual inspection. These degradation modes can serve as indicators for loss in electrical power output. They also provide valuable information for identifying the root cause of electrical degradation. For the 2018 All-India Survey, the visual inspection was done on basis of a modified NREL visual inspection check list [53] attached in Appendix-A. This chapter discusses various visual degradation modes observed in the field, and analysis on the basis of technology, age, climate zone, size of installation. We discuss visual degradation for silicon modules first and then in brief for thin film modules.

## 5.2 Visual Degradation Observed in Crystalline Silicon Modules

When exposed to outdoor environments, different components of PV modules degrade at different rates. Environmental factors like UV dosage, ambient and operating temperature of the module, and the outdoor humidity levels (with intermittent rainfall) affect the PV modules in different ways. The key degradation modes observed for crystalline silicon modules are discussed in the following sections.

### 5.2.1 Influence of Climatic Zone and Age on Visual Degradation Modes

***a) Discoloration of Encapsulant***

One of the most common causes of reduction in short circuit current ($I_{sc}$) is encapsulant discoloration (browning), which consequently reduces the power output of the field-aged PV modules. The PV module encapsulant has evolved over the years and undergone several changes in its composition to reduce cost, improve performance and provide adequate durability. Ethyl Vinyl Acetate (EVA) is the most widely used encapsulant due to its favourable properties and low cost. It is sensitive to photo-thermal degradation and has to be mixed with the proper additives to prevent untimely discoloration [54]. Even some young modules which were surveyed in the field show encapsulant discoloration as indicated in Fig. 5.1 and Table 5.1. Table 5.1 shows the percentage of modules affected by encapsulant discoloration (discoloration index less than 0.05 are considered “Not discoloured” as shown in Fig. 5.2) in different age groups and climatic zones. It is evident that the Hot zone (Warm & Humid, Hot & Dry, Composite) has more percentage of modules affected by encapsulant browning. The early onset of discoloration in the young modules in Hot zone (Table 5.1 and Table 5.2) raises concern about the material quality used in newer modules. However, after 10 years of exposure, most of the modules show discoloration even in the Non-Hot climates. The discoloured modules in the Non-Hot zone are located in Ladakh, where the high altitude leads to higher UV exposure on the PV modules. Interestingly one site in the Cold & Dry climate shows no encapsulant discoloration even after 20 years of field deployment (Fig. 5.1 (e)). This leads us to suspect that either the encapsulant used may not have been EVA, but some other high grade alternative, or the Cerium content of the front glass may be very high which could prevent UV rays from passing into the module, thereby preventing discoloration of the encapsulant [54].

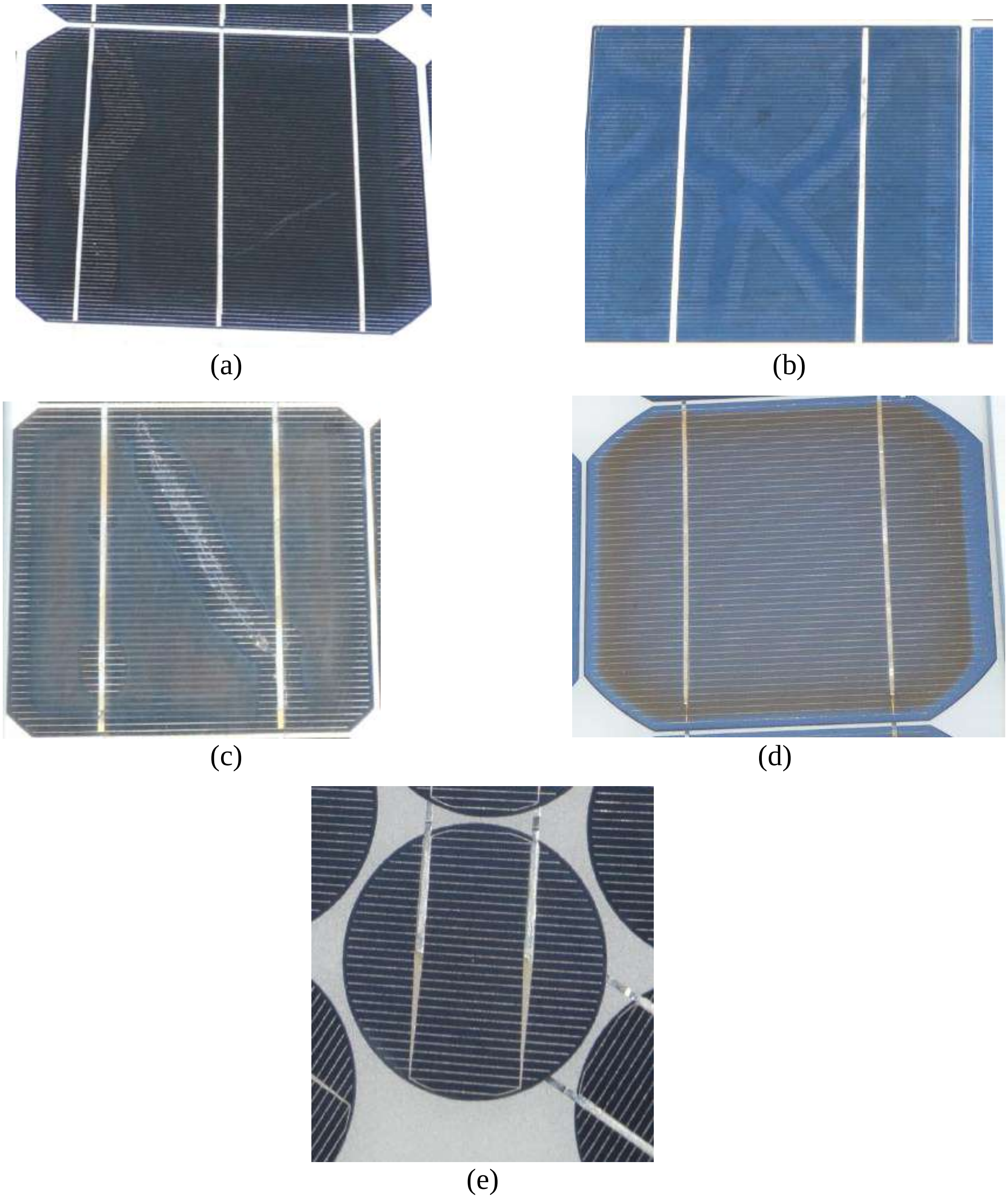

(a) (b) (c) (d) (e)

Fig. 5.1. Example of encapsulant discoloration observed during the survey- (a) Discoloration in 4-year-old module (with photo-bleaching effect along crack near bus bar) (b) discoloration in a 6 year old module with photo-bleaching (c) Discoloration of module and crack leading to photo-bleaching. (d) encapsulant discoloration of 20 year module in Cold & Sunny climate (e) no encapsulant discoloration of 20 year module in Cold & Sunny climate

Table 5.1. Percentage of c-Si modules affected by encapsulant discoloration in different climatic zones and age group (Total Number of samples is given in bracket)

| Climatic Zone | 0-5 year old | 5-10 year old | 10-15 year old | 15-20 year old | 20+ year old |
|---|---|---|---|---|---|
| **Warm & Humid** | 43% (59) | 84% (101) | 100% (33) | NA | NA |
| **Hot & Dry** | 5% (135) | 100% (179) | NA | 100% (18) | NA |
| **Composite** | 23% (188) | 3% (163) | NA | NA | NA |
| **Moderate** | 0% (27) | NA | NA | NA | NA |
| **Cold & Sunny** | NA | 0% (30) | 100% (26) | NA | 60% (20) |

It is necessary to quantify the severity of visual degradation in order to establish correlations with the electrical degradation. During the survey, it has been observed that discoloration is usually seen in all the cells of the affected modules, but some of the cells may show slightly larger discolored area or intensity (for example, cells with nameplate sticker or junction box at the back usually show slightly higher discoloration). There is some subjectivity involved in this visual estimation process, and it is possible that different persons will arrive at different estimations of the degree and area of discoloration for the same module. Hence the process of determining the Discoloration Index has been automated through an in-house software, which reads the colour of each pixel of the photographs of modules, and computes the average extent of yellowness in the module, which is referred to as the "Pseudo Yellowness Index" (PYI) [55]. Since the edges of the solar cells usually are photo-bleached, leaving the initial blue colour intact, this is used as the reference colour to identify the change in the colour of the modules due to field exposure and a Discoloration Index (DI) is defined, as indicated below. The detailed procedure for determination of the discoloration index is explained by S. Chattopadhyay, et al. [55].

$$DI = \frac{PYI_{Present} - PYI_{initial}}{PYI_{range}} \qquad \ldots\ldots\ldots (5.1)$$

Where,

$PYI_{present}$ = present value of Pseudo Yellowness Index

$PYI_{initial}$ = initial value of Pseudo Yellowness Index

$PYI_{range}$ = difference in PYI between the worst possible browning and the initial (blue) colour.

Examples of the Discoloration Index *DI* for some sample images are shown in Fig. 5.2, which shows that this technique is able to differentiate between various levels of discoloration in solar cells. The average discoloration severity in different age groups and climatic zones is given in Table 5.2. The total number of sample modules in Table 5.2 is lower than the total number of modules in Table 5.1, as the Discoloration Index could be computed only for modules which do not show high colour difference between grains in the crystalline silicon solar cells, and also for images captured at near-perpendicular angles under proper irradiance conditions (greater than 700 W/m$^2$). It is also observed that the modules have minor variations in solar cell colour even at the time of installation, with DI values less than 0.05. Modules with DI up to 0.05 have negligible $I_{sc}$ loss (less than 1%) and hence, only DI values higher than 0.05 have been considered in the analysis shown in Table 5.2. From Table 5.2, in "0-5 years" age group, it is clear that the severity of effect of the various climatic zones is in the order: Hot & Dry > Warm & Humid > Composite > Cold & Sunny > Moderate. The highest average discoloration is seen in modules with more than 20 years of field exposure. It can be observed that DI value of young modules in Hot zone (Hot & Dry, Warm & Humid and Composite) are higher than Non-Hot Zone (Moderate, Cold and Dry, Cold and Cloudy).

(a) DI = <0.05 (b) DI ~ 0.1 (c) DI ~ 0.3

Fig. 5.2. Examples of Discoloration Index for different extent of encapsulant browning

Table 5.2. Average severity of discoloration (Discoloration Index) in c-Si modules in different climatic zones and age groups (number of samples is given in brackets)

| Climatic Zone | 0-5 year old | 5-10 year old | 10-15 year old | 15-20 year old | 20+ year old |
|---|---|---|---|---|---|
| **Warm & Humid** | 0.13 (37) | 0.11 (21) | 0.12 (30) | NA | NA |
| **Hot & Dry** | 0.15 (3) | 0.11 (32) | NA | 0.13 (13) | NA |
| **Composite** | 0.12 (21) | 0.09 (1) | NA | NA | NA |
| **Moderate** | 0 (27) | NA | NA | NA | NA |
| **Cold & Sunny** | NA | 0.09 (27) | NA | NA | 0.32 (10) |

Based on the above, we can conclude that the Hot zone is harsher than the Non-Hot zone for the encapsulant (as per Fig. 5.1 and Table 5.2). This is not unexpected. The order of harshness is found to be: Hot & Dry > Warm & Humid > Composite > Cold & Sunny > Moderate.

***b) Front-side Delamination***

Delamination on the front side occurs due to loss of adhesion between the encapsulant and glass or between the encapsulant and solar cell. This loss of adhesion between different layers of the module increases the reflection losses from the affected area and the current gets reduced. In the 2018 Survey, front-side delamination has mostly been seen in the form of bubbles along cell cracks as shown in refer Fig. 5.3 (a). Also, at one site, all modules showed delamination along the gridlines as shown in Fig. 5.3 (b). Table 5.3 provides the statistics of front-side delamination in the surveyed c-Si modules. In most sites, small bubbles have been observed along cell cracks and snail tracks (which are also associated with cell cracks).

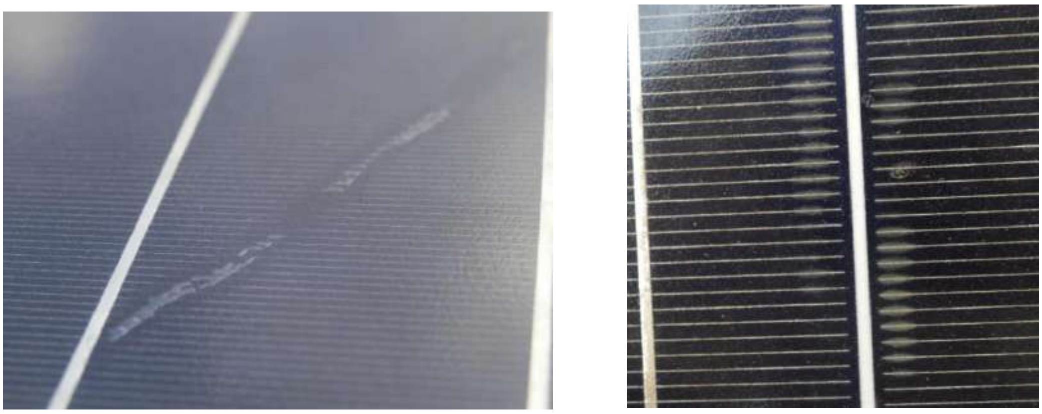

(a) (b)

Fig. 5.3. Examples of delamination observed during the survey (a) along snail track, (b) along fingers at cell edge

Table 5.3. Percentage of c-Si modules affected by delamination in different climatic zones and age groups (number of samples is given in brackets).

| Climatic Zone | 0-5 year old | 5-10 year old | 10-15 year old | 15-20 year old | 20+ year old |
|---|---|---|---|---|---|
| **Warm & Humid** | 0% (59) | 2% (101) | 79%(33) | NA | NA |
| **Hot & Dry** | 0% (135) | 16% (179) | NA | 0% (18) | NA |
| **Composite** | 10% (188) | 14% (163) | NA | NA | NA |
| **Moderate** | 0%(27) | NA | NA | NA | NA |
| **Cold & Sunny** | NA | 0% (30) | 0% (26) | NA | 0% (20) |

Table 5.4 provides the statistics for modules affected by delamination in the Hot and Non-Hot zones. It can be observed that this problem of delamination is mainly seen in the Hot climatic zone. Further analysis of the severity of delamination has not been done, since significant delamination (covering more than 5% cell area) has rarely been observed in the 2018 Survey, and in most cases, delamination (bubbles) has been found associated with snail tracks. Therefore, the delamination by itself is not responsible for significant power loss in PV modules observed in All-India Survey 2018.

Table 5.4. Delamination observed in survey in different climatic Hot and Non-Hot climatic zones

| Climate zone | 0-5 year old | 5-10 year old | 10-15 year old | 15-20 year old | 20+ year old |
|---|---|---|---|---|---|
| **Hot Zone** | 5% (382) | 12% (443) | 79% (33) | 0% (18) | NA |
| **Non-Hot Zone** | 0% (27) | 0% (30) | 0% (26) | NA | 0% (20) |

***c) Snail Tracks and Visible Cracks***

The encapsulant may be affected in different ways due to cracks in solar cells. In the old modules having discoloration, cracks in the cells allow oxygen to pass through to the discoloured encapsulant at the top of the cells, and this oxygen then bleaches the discoloration in the presence of sunlight [54]. On the other hand, in many of the newer modules, moisture and other gases are able to migrate through the cracks in the cells and cause a snail track formation on top of the cells [56]. Also, the spacing between the cells can serve as a pathway for moisture penetration up to the metallization on top of cells from the edges, and in some cases this leads to framing type snail tracks along the edges of the cells. Examples of the two types of snail tracks are shown in Fig. 5.4 (a). In the rest of the chapter, the term "snail tracks" shall be used for non-framing type snail tracks (unless otherwise stated), while the framing type snail tracks would be referred to as "framing" shown in Fig. 5.4 (b). In the survey, we have found good correlation between the cell cracks and snail tracks. Fig. 5.5 shows some examples of cracks (observed in EL image) and snail tracks (observed visually), in the same modules. The snail tracks are found to be associated with cracks in the solar cells. Both snail tracks (non-framing type) and photo-bleaching effects of the encapsulant serve as visual indications of cracks in the cells.

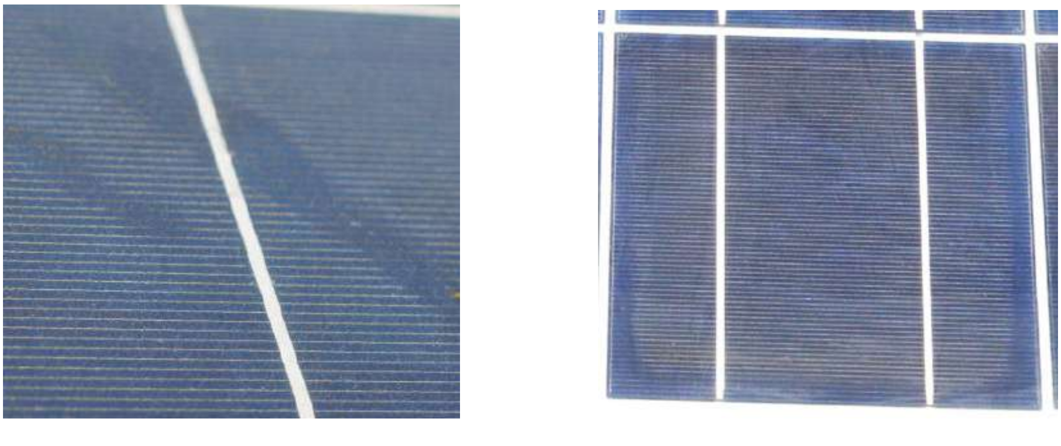

(a) (b)

Fig. 5.4. Snail track observed during the survey (a) Snail track in a young module in Hot and Dry zone and (b) framing type snail track in a young module in Warm and Humid climate

It is important to note that while the EL image also shows the area affected by the crack, snail tracks only delineate the crack's location but do not provide any indication about the severity of the crack (in terms of actual area affected by the crack). In this section, we shall first present the statistics related only to the snail tracks and then the overall statistics for visible indications of cracks (which includes both snail tracks and photo-bleaching). It is important to note that the cracks in the solar cells may not always lead to a visible sign (in terms of snail tracks or photo-bleaching) and EL imaging is the only way to check reliably for such cracks (discussed in more detail in Chapter 6).

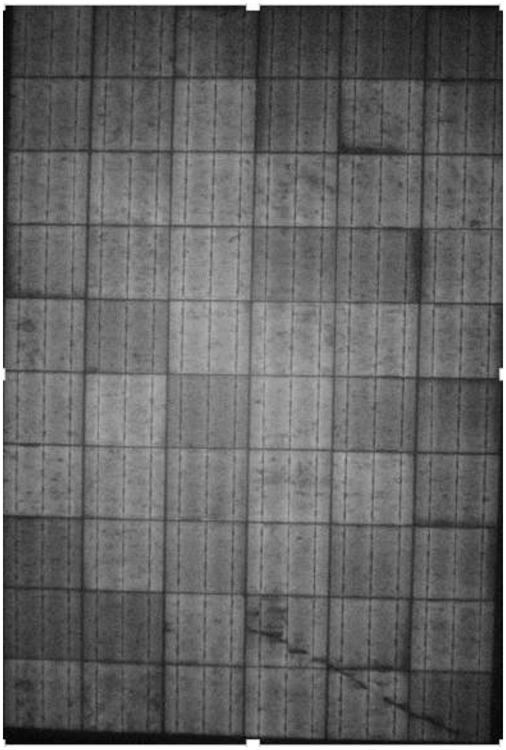

(a)

(b)

Fig. 5.5. Examples of cracks (shown in EL images on left side) and snail tracks (shown in digitally enhanced contrast-adjusted photographs on right side) observed during the survey

*Snail Tracks:*

The statistics of the snail tracks (generally associated with cracks in solar cells) are presented in Table 5.5. Snail tracks are predominantly seen in young modules with age less than 10 years, and their frequency is higher in the young modules in Composite and Hot & Dry climatic. Snail tracks have not been observed in the colder climates. Statistics of snail track in Hot zone and Non-Hot zone are presented in Table 5.6, where we see that modules in Hot zones are more likely to show snail trails.

Table 5.5. Percentage of c-Si modules affected by snail tracks in different climatic zones and age groups (number of samples is given in brackets)

| Climatic Zone | 0-5 year old | 5-10 year old | 10-15 year old | 15-20 year old | 20+ year old |
|---|---|---|---|---|---|
| **Warm & Humid** | 0 % (59) | 1% (101) | 0% (33) | NA | NA |
| **Hot & Dry** | 1% (135) | 6% (179) | NA | 0% (18) | NA |
| **Composite** | 12% (188) | 7% (163) | NA | NA | NA |
| **Moderate** | 0% (27) | NA | NA | NA | NA |
| **Cold & Sunny** | NA | 0% (30) | 0% (26) | NA | 0% (20) |

Table 5.6. Percentage of modules affected by snail tracks in Hot and Non-Hot zones

| Climate zone | 0-5 year old | 5-10 year old | 10-15 year old | 15-20 year old | 20+ year old |
|---|---|---|---|---|---|
| **Hot Zone** | 6% (382) | 5% (443) | 0% (33) | 0% (18) | NA |
| **Non-Hot zone** | 0% (27) | 0% (30) | 0% (26) | NA | 0% 20) |

The percentage of cells (out of all cells in all modules inspected in the zone) affected by snail tracks in a module has been considered as the criterion for determining severity of snail tracks. The average severity levels of snail tracks for the various climatic zones and age groups have been given in Table 5.7. The highest severity levels are seen in Composite, Hot and Dry.

Table 5.7. Average severity of snail tracks in c-Si

| Climatic Zone | 0-5 year old | 5-10 year old | 10-15 year old | 15-20 year old | 20+ year old |
|---|---|---|---|---|---|
| **Warm & Humid** | 0 (59) | 0.6 (101) | 0% (33) | NA | NA |
| **Hot & Dry** | 0.4 (135) | 1.2 (179) | NA | 0 (18) | NA |
| **Composite** | 2.4 (188) | 3.8 (163) | NA | NA | NA |
| **Moderate** | 0 (27) | NA | NA | NA | NA |
| **Cold & Sunny** | NA | 0 (30) | 0 (26) | NA | 0 (20) |

*Framing:*

Framing type snail tracks occur along the edges of the solar cells, and are not associated with cracks. The statistics for such snail tracks for the various climatic zones and age categories are presented in Table 5.8, and the climatic zones have been combined into Hot and Non-Hot in Table 5.9. Framing has been observed in the young modules with age less than 10 years, predominantly in the Hot zone.

Table 5.8. Percentage of modules affected by framing type snail tracks

| Climate zone | 0-5 year old | 5-10 year old | 10-15 year old | 15-20 year old | 20+ year old |
|---|---|---|---|---|---|
| **Warm & Humid** | 0 % (59) | 7% (101) | 0% (33) | NA | NA |
| **Hot & Dry** | 4% (135) | 15% (179) | NA | 0% (18) | NA |
| **Composite** | 32% (188) | 12% (163) | NA | NA | NA |
| **Moderate** | 4% (27) | NA | NA | NA | NA |
| **Cold & Sunny** | NA | 0% (30) | 0% (26) | NA | 0% (20) |

Table 5.9. Percentage of modules with framing type snail tracks in Hot and Non-Hot zones

| Climate zone | 0-5 year old | 5-10 year old | 10-15 year old | 15-20 year old | 20+ year old |
|---|---|---|---|---|---|
| **Hot Zone** | 15% (382) | 12% (443) | 0% (33) | 0% (18) | 0% (0) |
| **Non-Hot zone** | 0% (27) | 0% (30) | 0% (26) | 0% (0) | 0% (20) |

*Visible Cracks (Snail tracks and Photo-bleaching)*

As discussed earlier, snail tracks in young modules and photo-bleaching effects in the old modules can serve as visual indication of cracks, and in some cases the cracks in solar cells are wide enough to be visible without sophisticated tools, as shown in Fig. 5.6. Modules showing visible cracks in the solar cells, or indication of cracks in terms of snail tracks and photo-bleaching, have been identified and their statistics is shown in Table 5.10. About 27% (average for 0-10 year field aged modules) of the modules installed in the last decade show visible signs of cracks compared to about 34% (average for modules field aged greater than 10 years, dominated by Warm & Humid climate) of the older modules.

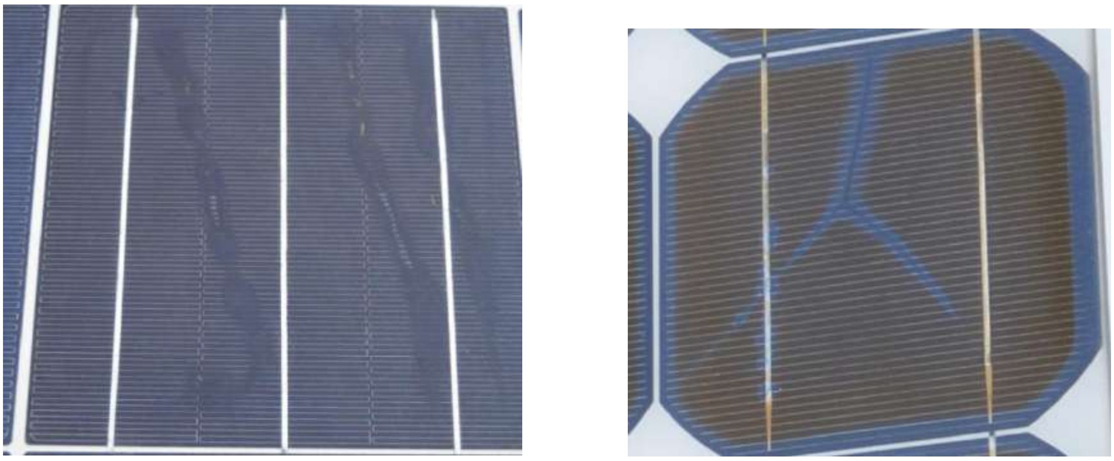

(a) (b)

Fig. 5.6. Cracks in the solar cell visible with naked eye, (a) Crack made visible by snail track and delamination, and (b) Crack made visible by photo-bleaching of discolored encapsulant

Table 5.10. Percentage of modules with visible indications of cracks (snail tracks and photo-bleaching) indifferent climatic zones and age groups (number of samples is given in brackets)

| Climatic Zone | 0-5 year old | 5-10 year old | 10-15 year old | 15-20 year old | 20+ year old |
|---|---|---|---|---|---|
| **Warm & Humid** | 34 % (59) | 49% (101) | 79% (33) | NA | NA |
| **Hot & Dry** | 2% (135) | 36% (179) | NA | 0% (18) | NA |
| **Composite** | 26% (188) | 31% (163) | NA | NA | NA |
| **Moderate** | 0% (27) | NA | NA | NA | NA |
| **Cold & Sunny** | NA | 0% (30) | 10% (26) | NA | 25% (20) |
| **All Climates** | 27% (882) | | 34% (97) | | |

***d) Discoloration on Metallization***

Metallization in solar panels includes the gridlines, busbars and interconnect ribbons, and their function is to conduct the current generated in the solar cells to the terminal box. Metallization discoloration can occur due to corrosion or poor material quality and sometimes due to improper manufacturing processes. Some examples of metallization discoloration are shown in Fig. 5.7. The statistics for metallization discoloration (including interconnects and output terminals inside junction box) for the different age groups and climatic zones is shown in Table 5.11. The discoloration of metallization in the young modules (0-5 years age category) is predominantly due to non-corrosion issues (like discoloration due to solder flux etc.) whereas in the older modules, corrosion is the predominant reason behind discoloration. As evident from the table, many young modules in the hot climates have discoloration issues that hint at poor material quality. Most of the panels aged more than 10 years have suffered from corrosion, irrespective of the climatic zone. In some cases, metallization discoloration is also observed along a cell crack. This may be due to the ingress of moisture through the crack in the solar cell.

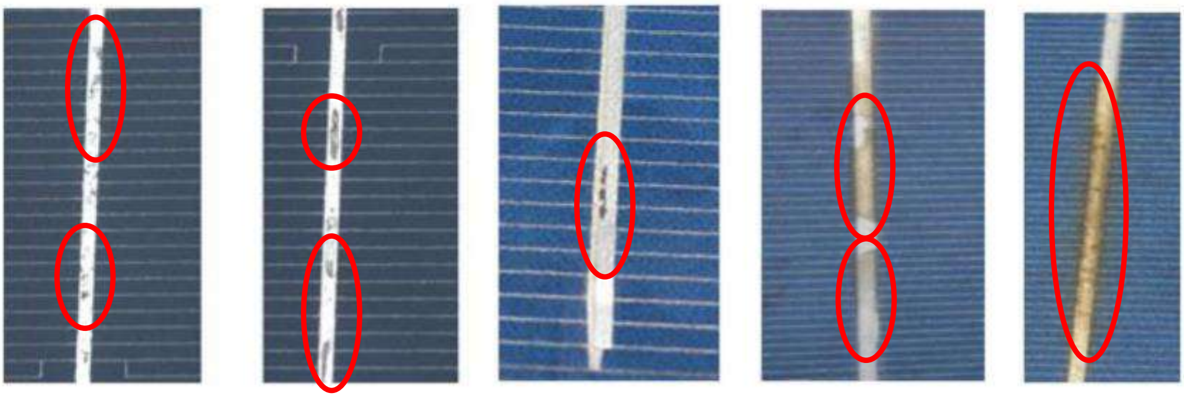

Fig. 5.7. Metallization discoloration observed during the survey

Table 5.11. Percentage of modules in c-Si modules affected by discoloration on metallization in different climatic zones and age groups (number of samples is given in brackets)

| Climatic Zone | 0-5 year old | 5-10 year old | 10-15 year old | 15-20 year old | 20+ year old |
|---|---|---|---|---|---|
| **Warm & Humid** | 46% (59) | 60% (101) | 100% (33) | NA | NA |
| **Hot & Dry** | 82% (135) | 73% (179) | NA | 100% (18) | NA |
| **Composite** | 39% (188) | 30% (163) | NA | NA | NA |
| **Moderate** | 0%(27) | NA | NA | NA | NA |
| **Cold & Sunny** | NA | 0% (30) | 100% (26) | NA | 100% (20) |

Metallization discoloration has been mostly observed near cell cracks in the young modules, and is more predominant in the Hot climatic zone.

***e) Glass Degradation***

The front glass performs the role of protecting the solar cells from environmental factors like humidity and dust, while allowing the solar radiation to pass through to the cells. The deposition of dust and the use of hard water in cleaning the modules can lead to haziness in the glass (which can reduce the transmission of light to the cells). Also, improper handling can lead to scratches, chips and cracks (shattering) in the front glass, as shown in Fig. 5.8. Table 5.12 gives the statistics for the various degradation modes of front glass observed in the survey. Haziness is the most prevalent problem observed in the front glass of crystalline silicon modules, occurring mostly at the bottom edge of the module

Table 5.12. Percentage of modules with different glass degradation

| Defect | % of Modules (Total Modules: 979) |
|---|---|
| Glass Break | 0 |
| Foreign Particle | 0.1 |
| Glass Scratch | 3.8 |
| Brown spot | 0.7 |
| Glass Haziness | 29 |
| White spot | 4.3 |

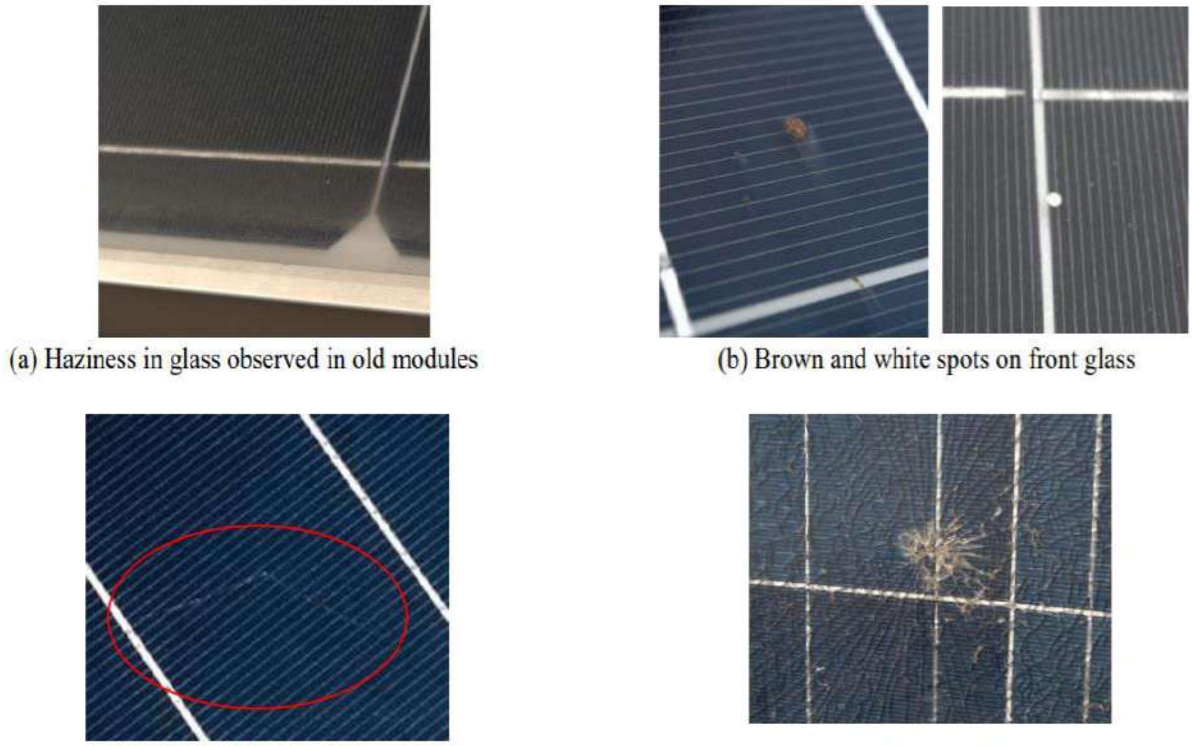

(a) Haziness in glass observed in old modules

(b) Brown and white spots on front glass

(c) Scratch on glass

(d) Shattered glass

Fig. 5.8. Glass degradation observed during the Survey

### 5.2.2 Correlation of Visual Degradation with Electrical Performance Degradation

***a) Encapsulant Discoloration***

Encapsulant browning primarily causes reduction in transmittance of light to underlying solar cells. This results in reduction of short circuit current and power output. The PV modules have been categorised into 5 categories (Table 5.13) based on their DI value.

Table 5.13. Categorization based on Discoloration Index

| **Discoloration Index** | 0-0.05 | 0.05-0.25 | 0.25-0.5 | 0.5-0.75 | 0.75-1 |
|---|---|---|---|---|---|
| **Discoloration Category** | 1 | 2 | 3 | 4 | 5 |

Figs. 5.9 and Figs. 5.10 show the effect of encapsulant discoloration on electrical performance degradation (total % and not %/year) for c-Si modules. In these plots, the average degradation values are indicated using the red horizontal lines (and the top and bottom edges of the red diamond indicate the 95% confidence interval). It may be noted that there are no modules in discoloration categories 4 and 5. It is seen that $P_{max}$ and $I_{sc}$ degradation both increase with Discoloration Category. In some cases, mostly in the young modules, the $P_{max}$ degradation has been found to be negative (which may be due to the uncertainty in the name plate data and also the uncertainty introduced by STC translation procedures which are discussed in detail in Chapter 3). It is interesting to note that the module with worst browning has suffered close to 30% drop in $P_{max}$ (in ~20 years of field exposure which means a degradation rate of ~1.4 %/year, after discounting 2% LID). It should be noted that this 30% drop is not entirely due to browning, as the power output is affected by many other degradation modes including metallization corrosion, solar cell cracks and other defects.

Many of the young modules with minor discoloration (category 1 & 2) show very high FF degradation and negative $V_{oc}$ loss. The negative degradation values may be due to name plate uncertainty, translation errors and/or underrating of the modules by the manufacturer. The worst discoloured modules have suffered about 10% degradation in $I_{sc}$ in 20 years of field exposure, so the average Linear $I_{sc}$ Degradation Rate for these modules is 0.5 %/year (after discounting 2% LID). The high *FF* degradation even in Category 1 modules may be due to cracks (more prevalent in young modules), metallization corrosion (mostly observed in old modules) or other localized defects. An increasing trend is seen for $V_{oc}$ degradation, which may be due to the degradation of the solar cells upon aging. From Fig. 5.9 (b) it can be observed that with the increase in discoloration index the $I_{sc}$ degradation increases affecting the net power output.

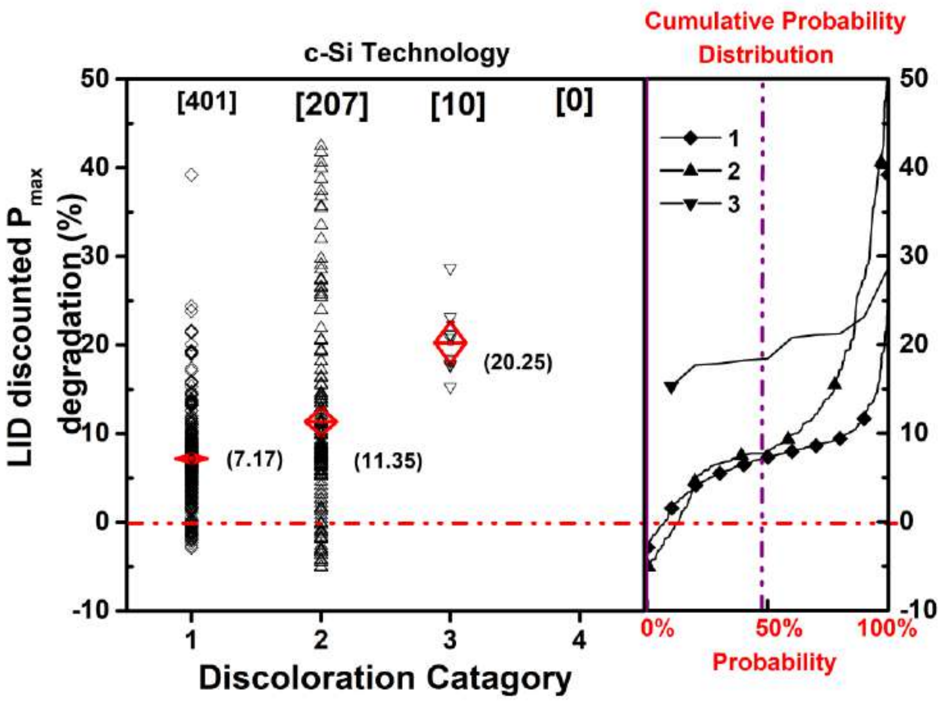


(a)

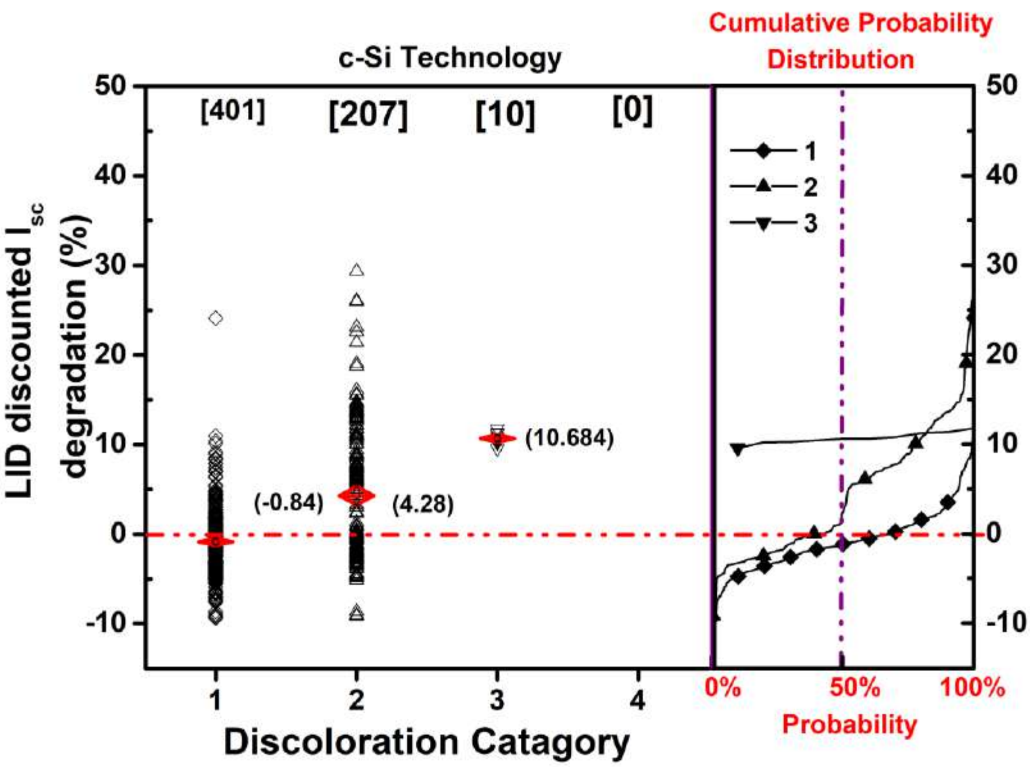


(b)

Fig. 5.9. Plot of electrical performance degradation versus severity of discoloration – (a) LID discounted $P_{max}$ degradation, (b) LID discounted $I_{sc}$

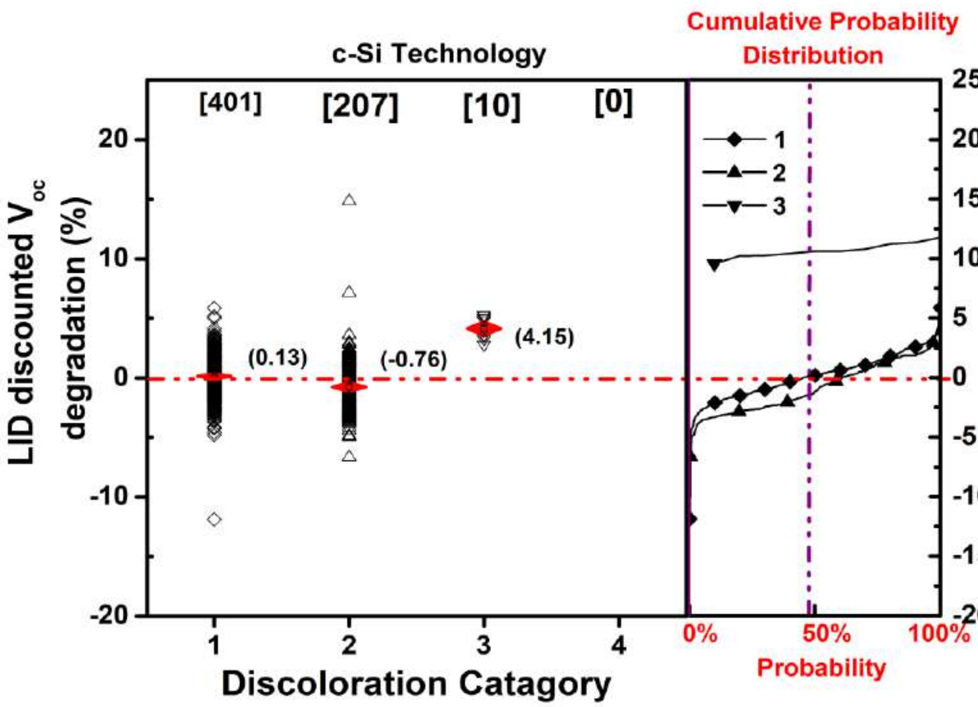


(a)

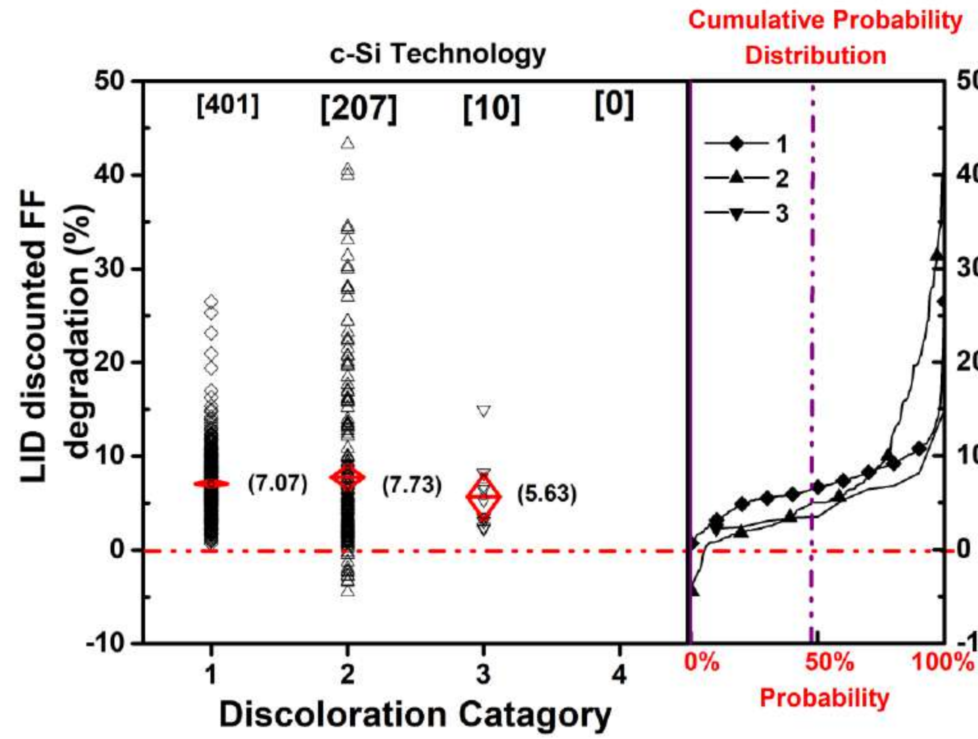


(b)

Fig. 5.10. Plot of electrical performance degradation versus severity of discoloration – (a) LID discounted $V_{oc}$ degradation (b) LID discounted *FF* degradation

***b) Metallization Discoloration***

Discoloration of metallization in modules is usually caused by corrosion in the older modules and also sometimes due to improper manufacturing techniques (which leave behind soldering flux on the metallization etc.). Metallization corrosion results in an increase in the series resistance of the module. The degradation in electrical parameters for modules with and without metallization discoloration is given in Figs. 5.11 and Figs. 5.12. It can be observed that modules with metallization discoloration have higher $P_{max}$, $I_{sc}$, and *FF* degradation (the p-values for Mann-Whitney U test are 0.00017, 0.006, 1.10e-06, respectively which means that the difference in degradation is statistically significant). Young modules show some discoloration on the interconnects which seems to correlate with the higher power degradation in these modules. This may be indicative of poor material/manufacturing quality of these modules.

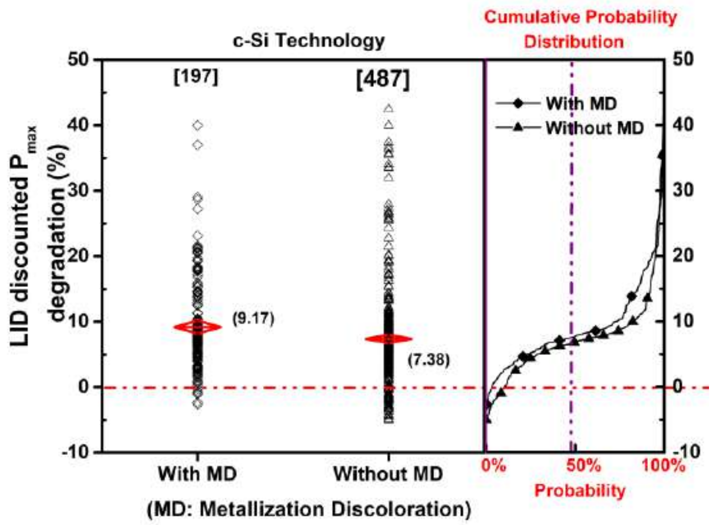


(a)

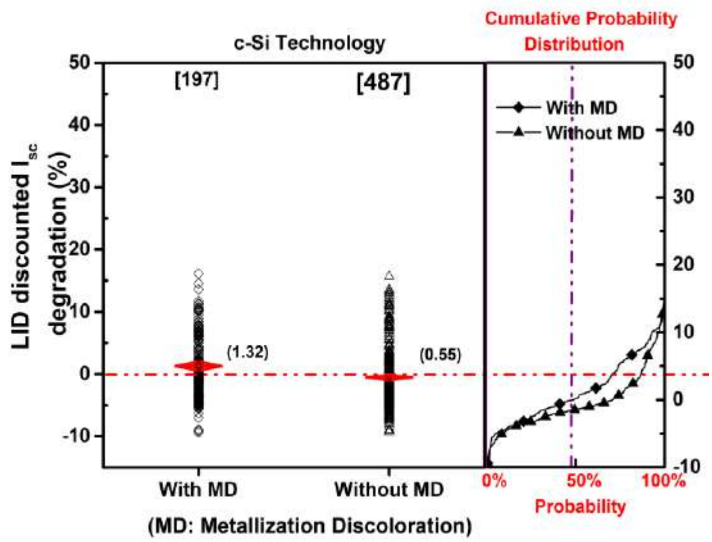


(b)

Fig. 5.11. Plots of electrical degradation versus severity of metallization discoloration: (a) $P_{max}$ degradation (%), (b) $I_{SC}$ degradation (%)

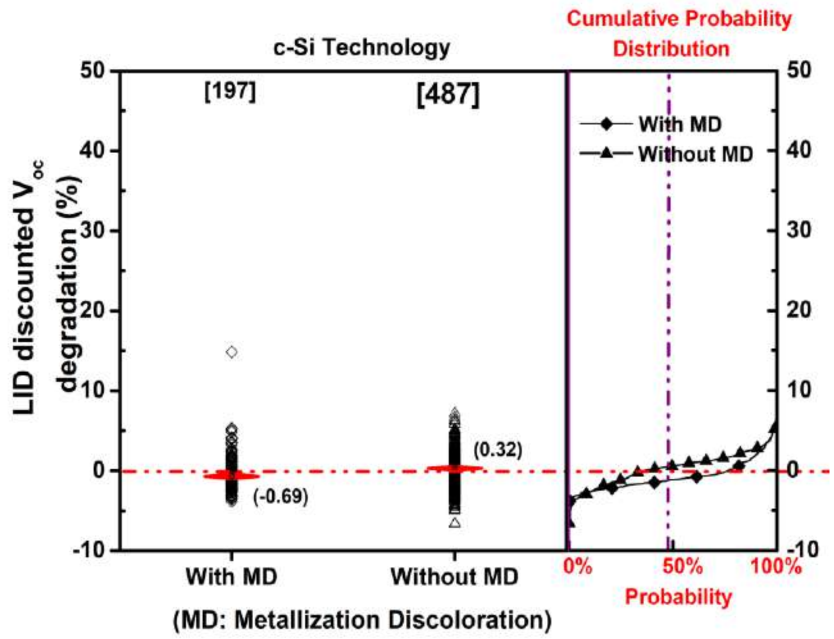


(a)

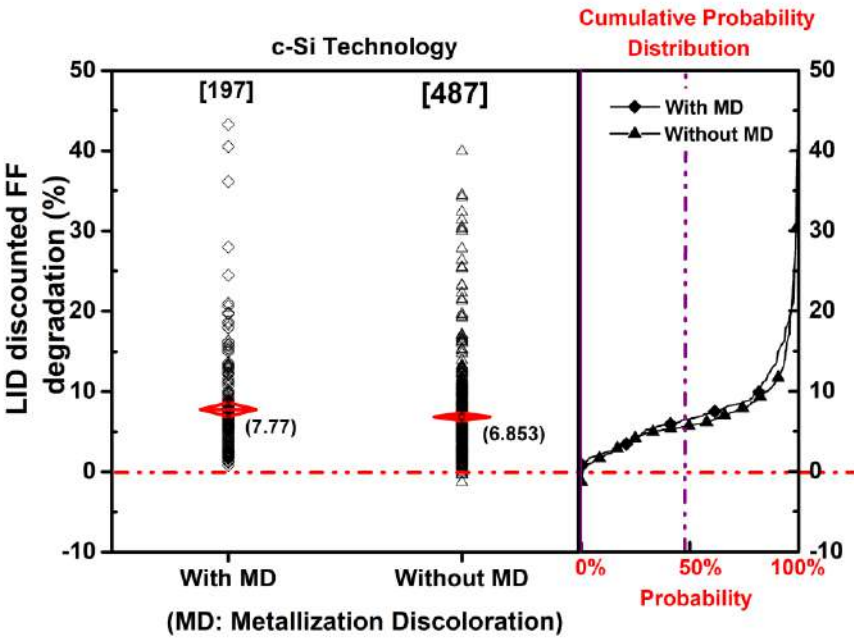


(b)

Fig. 5.12. Plots of electrical degradation versus severity of metallization discoloration: (a) $V_{OC}$ degradation (%), and (b) *FF* degradation (%)

***c) Visible signs of Cell Cracks (including Snail Tracks & Photo-bleaching)***

Snail tracks are observed in young modules for which the underlying cause is cracks in the solar cells. Also, sometimes these cracks in solar cells cause photo-bleaching in the old discoloured modules. Both (snail track and photo bleaching) serve as visible indicators of cracks in solar cell, even when the cracks themselves are not visible except by EL. However, it should also be kept in mind that not all cracks will lead to snail tracks or any other visible signs. The Linear Degradation Rates are plotted for modules with and without these visible signs of cracks in Fig. 5.13 and Figs. 5.14. The average degradation rates are indicated using the red horizontal lines (and the top and bottom edges of the red diamond indicate the 95% confidence interval). It is evident from the plot that the average $P_{max}$ degradation rates of the modules with and without visible signs of cracks are comparable. It should be noted here that the "No VC" category includes modules without any cracks and also modules with cracks which are not visible to the naked eye and can only be seen through EL imaging (discussed in Chapter 6). There is also some uncertainty in the name plate data and the uncertainty introduced by STC translation procedures (which are discussed in detail in Chapter 3).

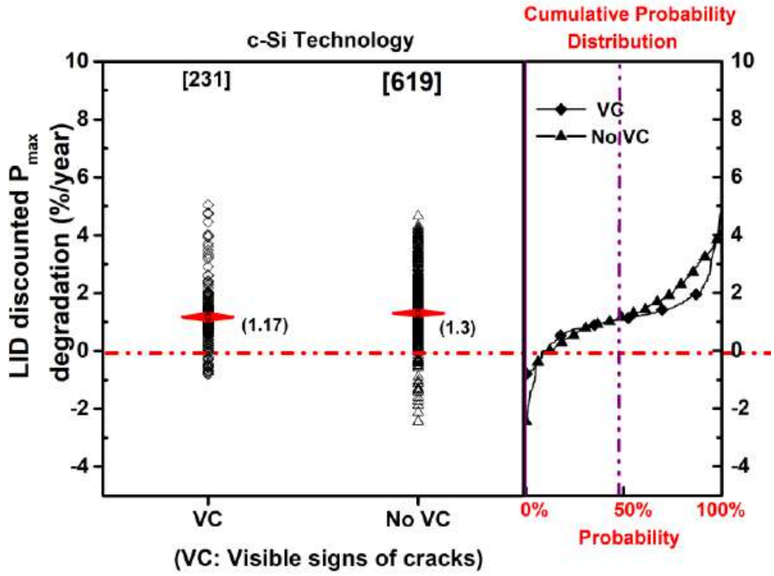


(a)

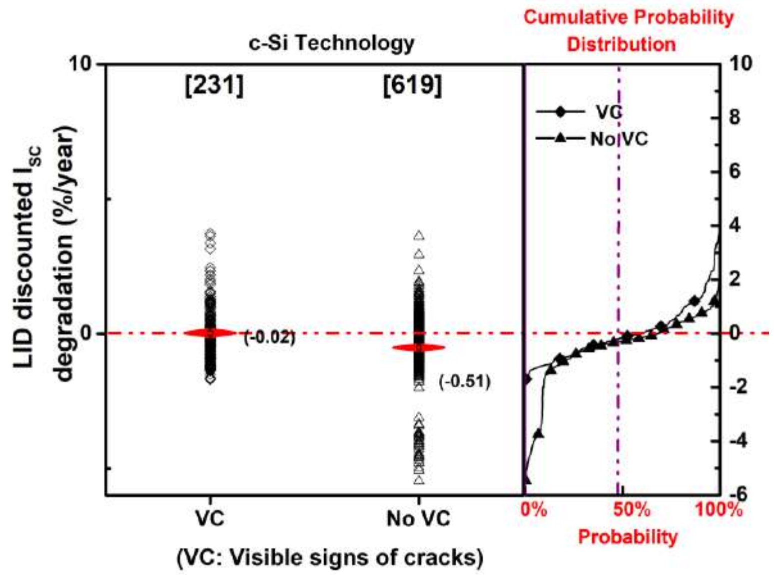


(b)

Fig. 5.13. Plots of electrical degradation versus visible signs of cell cracks: (a) $P_{max}$ degradation (%/year), (b) $I_{SC}$ degradation (%/year)

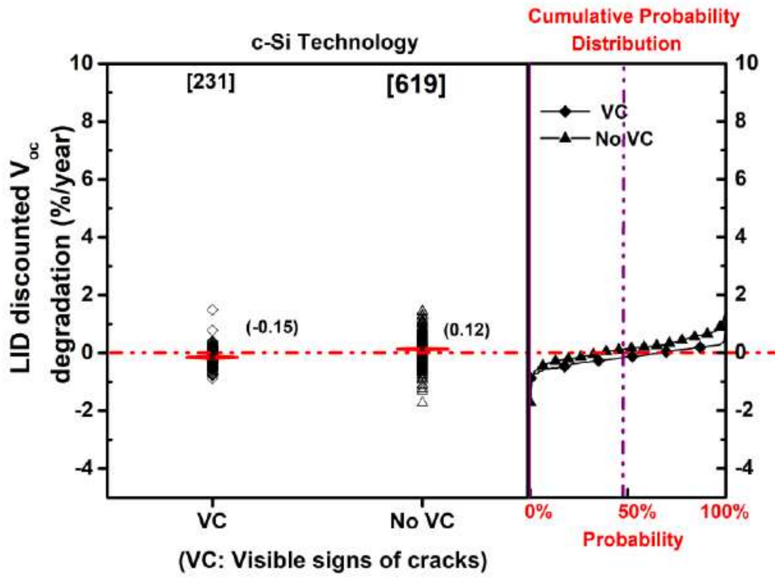


(a)

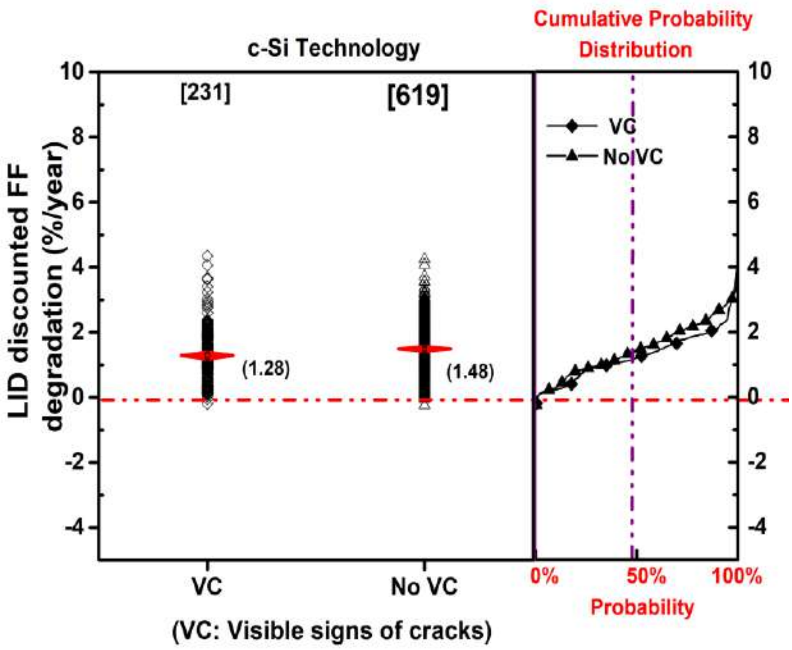


(b)

Fig. 5.14. Plots of electrical degradation versus visible signs of cell cracks: (a) $V_{OC}$ degradation (%/year) and (b) *FF* degradation (%/year)

## 5.3 Visual Degradation Observed in Thin Film modules

Thin Film modules are usually glass-glass modules with the active semiconductor material deposited on the top glass substrate. Moisture penetration into the laminate from the edges has been one of the most common causes of degradation in thin film modules since long time, which is being countered in the present generation of modules with the help of superior edge seals [57]. As part of the survey, we have inspected a total of 76 thin film modules, the majority of which were CdTe modules.

All of the modules were less than 10 years old, and were found only in the Hot climates (Hot & Dry, Warm & Humid, and Composite zones). Fig. 5.15 shows some of the most commonly seen degradation modes during our survey and Table 5.14 shows the statistics. White spots are commonly seen in thin film modules and are reported to be a visual indication of shunts, generated due to operation under partially shaded conditions [58, 59]. Delamination in the edge seal is also commonly seen, which can lead to TCO corrosion due to ingress of moisture into the module [57].

Table 5.14. Statistics of thin film modules affected by various degradation modes

| Technology | Total No. of Modules | Percentage of Modules Affected | | | | |
|---|---|---|---|---|---|---|
| | | White Spots | Cracked Glass | Non-Crack Damage | Cell Delamination | Edge Seal Delamination |
| **Amorphous Silicon** | 21 | 90% | 5% | 5% | 14% | 19% |
| **Cadmium Telluride** | 55 | 93% | 0% | 2% | 9% | 78% |

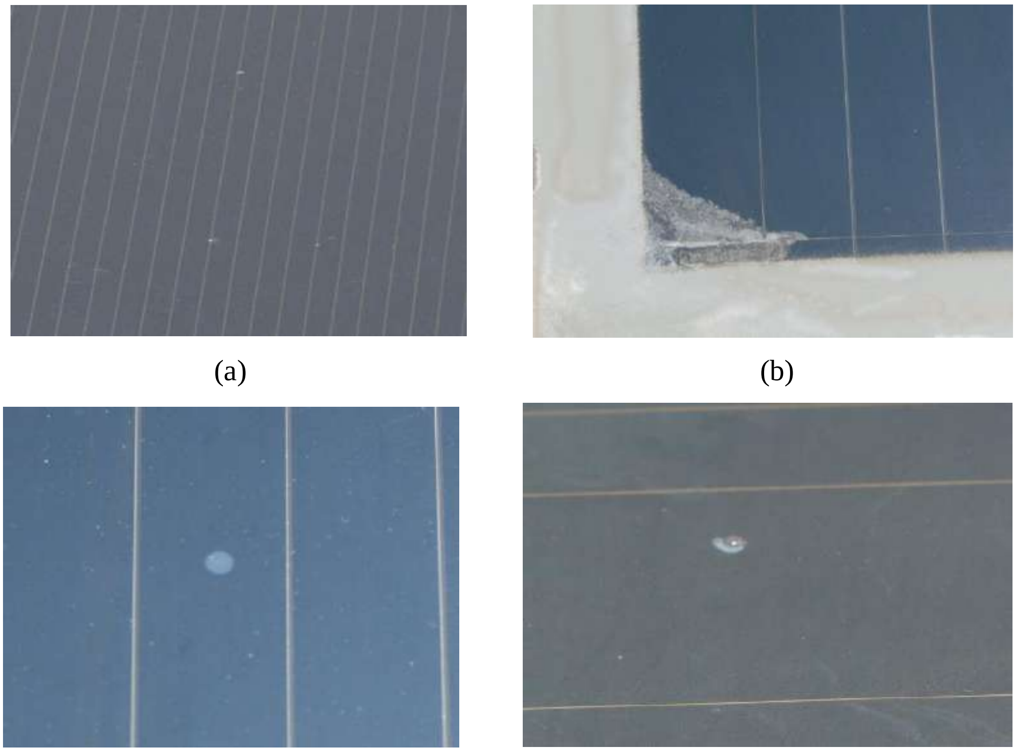

(a) (b) (c) (d)

Fig. 5.15. Degradation in Thin Film modules (a) White spot in CdTe module, (b) Delamination of edge seal and inside cells (bar graph corrosion) in CdTe module, (c) haziness in CdTe module, (d) Delamination (Bubble) in CdTe modules

## 5.4 Summary

A total of 979 crystalline silicon modules have been inspected for visual defects and an attempt has been made to correlate the defects with the electrical degradation. The major conclusions from the visual analysis are as follows:

- Hot zones are the harshest climates for the encapsulant. The order of harshness appears to be Hot & Dry > Warm & Humid > Composite > Cold & Sunny > Moderate. Encapsulant discoloration has started to appear in some of the young modules, which is a matter of concern.
- Delamination has been observed in Hot climatic zone, mostly in the form of bubbles along cell cracks in the young modules, but the area affected is less than 5%.
- Snail tracks are present predominantly in modules with age less than 10 year. Snail track (non-framing type) and photo-bleaching are associated with underlying crack as verified in EL image.
- The Hot zone is harsher for metallization than the Non-Hot zone, leading to discoloration (which is primarily corrosion in the older modules).
- Haziness is the most commonly seen degradation mode for the front glass.

# 6. Analysis of EL and IR Data

## 6.1 Introduction

Electroluminescence (EL) and Infrared (IR) imaging techniques are commonly used for characterization of PV modules. Various types of defects can be identified using EL imaging such as microcracks, cracks, inactive regions, finger and interconnect damage, PID etc. [60]. IR thermography shows the temperature distribution in the PV module and helps to identify the hot spots.

## 6.2 Analysis of Electroluminescence Data

Electroluminescence (EL) imaging provides valuable insight into the condition and quality of the semiconductor. In EL imaging technique, a constant forward bias (current) is applied to the PV module. Radiative recombination of carriers in silicon causes a small amount of near-infrared light emission. The images were captured with the help of a modified CMOS based digital camera developed at NCPRE. For EL imaging performed in the field, the current supplied was equal to the short circuit current of the module under test. For the 2018 Survey, EL images for over 700 modules were taken and analysed. Most of these modules belong to 'Young' category. Fig. 6.1 shows some images captured in the field with few defects, and Fig. 6.2 shows EL images captured in the field with multiple defects. In the EL images, dark areas indicate inactive cell areas.

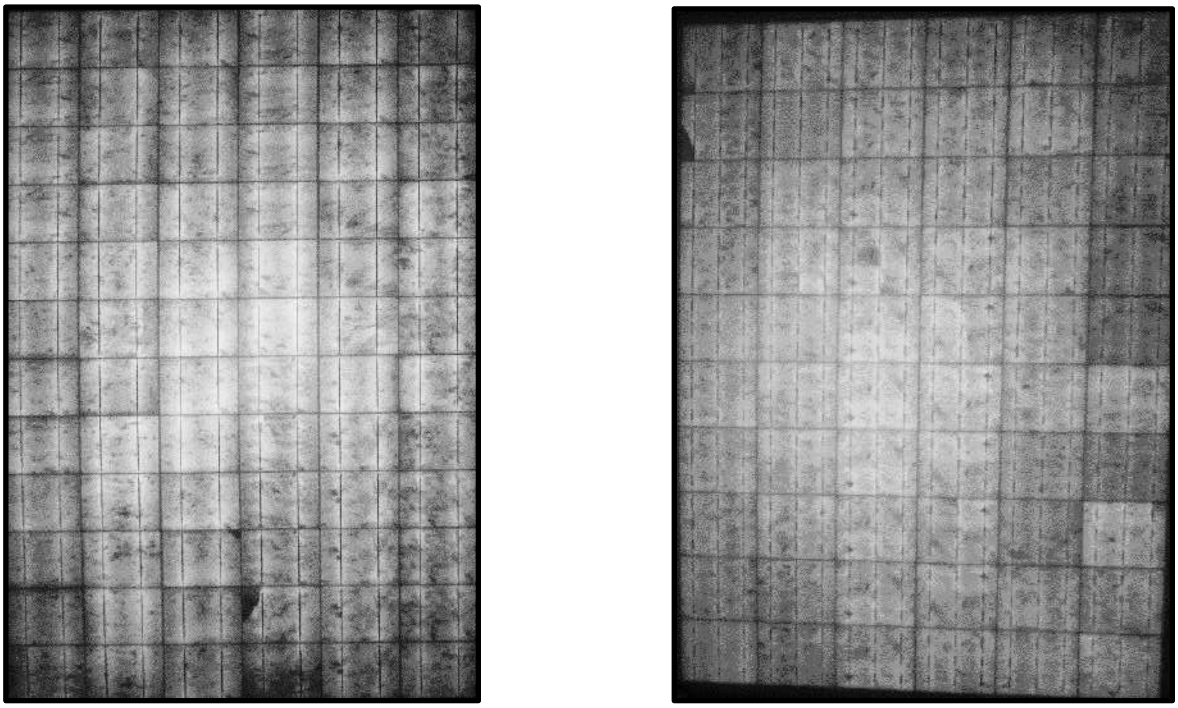

(a) (b)

Fig 6.1. EL images of fewer defects/cracks of Module (a) and (b)

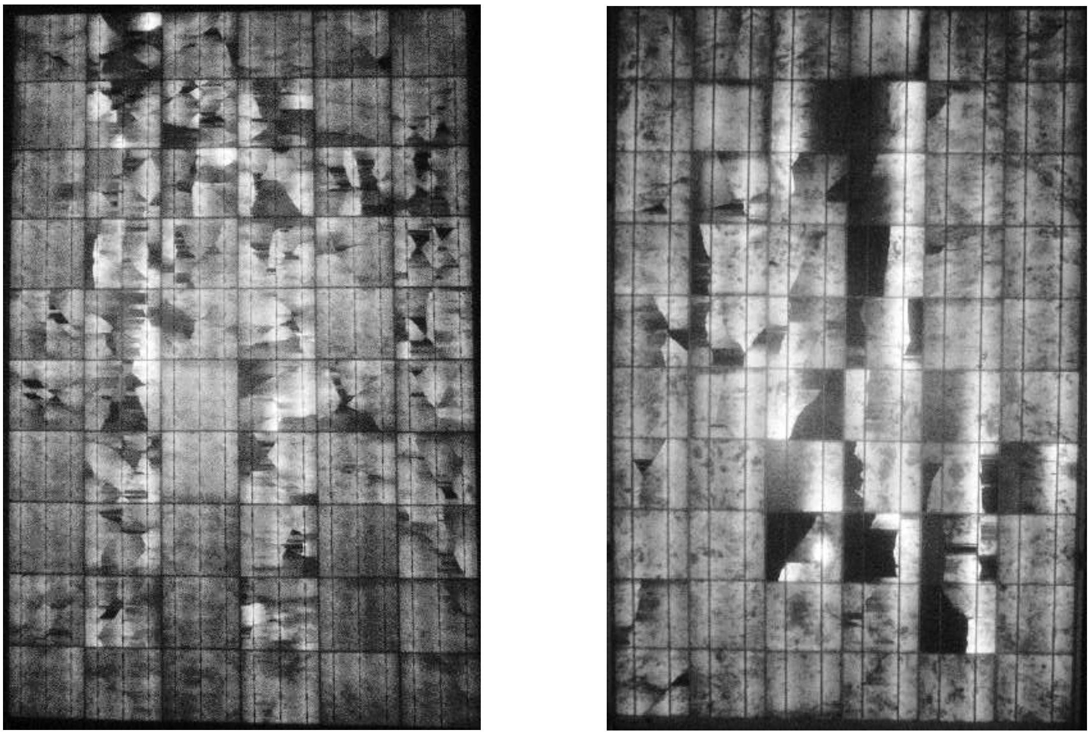

(a) (b)

Fig. 6.2. EL images of multiple defects/crack of Module (a) and (b)

In Fig. 6.1 (a) and (b), we can see dark portions in a few cells only. In Fig. 6.2 (a) and (b), there are multiple dark areas in many of the cells, which indicates the presence of cracks and interconnect failure that are affecting the charge collection and hence reducing the output power of the module. In Fig. 6.2 (b), for some cells (4th column from left), one-half of the cell is bright while the other half is dark. This indicates interconnect breakage in these cells, which is forcing current crowding through the intact interconnects. The higher number of cracks and defects may be due to poor manufacturing, transportation or installation practices.

## 6.2.1 Classification of Cracks

In general, cracks can be classified into three categories [61] based on the area affected by them. The three categories are as shown in Fig. 6.3.

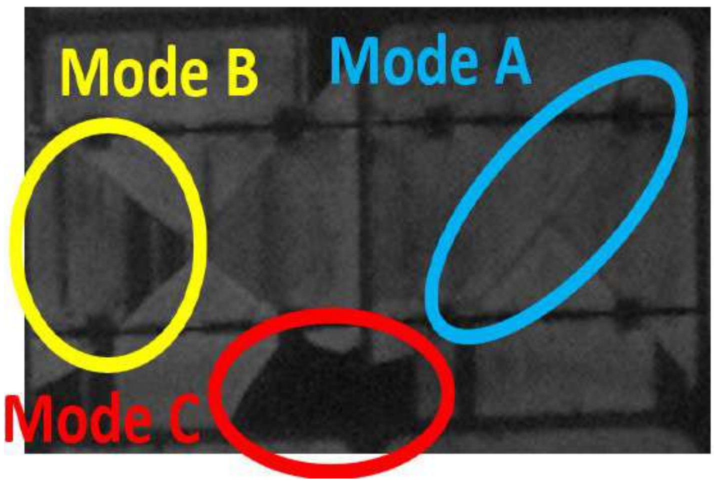


Fig. 6.3. Classification of cracks

a) Mode A cracks which are basically hair-line cracks, not associated with any dark area

b) Mode B cracks which are associated with a grey (not very dark) area in the cell

c) Mode C cracks which are associated with a dark area in the cell

The number of cells with different types of cracks is counted from the images taken in the survey and the statistics are shown in Table 6.1. We may observe that cells with Mode A type cracks are more in number. The statistics for ground and roof-mounted modules are shown in Table 6.2, which shows that the percentage of cracks is slightly higher in ground modules as compared to roof modules. This observation is in contrast with the results of the 2016 Survey, which showed the opposite. However, it should be noted that since the 2018 Survey focused on large (hence ground-mounted) systems, the number of samples for roof-mounted is small. In Table 6.3 we observe that small/medium installations suffer from more cracks than large installations.

Table 6.1. Percentage of cells affected by different types of cracks

| Percentage of cells with different types of crack | | | |
|---|---|---|---|
| Mode A | Mode B | Mode C | Number of cells checked |
| 8.32% | 4.39% | 1.14% | 37080 |

Table 6.2. Percentage of cells affected by different types of cracks in Rooftop and Ground-mounted systems

| Percentage of cells with different types of crack | | | | |
|---|---|---|---|---|
| | Mode A | Mode B | Mode C | Number of cells checked |
| Ground Mounted | 8.90% | 4.81% | 1.12% | 31368 |
| Roof Mounted | 5.13% | 2.01% | 0.82% | 5712 |

Table 6.3. Percentage of cells affected by different types of cracks in Large and Small/medium size systems

| Percentage of cells with different types of crack | | | | |
|---|---|---|---|---|
| | Mode A | Mode B | Mode C | Number of cells checked |
| Large System | 8.13% | 4.24% | 1.15% | 36000 |
| Small/medium System | 14.44% | 8.89% | 0.83% | 1080 |

### 6.2.2 Correlation of Performance Degradation with Number of Cracks

Fig. 6.4 shows the plot of the average Linear $P_{max}$ Degradation Rate (%/year) versus the total number of cells with different cracks in the module. For this analysis, only Mode B and Mode C type cracks are taken into account, as Mode A cracks do not cause power degradation. It can be observed in Fig. 6.4 that the degradation rate is not well correlated with number of cells with Mode B+C type cracks. This may indicate that for the 2018 Survey, cracks are not the dominant cause of high degradation rate seen in some PV modules (Chapter 4). In Fig. 6.5, it is seen that with an increase in the number of cells with cracks there is an increase in *FF* degradation rate (statistically significant between group with crack >20 with all other group of cell crack) which is understandable; however this does not appear to translate to a concomitant decrease in $P_{max}$. It should be noted that due to other degradation mechanism like PID, cell inter connect failure, encapsulant browning, etc. can lead to the power degradation.

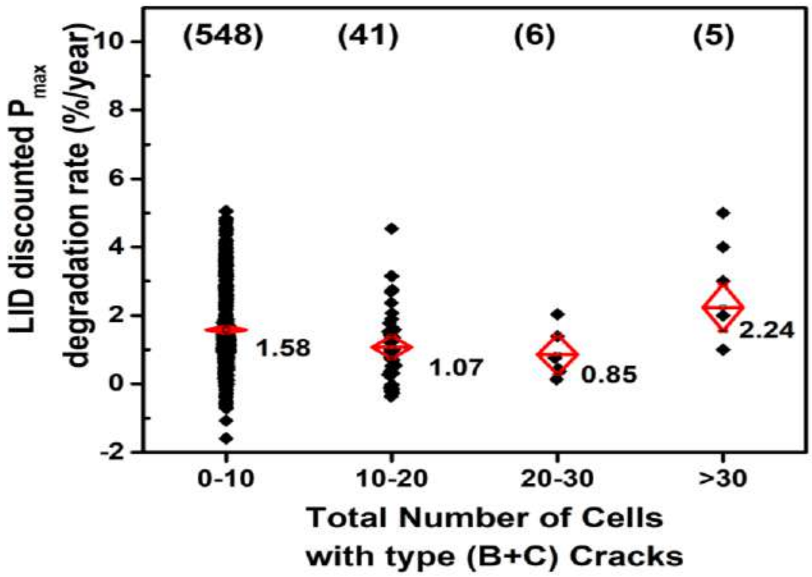


Fig. 6.4. $P_{max}$ degradation rate (%/year) versus the total number of cracks in the module

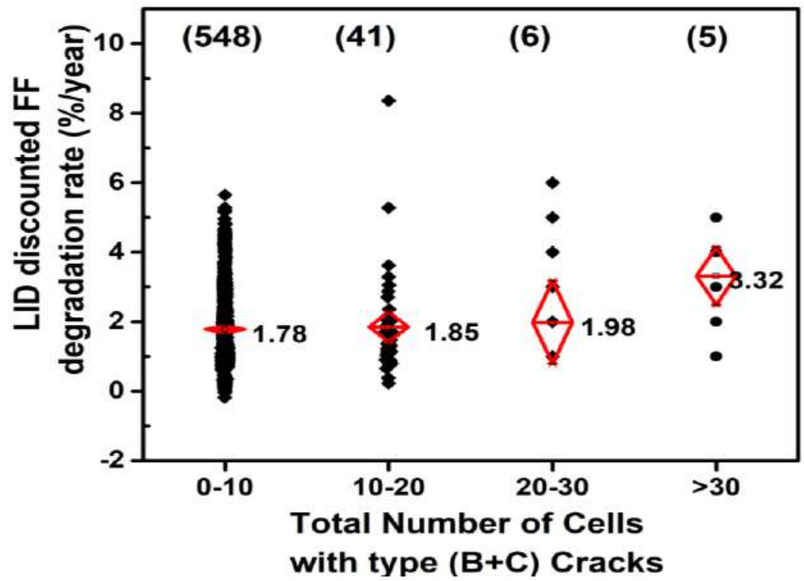


Fig. 6.5. FF degradation rate (%/year) versus the total number of cracks in the module

### 6.2.3 Correlation of Snail Trails with Electroluminescence Images

Snail trails have been observed in some modules during the survey, which has been described in detail in Chapter 5. The snail trails appear as black or brown curved lines running across the solar cells, and sometimes bordering them (like a frame). Usually, the EL images of the cells affected by snail tracks show cracks, as shown in Fig. 6.6. The cracks allow the moisture to reach the top side of the solar cells, where it aids the migration of the silver ions from the gridlines to the encapsulant layer. The silver ions then react with various chemicals from the encapsulant and backsheet producing various compounds of silver [62].

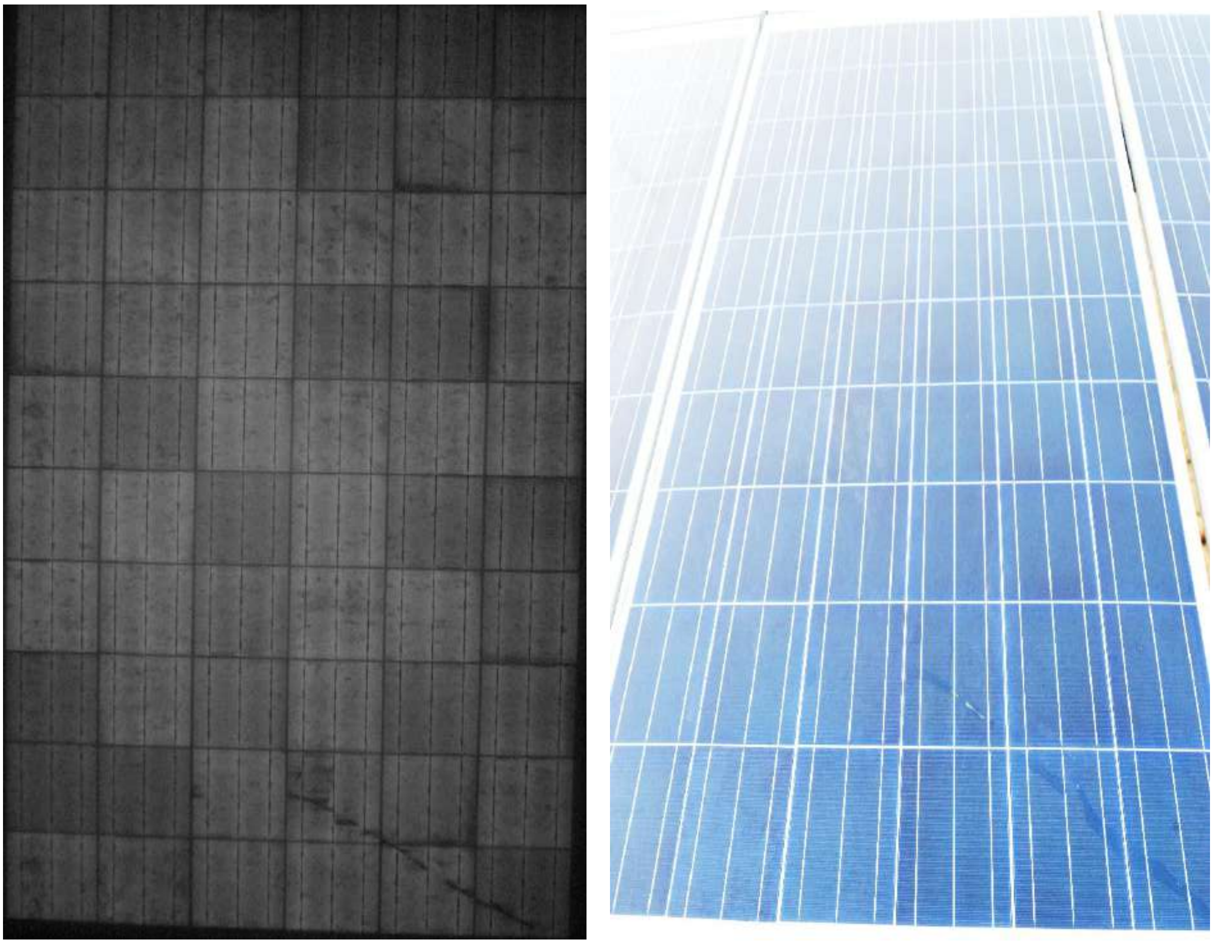

(a) (b)

Fig. 6.6. (a) EL image of the module showing the cell cracks, (b) Snail trails observed in the same PV module in Hot & Dry climate

### 6.2.4 Correlation of Interconnect Breakage with Electroluminescence Images

The electrical connections between the cells are provided by cell interconnects which help to conduct the electrical current to the external load from the cells in the PV module. The increase in the number of cell interconnect lines provides greater redundancy and reduces the resistive losses thereby improving the fill factor of the PV module. In the event of breakage of one interconnect the current flow shifts to the remaining intact interconnects, and this leads to darkening of the area corresponding to the broken interconnect. Fig. 6.7 shows half-dark cells which indicates interconnect breakage in the module.

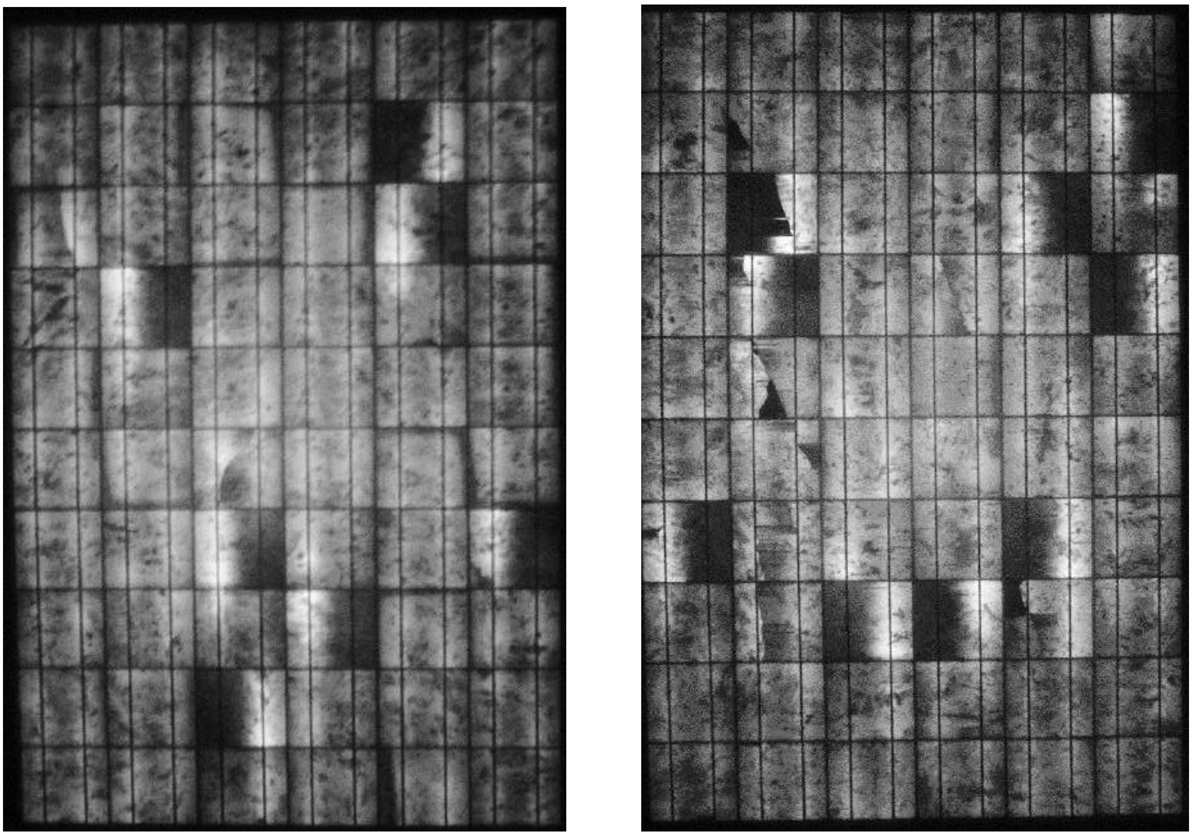

Fig. 6.7. Modules with suspected cell interconnect breakage

## 6.3 Analysis of the illuminated Infrared thermography data

Infrared (IR) thermography produces a thermal image of the Photovoltaic (PV) module, which is a first order analysis to identify defects in PV modules. It is a nondestructive characterization tool which can easily be done on a large sample size. Specific cameras are used for such analysis which can detect the infrared energy emitted from a PV module and convert it to temperature map of the image [38]. To understand the effect of temperature on PV modules, we took IR images of approximately 800 PV modules covering various installation types and climatic zones. From an IR image, we can measure the modal temperature (representative of the module temperature), maximum temperature and the $\Delta T$ (difference between maximum and modal temperature) which signifies the extent and degree of hot spots in a PV module. We can also detect the location of the hot spot from an IR image. Modal temperature is taken as the representative temperature of the module as it is the most frequently occurring temperature in the PV module (the average temperature is not considered as the representative temperature as the average value is highly influenced by surrounding objects like frame/mounting structures which inevitably appear in IR image).

IR images were taken under MPPT and short-circuited condition for our analysis. Maximum power point tracking (MPPT) conditions show the extent of hot spots in the typical operating condition, whereas the short-circuited image shows the enhanced effect. In short-circuit condition the current passed through the module is dissipated in the form of heat; this is useful in identifying minor defects which may increase with time. An example of IR images of a PV module captured under MPPT and short-circuited conditions is shown in Fig. 6.8. In this figure the vertical scale on the right side of the image shows the temperature range of the captured image (not the same for the two images), the top left numerical value shows the temperature of the pointer present in the center of the image. From the image, we may observe that the temperature of the short-circuited PV module is higher than the MPPT condition. We may also see the defined boundaries of hot spots/hot cells in short-circuited PV module (shown in Fig. 6.8), whereas in the MPPT IR image we may see a gradient of high to low temperature.

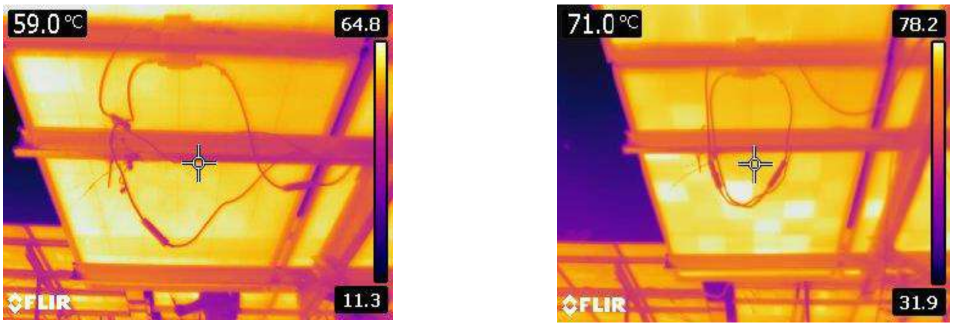


Fig. 6.8. IR image of a PV module under MPPT condition (left) and short-circuited condition (right)

Valuable data on Infrared thermography was collected from 33 sites during our Survey, which included IR images of 793 PV modules under load (MPPT) and 611 PV modules under short-circuited condition. All IR images were taken by FLIR E60 IR camera. It should be noted that at some of the sites, IR images were not taken due to site-specific constraints, so the total number of PV modules reported in this Section is lower than the numbers reported in Chapter 4. All images were taken at the plane of array (POA) irradiance above 700W/m$^2$. After changing the operating condition, we have given 15 min wait time for steady state measurements. Pixel-wise temperature data of each IR image was extracted in "CSV" format by using the FLIR tool. The CSV file was further processed by a semi-automated IR analysis software [15] which gives us the modal temperature (representative of the PV module temperature), maximum temperature and ΔT for the area of our interest. The GUI (graphical user interface) of the software is shown in Fig. 6.9. The software analyzed the images faster and enabled us to do sanity checks which produce better quality data. From Fig. 6.9, image (a) we select the PV module of our interest, which is then cropped and shown in Fig 6.9, image (b), and the histogram of the latter is shown at the bottom right of Fig. 6.9.

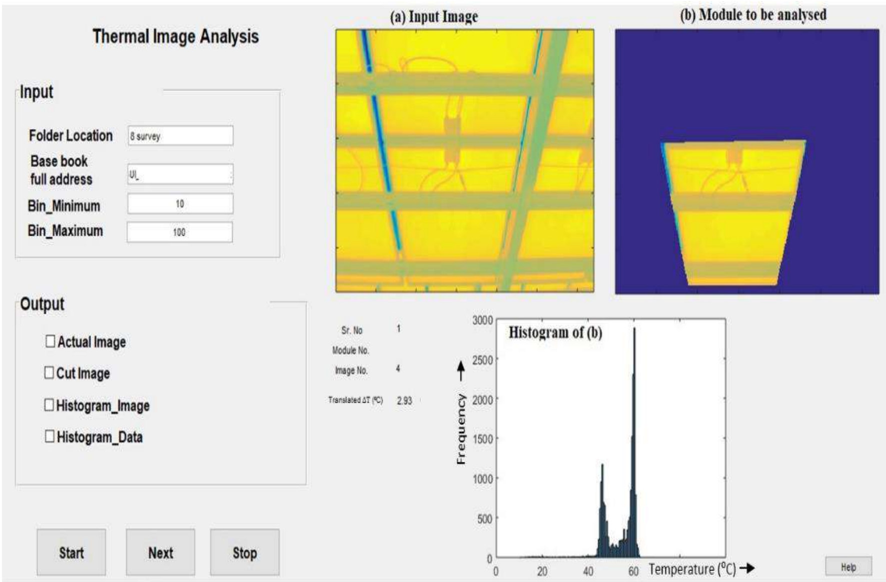


Fig. 6.9. GUI for Infrared (IR) thermography analysis.

In the software, the PV module (area of interest) to be analyzed is selected by the user for each image. After the selection of the PV module, the modal temperature (representative PV module temperature) is calculated from the histogram. The absolute maximum is taken as the maximum temperature of the selected PV module. Fig. 6.10 (a) shows the histogram of the measured module temperature (i.e., modal temperature) for c-Si PV modules, under MPPT condition. These values are presented as recorded on site without irradiance or temperature corrections. The lowest module temperature is 28.5 ºC (recorded in the Cold & Dry climate in Ladakh) whereas the highest module temperature is 71.5 ºC (recorded in the Hot &Dry climate in Maharashtra). The histogram of maximum temperature of the inspected PV modules is shown in Fig. 6.10 (b). The maximum temperature recorded under MPPT condition was 122 ºC (under POA irradiance of 842W/m$^2$ and ambient temperature of 35.6 ºC). The histogram of the module temperature and maximum temperature under short circuit condition is shown in Fig. 6.11. Under short circuit condition, module temperature ranges between 49 ºC to 69 ºC and the maximum temperature observed in short circuit condition was 120ºC. The histograms of Figs. 6.10 and 6.11 show that PV modules under short-circuited condition run hotter than MPPT condition.

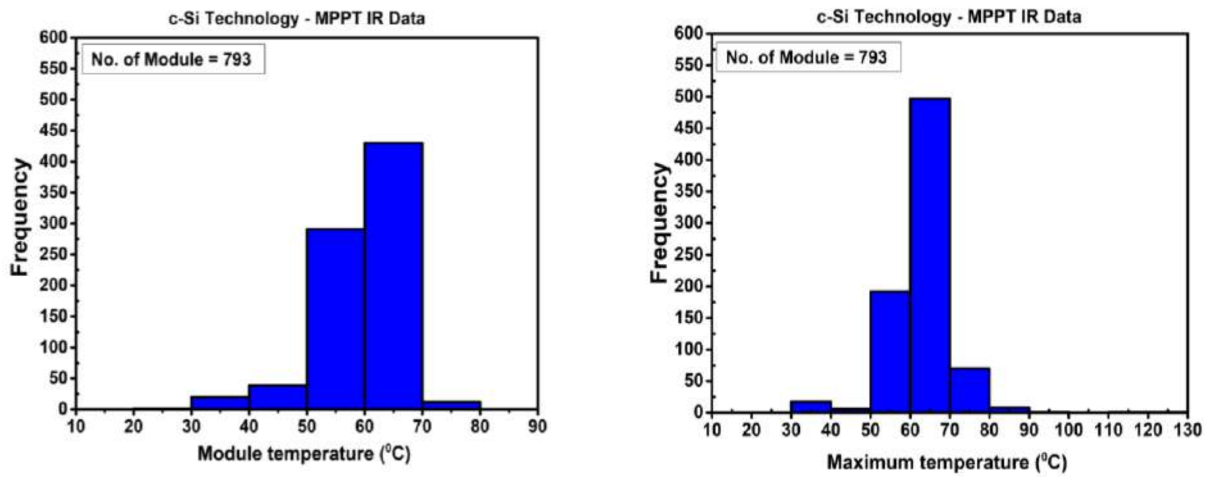


(a) (b)

Fig. 6.10. Histogram of Module (a) and Maximum (b) temperature under MPPT condition

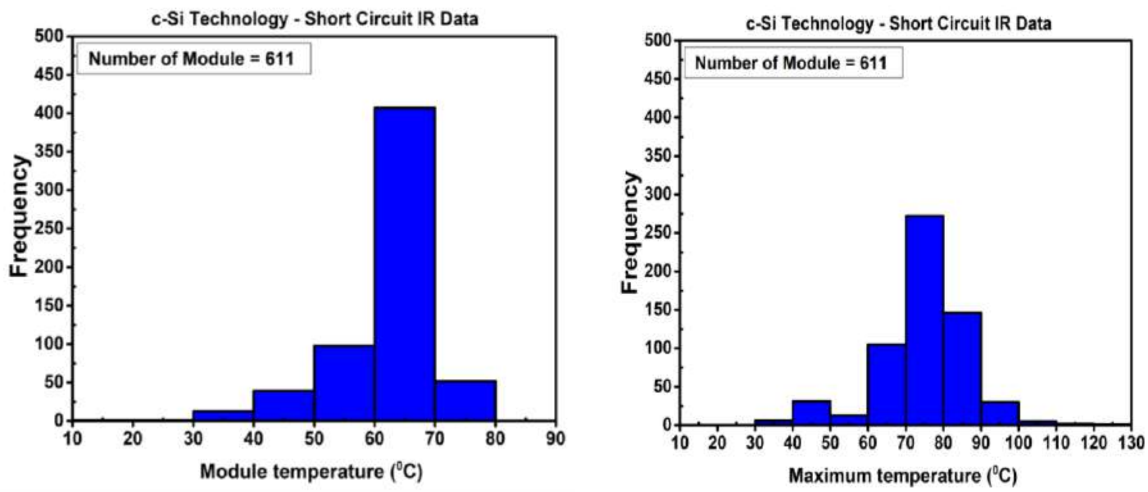


(a) (b)

Fig. 6.11. Histogram of Module (a) and Maximum (b) temperature under short circuit condition

### 6.3.1 Normalization of IR Data

In order to compare the temperature data of different sites, normalization was done. The temperature values were translated to reference conditions of 1000W/m$^2$ and 40 ºC based on the work done by Moreton *et al.* [63] and Oh *et al.* [64]. The equations used for the translation are given below:

$$T_{translated} = 40 + \frac{(T_{measured} - T_{ambient}) \times 1000}{Irradiance} \qquad \dots\dots\dots (6.1)$$

Where,

$T_{translated}$ = translated temperature of module under reference condition

$T_{measured}$ = measured temperature of module (obtained from IR image)

$T_{ambient}$ = ambient temperature measured at site

The temperature mismatch between the cells in a module is defined as Module ΔT, given as follows;

$$\text{Module } \Delta T = T_{maximum,\ translated} - T_{module,\ translated} \qquad \dots\dots\dots (6.2)$$

Where,

$T_{maximum,\ translated}$ = Translated maximum temperature of the module

$T_{module,\ translated}$ = Translated modal temperature of the module

Theoretically, the power loss in PV modules due to the formation of defects is proportional to the rise in temperature in the solar cell [65]. Based on energy balance in a PV module, by equating the incoming solar energy with the summation of the electrical power output and thermal power dissipation, it is possible to derive a relation of the form given below [15]:

$$\%\ Power\ loss\ in\ a\ PV\ module\ = \frac{U}{10 \times N \times \eta} \times \sum_N cells\ (T_{cell} - T_{module}) \qquad \dots\dots\dots (6.3)$$

Where,
U = Overall heat transfer coefficient
$T_{cell}$ = Cell Temperature
$T_{module}$ = Module's representative temperature (modal temperature)
$\eta$ = Initial efficiency of the PV module
N = Number of cells in the PV module

Many of the IR images taken in the 2018 Survey have parts of the frame or mounting structure blocking the cell of the module; also the images have irregular shapes, making it difficult to apply Eq. 6.3 to the IR data. Hence we have used a simplified version and defined a Thermal mismatch index (TMI) of the PV module as follows;

$$TMI = \frac{Module\ \Delta T}{\eta \times N} \qquad \dots\dots\dots (6.4)$$

Where,

$\eta$ = Efficiency of the PV module (taken from Datasheet)

N = Number of cells in the PV module

For standard module with 17% efficiency and 60 cell module, *TMI* = 1 implies Module Δ*T* of 10.2 ºC. Higher *TMI* indicates a higher extent of hot spot. PV modules have been grouped into 4 categories based on *TMI* values and different operating conditions.

## 6.3.2 Analysis of Normalized IR data

***a) Effect of Thermal mismatch on Electrical degradation***

To understand the effect of thermal mismatch/extent of hot spots on electrical degradation, PV modules have been grouped into four categories under MPPT and short circuit conditions. *TMI* categories under short circuit condition are referred as $TMI_{sc}$ and under MPPT condition as $TMI_{MPPT}$. In Table 6.4, we have calculated temperature ranges for each $TMI_{MPPT}$ category by equation 6.4, by taking average efficiency and the average number of cells of the complete data set (c-Si technology) for the 2018 Survey. Temperature ranges under short circuit conditions for each $TMI_{sc}$ categories are shown in Table 6.5.

In Fig. 6.12, we observe that the total power degradation increases with increase in $TMI_{MPPT}$ under MPPT condition. However, we do not see a statistically significant difference between $TMI_{MPPT}$ categories 1 and 2 nor between 3 and 4. This indicates that PV modules with temperature higher than 4 ºC ($TMI_{MPPT} > 0.5$) show a significant increase in power degradation. Statistically significant difference was verified by Mann Whitney U test, with a confidence interval of 95%. For p-values less than 0.05, we reject the null hypothesis. In Fig. 6.13, we observe that Fill Factor increases with $TMI_{MPPT}$. We see statistically significant difference only between $TMI_{MPPT}$ category "1 and 4", "2 and 4", not in any other categories. There was no trend found between short circuit current and open circuit voltage degradation with $TMI_{MPPT}$ shown in Fig. 6.14 and Fig 6.15. Please note that we have correlated the electrical parameters in terms of total degradation (%) and not degradation rate (%/year).

Table 6.4. Temperature mismatch category based on $TMI_{MPPT}$ values at MPPT condition ($TMI_{MPPT}$)

| Module $\Delta T$(ºC) | 0ºC - 2ºC | 2ºC - 4ºC | 4ºC - 9ºC | >9ºC |
|---|---|---|---|---|
| $TMI_{MPPT}$ | 0-0.25 | 0.25-0.5 | 0.5-1 | >1 |
| Category | 1 | 2 | 3 | 4 |

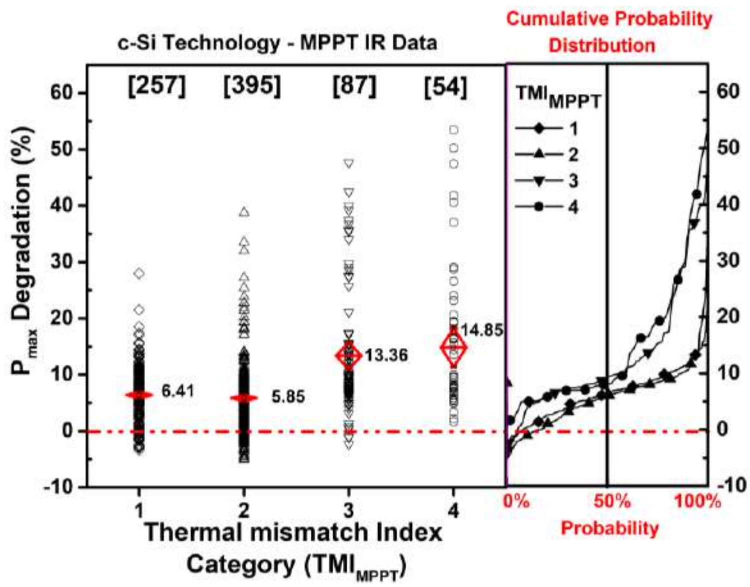


Fig 6.12. Correlation between $P_{max}$ degradation with respect to TMI categories under MPPT condition.

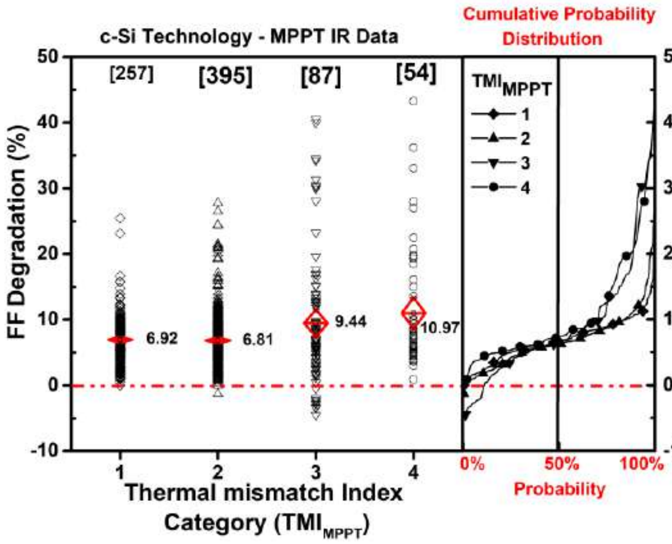


Fig. 6.13. Correlation between *FF* degradation with respect to TMI categories under MPPT condition

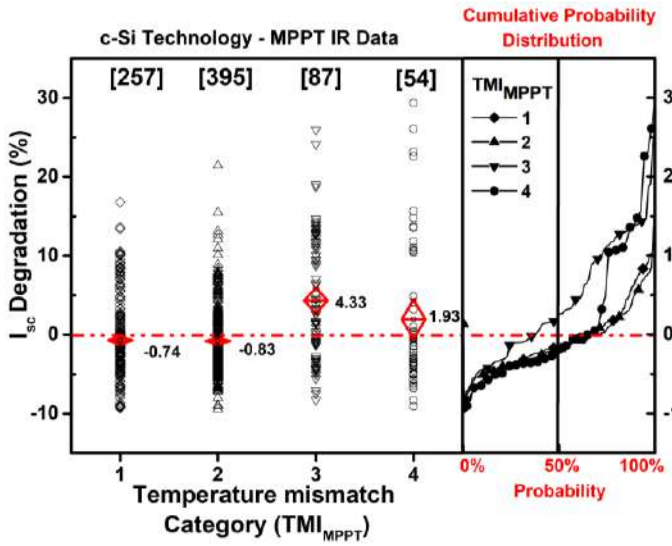


Fig. 6.14. Correlation between $I_{sc}$ degradation with respect to TMI categories under MPPT condition.

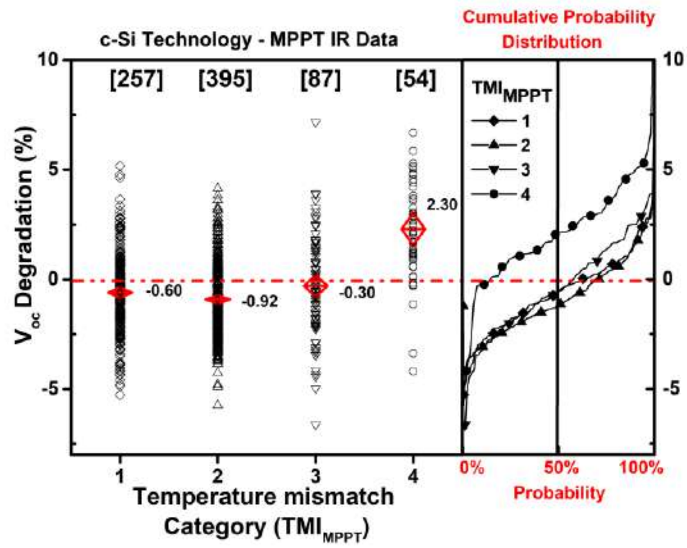


Fig. 6.15. Correlation between $V_{oc}$ degradation with respect to TMI categories under MPPT condition.

In short circuit condition, we observe higher temperatures (shown in Fig 6.10 and 6.11), thus the *TMI* categories are distributed in different temperature ranges than MPPT conditions. Table 6.5 shows $TMI_{SC}$ categories and their respective *TMI* and temperature values. Under short-circuited condition, we observe in Fig. 6.16 that the power degradation increases with $TMI_{SC}$, but the difference in $TMI_{SC}$ categories 1, 2 and 3 is not statistically significant (based on Mann Whitney U test). In Fill Factor degradation shown in Fig. 6.17, we observe that the distribution was statistically similar between all 4 categories (based on Mann Whitney U test statistics). There was no trend found in short circuit current and open circuit voltage degradation with $TMI_{SC}$, as shown in Fig 6.18 and Fig 6.19.

Table 6.5. Temperature mismatch category based on $TMI_{SC}$ values at SC condition ($TMI_{SC}$)

| Module Δ*T* (ºC) | 0ºC - 9ºC | 9ºC - 18ºC | 18ºC - 27ºC | >27ºC |
|---|---|---|---|---|
| $TMI_{SC}$ | 0-1 | 1-2 | 2-3 | >3 |
| Category | 1 | 2 | 3 | 4 |

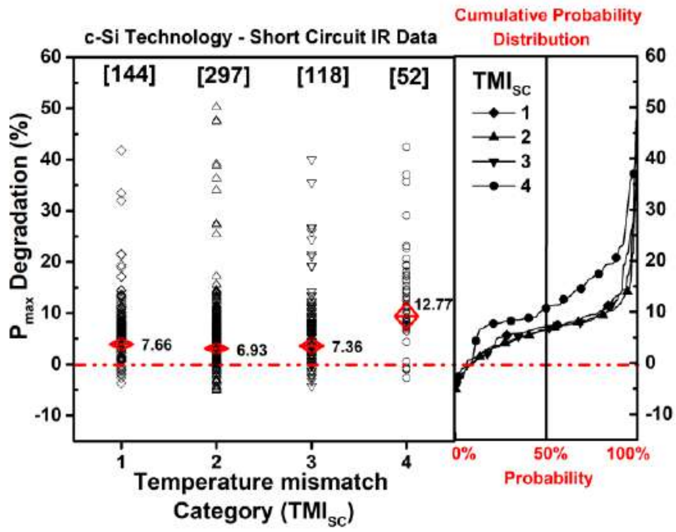


Fig. 6.16. Correlation between $P_{max}$ degradation with respect to TMI categories under Short circuit condition

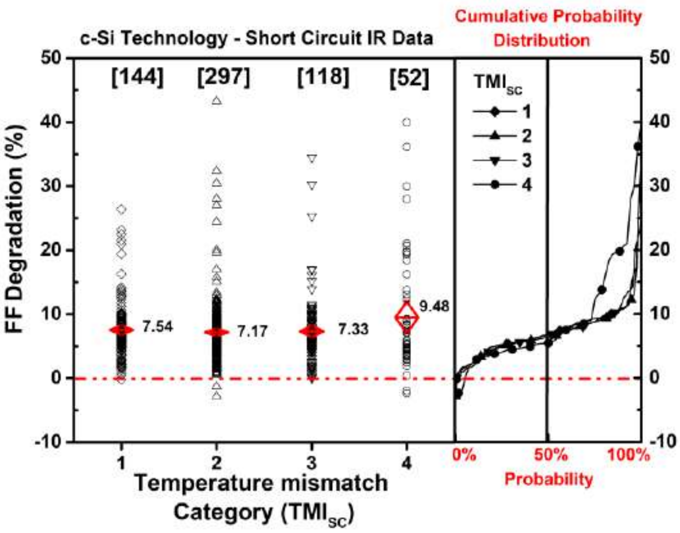


Fig. 6.17. Correlation between *FF* degradation with respect to TMI categories under Short circuit condition

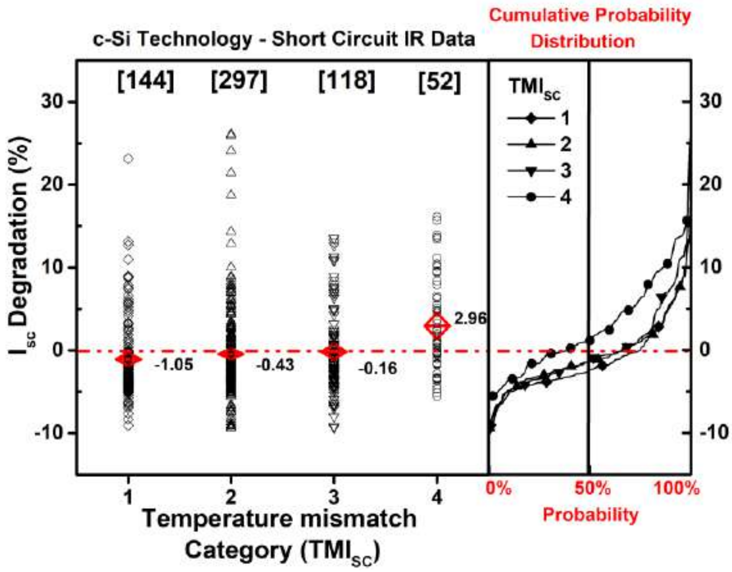


Fig. 6.18. Correlation between $I_{sc}$ degradation with respect to TMI categories under Short circuit condition

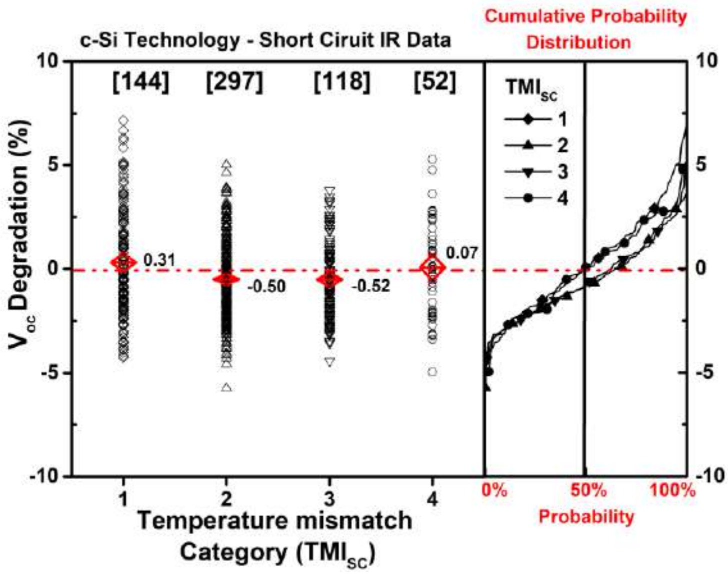


Fig. 6.19. Correlation between $V_{oc}$ degradation with respect to TMI categories under Short circuit condition

From this section we conclude that thermal mismatch correlates fairly well with power degradation of the PV module under MPPT/load condition, especially for low to high $TMI_{MPPT}$ categories. Similar effect was also seen under short circuit condition with low statistical significance (based on Mann Whitney U test statistics).

***b) Effect of Climatic zone***

In this section, we examine the effect of climatic zone. We have only used the MPPT IR data as it represents the present health of the PV module. Fig. 6.20 shows the effect of Hot zone and Non-hot zone on total power degradation (%). Modules deployed in hot zone are further divided into those that have a hot cell (HC) and those that don't have a hot cell (NHC)). A module with $TMI > 0.5$ is considered as a module with hot cell while those with TMI < 0.5 are considered to be without hot cell (NHC). From Fig. 6.20 (a) we observe that PV modules with hot cells (i.e., $TMI_{MPPT} > 0.5$) show higher degradation in all climatic conditions (both Hot and Non-hot zones). Especially note that hot cells in Hot zones have a significantly more deleterious effect on power than in Non-hot zones. This was also seen in the 2016 All-India Survey [5]. In Fig. 6.20 (b), *TMI* shows a similar trend, that hot cells have higher *TMI* in both Hot and Non-hot zones. The difference between the hot cell and the non-hot cell is statistically significant (based on Mann Whitney U test statistics) for all climatic conditions (Hot and Non-hot zones). Please note that we have correlated the electrical parameters in terms of total degradation (%) and not degradation rate (%/year).

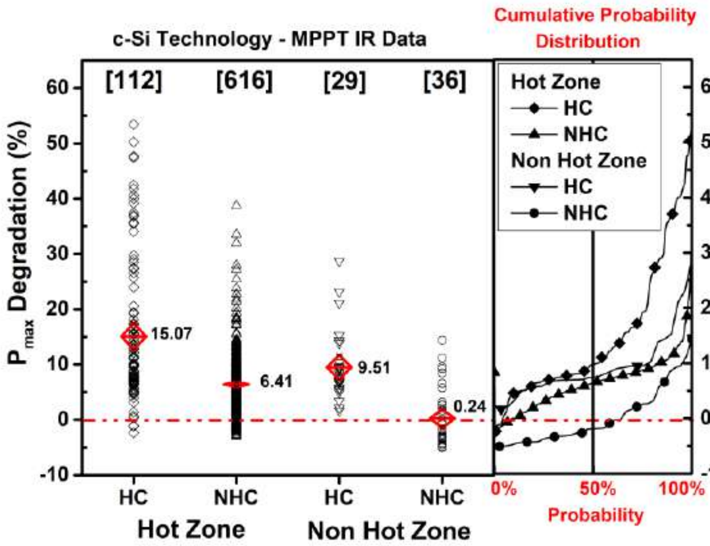


(a)

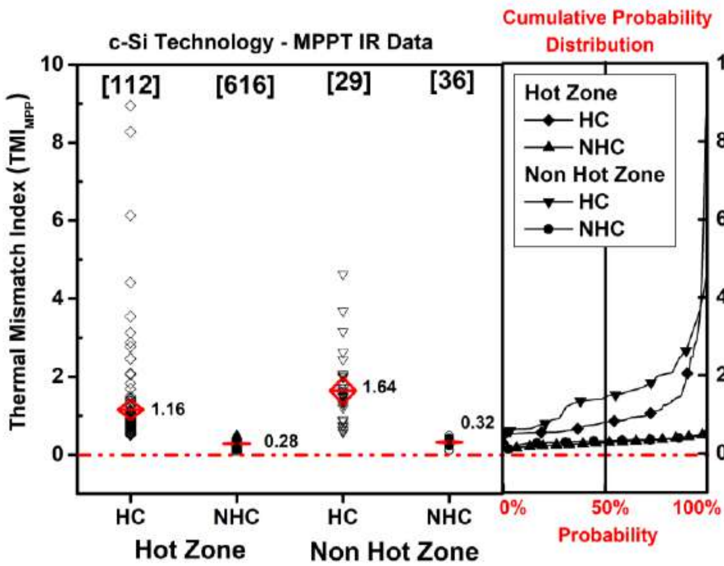


(b)

Fig. 6.20. Effect of hot cell on module performance in Hot and Non-hot zones (a) Power degradation (%), (b) Thermal mismatch index

***c) Effect of Mounting configuration***

To understand the effect of mounting configuration we have again only considered MPPT IR data. In Fig. 6.21 (a), we observe that roof mounted systems have significantly higher translated module temperature than ground mounted systems. Despite of both types of modules being mounted on 'open' racks. Statistically higher temperature of rack mounted modules on roof indicates that the air circulation around these modules is not as good as ground mounted modules. This could be because most of the roof mounted systems surveyed are in urban areas (thus surrounded by other buildings) and experience less wind speed. Also, the height from floor is generally less for roof-mounted systems as compared to ground mounted systems – thus leading to poorer air circulation. However, we observe in Fig. 6.21 (b) that Module $\Delta T$ (signifying the extent of hot spots) is higher for ground-mounted systems.

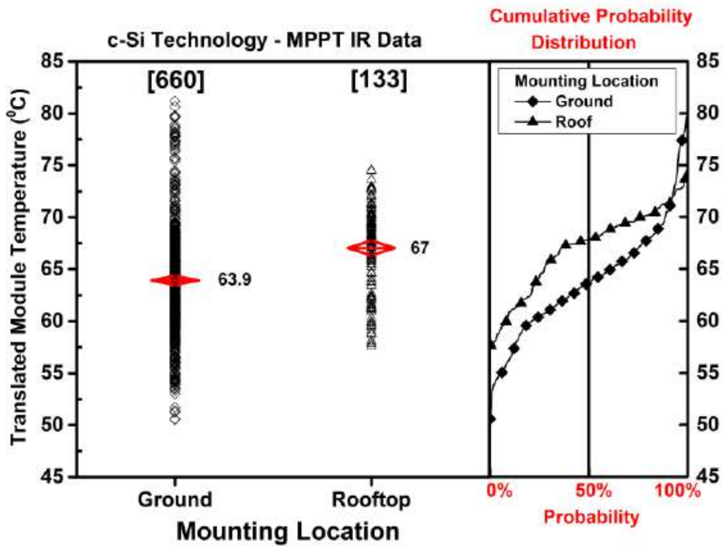


(a)

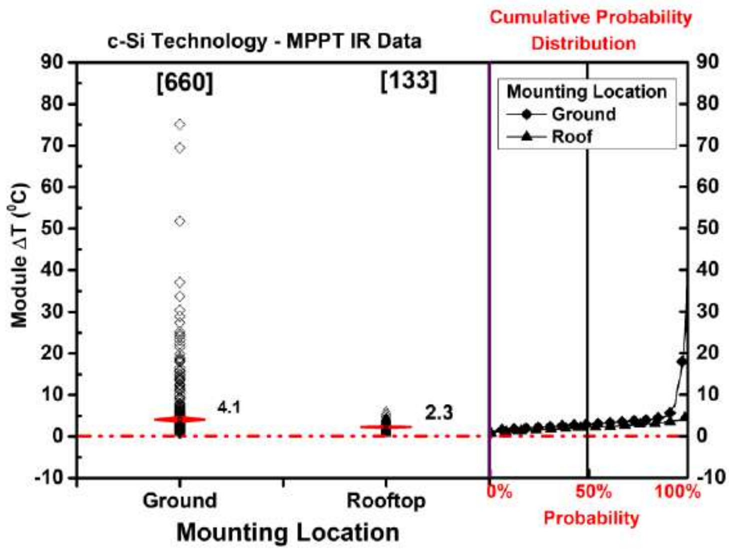


(b)

Fig. 6.21. Effect of mounting location on (a) Module (modal) temperature (ºC) and (b) Module ΔT (ºC) which signifies the extent of hot spots

***d) Correlation of Hot spots with Age***

Module $\Delta T$ (ºC) shows the temperature mismatch between the cells in a module and was taken as a metric to understand the correlation between hot spots and age. From Fig. 6.22, we may observe that old modules (Age > 5 Years) have higher Module $\Delta T$ (ºC) than young modules (Age – 1 to 5 years). One of the site (referred as the faulty site) which falls under "Old" category showed unusual high Module $\Delta T$, however even after removing the faulty site, the old modules show higher Module $\Delta T$ than young modules, and the difference was also seen to statistically significant. This shows that hot spots have increased significantly for module above age 5 years. This leads to a conclusion that hot spots are not one of the reasons for high degradation seen in young PV modules (Chapter 4).

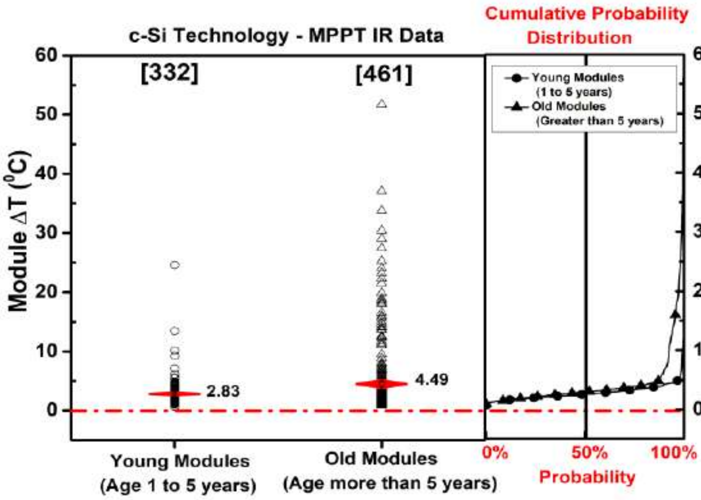


Fig. 6.22. Correlation of Age with Module ΔT (ºC) which signifies temperature mismatch between the cells in a module.

***e) Correlation of Hot spots with Visual and Electroluminescence (EL) Images***

There were some cases in which we observed a strong correlation between IR, visual, and EL images. In Fig. 6.23 (a) and (b), we observe, for two modules, browning in the visual image which was due to a significant cell crack (seen in electroluminescence imaging) that leads to a very severe hot spot (seen in IR image).

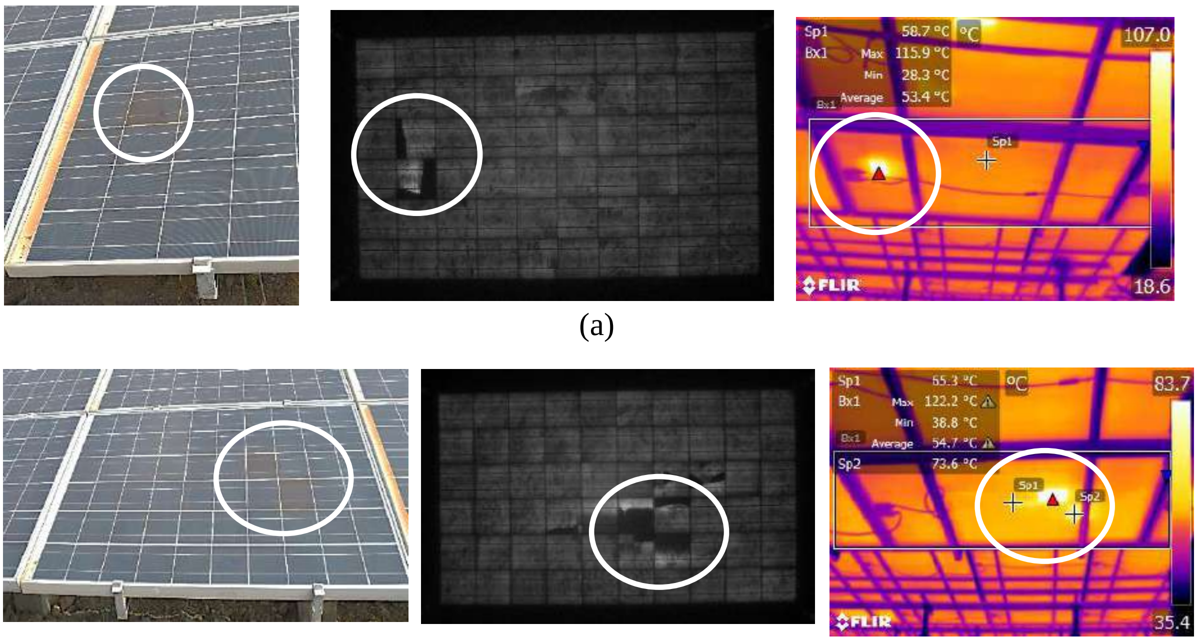


(a)

(b)

Fig. 6.23. Correlation of hot spots (right) with visual (left) and electroluminescence (centre) images for two modules (a) and (b)

***f) Comparison of Drone and FLIR based Infrared thermography***

We conducted drone-based IR thermography at 3 sites in All-India Survey 2018. However, only at one site comprehensive comparison of drone based thermography and ground based hand-held thermography could be performed. The results from that analysis are presented in this section. Drone-based imaging has several advantages, such as very high throughput, 100% inspection, no need for system disconnection, identification of different types of defects etc. It is especially useful if drone based imaging is followed up with an on-ground detailed inspection of affected modules. In this analysis, we performed drone-based imaging, which was followed by an on-ground detailed inspection; in which IR images were taken by hand-held portable FLIR E60 camera (FLIR based IR camera). In the ground-based inspection (done by FLIR based IR camera), we inspected modules that were detected by the drone as faulty and also modules which were not identified by the drone as faulty. Modules which had high Module $\Delta T$ (detected by drone and ground based IR image) were brought back to NCPRE (IIT Bombay), and detailed *I-V* curve and EL imaging were done in a laboratory environment. For this analysis, all images were taken under MPPT conditions for both drone and ground-based IR imaging. IR images were taken from the front side via drone, but FLIR based images were taken from the back side of the PV module. Drone imaging was done before the site survey, which was later compared with images taken by FLIR camera on site. In Fig. 6.24, we observe that hot spots identified by drone were also seen in images taken by FLIR based IR camera.

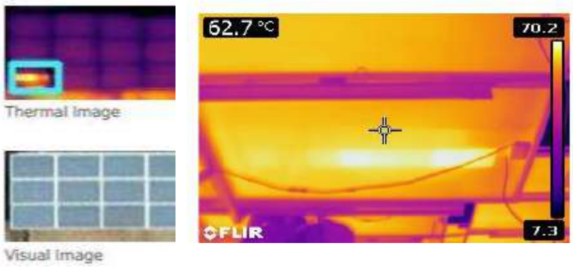


(a)

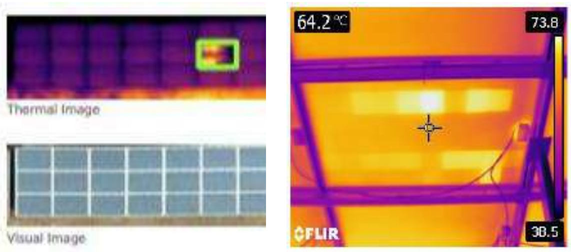


(b)

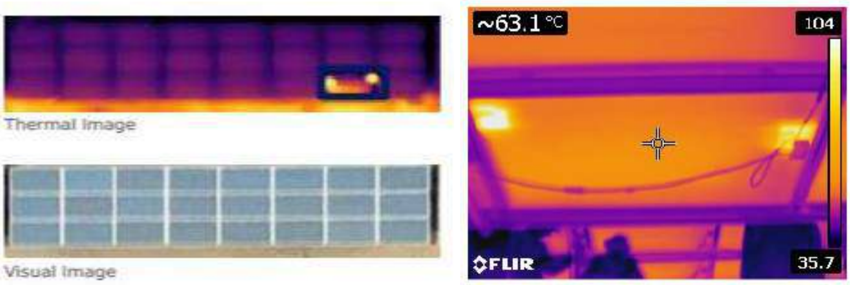


(c)

Fig. 6.24. IR image taken by Drone (left) and FLIR E60 portable camera (right) for three PV modules (a), (b) and (c)

Modules which showed high Module $\Delta T$ (detected by drone and FLIR imaging) were brought to NCPRE, IIT Bombay. By EL imaging and current-voltage characteristic curve done in the laboratory, we identified that these modules had diode failure, which can be seen in Fig. 6.25 where the entire sub-string of cells (first two and the last two strings in the PV module) appear dark in EL images. In Fig. 6.19 the current-voltage (*I-V*) characteristic curve was measured using SPIRE Sun Simulator 5600SLP under standard test conditions (1000W/m$^2$ and 25 $^0$C). Please note that PV modules shown in Fig 6.24 are different from PV modules shown in Fig 6.25.

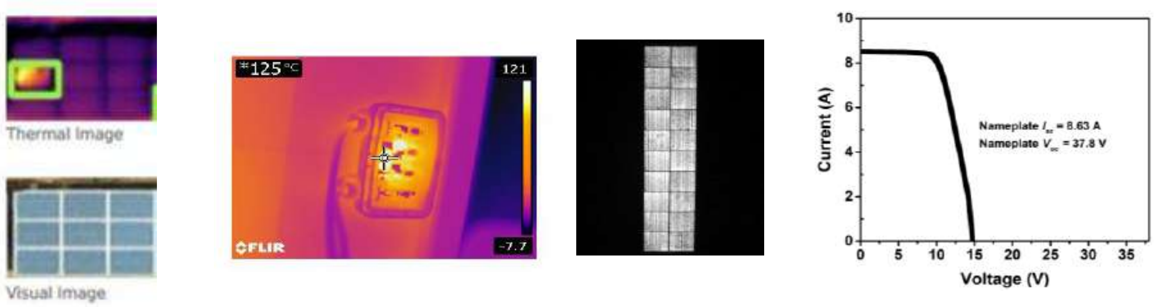


(a)

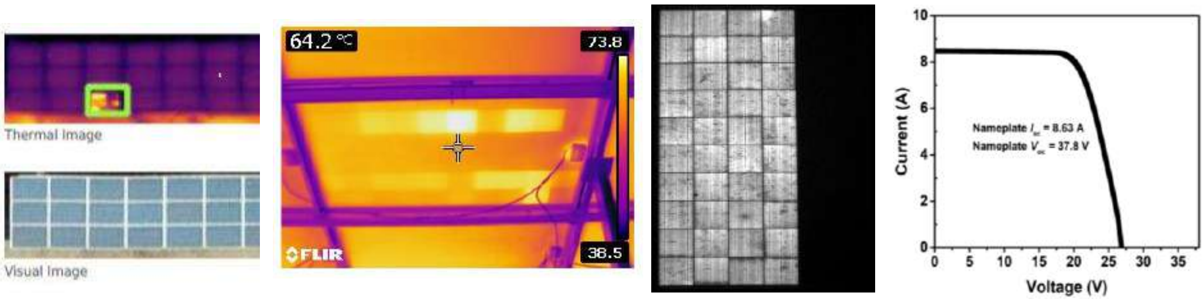


(b)

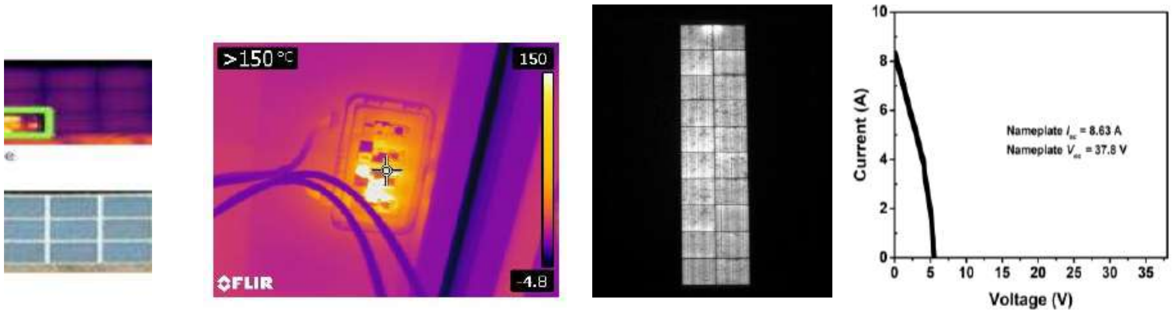


(c)

Fig. 6.25. IR image taken by Drone (extreme left) and FLIR E60 portable camera (middle left) of three modules (a), (b) and (c) in field. EL images (middle right) and STC *I-V* curve (extreme right) of the modules (a), (b) and (c) taken in laboratory conditions.

We also analysed some PV modules which did not show any hot spots in drone-based imaging. From these selected PV modules, we identified 3 PV modules (based on images taken from FLIR camera) which showed translated Module ΔT between 4 $^0$C to 5 $^0$C (shown in Fig 6.26), that may lead to an increase in $P_{max}$ degradation rates explained in section 6.3.2. , but was not identified by drone-based IR thermography. Under the conditions in which the drone images were collected, we observed greater sensitivity to identifying hot spots with Delta T greater than 4 $^0$C. For better sensitivity to identifying hot spots with smaller Module ΔT with drones, different flight and camera sensitivity parameters may be required. This study shows that the defects identified by the drone were also seen in ground-based imaging (done by FLIR camera). However, drone-based imaging was able to detect modules of higher $Module\ \Delta T$. Low $Module\ \Delta T$ may be detected by drone with different flight and camera sensitivity parameters.

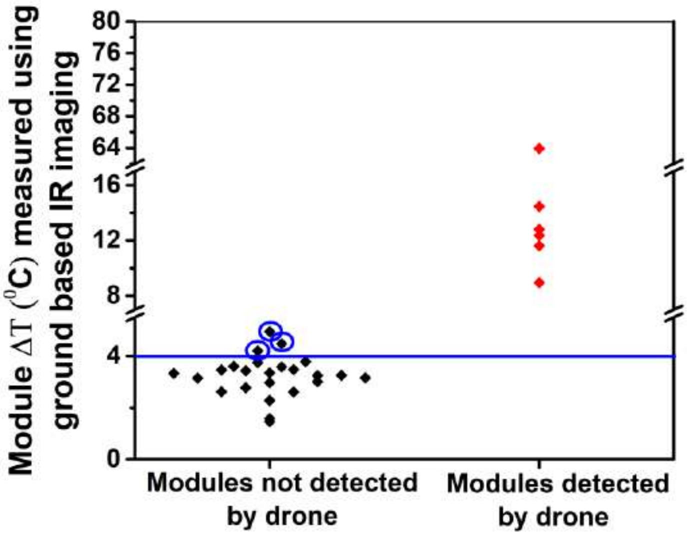


Fig. 6.26. $Module\ \Delta T$ measured by ground-based IR camera of modules which were detected (red) and not detected (black) by drone.

## 6.4 Summary

From the analysis of EL and IR images, we may conclude the following:

- Percentage of Mode A cracks is high, which may be due to poor transport and installation conditions, and also due to reduced thickness of wafers in Young modules. Although Mode A cracks do not result in power loss, they can later develop into Mode B and Mode C cracks which may cause power loss.
- Small/medium system sizes show more cracks compared to large system sizes.
- Power degradation correlates well with thermal mismatch under MPPT and short circuit conditions. Under MPPT condition PV modules with Module $\Delta T$ > 4 ºC show a significant increase in power degradation.
- 18% of PV modules inspected in the 2018 Survey show significant hot spots which lead to higher power degradation
- Modules with hot cells show higher degradation in both Hot and Non-hot zones, which was also seen in the 2016 All-India Survey. The effect of hot cells in Hot zones is particularly significant.
- Module $\Delta T$ which signifies temperature mismatch between the cells in a module is higher for old modules. This shows that hot spots / temperature mismatch is not one of the reasons for high degradation seen in Young PV modules (shown in chapter 4).
- We observed that some hot spots (with high Module $\Delta T$) show their signature in visual images in terms of browning, and cell cracks in electroluminescence imaging
- IR images taken by drone were able to identify hot spots which were verified by images taken on-ground by the FLIR camera. However, drone-based imaging was able to detect modules of higher $Module\ \Delta T$. Low $Module\ \Delta T$ may be detected by drone with different flight and camera sensitivity parameters.

# 7. Analysis of Sites Affected by Potential Induced Degradation (PID)

## 7.1 Introduction

Potential Induced Degradation (PID) is relatively recently identified degradation mechanisms in fielded PV modules that are subject to high (negative) voltages with respect to ground [66], [67]. PID was found to be the key degradation mechanism responsible for high degradation observed in some young sites in 2018 All-India Survey (see Fig. D.1, Appendix-D).

## 7.2 Techniques for Identification of PID

In order to identify whether a site was affected by PID, we followed a PV module selection procedure at the site, and adopted some techniques for detecting PID signatures in the data collected. In the new PV module selection procedure (described in Chapter 1), we have chosen three or four PV modules respectively from the beginning of the string (positive side), the middle of the string, and the end of the string (negative side). On these selected PV modules, we then performed all the detailed characterization tests like *I-V* measurement, IR imaging, and EL imaging as described earlier.

The primary step to detect PID was to observe the EL images of the modules with respect to the module position in the string from starting (positive side). If the solar cells in the border region (and/or the middle or other regions) of modules located only at (or near) the negative end of the string appear considerably dark, then we suspect them of being affected by PID [67]. The next step in the PID detection procedure was to look at the degradation rates of $P_{max}$, $I_{sc}$, $V_{oc}$, and *FF* of the modules in the suspected PID-affected string, and the calculation of shunt resistance ($R_{sh}$) from the *I-V*. All of these parameters are known to provide signatures for the presence of PID. A PID-affected module typically shows large power degradation, with the major contribution coming from FF degradation caused by reduced shunt resistance [67]. Finally, since PID affects modules near the negative end of the string, we also checked the positional dependence of the above parameters (dark cells in EL, $P_{max}$ degradation and $R_{sh}$ reduction). In particular, to check positional dependence of $P_{max}$, we calculated the Spearman Rank Correlation coefficient [68] for all the strings in the PID affected sites, by considering the position of the module in the string as the independent variable, and degradation of $P_{max}$ as dependent variable. In the next section, we show the results of the analysis for two of the PID-affected sites.

## 7.3 Results of PID affected sites

Out of the 36 sites that were inspected in the 2018 Survey, we observed PID signatures in 7 sites, of which 3 were roof-mounted and the remaining 4 were ground-mounted installations. In this section, we show all our analysis results for two such sites.

**Site 1:**

This is a Large and Ground-mounted site located in Hot & Dry climatic zone with an age of 6.25 years. We have performed all characterization tests at the site on the selected PV modules. We started with our primary step to detect PID which is observation of EL images of the PV modules in a string. As seen in Chapter 6, EL imaging is a powerful characterization technique to identify many of the defects in PV modules like cracks in the solar cell and interconnect breakage. It is also useful for primary identification of PID. We inspected three strings (String 2, String 4 and String 6), which were from Combiner Box 9 of Inverter 9 of this particular site. Fig. 7.1 shows the EL image of the 2nd PV module in String 4 (near the positive end), Fig. 7.2 shows the EL image of the 10th PV module in String 4 (near the middle), and Fig. 7.3 shows the EL image of the 22nd PV module in String 4 (near the negative end). We can clearly observe the difference between the EL images of the non-PID affected PV modules (2nd and 10th), and the PID affected PV module (22nd). Many of the border and some other cells in the middle of the 22nd PV module look very dark, and its location near the negative end leads us to suspect String 4 might be affected by PID.

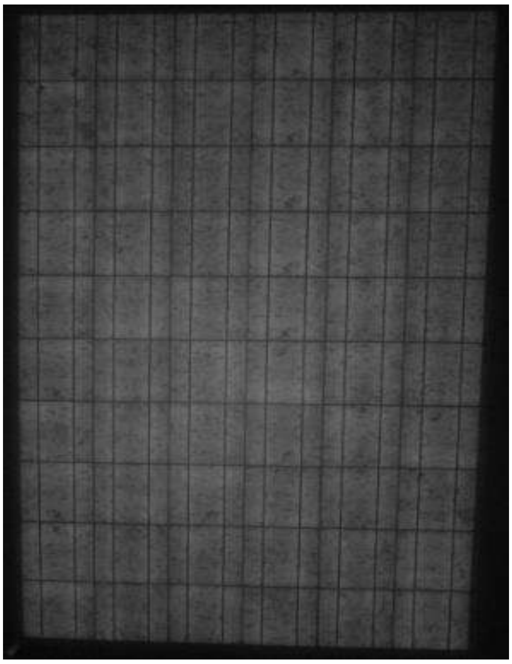

Fig.7.1. EL image of 2nd PV module of String 4

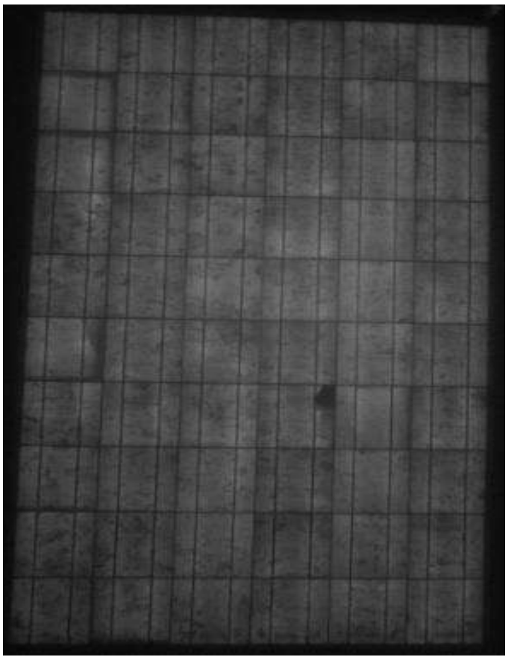

Fig.7.2. EL image of 10th PV module of String 4

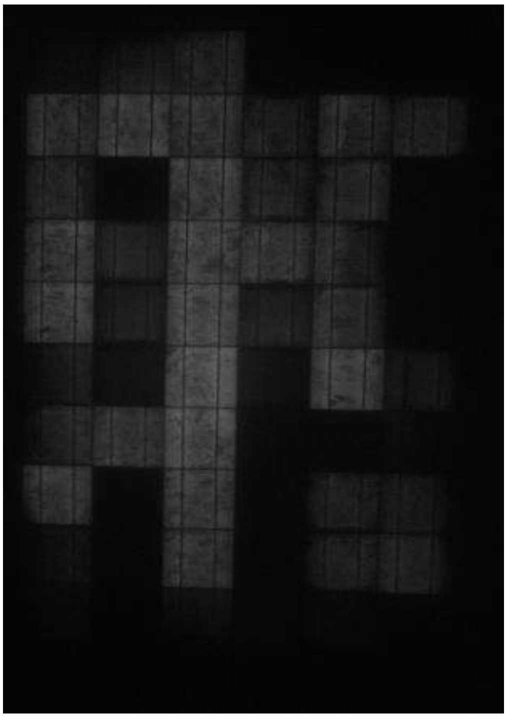

Fig.7.3. EL image of 22nd PV module of String 4

Fig. 7.4 shows the overall degradation and overall degradation rate on Y-axes, and position of each PV module in a string from the positive side on X-axis. As mentioned above, there were three strings which were inspected. Each string has 22 PV modules, and the overall degradation rate and total overall degradation of $P_{max}$ of the PV modules located at or near the negative end of the string are higher than those located towards the positive end or the middle, especially for String 4. One important point to mention is that even though the limit of our outliers is 5.21 %/year in the overall degradation rate of $P_{max}$, we have included such outliers in this PID analysis. Fig. 7.4 shows the maximum power of one of the PV modules has already degraded by 47%. This further supports the existence of PID in String 4 for which the EL images were shown earlier.

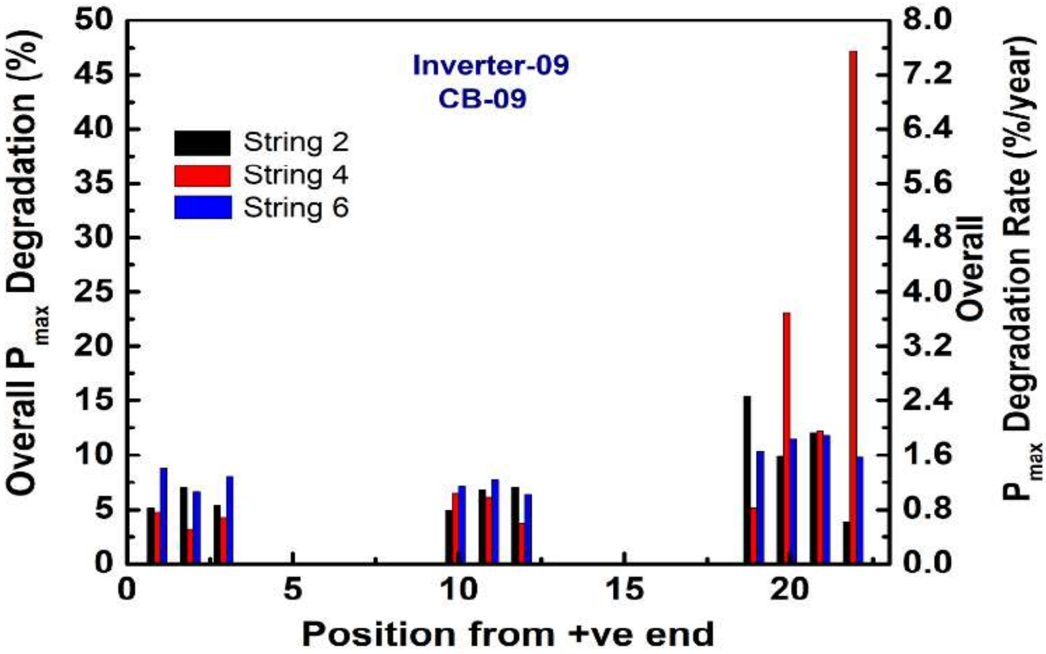


Fig. 7.4. Total overall degradation and overall degradation rate of $P_{max}$ of PV modules from positive side of the string for Strings 2, 4, and 6 of Combiner Box 9 of Inverter 9

We next calculate the Spearman Rank Correlation coefficient $r_s$ using the following formula

$$r_s = 1 - \frac{6\Sigma d_i^2}{n(n^2-1)} \qquad \text{.........(7.1)}$$

In Eqn. 7.1, $n$ is the number of PV modules characterized in a string, and $d_i$ is the difference between both the ranks, i.e. the difference between "Rank of Module No" and "Rank of degradation of $P_{max}$". The Rank of Module Number should be assigned based on position of the PV module in ascending order (from positive end), and Rank for degradation of $P_{max}$ should be assigned based on the overall degradation of $P_{max}$ of each PV module in ascending order.

The Spearman Rank Correlation coefficient is used to assess how well the relationship between two variables can be described using a monotonic function, even if their relationship is not linear. The value of Spearman Rank Correlation coefficient can be anywhere between −1 to +1. The sign of Spearman Rank Correlation coefficient indicates the direction of association between the independent variable (in this case, the position of PV module in the sting) and the dependent variable (in this case, overall degradation ($P_{max}$) of PV modules in the sting). If the dependent variable increases with the independent variable, the Spearman Rank Correlation coefficient is positive, and if it decreases, the coefficient is negative. If the coefficient is zero, it indicates that there is no tendency of dependent variable to either increase or decrease. For a perfectly monotonic increasing function, the magnitude of Spearman Rank Correlation coefficient is equal to 1. The extent of monotonicity depends on magnitude of this coefficient: a value of 0-0.39 implies weak monotonicity, 0.40-0.59 moderate, and 0.60-1.0 implies strong to strong monotonicity [68].

Tables 7.1, 7.2 and 7.3 show the percentage of overall degradation of $P_{max}$, Spearman Rank Correlation coefficient calculation and Shunt Resistance ($R_{sh}$) of all the PV modules that were inspected from Strings 2, 4 and 6 respectively.

Table 7.1. Spearman Rank Correlation coefficient and Shunt Resistance of String 2 PV modules

| Module No (from +ve end) | Degradation of $P_{max}$ (%) | Rank of Module No | Rank of Degradation of $P_{max}$ | $d_i$ | $d_i^2$ | Shunt Resistance (Ω) |
|---|---|---|---|---|---|---|
| 01 | 5.15 | 1 | 3 | -2 | 4 | 144.93 |
| 02 | 6.96 | 2 | 6 | -4 | 16 | 171.13 |
| 03 | 5.40 | 3 | 4 | -1 | 1 | 138.92 |
| 10 | 4.93 | 4 | 2 | 2 | 4 | 194.06 |
| 11 | 6.73 | 5 | 5 | 0 | 0 | 132.35 |
| 12 | 7.01 | 6 | 7 | -1 | 1 | 124.32 |
| 19 | 15.45 | 7 | 10 | -3 | 9 | 82.14 |
| 20 | 9.87 | 8 | 8 | 0 | 0 | 160.10 |
| 21 | 12.01 | 9 | 9 | 0 | 0 | 63.08 |
| 22 | 3.84 | 10 | 1 | 9 | 81 | 88.53 |
| **Spearman Rank Correlation Coefficient ($r_s$) = 0.297** | | | | | | |

Table 7.2. Spearman Rank Correlation coefficient and Shunt Resistance of String 4 PV modules

| Module No (from +ve end) | Degradation of $P_{max}$ (%) | Rank of Module No | Rank of Degradation of $P_{max}$ | $d_i$ | $d_i^2$ | Shunt Resistance (Ω) |
|---|---|---|---|---|---|---|
| 01 | 4.77 | 1 | 4 | -3 | 9 | 109.40 |
| 02 | 3.16 | 2 | 1 | 1 | 1 | 219.97 |
| 03 | 4.21 | 3 | 3 | 0 | 0 | 171.24 |
| 10 | 6.47 | 4 | 7 | -3 | 9 | 108.06 |
| 11 | 6.12 | 5 | 6 | -1 | 1 | 62.68 |
| 12 | 3.71 | 6 | 2 | 4 | 16 | 113.68 |
| 19 | 5.19 | 7 | 5 | 2 | 4 | 179.95 |
| 20 | 23.05 | 8 | 9 | -1 | 1 | 52.32 |
| 21 | 12.16 | 9 | 8 | 1 | 1 | 92.15 |
| 22 | 47.14 | 10 | 10 | 0 | 0 | 9.58 |
| **Spearman Rank Correlation Coefficient ($r_s$) = 0.745** | | | | | | |

Table. 7.3. Spearman Rank Correlation coefficient and Shunt Resistance of String 6 PV modules

| Module No (from +ve end) | Degradation of $P_{max}$ (%) | Rank of Module No | Rank of Degradation of $P_{max}$ | $d_i$ | $d_i^2$ | Shunt Resistance (Ω) |
|---|---|---|---|---|---|---|
| 01 | 8.79 | 1 | 6 | -5 | 25 | 144.93 |
| 02 | 6.61 | 2 | 2 | 0 | 0 | 171.13 |
| 03 | 8.05 | 3 | 5 | -2 | 4 | 138.92 |
| 10 | 7.06 | 4 | 3 | 1 | 1 | 194.06 |
| 11 | 7.77 | 5 | 4 | 1 | 1 | 132.35 |
| 12 | 6.35 | 6 | 1 | 5 | 25 | 124.32 |
| 19 | 10.36 | 7 | 8 | -1 | 1 | 82.14 |
| 20 | 11.45 | 8 | 9 | -1 | 1 | 160.10 |
| 21 | 11.80 | 9 | 10 | -1 | 1 | 63.08 |
| 22 | 9.78 | 10 | 7 | 3 | 9 | 88.53 |
| **Spearman Rank Correlation Coefficient ($r_s$)= 0.588** | | | | | | |

We can clearly observe from the tables that all the three strings have a higher power degradation for the PV modules located at the negative side. The shunt resistance of these PV modules is also very low. The Spearman Rank Correlation coefficient for String 4 is very high (0.745), so there exits strong monotonicity, for String 6 is quite high (0.588) implying moderate monotonicity, and for String 2, it is low (0.297) implying exits weak monotonicity. These results show that String 4 almost certainly shows PID, and probably Strings 2 and 6 also (the lower, but still positive, value of the coefficient can be due to other reasons for power degradation) shows PID signature, as we observed the border cells of negative side PV modules look dark in EL images of the PV modules of these strings also.

**Site 2:**

This is a Large and Roof-mounted site located in the Composite climatic zone with an age of 4 years. We have performed all characterization tests at the site on the selected PV modules. We inspected three strings (String 1, String 2 and String 3), which were from Combiner Box 1 of Inverter 2 of this particular site. Each string has 15 modules. We started with our primary step to detect PID, which is observation of EL images of the PV modules in a string. Fig. 7.5 shows the EL image of the 1$^{st}$ PV module in the String 1, Fig. 7.6 shows the EL image of the 7$^{th}$ PV module in the String 1, and Fig. 7.7 shows the EL image of the 13$^{th}$ PV module in the String 1. We can clearly observe the difference between the EL images of non PID affected modules (1$^{st}$ and 7$^{th}$) and the PID affected module (13$^{th}$). Some of the border cells in the latter module looks very dark, so we suspect that string to be affected by PID. Next, we inspect the $P_{max}$ degradation with respect to relative position of the PV module, starting from the positive side.

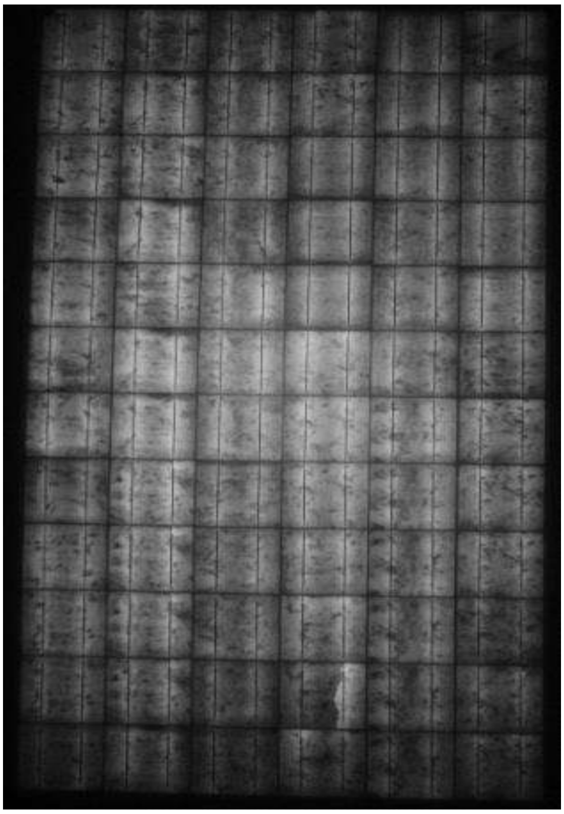

Fig.7.5. EL image of 1st PV module of String 1

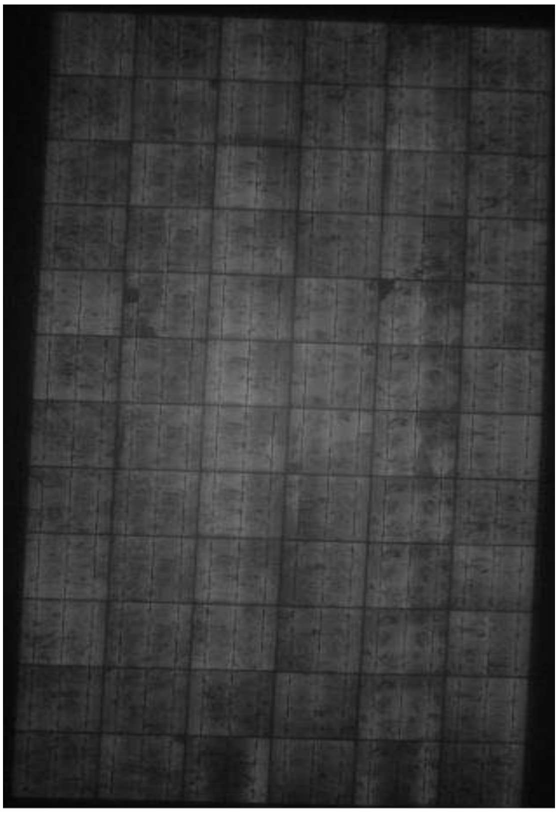

Fig.7.6. EL image of 7th PV module of String

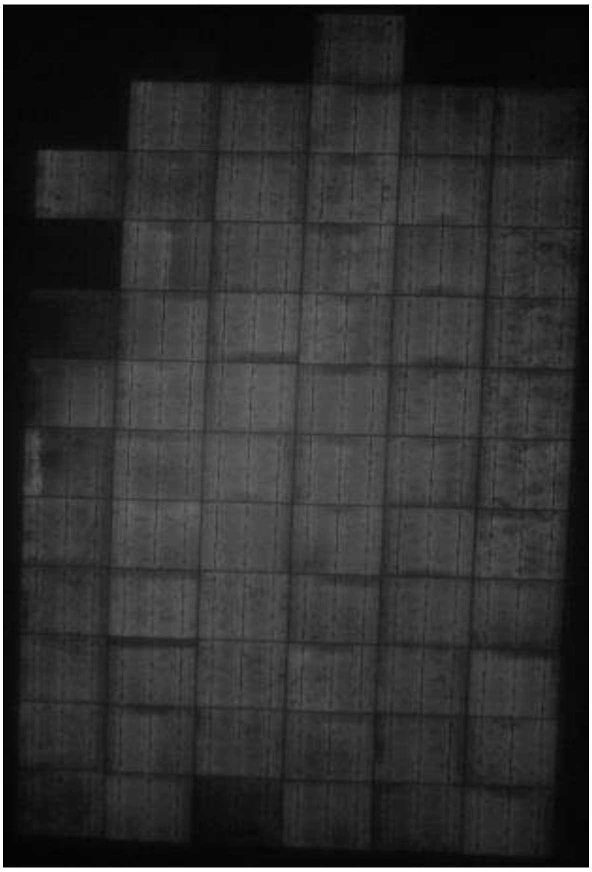

Fig.7.7. EL image of 13th PV module in String 1

Fig. 7.8 shows the overall degradation and overall degradation rate of $P_{max}$ on Y-axes and position of each PV module in a string from the positive side on X-axis. We can observe that for String 1 and String 2, the overall degradation rate and overall degradation of $P_{max}$ of the modules located at the negative end of the string are very high compared to those located towards the positive side or the middle of the string. String 3 seems to be not affected by PID.

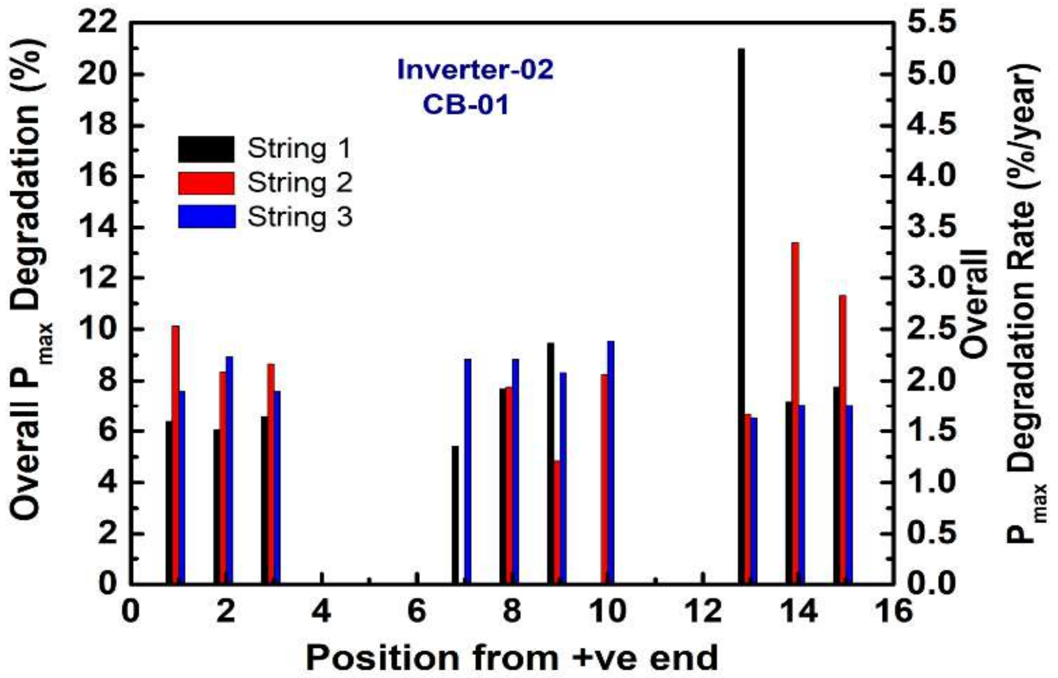


Fig.7.8. Overall degradation and degradation rate of $P_{max}$ of PV modules from positive side of the string for String 1, 2, and 3 of Combiner Box 1 of Inverter 2

Tables 7.4, 7.5 and 7.6 show the percentage of overall degradation of $P_{max}$, and the Spearman Rank Correlation coefficient calculation, as well as Shunt Resistance ($R_{sh}$) of all the PV modules that were inspected from Strings 1, 2 and 3. We can clearly observe from Table.7.4 and 7.5 that Strings 1 and 2 have higher overall power degradation for modules located at the negative end, and the shunt resistance of these PV modules also low. The Spearman Rank Correlation coefficient for String 1 is very high (0.7), so there exits strong monotonicity, whereas for String 2 is low but positive (0.091), so there exits very weak monotonicity. As seen from Table 7.6 for String 3, the PV modules located at the negative end do not show higher degradation compared to other PV modules, and the coefficient is negative (– 0.479). The shunt resistance is also not noticeably less for the modules located near the negative end. It therefore appears that String 3 is *not* affected by PID. Unfortunately, we do not have the EL images of negative side PV modules of String 3 to perform the primary analysis step of PID. But the other PID characterization parameters signifies, String 3 was not affected by PID. This indicates that all the strings from a particular site may not be equally affected by PID.

Table. 7.4. Spearman Rank Correlation coefficient and Shunt Resistance of String 1 PV modules

| Module No (from +ve end) | Degradation of $P_{max}$ (%) | Rank of Module No | Rank of Degradation of $P_{max}$ | $d_i$ | $d_i^2$ | Shunt Resistance (Ω) |
|---|---|---|---|---|---|---|
| 01 | 6.38 | 1 | 3 | -2 | 4 | 166.37 |
| 02 | 6.03 | 2 | 2 | 0 | 0 | 274.46 |
| 03 | 6.57 | 3 | 4 | -1 | 1 | 268.27 |
| 07 | 5.41 | 4 | 1 | 3 | 9 | 238.54 |
| 08 | 7.69 | 5 | 6 | -1 | 1 | 274.36 |
| 09 | 9.46 | 6 | 8 | -2 | 4 | 151.71 |
| 13 | 20.99 | 7 | 9 | -2 | 4 | 76.23 |
| 14 | 7.18 | 8 | 5 | 3 | 9 | 136.24 |
| 15 | 7.75 | 9 | 7 | 2 | 4 | 122.11 |
| **Spearman Rank Correlation Coefficient ($r_s$)= 0.7** | | | | | | |

Table. 7.5. Spearman Rank Correlation coefficient and Shunt Resistance of String 2 PV modules

| Module No (from +ve end) | Degradation of $P_{max\_LID}$ (%) | Rank of Module No | Rank of Degradation of $P_{max\_LID}$ | $d_i$ | $d_i^2$ | Shunt Resistance (Ω) |
|---|---|---|---|---|---|---|
| 01 | 10.13 | 1 | 8 | -7 | 49 | 222.57 |
| 02 | 8.34 | 2 | 6 | -4 | 16 | 227.68 |
| 03 | 8.66 | 3 | 7 | -4 | 16 | 302.26 |
| 08 | 7.76 | 4 | 4 | 0 | 0 | 355.00 |
| 09 | 4.84 | 5 | 1 | 4 | 16 | 340.10 |
| 10 | 8.25 | 6 | 5 | 1 | 1 | 156.48 |
| 11 | 6.44 | 7 | 2 | 5 | 25 | 165.54 |
| 13 | 6.66 | 8 | 3 | 5 | 25 | 391.71 |
| 14 | 13.41 | 9 | 10 | -1 | 1 | 98.40 |
| 15 | 11.31 | 10 | 9 | 1 | 1 | 172.01 |
| **Spearman Rank Correlation Coefficient ($r_s$)= 0.091** | | | | | | |

Table. 7.6. Spearman Rank Correlation coefficient and Shunt Resistance of String 3 PV modules

| Module No (from +ve end) | Degradation of $P_{max\_LID}$ (%) | Rank of Module No | Rank of Degradation of $P_{max\_LID}$ | $d_i$ | $d_i^2$ | Shunt Resistance (Ω) |
|---|---|---|---|---|---|---|
| 01 | 7.589 | 1 | 5 | -4 | 16 | 213.18 |
| 02 | 8.917 | 2 | 9 | -7 | 49 | 306.81 |
| 03 | 7.588 | 3 | 4 | -1 | 1 | 146.14 |
| 07 | 8.835 | 4 | 8 | -4 | 16 | 270.68 |
| 08 | 8.832 | 5 | 7 | -2 | 4 | 175.74 |
| 09 | 8.306 | 6 | 6 | 0 | 0 | 439.16 |
| 10 | 9.552 | 7 | 10 | -3 | 9 | 331.76 |
| 13 | 6.509 | 8 | 1 | 7 | 49 | 143.10 |
| 14 | 7.038 | 9 | 3 | 6 | 36 | 274.52 |
| 15 | 7.023 | 10 | 2 | 8 | 64 | 278.52 |
| **Spearman Rank Correlation Coefficient ($r_s$)= – 0.479** | | | | | | |

## 7.4 Summary

Potential Induced Degradation (PID) is observed to be one of the key degradation mechanisms responsible for high degradation rates seen in significant number of young sites. We used these signatures to identify PID: dark cells in EL images of PV modules near the negative end of the string, reduction in power of modules near the negative end, and reduction in shunt resistance near the negative end. We calculated the Spearman Rank Correlation coefficient to assess the positional dependence of power loss. Based on these tests, we did find evidence of PID, and we believe that 7 sites out of the 36 sites that we inspected, showed signs of PID. In this chapter, we have given typical results of 2 of these 7 sites.

# 8. Quantification of Reliability of PV Modules

## 8.1 Introduction

A proper quantification of the reliability of PV modules is necessary for choosing the reliable modules for installation in a power plant in a specific operating environment. The reliability of a PV module can be quantified by using the Risk Priority Number (RPN) analysis. PV modules have different failure modes or defects based on the materials used for the construction of the module and the operating conditions. In this survey, the team has found different failure modes in different climatic zones. Among the identified failure modes and their effects on the basis of priority ranking, a criticality analysis has been done by using a quantitative index, known as Risk Priority Number (RPN). This analysis is done based on Failure Modes, Effects and Criticality Analysis (FMECA) as per IEC 60812 [70]. RPN is estimated as per the following equation:

$$RPN = S \times O \times D \qquad \ldots(8.1)$$

Where, $S$ is the severity, representing the impact of failure mode or defects; $O$ is the occurrence, representing the probability of occurrence of failure mode based on the field data; and $D$ is the detection, representing the ability of recognizing or spotting and removing or preventing of failure modes of the analyzed system.

The failure modes/defects are observed in PV modules after long term exposure in the field conditions. In this analysis, there are 86 defects of PV modules which are used, and the details are given in Table 8.1 and Table 8.2. Table 8.1 shows 25 defects related to safety failures of PV modules. Table 8.2 shows 61 defects related to performance failure modes of PV modules [71, 72, and 73].

Table 8.1. Defects of PV module related to safety failures

| Glass | Frame | Junction box |
|---|---|---|
| Front glass crack<br>Front glass shattered<br>Rear glass crack<br>Rear glass shattered | Frame grounding severe corrosion<br>Frame grounding minor corrosion<br>Frame joint separation<br>Frame cracking | Junction box crack<br>Junction box burn<br>Junction box lose<br>Junction box lid fell off<br>Junction box lid crack<br>Junction box sealing will leak |
| **Backsheet** | **Wire** | **Cell** |
| Backsheet peeling<br>Backsheet delamination<br>Backsheet burn<br>Backsheet crack/cut under cell<br>Backsheet crack/cut between cell | Wires burnt<br>Wires animal bite/marks<br>Wire insulation cracked | Hot spot above 20 $^0$C<br>String interconnect arc tracks |

Table 8.2. Defects of PV module related to performance failure

| Glass | Frame | Junction box |
|---|---|---|
| Front glass lightly soiled<br>Front glass heavily soiled<br>Front glass crazing<br>Front glass chip<br>Front glass milky discoloration<br>Rear glass crazing<br>Rear glass chip | Major corrosion of frame<br>Minor corrosion of frame<br>Frame bent<br>Frame degraded<br>Frame oozed<br>Frame adhesive missing | Junction box lid loose<br>Junction box warped<br>Junction box weathered<br>Junction box adhesive loose<br>Junction box adhesive fell off<br>Junction box wire attachments loose<br>Junction box wire attachments fell off<br>Junction box wire attachments arced |
| **Cell** | **Encapsulant** | **Backsheet** |
| Cell discoloration<br>Cell burn Mark<br>Cell crack<br>Cell moisture penetration<br>Cell worm mark<br>Cell foreign particle embedded<br>Cell Interconnect discoloration<br>Gridline discoloration<br>Gridline blossoming<br>Busbar discoloration<br>Busbar corrosion<br>Busbar burn marks<br>Busbar misaligned<br>Cell Interconnect ribbon discoloration<br>Cell Interconnect ribbon corrosion<br>Cell Interconnect ribbon burn mark<br>Cell Interconnect ribbon break<br>String Interconnect discoloration<br>String Interconnect corrosion<br>String Interconnect burn mark<br>String Interconnect break<br>Hot spot less than 20˚C | Encapsulant delamination over the cell<br>Encapsulant delamination under the cell<br>Encapsulant delamination over the junction box<br>Encapsulant delamination near interconnect or fingers<br>Encapsulant discoloration -- (yellowing/browning) | Backsheet wavy<br>Backsheet discoloration<br>Backsheet bubble |
| **Edge Seal** | **Wires** | **Others** |
| Edge seal delamination<br>Edge seal moisture penetration<br>Edge seal discoloration<br>Edge seal squeezed/pinched out | Wires pliable degraded<br>Wires embrittled<br>Wires corroded<br>Wires soiled | Solder bond fatigue/failure<br>Potential Induced Degradation (PID) |

# 8.2 Methodology

## 8.2.1 Severity

Severity (*S*) ranking of defects in a PV module is analyzed based on the performance of the PV module in terms of power, short circuit current, fill factor and open circuit voltage. Severity was determined by ranking the failure mode of degradation from 1 to 10, where 1 indicates that the observed degradation mode has no effect on performance, and 10 indicates a major effect in terms of both power and safety [71, 72, and 73]. The severity ranking is done by performance analysis with different defects for individual PV power plants. Defects are divided into two categories: safety failure mode, and performance failure mode as shown in Tables 8.1 and 8.2. The degradation rates of PV modules in terms of $P_{max}$, $I_{sc}$, $V_{oc}$, and *FF* are analyzed for performance defects. The average degradation rate for each defect is arranged and grouped into different categories. The scale is discrete and not continuous because correlating specific degradation modes to certain power losses varies with operating conditions. For each defect observed in a power plant, a ranking is given for a group of average degradation values. For safety failure mode, the ranking is done based on the severity of safety and average degradation rate for the particular defect. However, it is very necessary to provide high ranking for a defect with the risk of electric shock.

## 8.2.2 Occurrence

Occurrence (*O*) ranking is done on the basis of defects observed in a power plant. The frequency of occurrence of each failure mode has been calculated by plotting the histogram of the number of modules for a particular defect. This ranking corresponds to the observed number of failures that are occurring for a cause over the operational life of the PV power plant. Failure modes are identified in terms of probability of occurrence, grouped into discrete levels. The cumulative number of module failures for each defect per thousand per year (CNF) is calculated by using the following formula:

$$\mathrm{NF}/1000 = \frac{(\text{cumulative \% of defects})/10}{\text{cumulative operating time}} = \frac{\sum_{\text{systems}} \frac{\text{\% defects}}{10}}{\sum_{\text{system}} (\text{operating time})} \qquad \ldots\ldots\ldots (8.2)$$

The ranking is done by making a group of CNF/1000 for different defects and ranking them from 1 to 10. The ranking is high with high occurrence.

## 8.2.3 Detection

Ranking of detection ($D$) of each failure mode is done based on the criteria of detection with monitoring system/procedure used during the survey. The inspection of the power plant is done through visual inspection and with sophisticated tools such as EL camera, *I-V* tracer, IR camera, insulation tester, digital camera, etc. The *D* ranking 1 of a defect is given if the defect is easily detectable by scheduled/regular maintenance or event-triggered inspections. In this study, lower-rank is given for the detection of defects with a visual inspection, middle-rank is given for the detection of defects which can be identified only with indirect calculation procedure, and high ranking is given for defects identified only by using sophisticated tools. However from the reliability perspective, the ranking of detection procedure should be normalized.

### 8.2.4 Performance and Safety RPN

In this study, modules are separated into two categories: modules with less than 5 years of exposure ('Young' modules) and modules with greater or equal to 5 years of exposure in the field condition ('Old' modules). RPN analysis of failure modes/defects is divided into two categories: performance RPN and safety RPN. The risk priority number is analyzed for failure defects related to performance defects (referred to as Performance RPN) and for failure defects of PV module related to safety issues (referred to as Safety RPN). Thus two different RPN (equation (8.1)) values are calculated.

It has been observed that some defects which are not easily detectable are also not very severe. But due to the high value of *D* (detection), the RPN is estimated to be high for such defects. This may lead the PV community to a wrong conclusion, and care should be exercised. The RPN analysis is also done for different power plant for each climatic zone individually. The distributions of the rank of different defects are plotted with the maximum value observed in the respective climatic zone.

## 8.3 Results and Discussion

All the modules are analyzed as per safety, reliability and durability failure definitions stated by Shrestha *et al.* [71]. Shrestha *et al.* have mentioned that defects with safety issues can be termed as safety failure, and modules with degradation rate more than 1 %/year (excluding modules with safety issues) are termed as modules with reliability failure; and modules with degradation rate less than 1 %/year (excluding modules with safety issues) but having other defects are termed as modules with durability failure. In Fig. 8.1, a pie chart of durability loss, safety failure, and reliability failures of the studied Old modules for the different climatic zones are plotted (note that our Survey did not have any Old modules in Moderate climatic zone). In Cold & Sunny zone, the percentage of reliability failure is the minimum as compared to all other climatic zones for the Old modules with failure modes. The percentage value of reliability failure is the highest in Hot & Dry climatic zone as compared to other zones for the Old module with failure modes.

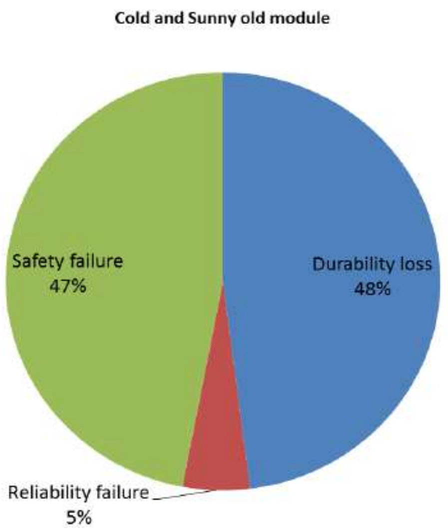


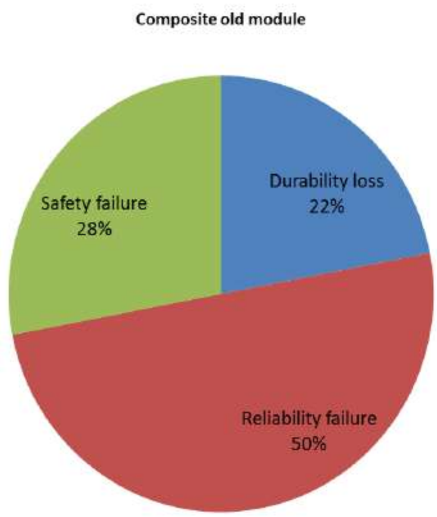

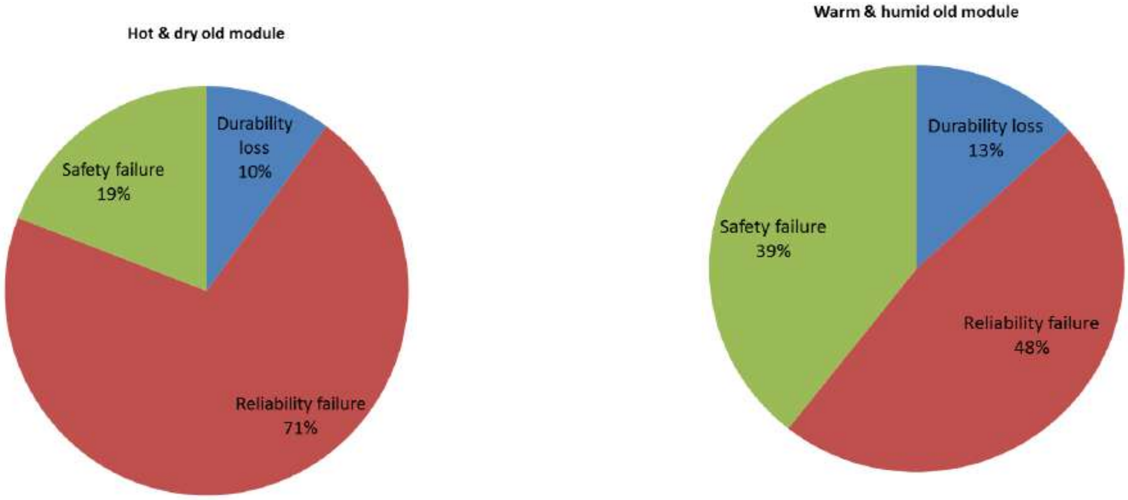


Fig. 8.1. Safety failure, Reliability failure and Durability loss of Old modules for different climatic zones

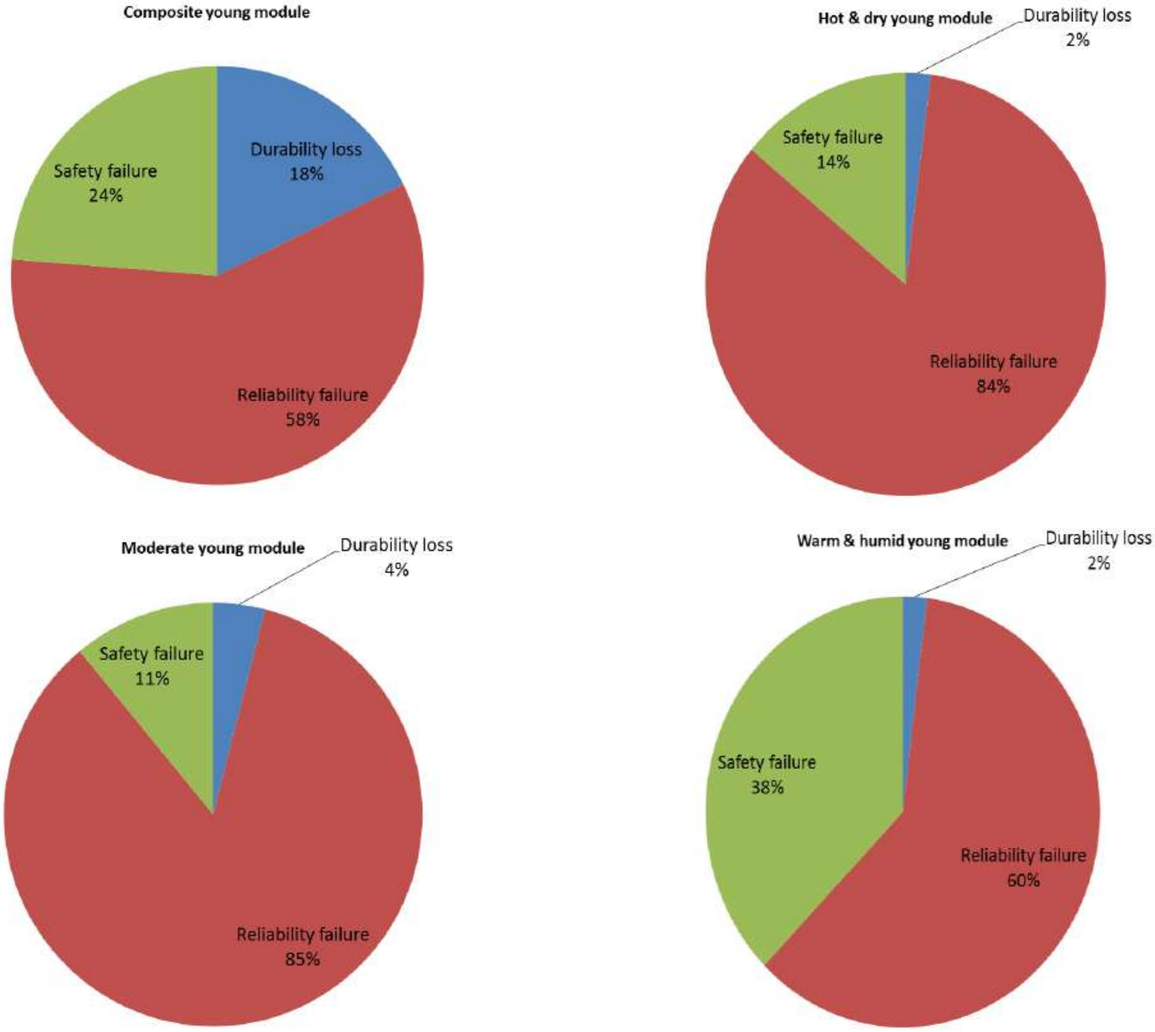


Fig. 8.2. Safety failure, Reliability failure and Durability loss of Young modules for different climatic zones

Fig. 8.2 shows a pie chart of durability loss, safety failure, and reliability failures of the studied Young modules for the different climatic zones (note that our Survey did not have any Young modules in Cold & Sunny climatic zone). In the Composite zone, the percentage of reliability failure is minimum as compared to all other climatic zones for Young modules with failure modes. The percentage of reliability failure is the highest in Moderate and Hot & Dry climatic zones as compared to other zones for Young modules with failure mode.

## 8.3.1 Severity rank of failure modes

The severity ranking *S* of failure modes is based on the performance of the PV module in terms of power, short circuit current, fill factor and open circuit voltage. First we divide the failure modes into two parts: Safety failure mode, and Performance failure mode. For a given severity rank of safety failure mode, the degradation rate of the PV module is estimated for different electrical parameters. The average degradation rate for each failure mode is estimated for different PV modules and given a rank based on the degradation rate. Fig. 8.3 shows the severity rank of performance failure modes for different climatic zones of Old modules. Fig. 8.4 shows the same for Young modules in different climatic zones. For Old modules the highest rank of severity for performance failure occurs for Potential Induced Degradation, solder bond failure, busbar burn marks, cell burn marks and snail tracks. The severity rank for performance failure modes in Young modules is generally high as compared to Old modules for different climatic zones. This again supports our observation that Young modules are appearing to perform worse than Old modules.

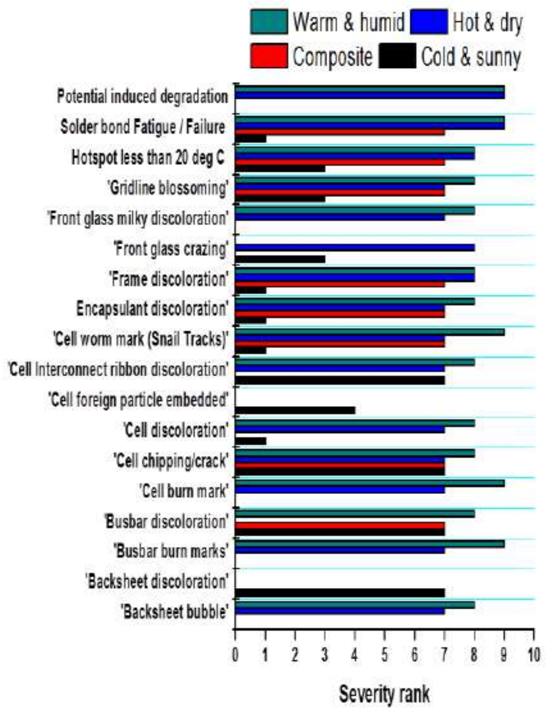


Fig. 8.3. Severity rank of performance failure mode in Old PV modules

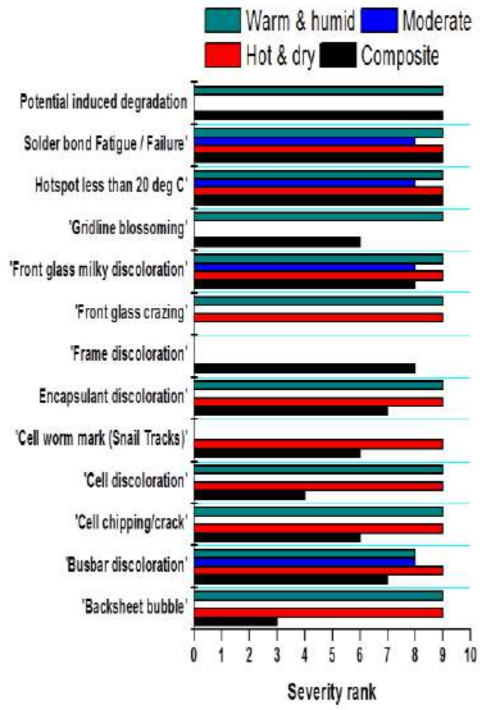


Fig. 8.4. Severity rank of performance failure mode in Young PV modules

Fig. 8.5 shows the severity rank of safety failure mode found in PV modules of different climatic zones. The rank of severity in safety failure modes is estimated based on its effect on performance and safety.

In the case of Young modules in *Moderate climatic zone*, the maximum degradation rate of 1.95 %/year is observed in the modules with glass discoloration. All the modules from this zone with different failure modes have shown average degradation rate more than 1.5 %/year. The highest performance severity rank of value 8 is assigned for this category of module with these failure modes: Front glass discoloration, Busbar discoloration, Solder bond failure, and Hot spot. The highest safety severity rank 9 is assigned to hot spot with high-temperature difference in the Moderate climatic zone.

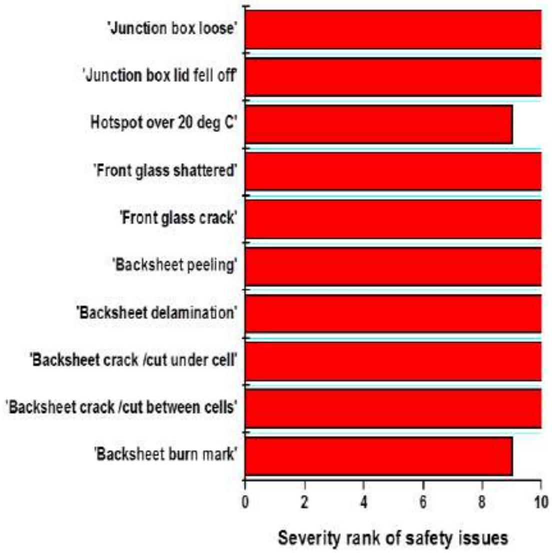


Fig. 8.5. Severity rank of safety failure mode in PV modules

In the case of *Warm & Humid climatic zone*, the degradation rate of more than 3.4 %/year is observed in the Old modules with busbar burn marks, cell burn marks, and cell worm marks. The maximum degradation of 6.5 %/year (outlier module) is observed in the Old module with PID. Those modules under study with defects have shown degradation rate of more than 1.6 %/year. The highest value of performance severity rank is assigned for these failure modes: Busbar burn marks, Cell burn mark, Cell worm mark, solder bond Fatigue, and PID. The highest value of safety severity rank is assigned for these failure modes: Problem in front glass, backsheet delamination & backsheet crack /cut. In case of Young modules in Warm & Humid climatic zone, degradation rate of more than 3.4 %/year is observed in modules with Gridline blossoming, Cell discoloration, Cell chipping/crack. Those modules under study in this category with defects have shown degradation rate more than 1.8 %/year. The maximum degradation of 7.1 %/year (outlier module) is observed in the Young modules with PID. The highest value of performance severity rank is assigned for these failure modes: problem in front glass, back sheet bubble, gridline blossoming, cell discoloration, cell crack, solder bond failure, hot spot, encapsulant discoloration and PID. The highest value of safety severity rank is assigned for this failure mode: hot spot with high temperature.

In the case of Old modules in *Hot & Dry climatic zone*, degradation rate of more than 2.1 %/year is observed in the module with solder bond failure defect. The maximum degradation of 7.5 %/year (outlier module) is observed in the Old module with PID. The highest value of performance severity rank is assigned to solder bond fatigue and to PID. The highest value of safety severity rank is assigned for these failure modes: front glass shattered, back sheet peeling, back sheet delamination, back sheet crack /cut. In case of Young module in Hot & Dry climatic zone, maximum degradation rate of 3.2 %/year is observed in the module with these failure modes: cell discoloration, solder bond fatigue, and hot spot. The highest value of performance severity rank is assigned for these failure modes: problem in front glass, back sheet bubble, busbar discoloration, cell discoloration, cell chipping & worm mark, solder bond fatigue, hot spot, and encapsulant discoloration. The highest value of safety severity rank is assigned for these failure modes: problem in front glass, back sheet burn mark, back sheet crack /cut, and hot spot.

In the case of the Old modules in *Composite climatic zone*, maximum degradation rate of 1.3 %/year is observed in the module with encapsulant discoloration. The highest value of performance severity rank is assigned for these failure modes: frame discoloration, gridline blossoming, busbar discoloration, cell chipping & worm mark, solder bond fatigue, hot spot, and encapsulant discoloration. The highest value of safety severity rank is assigned for these failure modes: front glass shattered, back sheet delamination. In case of Young modules in Composite climatic zone, degradation rate of 2.3 %/year is observed in the modules with solder bond fatigue, hot spot. The maximum degradation of 7.5 %/year (outlier module) is observed in the Young module under this zone with PID. The highest value of performance severity rank is assigned for these failure modes: solder bond fatigue, hot spot and PID. The highest value of safety severity rank is assigned for these failure modes: problem in front glass, back sheet delamination, hot spot with high temperature.

In the case of the Old module in *Cold & Sunny climatic zone*, maximum degradation rate of 1.1 %/year is observed in the module with cell crack. The highest value of performance severity rank is assigned for these failure modes: backsheet discoloration, busbar discoloration, cell interconnect ribbon discoloration, encapsulant discoloration and cell crack. The highest value of safety severity rank is assigned for failure mode: junction box lose, junction box lid fell off and backsheet peeling.

## 8.3.2 Occurrence

As mentioned above, the occurrence rank of failure mode is estimated based on the frequency of occurrence of particular failure mode in different PV power plant of a climatic zone. The cumulative number of module failures for each defect per thousand per year (CNF) is calculated using equation (8.2).

Fig. 8.6 & 8.7 show the occurrence rank of different failure modes observed in Young and Old modules of different climatic zones. In the case of the Young module in *Moderate climatic zone*, the CNF is the highest for solder bond failure and its value is 187 and busbar discoloration has the lowest CNF and its value is 7. In case of Old modules in *Warm & Humid zone*, the CNF is highest for cell discoloration, PID and the CNF is the lowest for failure mode: busbar burn marks, cell burn mark, and cell worm mark. In case of Young modules in *Warm & Humid zone*, the CNF is high for solder bond fatigue and next PID. The CNF is the lowest for failure mode: front glass crazing, busbar discoloration, and its value are 5. In case of Old modules in *Hot & Dry zone*, the CNF is high for cell discoloration and PID. The CNF is the lowest for problem in front glass and its value is 0.5. In case of Young module in *Hot & Dry zone*, the CNF is the highest for failure modes: problem in front glass, solder bond fatigue and its value is more than 120. The CNF is the lowest for failure mode: problem in front glass, backsheet bubble, cell chipping, cell worm mark, and its value are 1.6. In case of Old modules in *Composite zone*, the CNF is the highest for solder bond fatigue and its value is 71. The CNF is the lowest for cell worm mark and its value is 1.3. In case of Young module in *Composite zone*, the CNF is the highest for solder bond fatigue and next PID. The CNF is the lowest for the back sheet bubble and its value is 1.3. In case of Old module in *Cold & Sunny zone*, the CNF is the highest for cell discoloration and its value is 36. The CNF is the lowest for foreign particle embedded and its value is 0.6.

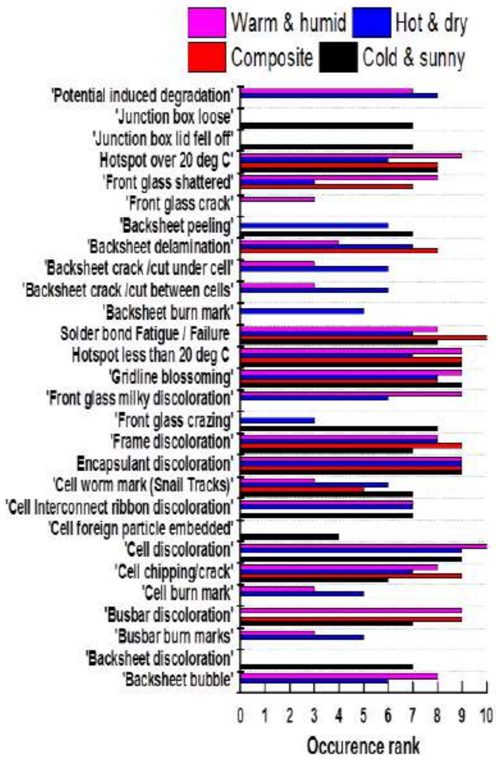


Fig. 8. 6. Occurrence rank of performance failure mode in Old PV modules

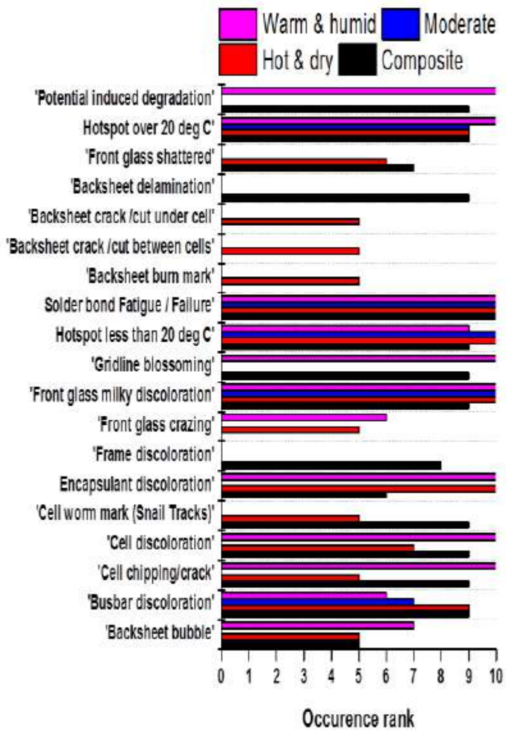


Fig. 8. 7. Occurrence rank of performance failure mode in Young PV modules

## 8.3.3 Detection

Fig. 8.8 shows the detection (*D*) rank of different failure modes observed in different climatic zones. The detection rank of different failure modes is based on the criteria of detection. In this study, almost all the failure modes are detected in the field except the solder bond defect and PID. The solder bond defect, hot spot detection and PID include calculation and analysis after collecting data. The detection rank of hot spot is 5 and for solder bond fatigue and PID, it is 8. The rank of all the other failure modes is assigned the value 2.

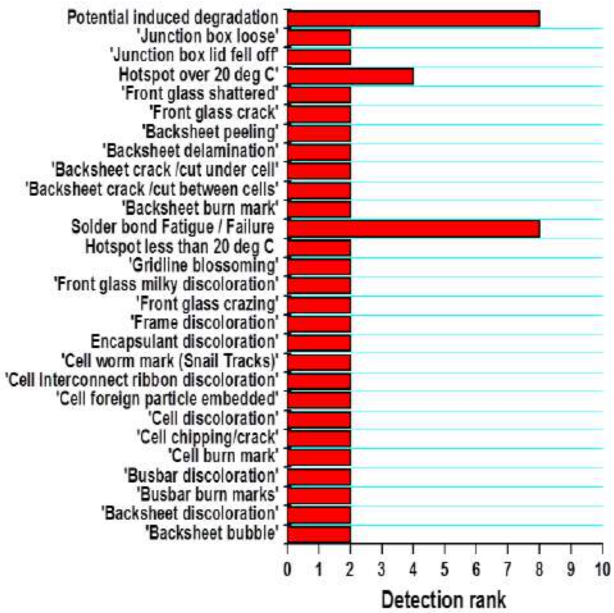


Fig. 8. 8. Detection rank of failure mode in PV modules

### 8.3.4 Performance RPN

Figs. 8.9 and 8.10 show the RPN values of performance failure modes in Old and Young modules for different climatic zones. In the case of the Young modules in *Moderate climatic zone*, solder bond fatigue shows the highest performance RPN value and its value is 640. The parameter which is mainly affected for this defect is the *FF* and the RPN for *FF* for solder bond failure mode is 560. The lowest performance RPN is estimated for busbar discoloration and its value is 112.

In case of the Old modules in *Warm & Humid climatic zone*, the highest severe performance failure mode is found to be the solder bond fatigue and its value is 576. The electrical parameters which are mainly affected for this defect are $I_{sc}$ and *FF*. The RPN for $I_{sc}$, in this case, is 384 and for *FF* it is 448. The second highest performance failure mode for this climatic zone is PID and its RPN value is 448. The lowest performance RPN value found in these failure modes: busbar burn mark, cell burn mark, cell worm mark. In case of Young modules in Warm & Humid climatic zone, solder bond failure is the highest severe failure mode with RPN value of 720. The electrical parameters which are mainly affected are $I_{sc}$ and *FF*. The RPN value of $I_{sc}$ is 480 and for *FF* it is 560. The second most severe defect for this climatic zone is PID and its RPN value is 640. The lowest value of performance RPN is found in busbar discoloration.

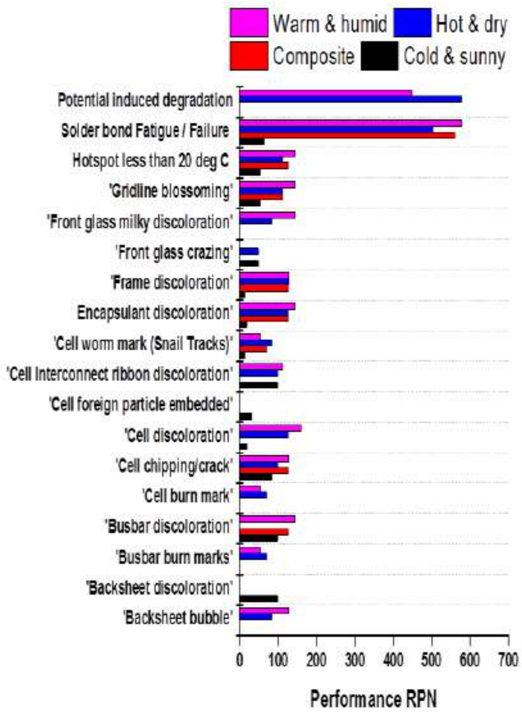


Fig. 8. 9. Performance RPN of failure mode in Old PV modules

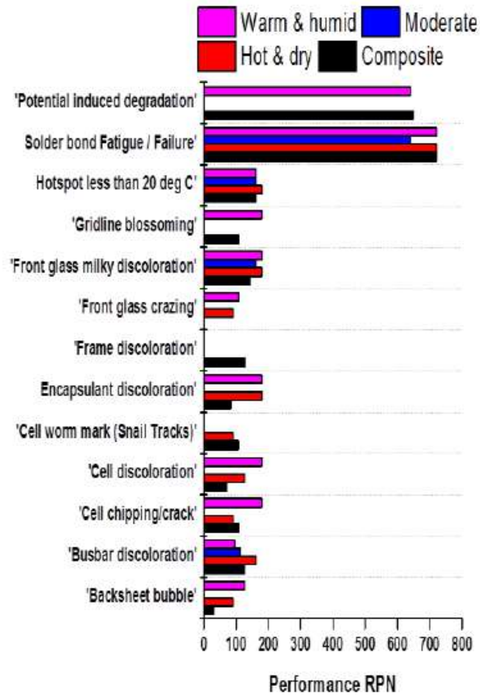


Fig. 8. 10. Performance RPN of failure mode in Young PV modules

In the case of the Old modules in *Hot & Dry climatic zone*, the performance RPN value is highest for PID with value 576. The performance RPN value is second highest for solder bond fatigue with value 504 and the main affected parameter is *FF* with RPN value 392. The third-highest performance RPN value is found in the case of frame discoloration for this category of module. The lowest performance RPN value is found for problem in glass. In case of Young modules in Hot & Dry climatic zone, the performance RPN value is the highest for solder bond fatigue with RPN value 720. The main affected parameters are $V_{oc}$ and *FF*. The value of RPN for $V_{oc}$ is 400 and for *FF* it is 560. The second highest of the performance RPN values (180) are observed for these failure modes: problem in front glass, hot spot, encapsulant discoloration. The lowest performance RPN value is observed for these failure modes: problem in front glass, back sheet bubble, cell crack, cell worm mark.

In the case of the Old modules in *Composite climatic zone*, solder bond fatigue is the most severe performance defect with RPN value 560. The main affected parameter is *FF* and its RPN value is 560. The second-highest performance RPN value observed for these failure modes: frame discoloration, busbar discoloration, cell crack, hot spot, and encapsulant discoloration. The lowest performance RPN observed is the cell worm mark failure mode for this category of modules. In the case of Young modules in Composite zone, solder bond fatigue is the most severe performance failure mode with RPN value 720. The parameter which is mainly affected is *FF* and its RPN value is 560. The second most severe performance failure mode is PID with RPN value 648. The lowest performance RPN value observed is back sheet bubble failure mode for this category of modules.

In the case of the Old modules in *Cold & Sunny zone*, the most severe performance failure modes are back sheet discoloration, busbar discoloration, cell interconnect ribbon discoloration with RPN value of 98, and the second most severe performance failure mode is cell cracks. The lowest performance RPN is observed in case of cell worm mark failure mode.

## 8.3.5 Safety RPN

Figs. 8.11 and 8.12 show the safety RPN of failure modes in Young and Old PV modules of different climatic zones. In the Young modules of *Moderate climatic zone*, the only safety failure mode observed is a hot spot with high temperature and its RPN value is 324. In the case of the Old modules in *Warm & Humid climatic zone*, the most severe safety failure mode is hot spot with high temperature and its RPN value is 324. The second most severe safety failure mode is problem in the front glass. In the Young modules of *Warm & Humid climatic zone*, only safety failure mode observed is hot spot with high temperature and its RPN value is 400. In case of Old modules in *Hot & Dry climatic zone*, the most severe safety failure mode is hot spot with high temperature and its RPN value is 216. The second most severe safety failure is back sheet delamination and its RPN value is 140. In Young modules of *Hot & Dry climatic zone*, the most severe safety failure mode is hot spot with high temperature and its RPN value is 360. The second most severe safety failure mode is problem in front glass with RPN value 120. In case of Old modules in *Composite zone*, the most severe defect is hot spot with high temperature and its RPN value is 288. The second most severe safety failure mode is problem in front glass with RPN value 140. In case of Young modules in *Composite zone*, the most severe safety defect is hot spot with high temperature and its RPN value is 360. The second most severe safety failure mode is problem in front glass with RPN value 140. In case of Old modules in *Cold & Sunny climatic zone*, the most severe safety defect is hot spot with high temperature and its RPN value is 360. The second most severe safety failure modes are junction box loose, junction box lid fell off, back sheet peeling and the value of RPN is 140. It can be seen that hot spots pose the most common risk as far as safety is concerned.

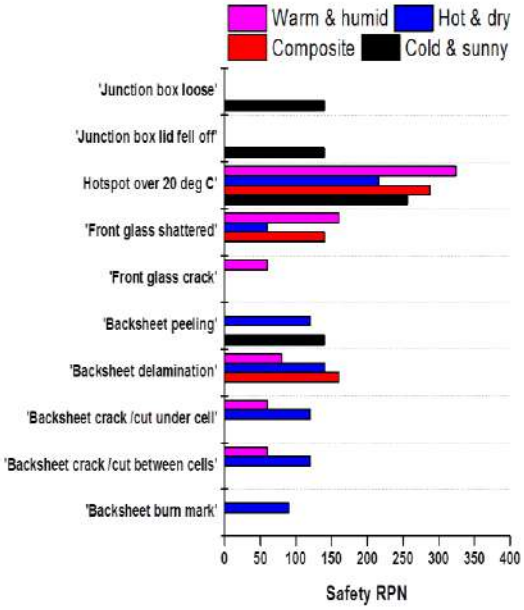


Fig. 8.11. Safety RPN of failure mode in old PV Old PV modules

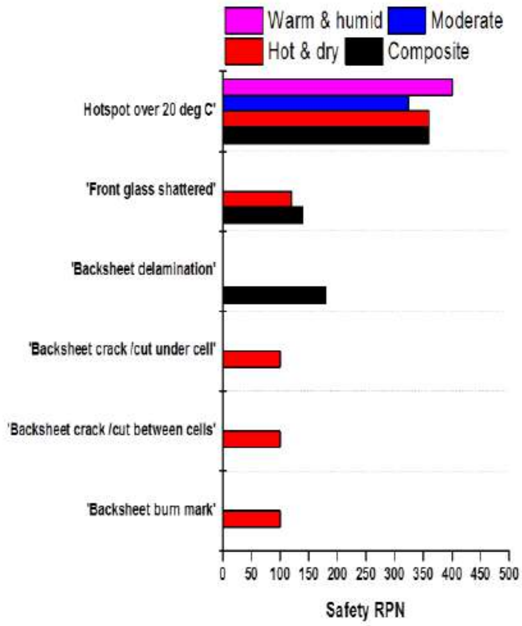


Fig. 8.12. Safety RPN of failure mode in Young PV modules

## 8.4 Summary

The quantification of the reliability of PV modules inspected during the survey has been performed as per IEC 60812 standard. The performance failure rates of PV modules are high in Young modules (age < 5 years) as compared to Old modules (age > 5 years). Modules deployed in Cold & Sunny climate had a considerably lower variety of failure modes of degradation for the studied modules. Solder bond fatigue/failure is one of the common defects in all climatic zones. PID, delamination and junction box issues are more prevalent in Hot & Dry, Warm & Humid and Composite climates than in other climates. The highest concerns in case of Young modules for Hot zones are PID and solder bond defect, although modules are qualified as per IEC standards. So, new testing conditions need to be explored for the climatic conditions of India for these failure modes. The highest concerns of systems with Old modules appear to be hot spots, the problem in internal circuitry, and problems in the back sheet. Snail tracks are common in both Young and Old modules in all the climates. Hot spot with high temperature is one of the common safety failure modes for all the climatic zones.

# 9. Conclusions and Recommendations

## 9.1 Conclusions

We present below the major conclusions of the 2018 All-India Survey of Photovoltaic Module Reliability conducted during March - May 2018. The survey covered 1199 modules in 36 sites spread over five climatic zones of India. The age of the modules ranged from 1 year to more than 25 years, and included 7 technologies, though the majority was crystalline silicon (both multi and mono). In the 2018 Survey, a special effort was made to include more utility-scale power plants, as these represent the increasingly dominant type of installations in India. Of the 36 sites, 27 were large installations with installed capacity more than 100 kW (many were above 1 MW), and 23 of these were ground-mounted sites. Of the 36 sites, 17 were ‘repeat’ sites (they had been also inspected in the 2014 and/or 2016 Surveys), and 19 were fresh sites being inspected for the first time in 2018.

Broadly speaking, the results obtained during the 2018 All-India Survey of Photovoltaic Module Reliability are in consonance with the results of the earlier 2016 and 2014 Surveys. This lends confidence to the results obtained during the surveys. By and large, we see again that there is a wide distribution of the observed degradation rate (%/year), meaning that there are some sites which perform well, whereas some sites do not. Modules in ‘Hot’ climates show, on average, higher degradation rates than those in ‘Non-Hot’ climates. Young modules (whose age is less than 5 years) show higher degradation than Old modules (age > 5 years), even after accounting for the initial rapid decline due to LID and other causes. PID, interconnect damage and hot spots were identified to be the key degradation mechanisms responsible for higher degradation rates seen in some of the Young sites. Ground-mounted modules perform better than roof-mounted modules in terms of degradation rate. Cracks and micro-cracks (observed through EL) are observed in many modules. We compare later in this Section the 2018 results with those of the 2016 and 2014 Surveys.

These main results of the 2018 Survey are given below in bulleted form. Arising out of these results, we make several recommendations which are presented in the next Section. These recommendations, if adopted with seriousness, will ensure that the installations coming up in future will show better overall performance than we have seen thus far, and thereby ensure success of the National Solar Mission.

- The performance of PV modules surveyed is found to vary widely. The Annual ‘Linear’ Degradation Rates for crystalline silicon modules vary from less than 0 %/year to more than 5%/year, even after discounting 2% degradation in initial power output due to LID. (Some negative degradation rates seen in the field for young modules are ascribed to measurement/translation error, under-rating by the manufacturer and uncertainty in initial degradation.) Observations made by visual, IR, EL and other means also show significant variation in the degradation of PV modules.

- The average linear degradation rate is 1.22 %/year for the 1199 modules encompassing all technologies, and 1.47 %/year if only c-Si modules are considered. These numbers, especially for c-Si, are rather high, and the reasons have been analysed carefully in this work.

- Young modules (age < 5 years) show a higher degradation rate than old modules (age > 5 years old). The observed average rates for c-Si modules are 1.85 %/year for Young modules and 1.14 %/year for Old modules. Note that these are the 'linear' degradation rates, in which the LID effect has been discounted. There are several possible factors responsible for higher LID discounted degradation rates seen in Young modules. For example, significant number of Young sites were observed to be affected by PID and interconnect degradation. The results suggest that newer installations have poorer quality of modules and/or installation practices, and also possibly over-rating of modules supplied in recent years. For Young modules, the main, indeed only, contributor for $P_{max}$ degradation is the fill factor (*FF*). For the Old modules, *FF* degradation again dominates but short circuit current ($I_{sc}$) degradation also plays a role.

- A detailed climatic zone analysis was performed. We find that c-Si modules in Warm & Humid (2.07 %/year) and Hot & Dry (1.53 %/year) climates degrade fastest. Modules in the benign Cold & Sunny climate perform very well, degrading at an average rate of just 0.23 %/year. Clubbing Hot & Dry, Warm & Humid, and Composite climates as 'Hot' climates, and the others (Moderate and Cold & Sunny) as 'Non-Hot' we see that modules in Hot climates degrade on average at 1.57 %/year, whereas those in Non-Hot climates degrade at 0.52 %/year. This stark difference between performance in Hot and Non-Hot climates was observed in previous surveys also. This is likely to be partly because of the higher incidence of encapsulant discoloration and metallization discoloration observed in the 'Hot' climates. Moreover, higher temperatures are known to accelerate several degradation mechanisms leading to faster wear out.

- Technology-wise, c-Si modules degrade faster than thin films: 1.47 %/year compared with ~ 0 %/year. However, this may be a reflection of the quality of manufacturing (all thin films come from a small number of reputed manufacturers whereas c-Si come a wide variety of manufacturers, some unknown), rather than an intrinsic technology dependence. Moreover, meta-stability and spectral effects in thin film modules are likely to introduce higher errors during STC translation.

- There does not appear to be much difference of degradation based on system size – large installations (>100 kW) show about the same rate of degradation as small/medium installations (<100 kW).

- Roof-(rack)-mounted modules suffer from a higher degradation rate as compared to ground-mounted modules, the respective values being 1.99 %/year and 1.33 %/year. Such a difference was observed in earlier Surveys as well. This means special attention is needed for the 40 GW rooftop target of India's National Solar Mission.

- We have performed a 'multi-point' analysis of degradation rates for modules which were inspected in earlier Surveys. This analysis shows that 'year-to-year' data matches well with data obtained by considering only the 2018 measured and the initial nameplate value. This lends good credibility to the measurements made in the 2018 and earlier Surveys.

- We have made a systematic effort in the 2018 Survey to identify the occurrence of PID. This was done by evaluating EL images, shunt resistance and positional dependence of the module (within the string). We see clear indications of PID in some strings in 7 sites of the 36 surveyed. Of the 7 sites, 3 were roof-mounted and 4 ground-mounted. Significant number of these PID affected sites belonged to the 'Young' category.

- Our analysis shows that the main causes of excess degradation, especially in the Young modules, are PID, finger/interconnect damage, hot spots, encapsulant discoloration and cell cracks. Further, there are several sites, most of them belonging to 'Young' category, where high degradation rates were observed, but no prominent signature of any failure mechanism was seen through various characterization techniques. For such sites, we suspect an unethical over-rating on the module nameplate, which might have resulted in an apparently excessive degradation rate, especially for Young modules.

- We have performed an extensive visual inspection of the modules. We have seen many visible signs of degradation, including encapsulant discoloration, delamination of front and back encapsulants, metallization discoloration and/or corrosion, visible cracks in the cells, snail tracks, backsheet scratches, and front glass haziness and cracks.
- Encapsulant discoloration is highest in the Hot climates (specifically Warm & Humid and Hot & Dry). Increased discoloration is one of the reasons for higher degradation rates observed in Hot climates, and we have observed a clear correlation between power loss and amount of discoloration as quantified by the Discoloration Index. Similarly, delamination is more prevalent in the Hot climates, especially the Warm & Humid climate.
- Cracks in the cells are often visible to the naked eye, enhanced by the presence of snail tracks and photobleaching. We find the prevalence of these to be more in Young modules, indicating problems in the installation process, or perhaps the quality of the cells themselves.
- Metal discoloration or corrosion is also more prevalent in Hot climates, and can be another reason for higher degradation rates seen in such climates. Indeed, we do see that modules with metal discoloration show, on average, higher degradation.
- Since cracks and micro-cracks are defects which we see often, we have performed extensive electroluminescence (EL) imaging, covering over 700 modules in our Survey. We used special portable EL cameras together with an image processing technique to obtain EL images in the evening, not having to wait till darkness. This extensive EL study also enabled us to identify PID-affected sites.
- We have found that cracks and micro-cracks are more prevalent in large ground-mounted systems, which is different from our observation of the 2016 Survey, where small roof-mounted systems showed higher prevalence of cracks. The reason for this difference is not clear, but may be related to the fact that this year we have many more large ground-mounted systems, which are all very young. It is possible that the 'youngness' of the sites has a dominant effect.
- Detailed IR thermography was performed under both MPPT and short-circuit conditions. This showed that 18% of the PV modules inspected in 2018 survey have significant hot spots that are responsible for higher power degradation. The power degradation observed correlated well with the module $\Delta T$, which is a measure of the temperature of the hot spot above the rest of the module. Under MPPT conditions, PV modules with Module $\Delta T$ > 4 ºC show a significant increase in power degradation. We also see that the effect of hot cells in Hot climates is significantly more pronounced than that of hot cells in Non-Hot climates – another reason that modules degrade faster in Hot climates. Overall translated module temperatures (at 1000 W/m$^2$ irradiance and 40 $^o$C ambient temperature) are higher for roof-mounted rather than ground-mounted systems. This indicates that the air circulation around the roof mounted modules on racks was poorer as compared to the air circulation around ground mounted modules on racks. Interestingly, the module $\Delta T$ is higher for ground-mounted modules. Usually higher extent of cracks can lead to such observation, however, in this survey, we have not seen significant

difference in the extent of cracks in ground mounted and roof mounted modules finally, we see that severity of hot spots in older modules is more than that in young modules.

- For the first time, we also performed drone-based IR thermography at one site, which was followed up with a detailed ground-based survey. Under the conditions in which the drone images were collected, we observed greater sensitivity to identifying hot spots with ΔT greater than 4 $^{o}$C. For better sensitivity to identifying hot spots with smaller ΔT with drones, different flight and camera sensitivity parameters may be required. Drone based IR imaging was found to be a promising technique for quick, 100% IR imaging of PV modules in a plant to identify modules with catastrophic failures or severe hot spots. Intelligent drone image processing software can significantly reduce the time required to provide actionable feedback to the PV plant O &M teams on poorly performing modules / strings.
- 99% of the surveyed modules have passed the dry insulation test (933 modules out of 943 modules for which the measurement was done).
- The 'Hot' climatic zones of India – 'Hot & Dry', 'Warm & Humid' and 'Composite', where most of the installations are likely to take place, present a challenging environment for PV modules in India. Problems encountered in these zones include higher annual degradation rates, greater incidence of hot cells, more encapsulant discoloration, and higher metal corrosion.
- The Risk Priority Number (RPN) analysis indicates again that performance failure rates are higher in Young modules compared to Old modules
- The RPN analysis shows that modules deployed in the Cold & Sunny zone have a very low variety of failure modes, thus lending further support to the observation of excellent performance in this climatic zone.
- The RPN analysis shows that solder bond fatigue/failure is very widespread, and also that PID, delamination and junction box issues are also prevalent in Hot climates.

It is worthwhile comparing the procedures and results obtained during the 2018 Survey with the results of the 2014 and 2016 Surveys. One important difference in the 2018 Survey was our procedure to choose the modules being inspected. In earlier Surveys, the process was random. In 2018, we chose modules from best, medium and worst performing strings of the best and worst performing inverters. (This was not done for repeat sites where we preferred to inspect the same modules as in the previous Surveys.) The new procedure enabled us to cover strings containing a total of 11270 modules, of which 1199 individual modules were selected for detailed analysis. Other measurement protocols were very similar in all surveys. However, during the analysis, we chose, in 2018, *not* to artificially separate out the Group X ('good') sites and Group Y ('bad') sites as we had done in previous years. In terms of the main results obtained, very similar conclusions emerge from all these Surveys. There is a wide variability in the performance – modules at some installations perform well, while those at other installations do not. This wide variability in performance indicates significant differences in the quality of modules being procured, and in installation practices being followed. There also appears to be evidence of under-rating of modules by conservative manufacturers, which give rise to very low or negative degradation rates, and over-rating by unethical ones, which give rise to unrealistically high rates. The average linear degradation rate observed in 2018 for c-Si modules is 1.47 %/year, which is same as that of observed in 2016. Nevertheless, it's still a high value and is certainly a cause for concern. In all our Surveys, we have consistently seen that modules in Hot climates degrade faster than those in Non-Hot climates; and modules on rooftops degrade faster than those which are ground-mounted. Furthermore, many of the defects seen by visible inspection and IR imaging and EL imaging also show similar trends in the two Surveys: encapsulant discoloration is prevalent in Hot climates, especially in older modules; and hot spots occur more frequently and have a more marked effect on degradation in Hot climates. On the other hand, we see a difference in the EL results in the 2016 and 2018 Surveys: cell cracks are seen to be more prevalent in ground-mounted installations than roof-mounted in 2018.

## 9.2 Recommendations

Based on, and arising out of, the above conclusions, we propose the following recommendations. Many of these are the same as we had made after the 2016 Survey, and we are happy to note that some of them have been useful to the photovoltaic community.

- Quality of modules can vary significantly, so due diligence should be exercised while selecting and procuring modules. This may include verifying the antecedents of the manufacturer, and independent checks on the quality of the module(s). Although most modules available in the market carry the IEC certification, it should be noted that the IEC certification is really a certification of the module design, and does not guarantee that the module will perform adequately through its intended life. The tender specifications need to be much more elaborate than currently being used.
- Materials used in modules are important. EVA and backsheet particularly can be of different qualities, and should be specified carefully in the tender document for procurement.
- Some cases of 'over-rating' of modules have definitely been observed. Owners and installers of power plants should be vigilant about this malpractice. Random measurements should be made on modules, and such checks should be specified in the tender documents as well. An independent audit of modules and installations by third party is recommended.
- Module manufacturers and installers should place more emphasis on proper packaging and handling of the modules during transportation since improper handling can induce cracks in the solar cells and lead to long-term degradation.
- It is recommended that a field-based electroluminescence (EL) study be performed after receiving the modules at site and after installation to reveal micro-cracks which may have been caused during the transport and installation phases.
- The presence of some modules suffering from PID in as many at 20% of the sites surveyed indicates the need to be cognizant of this failure mode, and to take appropriate steps, including attention to grounding, and installation of 'PID-free' modules. The use of instruments providing 'PID-reversal' may be explored at sites that are severely impacted by PID.
- It has been noted that the 'Hot' climates present a harsh operating environment for PV modules. An intensive study of degradation phenomena in hot climates, which has not been emphasized sufficiently by the PV community so far, is needed. This is particularly important for India, since much of the 100 GW is expected to come up in the 'Hot' zones of the country.
- The IEC certification protocols (e.g. 61215), and other standards are currently being updated to take into account the hot climate phenomena. This has arisen partly out of our All-India Survey reports which have consistently shown in 2013, 2014, 2016, and now in 2018 that modules in Hot climates degrade faster. The upcoming IEC technical specification (IEC 63126) would provide harsher accelerated tests for modules deployed in high temperature end use environments.

- Modules and sites perform very well in the 'Cold & Sunny' climate of Ladakh, as seen from all perspectives including the RPN analysis. We had recommended earlier that power plants should be set up in this region, as these would enjoy not only low degradation rates and higher performance ratios, but also excellent irradiance and easy availability of land. With the proposed grid links to Ladakh under construction, it is now appropriate that MNRE is pursuing 23 GW of solar PV in the region.
- It is felt that some of the quality issues seen especially in the young modules are the result of aggressive pricing and timelines and improper handling/installation. Reverse bidding has been extremely valuable to discover lower tariffs and bring down the cost of PV in India. However, now that the cost of PV electricity is comparable (or lower) with that of fossil fuel based generation in most parts of the country, it is recommended that clauses to ensure quality and reliability be included in the tenders. These clauses should attempt to go beyond the minimum IEC certification criteria to proactively ensure good quality of PV modules in the entire chain - from manufacturing to installation. The RPN data may help in identifying such clauses. This may result in stabilization of the tariffs to current values for some time (instead of further lowering), however, the benefit in terms of increased energy production during the service life of PV plants would outweigh the slightly higher initial costs.

# References


[1] https://mnre.gov.in/physical-progress-achievements

[2] https://m.economictimes.com/industry/energy/power/india-will-add-225-gw-renewable-energy-project-capacity-by-2022-r-k-singh/articleshow/64461995.cms

[3] R. Dubey, S. Chattopadhyay, V. Kuthanazhi, J. John, C. S. Solanki, A. Kottantharayil, B. M. Arora, K. Narsimhan, J. Vasi, B. Bora, Y. Singh and O.S. Sastry, *All-India Survey of Photovoltaic Module Degradation: 2013*, [Online] Available at: http://www.ncpre.iitb.ac.in/research/reports.html

[4] R. Dubey, S. Chattopadhyay, V. Kuthanazhi, J. John, F. Ansari, S. Rambabu, B. M. Arora, A. Kottantharayil, K. L. Narasimhan, J. Vasi, B. Bora, Y. K. Singh, K. Yadav, M. Banger, R. Singh and O. S. Sastry, *All-India Survey of Photovoltaic Module Reliability: 2014*, available at: http://www.ncpre.iitb.ac.in/research/reports.html

[5] S. Chattopadhyay, R. Dubey, V. Kuthanazhi, S. Zachariah, S. Bhaduri, C. Mahapatra, S. Rambabu, F. Ansari, A. Chindarkar, A. Sinha, H. K. Singh, N. Shiradkar, B. M. Arora, A. Kottantharayil, K. L. Narasimhan, S. Sabnis, J. Vasi, B. Bora, G. Kumar, Y. K. Singh, M. Bangar, M. Kumar, A. K. Haldkar, R. Singh, S. Raghava, M. Morampudi, G. Ganesh, R. Kumar and O. S. Sastry, *All-India Survey of Photovoltaic Module Reliability: 2016*, available at: http://www.ncpre.iitb.ac.in/research/reports.html

[6] R. Dubey, S. Chattopadhyay, V. Kuthanazhi, A. Kottantharayil, C. S. Solanki, B. M. Arora, K.L. Narasimhan, J. Vasi, B. Bora, Y. K. Singh and O.S. Sastry, "Comprehensive study of performance degradation of field-mounted PV modules in India," *Energy Science and Engineering* vol. 5, p. 51, 2017.

[7] S. Chattopadhyay, R. Dubey, V. Kuthanazhi, J. J. John, C. S. Solanki, A. Kottantharayil, B. M. Arora, K.L. Narasimhan, V. Kuber, J. Vasi, A. Kumar, O.S. Sastry, "Visual Degradation in Field-aged Crystalline Silicon PV Modules in India and Correlation with Electrical Degradation," *IEEE Journal of Photovoltaics* vol. 4, p. 1470, 2014.

[8] R. Dubey, S. Chattopadhyay, V. Kuthanazhi, J. J. John, J. Vasi, A. Kottantharayil, B. M. Arora, K.L. Narsimhan, C.S. Solanki, A. Kumar, O.S. Sastry, "Performance Degradation in Field-aged Crystalline Silicon PV Modules in Different Indian Climatic Conditions," *40th IEEE Photovoltaic Specialists Conference*, Denver, USA, 2014.

[9] S. Chattopadhyay, R. Dubey, V. Kuthanazhi, J. J.John, C. S. Solanki, A. Kottantharayil, B. M. Arora, K.L. Narasimhan, J. Vasi, B. Bora, Y. K. Singh and O.S. Sastry, "All-India Survey of Photovoltaic Module Degradation 2014: Survey Methodology and Statistics," *42nd IEEE Photovoltaic Specialists Conference*, New Orleans, USA, 2015.

[10] R. Dubey, S. Chattopadhyay, V. Kuthanazhi, J. J. John, C. S. Solanki, A. Kottantharayil, B. M. Arora, K.L. Narasimhan, J. Vasi, B. Bora, Y. K. Singh and O.S. Sastry, "Correlation of Electrical and Visual Degradation seen in Field Survey in India," *43rd IEEE Photovoltaic Specialists Conference*, Portland, USA, 2016.

[11] R. Dubey, S. Chattopadhyay, V. Kuthanazhi, A. Kottantharayil, C. S. Solanki, B. M. Arora, K.L. Narasimhan, J. Vasi, B. Bora, Y. K. Singh and O.S. Sastry, "Comprehensive study of performance degradation of field-mounted PV modules in India," *Energy Science and Engineering* vol. 5, p. 51, 2017.

[12] R. Dubey, S. Zachariah, S. Chattopadhyay, V. Kuthanazhi, S. Rambabu, S. Bhaduri, H. K. Singh, A. Sinha, C. S. Solanki, A. Kottantharayil, B. M. Arora, K. L. Narasimhan, J. Vasi, B. Bora, R.

Kumar, and O. S. Sastry, "Performance of Field-Aged PV Modules in India: Results from 2016 All-India Survey of PV Module Reliability," *44th IEEE Photovoltaic Specialists Conference*, Washington DC, USA, 2017.

[13] R. Dubey, S. Chattopadhyay, S. Zachariah, S. Rambabu, H. K. Singh, A. Kottantharayil, B. M. Arora, K. L. Narasimhan, N. Shiradkar, and J. Vasi, "On-Site Electroluminescence Study of Field-Aged PV Modules," *7th World Conference on Photovoltaic Energy Conversion and 45th IEEE Photovoltaic Specialists Conference*, Waikoloa, Hawaii, USA, 2018.

[14] R. Dubey, S. Chattopadhyay, S. Zachariah, V. Kuthanazhi, S. Rambabu, S. Bhaduri, H.K. Singh, A. Kottantharayil, B. M. Arora, K.L. Narasimhan, N. Shiradkar, B. Bora, O.S. Sastry and J. Vasi, "Investigation of Poor Performing PV Modules Observed in All-India Survey of PV Module Reliability," *7th World Conference on Photovoltaic Energy Conversion and 45th IEEE Photovoltaic Specialists Conference*, Waikoloa, Hawaii, USA, 2018.

[15] S. Chattopadhyay, R. Dubey, S. Bhaduri, S. Zachariah, H. K. Singh, C. S. Solanki, A. Kottantharayil, N. Shiradkar, B. M. Arora, K. L. Narasimhan, and J. Vasi, "Correlating Infrared Thermography with Electrical Degradation of PV Modules Inspected in All-India Survey of Photovoltaic Module Reliability 2016," *IEEE Journal of Photovoltaics* vol. 8, p. 1800, 2018.

[16] D. C. Jordan, S. R. Kurtz, K. VanSant and J. Newmiller, "Compendium of photovoltaic degradation rates", *Progress in Photovoltaics: Research and Applications*, vol. 24, pp. 978–989, 2016. DOI: 10.1002/pip.2744

[17] D. C. Jordan, T. J. Silverman., J. Wohlgemuth, S. R. Kurtz, and K. T. VanSant, "Photovoltaic failure and degradation modes," *Progress in Photovoltaics: Research and Applications*, vol. 25, pp. 318–326, 2017. DOI: 10.1002/pip.2866

[18] D. C. Jordan, T. J. Silverman, B. Sekulic and S. R. Kurtz, "PV degradation curves: non-linearities and failure modes", *Progress in Photovoltaics: Research and Applications*, vol. 25, pp. 583–591, 2017. DOI: 10.1002/pip.2835

[19] D. C. Jordan, C. Deline, S. R. Kurtz, G. M. Kimball and M. Anderson, "Robust PV degradation methodology and application," *IEEE J. Photovoltaics*, vol. 8, pp 525-531, 2018.

[20] D.L. Staebler, C.R. Wronski, "Reversible conductivity changes in discharge-produced amorphous Silicon", *Applied Physics Letters*, vol. 31, p. 292, 1977. DOI: http://dx.doi.org/10.1063/1.89674

[21] R. Rüther, J. Livingstone, "Seasonal variations in amorphous silicon solar module outputs and thin film characteristics", *Solar Energy Materials and Solar Cells*, vol. 36, no. 1, pp. 29-43, 1995. DOI: 10.1016/0927-0248(94)00165-O

[22] S. Demtsu, S. Bansal, and D. Albin, "Intrinsic stability of thin-film CdS/CdTe modules," *35th IEEE Photovoltaic Specialists Conference*, Hawaii, 2010, pp. 1161-1165. DOI: 10.1109/PVSC.2010.5614753

[23] J. A. del Cueto and B. von Roedern, "Long-term transient and metastable effects in cadmium telluride photovoltaic modules," *Progress in Photovoltaics: Research and Applications*, vol. 14, no. 7, pp. 615-628, 2006. DOI: 10.1002/pip.687

[24] T. J. Silverman, U. Jahn, G. Friesen, M. Pravettoni, M. Apolioni, A. Louwen, W van Sark, M. Schweiger, G. Belluardo, J. Wagner, A. Tetzlaff, P. Ingenhoven, D. Moser, "Characterization of Performance of Thin Film Photovoltaic Technologies", International Energy Agency Report No. IEA-PVPS T13-02:2014, May 2014.

[25] Vikram Solar, "Limited and Linear Warranty for PV Modules", [Online] Available: https://www.vikramsolar.com/wp-content/uploads/2016/03/Warranty-Certificate_Dec16.pdf

[26] Jinko Solar, "Limited Warranty", [Online] Available: https://www.jinkosolar.com/download.html?downid=223

[27] JA Solar, "Limited Warranty", [Online] Available: http://en.jasolar.com/site/pdf/594

[28] S. Pingel, D. Koshnicharov, O. Frank, T. Geipel, Y. Zemen, B. Striner and J. Berghold, "Initial Degradation of Industrial Silicon Solar Cells in Solar Panels", *25th European PV Solar Energy Conference and Exhibition,* Valencia, Spain, 2010. DOI: 10.4229/25thEUPVSEC2010-4AV.3.20

[29] PVSyst, "LID (Light Induced Degradation) Loss", [Online] Available: http://files.pvsyst.com/help/lid_loss.htm

[30] System Integration Technical Briefing "Light-Induced Degradation newly addressed – Predicting long-term yield loss of high-performance PV modules", www.pv-tech.org

[31] J. H. Reiss, R. R. King, and K. W. Mitchell, "Characterization of diffusion length degradation in Czochralski silicon solar cells", *Applied Physics Letters*, vol. 68, pp. 3302, 1996. DOI: 10.1063/1.116581

[32] K. Peter, P.Preis, P.E. Díaz-Pérez, J. Theobald, E. Enebakk, Anne-Karin Soiland, A. Savtchouk, M. Wilson and J. Lagowski, "Light Induced Degradation in Multicrystalline Solar Grade Silicon Solar Cells Evaluated using Accelerated LID", 26th *European PV Solar Energy Conference and Exhibition*, 2011. DOI: 10.4229/26thEUPVSEC2011-2BV.4.21

[33] B. Sopori, P. Basnyat, S. Shet, V. Mehta, Jeff Binns and Jesse Appel, "Understanding Light-Induced Degradation of c-Si Solar Cells", *38th IEEE Photovoltaic Specialists Conference*, Austin, 2012. DOI: 10.1109/PVSC.2012.6317798

[34] K. M. Broek, I.J. Bennett, M.J. Jansen, N.J.C.M. van der Borg and W. Eerenstein, "Light and current induced degradation in p-type multi-crystalline cells and development of an inspection method and a stabilisation method", in proceedings of the *27th European PV Solar Energy Conference and Exhibition,* Frankfurt, 2012. DOI: 10.4229/27thEUPVSEC2012-4DO.6.5

[35] C. Packard, J. H. Wohlgemuth and S. R. Kurtz, "Development of a visual inspection data collection tool for evaluation of fielded PV Module condition," NREL, Technical Report no. NREL/TP-5200-56154, Golden, Colorado, 2012.

[36] S. V. Spataru, D. Sera, P. Hecke, T. Kerekes and R. Teodorescu, "Fault identification in crystalline silicon PV modules by complementary analysis of the light and dark current–voltage characteristics," *Progress in Photovoltaics: Research and Applications*, 2015.

[37] G. A. Gueymard, "SMARTS2: A Simple Model of the Atmospheric Radiative Transfer of Sunshine: Algorithms and Performance Assessment", Florida Solar Energy Center Technical Report No. FSEC-PF-270-95, 1995, Florida.

[38] C. Buerhop, D. Schlegel, M. Niess, C. Vodermayer, R. Weißmann and C. Brabec, "Reliability of IR Imaging of PV Plants under operating conditions," *Solar Energy Materials and Solar Cells,* vol. 107, pp. 154-164, 2012.

[39] M. Kempe, M. Reese, A. Dameron and T. Moricone, "Types of Encapsulant Materials and Physical Differences Between Them," *NREL Photovoltaic Module Reliability Workshop,* Denver, USA, 2010.

[40] A. Mansouri, M. Zettl, O. Mayer, M. Lynass, M. Bucher, O. Stern and R. Burhenne, "Defect detection in photovoltaic modules using electroluminescence imaging," *27th European PV Solar Energy Conference and Exhibition,* Frankfurt, Germany, 2012, pp. 3374-3378.

[41] R. Dubey, S. Chattopadhyay, V. Kuthanazhi, J. John, C. S. Solanki, A. K., B. M. Arora, K. Narsimhan and J. Vasi, "Daylight Electroluminiscence Imaging of Photovoltaic Modules by Image Difference Technique," *6th World Conference on Photovoltaic Energy Conversion,* Kyoto, 2014.

[42] Bureau of Indian Standards, *National Building Code of India*, SP 7:2005, 2005.

[43] N. K. Bansal and G. Minke, *Climatic Zones and Rural Housing in India*, Julich: Forschungszentrum Julich GmbH, 1995.

[44] P. Mundle, N. Shiradkar, J. Vasi and S. Patwardhan, “Photovoltaic Climate Classification for Degradation Study,” *35th European Photovoltaic Solar Energy Conference (EUPVSEC)*, Brussels, Belgium, 2018.

[45] IEC 60891 Standard Edition 2.0, 2009-12

[46] A. J. Anderson, “Photovoltaic Translation Equations: A New Approach”, *NREL*, January 1996.

[47] Hemant K. Singh, R. Dubey, S. Zachariah, K. L. Narasimhan, B. M. Arora, A. Kottantharayil, and J. Vasi, “Modified STC Correction Procedure for Assessing PV Module Degradation in Field Surveys”, *45th IEEE Photovoltaic Specialists Conference*, Waikoloa, Hawaii, USA, 2018.

[48] W. Herrmann, “Current-Voltage Translation Procedure for PV Generators in the German 1000 Roofs Programme” [online], Available: http://www.f09.fhkoeln.de/imperia/md/content/personen/wiesner_wolfgang/veroeffentlichungen/26_proceed.pdf, [Accessed Feb. 20, 2014].

[49] Haider Ibrahim, and Nader Anani, “Variations of PV module parameters with irradiance and temperature” *9th International Conference on Sustainability in Energy and Buildings*, SEB-17, 5-7 July 2017, Chania, Crete, Greece.

[50] Mohammad Hejri, Hossein Mokhtari, Mohammad Reza Azizian and Lennart Soder, “An analytical- numerical approach for parameter determination of a five-parameter single-diode model of photovoltaic cells and modules”, *International Journal of Sustainable Energy*.

[51] Sakaros Bogning Dongue, Donatien Njomo, and Lessly Ebengai, “An Improved Nonlinear Five-Point Model for Photovoltaic Modules”, *International Journal of Photoenergy*, Volume 2013, Article ID 680213

[52] C. Mahapatra, R. Dubey, S. Chattopadhyay, S. Zachariah, and S. Sabnis, "Statistical Analysis of Degradation Data for c-Si modules observed in India in 2016", *44th IEEE Photovoltaics Specialists Conference*, Washington D.C., 2017.

[53] C. Packard, J. H. Wohlgemuth and S. R. Kurtz, “Development of a visual inspection data collection tool for evaluation of fielded PV Module condition,” NREL, Technical Report no. NREL/TP-5200-56154, Golden, Colorado, 2012

[54] A. W. Czanderna and F. Pern, "Encapsulation of PV Modules using ethylene vinyl Acetate Co-polymer as a pottant : A Critical review," Solar Energy Materials & Solar Cells, vol. 43, pp. 101-181, 1996

[55] S. Chattopadhyay, S. Tatapudi, C. S. Solanki, A. Kottantharayil, K.L. Narasimhan, J. Vasi, G. TamizhMani, “Quantification of PV Module Discoloration using Visual Image Analysis”, 44th IEEE Photovoltaic Specialist Conference, Washington DC, 2017

[56] M. Kontges, I. Kunze, V. Naumann, S. Richter, C. Hagendorf, J. Berghold and M. Roericht, "Snail Tracks (Schneckenspuren), Worm marks & Cell Cracks," [Online]. Available: http://ieapvps.org/index.php?id=223&eID=dam_frontend_push&docID=1272. [Accessed 3/12/2017].

[57] M. D. Kempe, A. A. Dameron, T. J. Moricone, and M. O. Reese, “Evaluation and Modeling of EdgeSeal Materials for Photovoltaic Applications”, 35th IEEE Photovoltaic Specialist Conference, Honolulu, 2010

[58] M. Kontges, C. Packard, S. Kurtz, U. Jahn, K. A. Berger, K. Kato, T. Friesen, H. Liu, "Review of Failures of Photovoltaic Modules," International Energy Agency, Technical Report no. IEA-PVPS, T13-01, 2014

[59] Sharp Corporation, "SHARP Installation Manual" [Online]. Available: http://www.becksolar.de/fileadmin/user_upload/Datenblaetter/Sharp/InstallationManual_SHARP_NA_FxxxGK_KTA10 007_Ver3-11.pdf

[60] K. J. Havens and E. J. Sharp, *Thermal Imaging*. 2016. Available online: https://www.sincedirect.com/topics/earth-and -planetary sciences/thermal-imaging/pdf

[61] M. Kontges, I. Kunze, S. Kajari-Schroder, X. Breitenmoser and B. Bjorneklett, "The risk of power loss in crystalline silicon based photovoltaic modules due to micro-cracks," Solar Energy Materials & Solar Cells, vol. 95, pp. 1131-1137, 2011

[62] S. Meyer, S. Timmel, S. Richter, M. Werner, M. Gläser, S. Swatek, U. Braun and C. Hagendorf, "Silver nanoparticles cause snail trails in photovoltaic modules," Solar Energy Materials and Solar Cells, vol. 121, pp. 171-175, 2014

[63] R. Moreton, E. Lorenzo, J. Leloux and J.M.Carrillo, "Dealing in Practice with Hot Spots," in *29th European Photovoltaic Solar Energy Conference and Exhibition*, Amsterdam, 2014, pp. 2722-2727

[64] J. Oh and G. TamizhMani, "Temperature Testing and Analysis of PV modules per ANSI/UL 1703 and IEC 61730 standards," in *35th IEEE Photovoltaic Specialist Conference*, Honolulu,, 2010, pp. 984-988

[65] I. A. Tsanakas, E. Pilat, L. D. Ha, F. A. Shakarchi, "Early Reliability Issues and Symptoms Evaluated in Four Large PV Plants in Southern France", *NREL PV Module Reliability Workshop*, Denver, 2017

[66] Omron Europe B.V, "White Paper" *Omron Corporation*, 1st April, 2013

[67] S. Pingel, O. Frank, M. Winkler, S. Daryan, T. Geipel, H. Hoehne and J. Berghold, "Potential Induced Degradation of Solar Cells and Panels", *EU PVSC*, 2010

[68] http://www.statstutor.ac.uk/resources/uploaded/spearmans.pdf

[69] "Koppen Climatic Classification" [Online] Available: http://www.thesustainabilitycouncil.org/resources/the-koppen-climate-classification-system/

[70] IEC 60812 Failure modes and effects analysis (FMEA and FMECA)

[71] S. Shrestha, J. Mallineni, S. Tatapudi, B. Knisely, K. Yedidi, J. Kuitche and G. TamizhMani "FMECA on Field Deployed c-Si Modules under Hot-Dry Desert Climate for Determining Dominant Failure Modes", *IEEE PVSC*, 2014.

[72] J.M. Kuitche, R. Pan, and G. TamizhMani "Investigation of Dominant Failure Mode(s) for Field-aged Crystalline Silicon PV Modules under Desert Climatic Conditions", JPV-12-0393-R.R1, 2013.

[73] O.S. Sastry, Birinchi Bora, Yogesh Kumar Singh, Manander Bangar, Rashmi Singh, Renu, Mithilesh Kumar, Kamlesh Yadav, Ramayan Singh, Avinash Kumar and Supriya Rai, "RPN analysis of field exposed mono crystalline Silicon PV modules under composite climate of India", *42nd IEEE PVSC*

# Appendix A
# Survey Checklists

Form 0A

| Identification ID | | | | | | Module Nameplate Data | | | | | | | |
|---|---|---|---|---|---|---|---|---|---|---|---|---|---|
| S. No | Module ID | Serial Number | Module Manufacturer | Model | Module position from positive end in string | $P_{max}$ (W) | $V_{oc}$ (V) | $I_{sc}$ (A) | $V_{mp}$ (V) | $I_{mp}$ (A) | Sys Voltage (V) | Date of Installation/ Commission | Remarks |
| | | | | | | | | | | | | | |
| | | | | | | | | | | | | | |
| | | | | | | | | | | | | | |
| | | | | | | | | | | | | | |
| | | | | | | | | | | | | | |
| | | | | | | | | | | | | | |
| | | | | | | | | | | | | | |
| | | | | | | | | | | | | | |
| | | | | | | | | | | | | | |
| | | | | | | | | | | | | | |
| | | | | | | | | | | | | | |
| | | | | | | | | | | | | | |
| | | | | | | | | | | | | | |
| | | | | | | | | | | | | | |

Module ID: INSMSTMO where IN: Inverter no (2 digits), SM: SMU no in given inverter (2 digits), ST: String No in given SMU (2 digits), MO: Module no/position from positive in given string (2 digits)

Form A1

System Information

| Module ID | System Design (Single Module/ Multiple Module/ Unknown) | If Multiple Module System | | | | | | |
|---|---|---|---|---|---|---|---|---|
| | | Module location/no. in a series string (from positive) | No. of Modules in series string | No. of Strings in parallel (array) | No. of Bypass diodes | Rating and Model No.of Bypass diode | No. of modules per Blocking diode | Rating and Model No.of Blocking diode |
| | | | | | | | | |
| | | | | | | | | |
| | | | | | | | | |
| | | | | | | | | |
| | | | | | | | | |
| | | | | | | | | |
| | | | | | | | | |
| | | | | | | | | |
| | | | | | | | | |
| | | | | | | | | |
| | | | | | | | | |
| | | | | | | | | |
| | | | | | | | | |

Form A2

I-V data Info (Strings)

Site Name: Site No: Date: Filled By:

| String No/ID | Tracer Used | I-V Curve File Name | RH (%) | Ambient Temperature ($^0$C) | Remarks |
|---|---|---|---|---|---|
| | | | | | |
| | | | | | |
| | | | | | |
| | | | | | |
| | | | | | |
| | | | | | |
| | | | | | |
| | | | | | |
| | | | | | |
| | | | | | |
| | | | | | |
| | | | | | |

Module ID: INSMST where IN: Inverter no (2 digits), SM: SMU no in given inverter (2 digits), ST: String No in given SMU (2 digits)

Form A2

I-V data Info (Modules)

Site Name: Site No: Date: Filled By:

| Module ID | Serial Number | Tracer Used | I-V Curve File Name | RH (%) | Ambient Temperature ($^0$C) | Remarks |
|---|---|---|---|---|---|---|
| | | | | | | |
| | | | | | | |
| | | | | | | |
| | | | | | | |
| | | | | | | |
| | | | | | | |
| | | | | | | |
| | | | | | | |
| | | | | | | |
| | | | | | | |
| | | | | | | |
| | | | | | | |

Module ID: INSMSTMO where IN: Inverter no (2 digits), SM: SMU no in given inverter (2 digits), ST: String No in given SMU (2 digits), MO: Module no/position from positive in given string (2 digits)

Form C2

IR (MPPT)

Site Name: Site No: Date: Filled By:

| Module ID | Image No. (MPPT) | Irradiance (W/m$^2$) | Ambient Temperature ($^0$C) | Hot Spot (Y/N) | Remarks |
|---|---|---|---|---|---|
| | | | | | |
| | | | | | |
| | | | | | |
| | | | | | |
| | | | | | |
| | | | | | |
| | | | | | |
| | | | | | |
| | | | | | |
| | | | | | |
| | | | | | |
| | | | | | |

Module ID: INSMSTMO where IN: Inverter no (2 digits), SM: SMU no in given inverter (2 digits), ST: String No in given SMU (2 digits), MO: Module no/position from positive in given string (2 digits)

Form C2

IR (SC)

Site Name: Site No: Date: Filled By:

| Module ID | Image No. (SC) | Irradiance (W/m$^2$) | Ambient Temperature ($^0$C) | Hot Spot (Y/N) | Remarks |
|---|---|---|---|---|---|
| | | | | | |
| | | | | | |
| | | | | | |
| | | | | | |
| | | | | | |
| | | | | | |
| | | | | | |
| | | | | | |
| | | | | | |
| | | | | | |
| | | | | | |
| | | | | | |

Module ID: INSMSTMO where IN: Inverter no (2 digits), SM: SMU no in given inverter (2 digits), ST: String No in given SMU (2 digits), MO: Module no/position from positive in given string (2 digits)

# Visual Checklist (Group-D)

| Location: ………….……… Lat/Long: ………..……… Altitude: …………….. | |
|---|---|
| **Module Details:**<br>Manufacturer: ……<br>Type of Module: *Mono-cSi / Multi-cSi / Thin Film (……….....)* No. of Cells: ……<br>Dimension of Cells (cm): …..… x …..…<br>Dimension of Module (cm): ……… x ……… | **Module Name Plate Available:** Y/N<br>Model No. & Sl. No. : ……<br>Name Plate Condition: *Like New / Discolored / Torn*<br>Certification: *IEC61215 / IEC61646 / IEC61730 / UL1703*<br>Estimated deployment date: ….... |
| **Crystalline Silicon Module** : Y/N<br>Cells in each string x strings in series/parallel: …… x ……<br>**Spacing:** Cell to cell = …….. mm<br>Frame to cell (mm) = ….. (top), ……. (bottom), …… (left), …….. (right)<br>Module Discoloration: *None / Light / Dark, (……% area)*<br>No. of cells discoloured: ………<br>Discoloration Location : *Overall / Module centre / Module edges / Cell Center / Cell edges / over fingers / over busbars / over tabbing / between cells / individual cells darker than others / partial cell discoloration/others (…………)*<br>Effect in JB area: *Same as elsewhere / more / less*<br>Effect in Name Plate area: *Same as elsewhere / more / less*<br>Damage : *Burn marks / Cracks / Moisture /Snail tracks / foreign particles embedded*<br>Burn marks (nos.): …… Cells cracked (nos.): ……<br>Cells with Snail Tracks (nos.): …..…. Cells with Framing (nos.): ….. Area Delaminated: *Nil /Over cells (…%), Between cells (…%), uniform / from edges / at corners / near JB / near Interconnects (cell or string)* | **Backsheet Applicable:** Y/N<br>Texture: *Like New / Wavy (Delam / No Delam) / Dented*<br>Damage: *None / Small Localized / Extensive*<br>Discoloration: *Like New / Major / Minor*<br>Chalking: *None / Slight / Significant*<br>Delaminated area (%):*<5 / 5-25 / 25-50 / 50-75 />75%*<br>Bubbles (nos., dimension): … , *<5mm / 5-30mm />30mm*<br>Fraction of area with bubbles > 5mm: *<5% / 5-25% / 25-50% / 50-75% />75%*<br>Cracks/scratches (nos. & location): ……………., *random/ over cells / between cells*<br>Cracks location: *Only Near JB / Only near Nameplate / Other (………..)*<br>Fraction of cracks/scratches that exposes the circuit: *<5% / 5-25% / 25-50% / 50-75% />75%*<br>Burn Marks (nos. & area): ……, *<5% / 5-25% / 25-50% / 50-75% />75%* |
| **Frame Applicable:** Y/N<br>Appearance: *Like New / Damaged / Missing*<br>Damage: *Corrosion (major or minor) / Bent/ Joints separated/ Cracking*<br>Frame Adhesive : *Not visible / Like New / Degraded / oozed out / missing in some areas* | **Frame Grounding Present:** Y/N<br>Original State : *No ground / Wired / Resistive/ Unknown*<br>Corrosion : *Nil / Minor / Major*<br>Functionality: *Well Grounded / No Connection* |

**Wires**:
*NA / Like New / pliable but degraded / embrittled / Cracked or disintegrated insulation / burnt / corroded / animal bites /soiled*

**Connectors**: Y/N
Type: *MC3 or MC4 / Tyco / Others*
Condition: *Like New / pliable but degraded / embrittled / Cracked or disintegrated insulation / burnt / corroded / animal bites / soiled*

**Junction Box (JB) Applicable:** Y/N
Physical state : *Intact / unsound / weathered / cracked / burnt/ warped/ output terminals corroded*
Lid : *Intact(potted) / loose / fell off / cracked*
Attachment : *Well attached / loose / fallen off*
Wire attached in JB : *Well attached / Loose / Fell off/ arced / caused fire*
Seal : *Good sealing / will Leak*

**Mounting Structure Details:**
Material: ………..
Condition of structure: *Good / rusted / bent / broken*
Installation Site : Roof top / Ground
Type of Floor: Soil / Cement / Other (………………………….)
Tilt Angle: …… Direction of PV Panels: ……
Height of lowest part of module from floor: ………..

**Rear-Side Glass Applicable:** Y/N
Damage: *None/ Small Localized / Extensive*
Crazing (or other non-crack damage): ……
Shattered (tempered/non-tempered): ……
Cracks: nos. : *1 / 2 / 3 / 4-10 / >10*
Cracks start from: *mod. Corner / mod. edge / cell / JB / foreign object impact spot*
Chips: nos. : *1 / 2 / 3 / 4-10 / >10*
Chipping location: *module corner / module edge*

**Frameless Edge Seal Applicable:** Y/N
Appearance: *Like New / discolored / Visibly degraded*
Discoloration area : *<5% / 5-25% / 25-50% / 50-75% / >75%*
Material Problems : *Squeezed Out / signs of moisture penetration*
Delamination : *Localized / widespread*
Delaminated area (%) : *<5 / 5-25 / 25-50 / 50-75 />75%*

**Thin Film Module** : Y/N
Cells in each string (nos.): ……
Strings in parallel (nos.): ……
Distance between frame and cell : ……. mm
Module Discoloration: *None / Light / Dark, (…… % area)*
Discoloration Type : *White Spots/ Haze/ Other*
Discoloration Location : *Overall / Module centre / Module edges / Cell Center / Cell edges / near cracks*
Damage : *No / Small Localized / Extensive*
*Damage Type : Burn Marks / Cracking / Moisture / Foreign particles embedded*
Delamination : *None / Small Localized / Extensive*
Delamination Location: *From edges / uniform / corners/ near junction box / near busbar / along scribe lines*
Delamination Type : *Absorber delamination/ AR Coating delamination/ Other*

Remarks:

Form E

EL Checklist

Site Name: Site No: Date: Filled By:

| Module ID | Image ID | | Biased Current for EL (A) | Voltage Reading (V) | Remarks |
|---|---|---|---|---|---|
| | EL With Bias | EL Without Bias | | | |
| | | | | | |
| | | | | | |
| | | | | | |
| | | | | | |
| | | | | | |
| | | | | | |
| | | | | | |
| | | | | | |
| | | | | | |
| | | | | | |
| | | | | | |

Module ID: INSMSTMO where IN: Inverter no (2 digits), SM: SMU no in given inverter (2 digits), ST: String No in given SMU (2 digits), MO: Module no/position from positive in given string (2 digits)

Form F

Bypass Diode Test

Site Name: Site No: Date: Filled By:

| Module ID | No. of Bypass Diodes | No. of cells per Bypass diode | Status (√/X/NA) For the diode positioned at… from (+ve) end | | | | | Remarks |
|---|---|---|---|---|---|---|---|---|
| | | | 1 | 2 | 3 | 4 | 5 | |
| | | | | | | | | |
| | | | | | | | | |
| | | | | | | | | |
| | | | | | | | | |
| | | | | | | | | |
| | | | | | | | | |
| | | | | | | | | |
| | | | | | | | | |
| | | | | | | | | |
| | | | | | | | | |
| | | | | | | | | |

Module ID: INSMSTMO where IN: Inverter no (2 digits), SM: SMU no in given inverter (2 digits), ST: String No in given SMU (2 digits), MO: Module no/position from positive in given string (2 digits)

Form G

Insulation Resistance Test

Site Name: Site No: Date: Filled By:

| Module ID | Dry Resistance (MΩ) | Wet Resistance (MΩ) | Remarks |
|---|---|---|---|
| | | | |
| | | | |
| | | | |
| | | | |
| | | | |
| | | | |
| | | | |
| | | | |
| | | | |
| | | | |
| | | | |
| | | | |

Module ID: INSMSTMO where IN: Inverter no (2 digits), SM: SMU no in given inverter (2 digits), ST: String No in given SMU (2 digits), MO: Module no/position from positive in given string (2 digits)

# Form H
# SOILING & SHADING CHECKLIST

Site Name: Site No.: Date: Filed By:

**C1. Surroundings:**

**Soiling**

Image of the Module: Soiled _____________Cleaned ____________

Appearance of Glass: ☐ Clean ☐ Lightly soiled ☐ Heavily soiled

Location of soiling: ☐ Locally soiled near frame

☐ Left ☐ Right ☐ Top ☐ Bottom ☐ All sides

☐ Locally soiled on glass / Bird droppings

Soiling sample taken on glass slides ☐ Yes ☐ No
Minimum 4 grams

Cleaning interval ___________________________________________________________________

Last cleaned on (date) : ___________________________________________________________________

I-V of Soiled and Cleaned Modules: Soiled: ________________________Cleaned: _______________________

**Shading**

Kind of shading: ☐ Building ☐ Trees

Any reflecting surface nearby: ☐ Yes ☐ No

Debris ☐ Yes ☐ No

**Solar Path Finder Details:** Camera used:

| | | | | | |
|---|---|---|---|---|---|
| Corner 1 | Corner 2 | Corner 3 | Corner 4 | Corner 5 | Corner 6 |
| Pic No: | Pic No: | Pic No: | Pic No: | Pic No: | Pic No: |

**IR Images of system**

IR Image before cleaning:

IR image after cleaning:

**Weather Type**

- ☐ Occurrence of due or fog in early Morning / Humid
- ☐ Dry

# Appendix B
# Koppen-Giger Climatic Classification

Throughout this report, we have used the six-climate classification of Bansal *et al.* [43] for the analysis of the survey data (as discussed in Chapter 1). In chapter 4, we have presented some of the important climate-dependent analysis in in detail, in terms of internationally accepted Koppen-Geiger climate classification system also. This Appendix shows climatic zones of India according to the Koppen-Geiger system, and also lists the climatic zone of all sites visited as per this classification.

Unlike the six-climate classification system of Bansal *et al.*, which uses temperature and relative humidity as the classification criteria, the Koppen-Geiger system uses temperature and precipitation [42]. The detail methodology of Koppen-Geiger climatic classification was explained in 2016 All-India Survey Report [5], and the interested readers can refer to it. Fig. B.1 shows the different climatic zones of India according to the Koppen-Geiger classification.

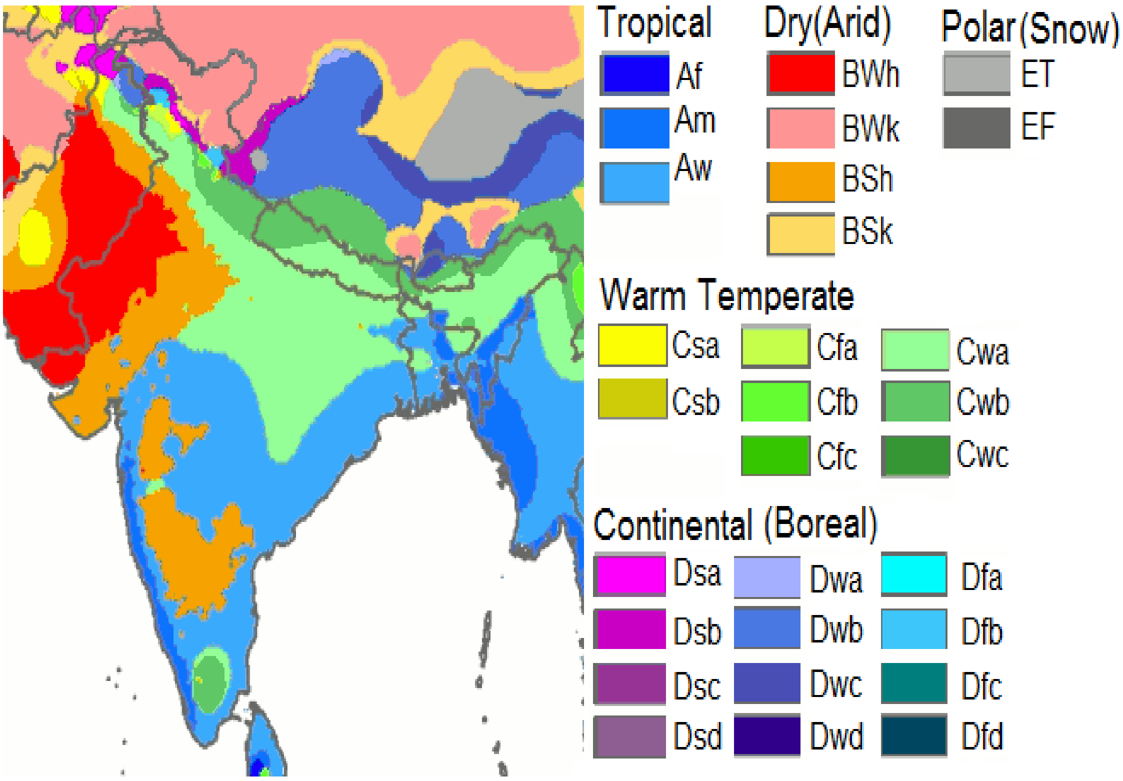


Fig. B.1. Koppen-Geiger Climate classification Map of India (based on [69])

Table B.1 shows the All-India Survey sites that were inspected in 2018, and the climatic zones they belong to according to the Bansal *et al.*[43], and Koppen-Geiger [69] classifications.

Table B.1. Climate wise classification of the inspected sites in 2018 survey

| **Survey Site** | **Classification as per Bansal *et al.*** | **Hot/Non-Hot** | **Koppen-Geiger Classification** |
|---|---|---|---|
| Osmanabad | Hot & Dry | Hot | Tropical Savanna (Aw) |
| Latur | Hot & Dry | Hot | Tropical Savanna (Aw) |
| Itnal | Warm & Humid | Hot | Arid Semi Hot (BSh) |
| Bangalore | Moderate | Non-Hot | Tropical Savanna (Aw) |
| Wayanad | Warm & Humid | Hot | Tropical Monsoon (Am) |
| Cochin | Warm & Humid | Hot | Tropical Monsoon (Am) |
| Kayamkulam | Warm & Humid | Hot | Tropical Monsoon (Am) |
| Trivandrum | Warm & Humid | Hot | Tropical Savanna (Aw) |
| Auroville | Warm & Humid | Hot | Tropical Savanna (Aw) |
| Sricity | Warm & Humid | Hot | Tropical Savanna (Aw) |
| Medimakulapally | Hot & Dry | Hot | Arid Semi Hot (BSh) |
| Midjil | Hot & Dry | Hot | Tropical Savanna (Aw) |
| Bidar | Composite | Hot | Tropical Savanna (Aw) |
| Nirna | Composite | Hot | Tropical Savanna (Aw) |
| Hyderabad | Composite | Hot | Arid Semi Hot (BSh) |
| Ramagundam | Composite | Hot | Tropical Savanna (Aw) |
| Rajgarh | Composite | Hot | Tropical Savanna (Aw) |
| Sakri | Composite | Hot | Arid Semi Hot (BSh) |
| Charanka | Hot & Dry | Hot | Arid Semi Hot (BSh) |
| Bap | Hot & Dry | Hot | Arid Desert Hot (BWh) |
| Tiloniya | Hot & Dry | Hot | Arid Semi Hot (BSh) |
| Jaipur | Hot & Dry | Hot | Arid Semi Hot (BSh) |
| Gurgaon | Composite | Hot | Arid Semi Hot (BSh) |
| Hanle | Cold& Sunny | Non-Hot | Arid Desert Cold (BWk) |
| IIT Bombay | Warm & Humid | Hot | Tropical Savanna (Aw) |
| Dadri | Composite | Hot | Arid Semi Hot (BSh) |
| Anantapur | Hot & Dry | Hot | Arid Semi Hot (BSh) |

# Appendix C
# Outliers and other Excluded PV Modules

## C.1 Introduction

Out of 1386 PV modules that were inspected in detail, 100 PV modules were not considered for analysis due to their age is less than one year, and another 27 PV modules which were measured at an irradiance level of below 700 W/m$^2$ were also not considered for analysis. Out of remaining 1259 PV modules on which the primary analysis was done, 8 PV modules have Front Glass Breakage issue, 3 PV modules have Shading issue, and in 3 PV modules Bypass Diodes got activated. All of these were discarded for detailed analysis. In remaining 1245 PV modules, 46 PV modules have Overall degradation rate of $P_{max}$ is higher than 5.21 %/year, hence we separated them as "Outliers" and not included in detailed analysis. The separation of outliers was done based on statistical analysis, which was mentioned in Chapter 3. In this section we explain briefly about the PV modules with Front Glass Breakage, with Activated Bypass Diodes, and then we explain the analysis of "Outliers" in some detail.

## C.2 PV Modules with Front Glass Breakage and Shading

In this 2018 All-India Survey, we have inspected 8 PV modules with the Front Glass Breakage issues, and 3 with Shading. After talking to the site engineers/technicians, we figured out that stone pelting is the reason for Front Glass Breakage in most of these cases. The machines used for cutting grass or vegetation in the gap between the adjacent structures in the site, pelt small stones on the PV modules. We could clearly see the impact of this, at some particular locations of glass and propagation of cracks throughout the tempered glass from impact location. The Visual, EL, and IR images of one such module is shown in Fig.C.1, Fig.C.2, and Fig.C.3

Fig. C.1. Visual Images of a Glass Broken PV Module

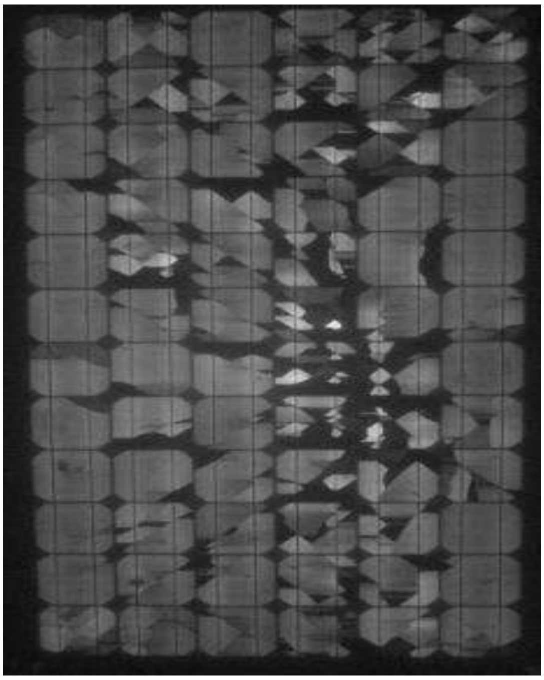

Fig. C.2. EL Image of PV Module shown in Fig. C.1

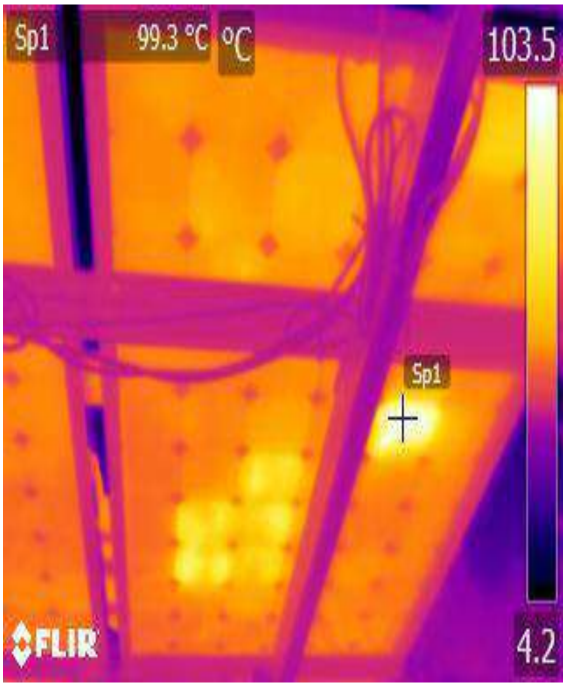


Fig. C.3. IR Image of PV Module shown in Fig. C.1

From the EL and IR images of a Glass Broken PV module, we can see that there are many cracks in the cells, and the impact locations are having hot spots. The *I*-*V* of this type of PV modules is very random, and unpredictable. They show very high power degradation, and it is mainly due to *FF* degradation, $I_{sc}$ degradation, and sometimes degradation of $V_{oc}$ also present (If Bypass Diode gets activated). Most importantly these PV modules impose safety issues, and one should not touch and clean (wet) these modules. At few sites we suggested the cleaning staff to avoid cleaning these type PV modules with water, after observing them doing so. 3 PV modules at a particular site were shaded by the surrounding trees in the evening times, that showed temperature mismatch which can be observed in Fig C.4.

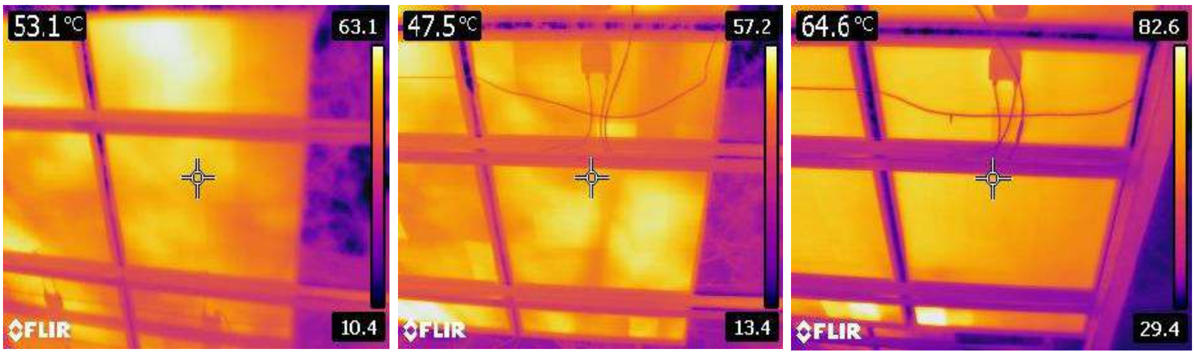


(a) (b) (c)

Fig C.4. IR images of PV Modules (a), (b) and (c) partially shaded by trees

## C.3 Bypass Diode Activated PV Modules

In this 2018 All-India Survey, we have inspected 3 PV modules with the problem of Bypass Diode Activation. Fig. C.5, Fig. C.6 shows the EL image, and IR image of the PV module in which one of the bypass diode has activated. In these cases, the PV module $V_{oc}$, and $P_{max}$ will reduce by one third of its actual value. In EL image we can see that one string of the cells appears completely dark, and the Bypass Diode connected to that string of cells got activated. In IR image also we can see, that the Junction Box is running at very high temperature.

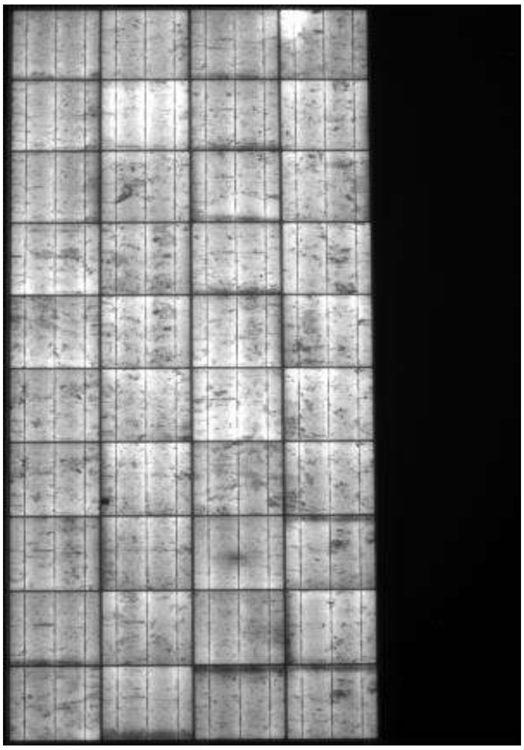

Fig. C.5. EL Image of Bypass Diode Activated PV Module

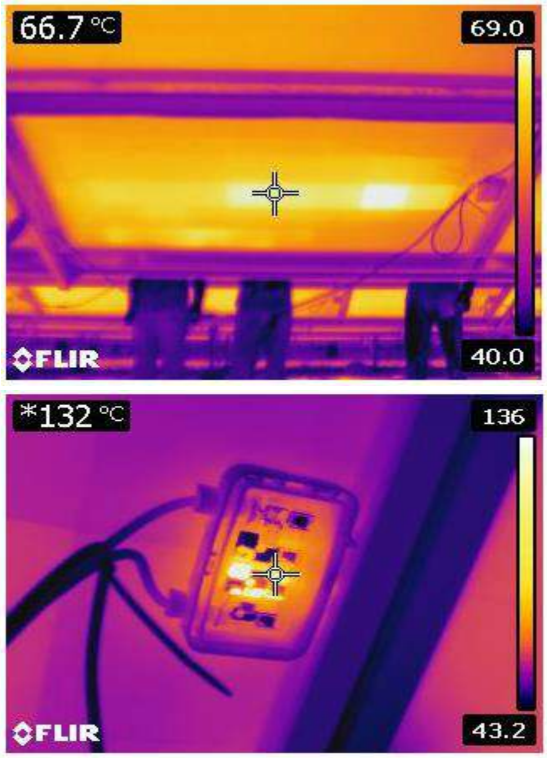


Fig. C.6. IR Images of Bypass Diode Activated PV Module

## C.4 Outlier PV Modules

In this 2018 All-India Survey, 46 PV modules have Overall degradation rate of $P_{max}$ higher than 5.21 %/year, hence we separated them as "Outliers". All these are of c-Si technology PV modules only. Out of these 46 PV modules, 17 of them were affected by PID (15 of them were "Young"), another 16 PV modules are from a "Young" site, but we could not find any signatures of degradation modes through any of our measurement or techniques. For these 16 modules, we observed high degradation in all the parameters like $V_{oc}$, $I_{sc}$, and $FF$. So we suspect the reasons might be might be high LID, and/or Overrating. Remaining PV modules have different issues like hot spots, high $R_s$, and low $R_{sh}$, but we don't have field EL and IR images for many of these PV modules to understand exact degradation modes.

Fig. C.7 shows the age of the PV modules, which we separated as Outliers. We can observe that 44 out of 46 PV modules, are of "Young". So this indicates that due to many reasons like PID, LID, and Overrating, etc. the Young modules have very high degradation rates.

## C.4.1 Electrical Analysis

Fig. C.8, and Fig. C.9 shows the histograms of "Overall", and "Linear" degradation rates of $P_{max}$ of all the Outlier PV modules. In Fig. C.8, the distribution of Overall degradation rates of $P_{max}$ is wide, starting from 5.22 %/year, going till 7.73 %/year, with an average of 6.14 %/year. In Fig. C.9, the distribution of Linear degradation rates of $P_{max}$ is also wide, starting from 4.38 %/year, going till 7.48 %/year, with an average of 5.48 %/year.

Fig. C.10 shows the effect of Hot and Non-Hot climatic zones on the Outlier PV module performance, in which linear degradation rate of $P_{max}$ was plotted. Fig. C.10 also consists of CDF of probability for the Young and Old PV modules in the Hot climatic zone. We can observe that all the Outlier PV modules are from Hot zone only, and we do not have any sample from Non-Hot zone. But one thing we suggest the reader to remember is that we inspected less number of PV modules from this Non-Hot zone in our 2018 All-India Survey.

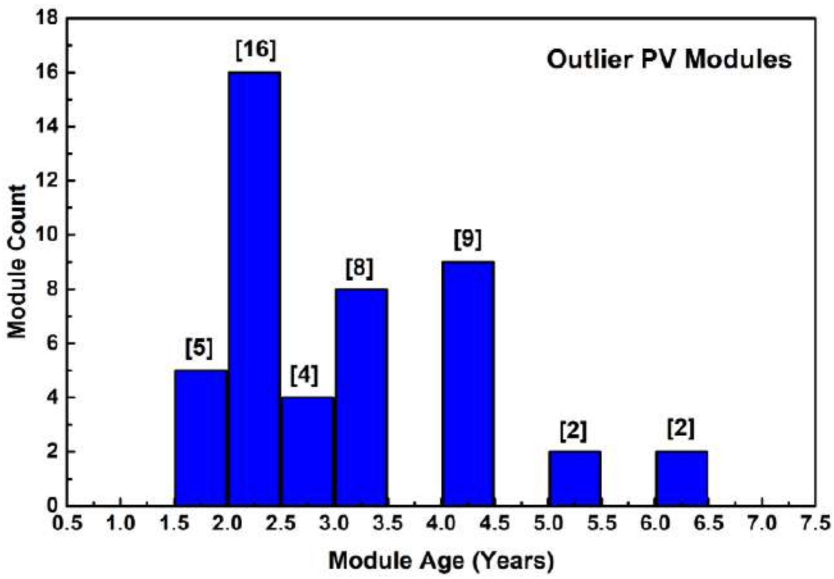


Fig. C.7. Age distribution of Outlier PV modules

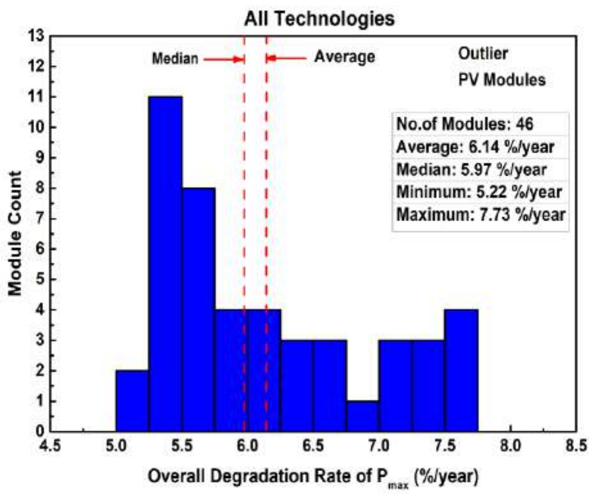


Fig. C.8. Overall degradation rate of $P_{max}$ for Outliers

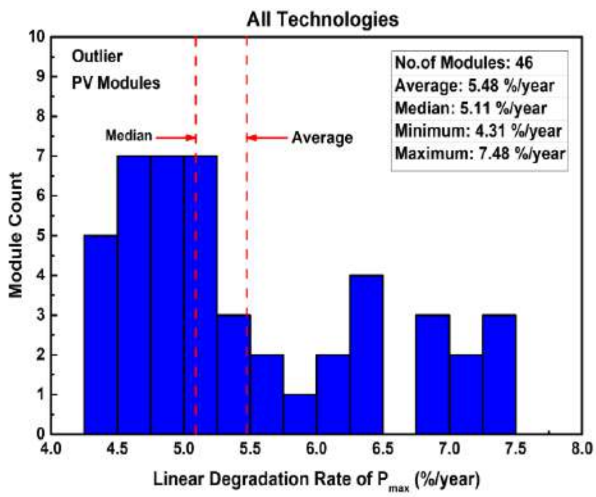


Fig. C.9. Linear degradation rate of $P_{max}$ for Outliers

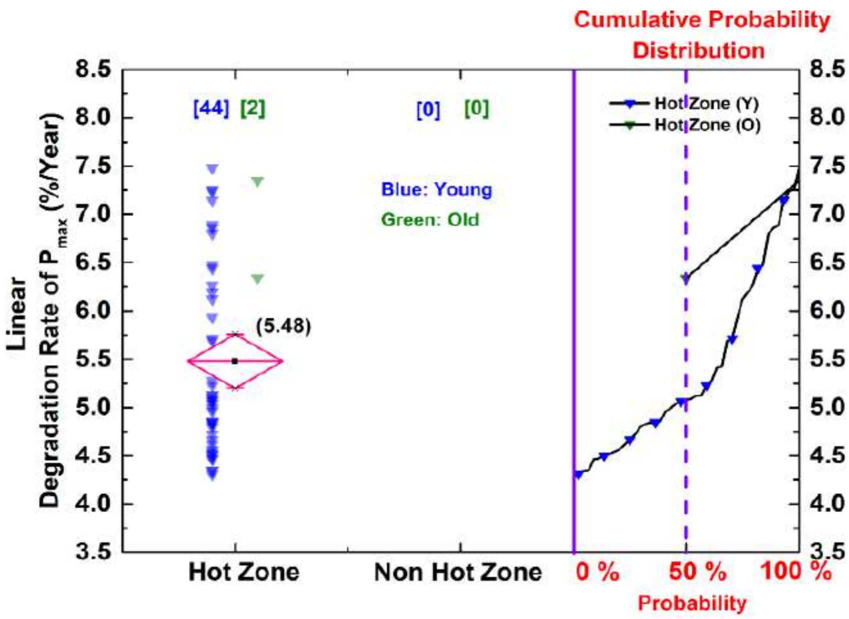


Fig. C.10. Influence of Hot and Non-Hot zones on Outlier performance

Fig. C.11 shows the linear degradation rate of all the performance parameters of Outlier PV modules, and the degradation in *FF* is the major reason for $P_{max}$ degradation in most of the PV modules, and in some PV modules, there are contributions of $V_{oc}$, and $I_{sc}$ degradations along with *FF* degradation. The main reasons for *FF* degradation is PID, LID, Cracks and in some cases it might be because of possible Overrating. The main reasons for *Voc*, and *Isc* degradation in some Outlier PV modules are LID, and possible Overrating.

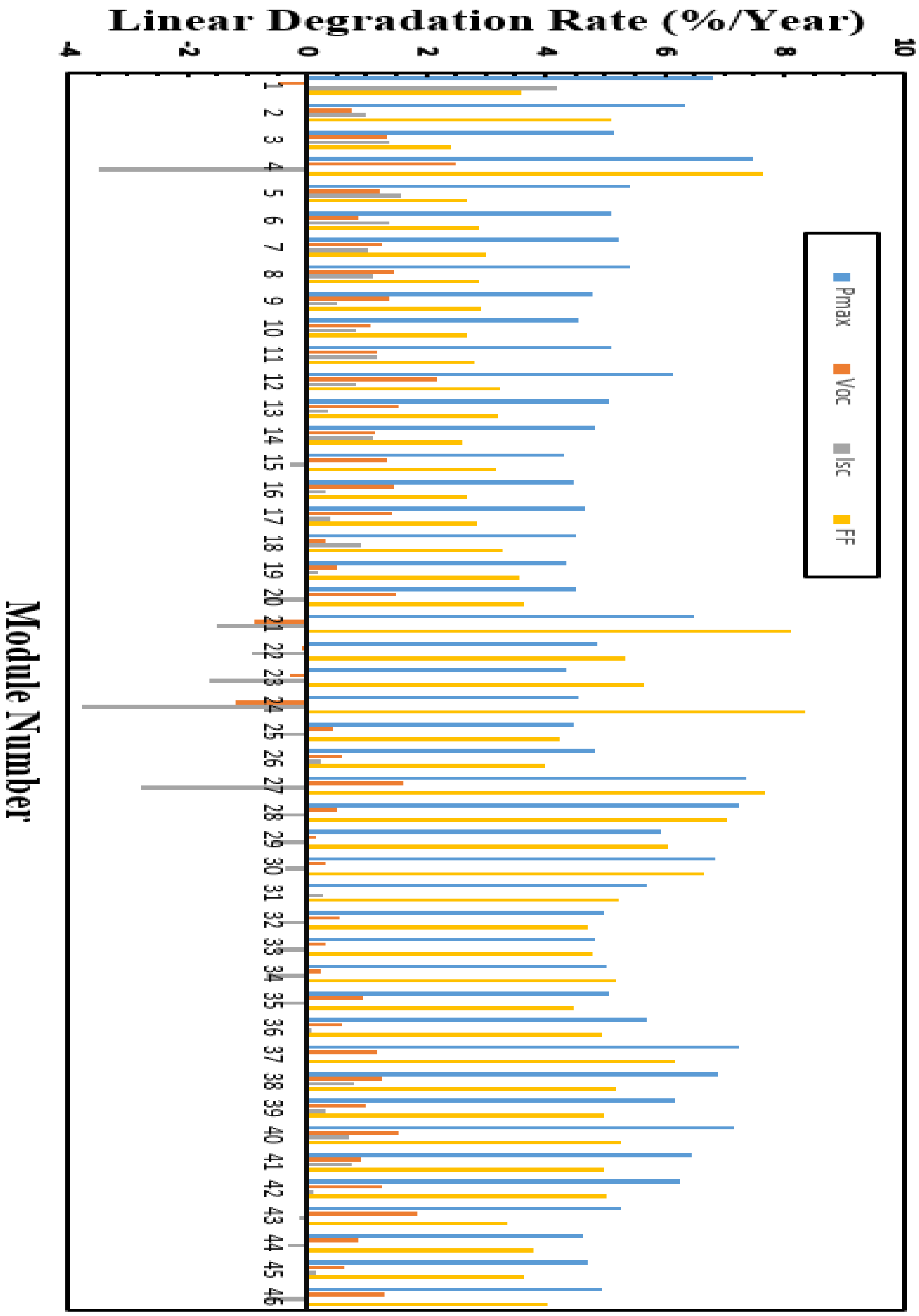


Fig. C.11. Linear degradation rates of different electrical parameters of Outlier PV modules

### C.4.2 Visual Degradation and Correlation to Electrical Degradation

In the 2018 survey it is observed that one of the cause of modules (17 modules) to be outlier is PID. For these modules there is no visual defects observed. Fig C.12. (a), and C.12. (b) Shows the visual images of two PID affected PV modules. The respective EL images those PV modules are shown in section C.4.3, Fig. C.13. (a) and C.13. (b). The other 16 modules which lies in outlier category are young (age < 5 years) and the do not have any encapsulant browning or any other visual defects, as can be seen in Fig. C.12. (c) and Fig. C.12. (d).

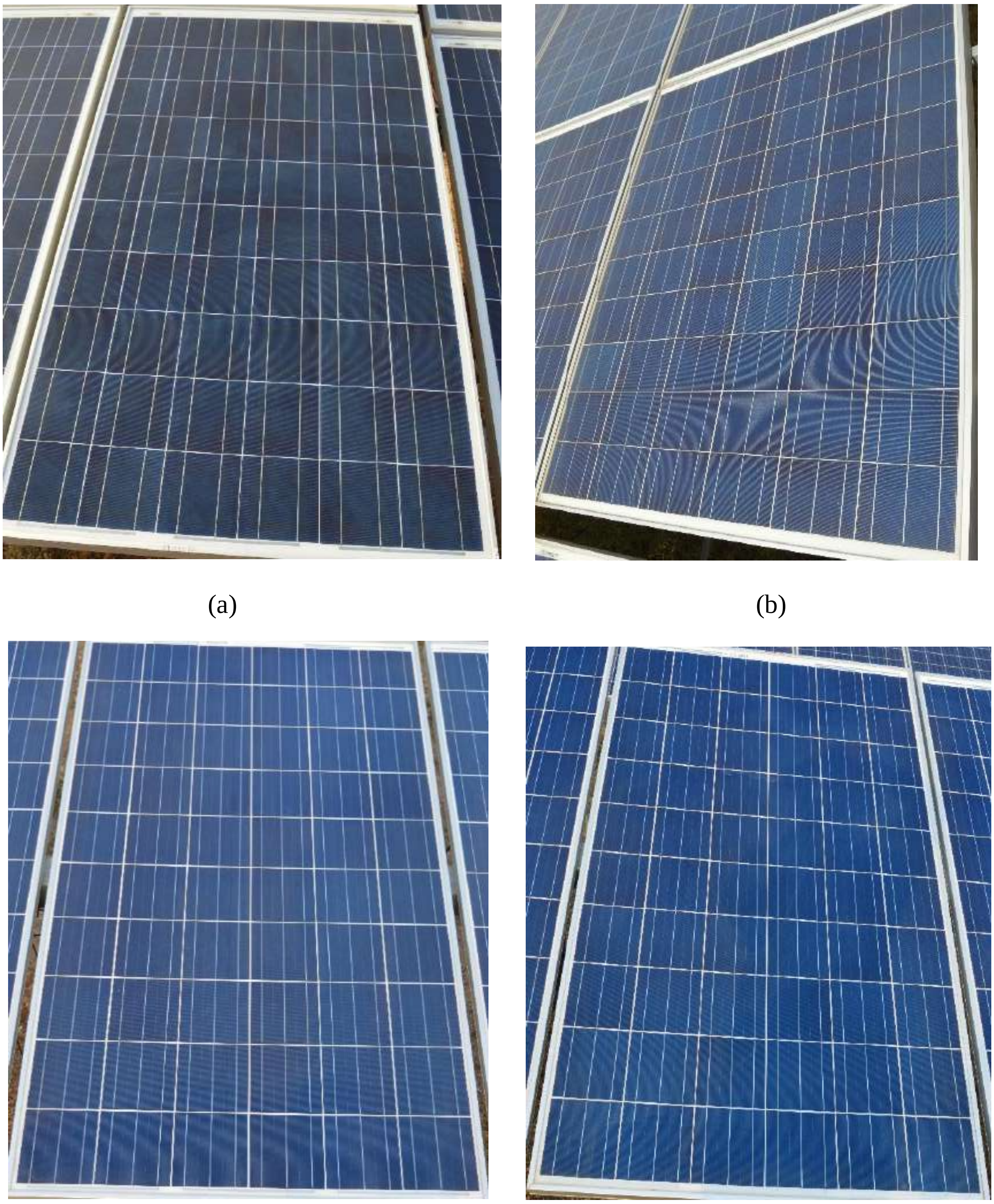

(a) (b) (c) (d)

Fig. C.12. Visual image of outlier modules (a) Module in composite climate with no visual degradation but with linear $P_{max}$ degradation of 7.35 %/year (b) Module in composite climate with no visual degradation but with linear $P_{max}$ degradation of 7.25 %/year (c) Module in Hot and Dry climate with no visual degradation but with linear $P_{max}$ degradation of 4.80 %/year (d) Module in Hot and Dry climate with no visual degradation but with linear $P_{max}$ degradation of 4.50 %/year.

### C.4.3 Electroluminescence Imaging and IR Thermography Results

From the EL images of the outlier PV modules, we observed that most of the modules with PID signature show high linear degradation rate compared to other outlier modules. In Fig. C.13. (a) and Fig. C.13. (b) EL image of modules with PID signature are shown. In other modules (16 modules from Hot and Dry climate) the EL images show defect as edge wafer in multiple cells and apart from this, no other defect were observed as seen in Fig. C.13. (c) and Fig. C.13. (d).

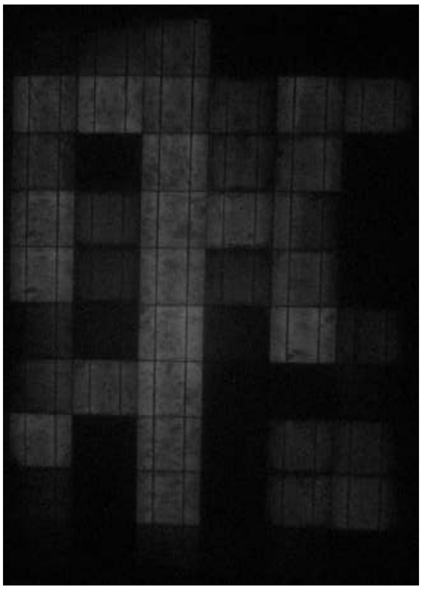

(a)

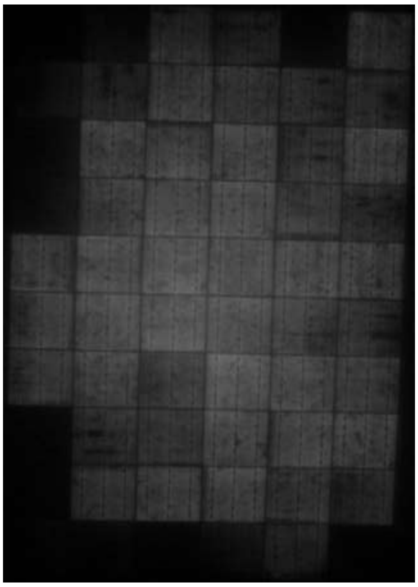

(b)

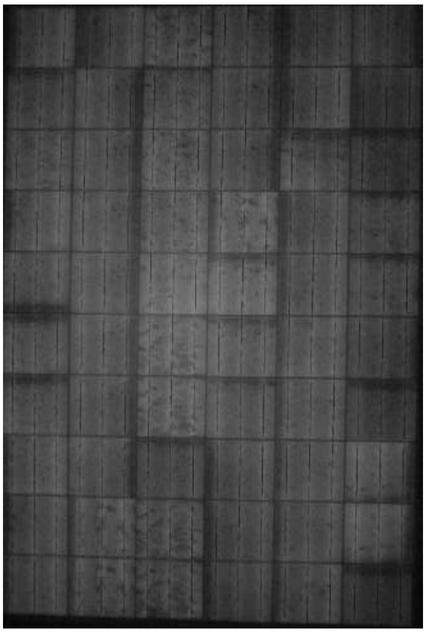

(c)

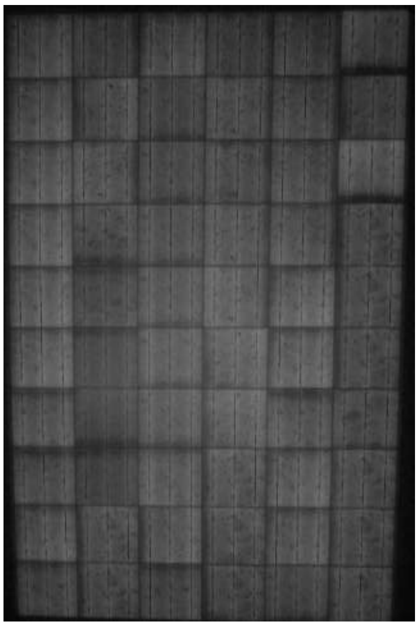

(d)

Fig. C.13. EL image of outlier PV modules (a) Module in composite climate with PID signature and linear $P_{max}$ degradation of 7.35 %/year (b) Module in composite climate with PID signature and linear $P_{max}$ degradation of 7.25 %/year (c) Module in Hot and Dry climate with linear $P_{max}$ degradation of 4.80 %/year (d) Module in Hot and Dry climate with linear $P_{max}$ degradation of 4.50 %/year.

As in some PV modules (count-16) not major defect was observed in EL images apart from edge wafer, this opens the discussion and possibility high LID, and/or Overrating in these modules. 4 modules showed Module $\Delta T$ between 4 ºC – 6 ºC which lead to increase in $P_{max}$ degradation. IR Images of these 4 modules are shown in Fig (shown in Fig. C.14). All IR images shown in Fig. C.14 are taken under MPPT condition. Many outlier modules were not considered for analysis due to high reflection and IR images taken at low Irradiance (<700W/m$^2$)

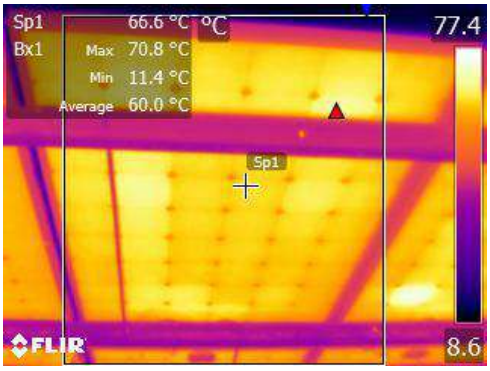


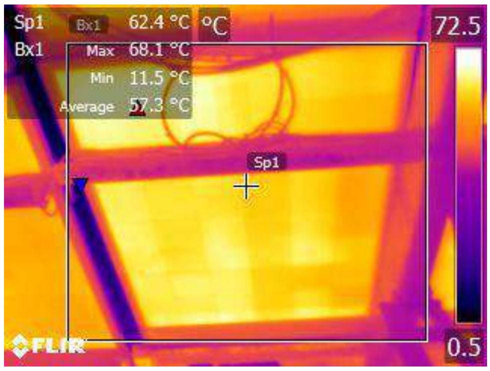


(a)

(b)

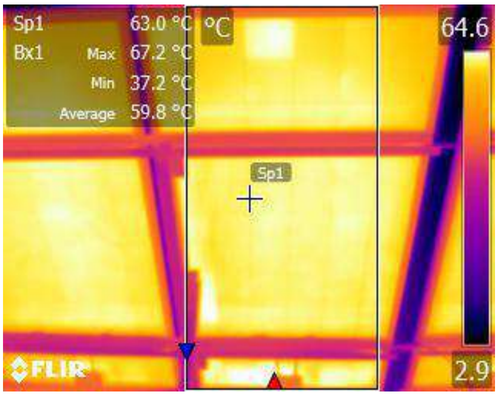


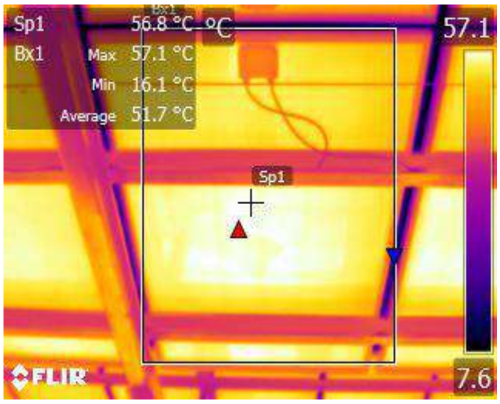


(c)

(d)

Fig. C.14. IR images of PV modules (a), (b), (c) and (d) of Outlier PV modules with high Module $\Delta T$

# Appendix D
# Major Degradation Modes Identified in All-India Survey of PV Module Reliability: 2018

## D.1 Introduction

Out of the 36 sites we inspected in All-India Survey of PV Module Reliability (AISPVM) 2018, 33 sites have only c-Si technology, and 2 sites have both c-Si and Thin film technology, and 1 site has only Thin film technology PV modules. In this Appendix D we focus on the major degradation modes identified in the c-Si sites which have average degradation rate greater than the median of all the 35 (33 + 2) sites, which is 1.75 %/year. This gives us the idea about the problems facing by the fielded c-Si PV modules in the country.

## D.2 Major Degradation Modes Identified

Fig. D.1, D.2 shows the graphs of average overall and linear degradation rate of $P_{max}$ for all the 35 c-Si sites with respect to their age. Fig. D.1 also shows the dominant degradation modes identified in all the sites with degradation rate higher than the median value that was observed from all the c-Si sites. Some of these sites may have multiple degradation modes also, but we have indicated the dominant degradation mode for each site.

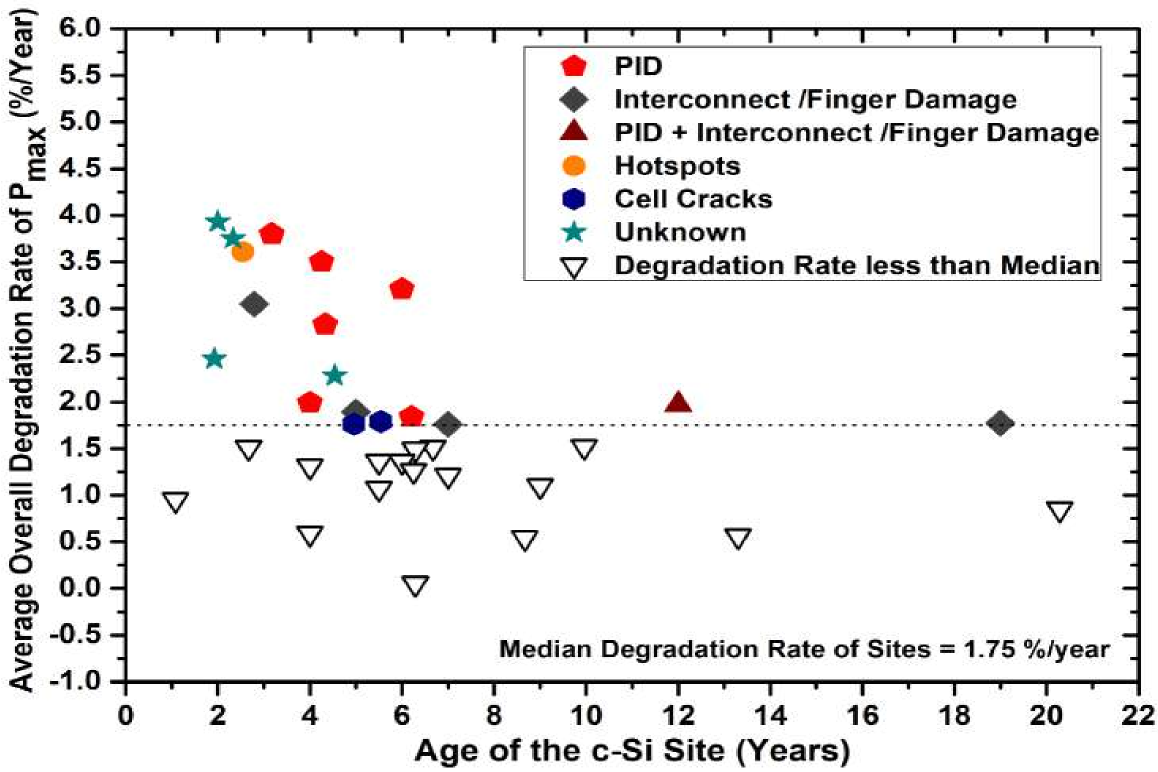

Fig. D.1. Average overall degradation rates of $P_{max}$ for all c-Si sites with respect to their Age and dominant degradation modes observed in sites with degradation rates higher than the median (1.75 %/year)

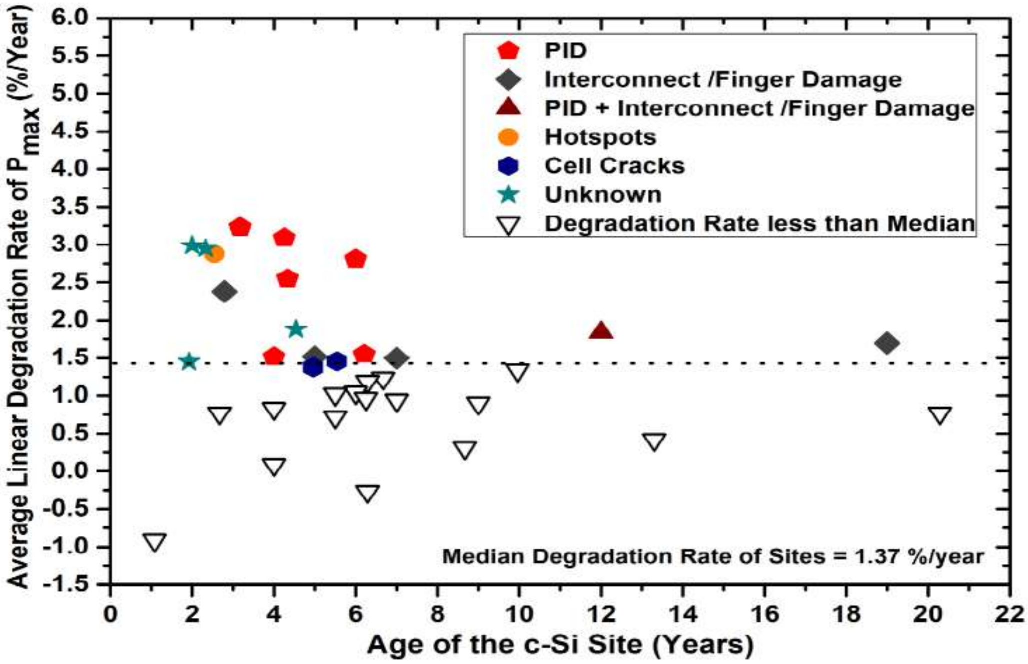


Fig. D.2. Average linear degradation rates of $P_{max}$ for all c-Si sites with respect to their Age and dominant degradation modes observed in sites with degradation rates higher than the median (1.37 %/year)

Potential Induced Degradation (PID) is seen as one of the severe degradation mode observed in this 2018 survey, it is also one of the major reason for the higher degradation mode observed in "Young" c-Si sites. We observed high Fill Factor (*FF*) degradation rate in the PV modules inspected from these PID affected sites. Interconnect and (or) Finger damage is the next severe degradation mode observed in this survey after PID. We identified corrosion of fingers and busbars of the solar cells in some sites, especially severity of corrosion is more in the sites located in Warm & Humid climatic zone. We also observed interconnect damage due to thermal cycling in some of the sites located in Hot climatic zones of the country. In the sites, the PV modules affected by Interconnect and (or) Finger damage have shown high Series Resistance ($R_s$) than other PV modules. Due to high Series Resistance ($R_s$), these PV modules have shown high *FF* degradation rates. We have also seen severe hot spots in one of the "Young" site, and those are due to improper installation practice. In this particular site, the clamps are partially shading the PV module at four corners, and causing hot spots, and which led to high *FF* degradation rates. Cell Cracks were observed in all most all the sites, but the severity of cracks is more in couple of sites. We observed large number of mode B and C cracks in most of the PV modules inspected from these sites. In these sites also high *FF* degradation rates were observed. Snail Trails were also seen in some of the sites, and they led to high *FF* degradation rates in those PV modules.

In some of "Young" sites even though we have observed very high degradation rates, but we could not find any degradation mode from our field characterization techniques and analysis techniques. But in all these sites the manufacturer specification for Light Induced Degradation (LID) is more than we have discounted (2% in power) in our analysis. Even though the excess LID is not only the reason to explain very high degradation rates in these sites, but the contribution of this excess LID cannot be ignored. Other major reason we suspect is that possible overrating of the PV modules in these sites. We also observed discoloration of encapsulant in very old sites and the Short Circuit Current (*Isc*) degradation is the major degradation mode in these sites. Delamination was observed in few cases but the extent of delamination is not high in any of the inspected sites.